Università degli Studi Roma Tre
Dipartimento di Scienze Geologiche

Scuola Dottorale in Geologia dell'Ambiente e delle Risorse
Sezione Geologia delle Risorse
Ciclo XXIII

In situ brecciation and fluid migration in seep carbonates:
the case study of the Messinian Limestones in the Western Mediterranean Basin

Annalisa Iadanza

Tutor: Domenico Cosentino

SCUOLA DOTTORALE IN

GEOLOGIA DELL'AMBIENTE E DELLE RISORSE

(SDIGAR)

Ciclo XXIII

IN SITU BRECCIATION AND FLUID MIGRATION IN SEEP

CARBONATES:

THE CASE STUDY OF THE MESSINIAN LIMESTONES

IN THE WESTERN MEDITERRANEAN BASIN

Annalisa Iadanza

A.A. 2010/2011

Tutor
Prof. Domenico Cosentino

Direttore SDIGAR
Prof. Domenico Cosentino

Revisori
Prof. Francesco Dela Pierre
Università degli Studi di Torino
Dipartimento di Scienze della Terra

Prof. Maria Mutti
Universität Potsdam
Institut für Erd- und Umweltwissenschaften

Annalisa Iadanza

XXIII ciclo dottorale – 2008-2010

email: aiadanza@uniroma3.it
         annalisa.iadanza@gmail.com

Università degli Studi "Roma Tre"
Dip. Scienze Geologiche L.go S. Leonardo Murialdo 1
00146 Roma, Italia

Reviewers

Prof. Francesco Dela Pierre
Università degli Studi di Torino
Dipartimento di Scienze della Terra

Prof. Maria Mutti
Universität Potsdam
 Institut für Erd- und Umweltwissenschaften

Examining Commitee:

Prof. Roberto Bartole
Dipartimento di Geoscienze
Università degli Studi di Trieste

Prof. Antonio Caruso
Dipartimento di Scienze della Terra e del Mare
Università degli studi di Palermo

Prof.ssa Daniela Ducci
Dip. Ingegneria Idraulica, Geotecnica e Ambientale (DIGA), Sez. Geologia Applicata
Università degli Studi di Napoli

Dott. Domenico Grigo
eni spa - exploration & production division
San Donato Milanese (Milan) Italy

Prof. François Roure
IFI-Energies Nouvelles
Département de Géologie-Géochimie-Géophysique
Ruel-Malmaison Cedex

Direttore della Scuola Dottorale in Geologia dell'Ambiente e delle Risorse
Prof. Domenico Cosentino

Coordinatore della Sezione Risorse
Prof. Giuseppe Capelli

ai Guerrieri della Luce

"I shall consider this paper an essay in geopoetry.
In order not to travel any further into the realm of fantasy
than is absolutely necessary I shall hold as closely as possibly to a uniformitarian approach;
even so, at least one great catastrophe will be required early in the Earth's history."

Harry Hammond Hess, 1962

*"**In situ brecciation and fluid migration in seep carbonates: the case study of the Messinian Limestones in the Western Mediterranean Basin**"*

Abstract

Brecciated fabrics, coupled with authigenic carbonate precipitation, extensively affect the carbonatic units developed during the Messinian Salinity Crisis (MSC) of the Mediterranean Sea. These limestones represent a complex unit in terms of genesis and stratigraphy: they show a rich facies inventory and are intimately related to a major basin-scale unconformity (the MES, Messinian Erosional Surface). The brecciated limestones are known as "Calcare di Base" Fm. (basal limestone) and show sulphur-bearing lithofacies at places. They have been long investigated and the attempt to group them on the basis of sedimentological, mineralogical and geochemical datasets results in still fragmentary models, where the fabric aspects have not been highlighted yet, nor the trigger for the wholesale brecciation hasn't been clearly defined. Two different triggers for brecciation have been so far claimed: evaporitic collapse and mass wasting processes.

The relation between the upper Messinian breccias and fluid migration, to date only speculated, is tested in the present study using a suite of sedimentary techniques (outcrop facies analysis, natural radioactive measurements, facies and fabric investigations) and geochemical techniques (XRD and EDS analyses, stable isotopes $\delta^{18}O$ and $\delta^{13}C$, organic geochemistry). The brecciated limestones widely crop out in the Western Mediterranean area: some key-sections located in Italy (Maiella area; Calabrian Arc; Sicily) have been chosen in this thesis to obtain an exhaustive stratigraphic framework and a genetic model for the Upper Messinian breccias. The overall challenge is to validate the role of investigating brecciated fabric as: 1) a sedimentological tool for detecting ancient cold seeps, offering a contribute to the "paleo-seep search strategy"; 2) an opportunity to achieve an outstanding insight into the processes taking place below the seafloor in modern seepage settings.

The Messinian breccias are made up of limestones exhibiting high variability in facies and thickness: their geometry varies from a patchy distribution within a host sediment to massive or stratified thick bodies interbedded with pelitic horizons. The carbonatic beds consist of locally brecciated marly lime mudstones, highly cemented, devoid of gravity segregation and any preferential distribution. Generally brecciation overprints the primary fabric, resulting in fabric-retentive breccias (in situ brecciation). Breccias are typified by monomictic subangular clasts, showing scale-invariant fabric and lithology-independent patterns.

Brecciation, accompanied by fluid migration pathways occurring at any scale of observation, is a diffused phenomenon at the mesoscale, but localized at the microscale. This possibly accounts for variation in the energy input of the fluids, supposed to have triggered brecciation in such environments.

The co-occurrence of plastic and brittle behaviour proxies point to fluidification and associated brecciation phenomena taking place in a partly unlithified sedimentary column, typified by differential diagenesis.

Both the carbonates and the pelitic fraction show an intense natural radioactivity (up to 63 Cps), mostly related to authigenic ^{238}U.

The geochemical dataset is complex and shows wide ranges both in δ^{18}O (+7.74 down to -9.64 ‰ PDB) and δ^{13}C values (+4.14 down to -43.7 ‰ PDB). This is the result of: 1) originally mixed carbon sources involved in authigenesis; 2) a complex fluid-rock interaction; 3) different fluid composition in the different basins (in the Maiella Basin and at Capodarso - in the Caltanissetta basin - they were enriched in hydrocarbons; in the Calabrian Arc and in Centuripe - in the Caltanissetta basin - the nature of the fluids, was possibly saline). In addition, the coupled positive δ^{18}O - negative δ^{13}C widely typifying the Calcare di Base both in Sicily and Calabria, could be related to gas hydrate destabilization processes, since textures resembling gas-hydrate bearing sediments were observed as well.

A revisiting of the term "seep limestone" is proposed herein, since the aforementioned facies and fabric association enucleates important sedimentological proxies for the detection of seep limestones: (a) irregular geometries of the geobodies; (b) primary fabric overprinting; (c) peculiar textural characters of breccias; (d) scale-independent and lithology-independent patterns; (e) complex rheology; (f) fabric resembling gas-hydrate infilling sediments.

The upper Messinian brecciated limestones occur in correspondence to different phases of the Messinian Salinity Crisis, but are strictly related to the regional unconformity: the MES played a critical role in the brecciation processes. There is no evidence to consider the upper Messinian breccias as a stratigraphic unit: the processes of brecciation and widespread fluid migration took place, involving different stratigraphic levels, according to their rheology and to the structural local setting. The age of this processes is constrained to the early upper Messinian phase, before the development of the Lago-Mare event.

The major drawdown of the Mediterranean Sea recorded by the MES corresponds to a huge sea level drop: this most likely represents the primary trigger for fluid migration: the high depressurization experienced by the sedimentary column after the removal of at least 1 km of water column, could have likely favoured a catastrophic migration of overpressured fluids from below.

1 - INTRODUCTION

Brecciated fabrics, coupled with authigenic carbonate precipitation, extensively affect the carbonatic units developed during the Messinian Salinity Crisis (MSC) of the Mediterranean Sea. These limestones represent a complex unit in terms of genesis and stratigraphy: they show a rich facies inventory and are intimately related to a major basin-scale unconformity (the MES, Messinian Erosional Surface).

The brecciated limestones are known as "Calcare di Base" Fm Auctt., since they have been traditionally interpreted to mark the onset of the crisis: a deposit related to an early evaporitic environment, that experienced in situ-brecciation after evaporitic collapse (McKenzie, 1985; Decima et al., 1988; Pedley & Grasso, 1993). Their primary vs secondary nature and the occurrence of sulphur-bearing lithofacies at places, have nonetheless kept an animated discussion about the genesis.

Recently they have been even interpreted as the product of mass wasting processes occurring after the first phases of the crisis (Roveri et al., 2008; Manzi et al., 2010). This led for the first time to the review of their stratigraphic position too (CIESM, 2008).

The basal limestones have been long investigated in the attempt to group them on the basis of sedimentological, mineralogical and geochemical datasets. Yet, this still results in fragmentary models, since the fabric aspects have not even been highlighted and the trigger for the wholesale brecciation hasn't been clearly defined yet.

The brecciated limestones widely crop out in the Western Mediterranean area: some key-sections located in Italy (Maiella area; Calabrian Arc; Sicily) have been chosen in this thesis to obtain a genetic model for the upper Messinian breccias, thus clarifying in turn the unsettled stratigraphy. This model is finally placed in the larger context of the major events of the Messinian Salinity Crisis, as a contribute to the still lively "Messinian debate".

Fluid flow processes and their wide spectra of products have been documented from every kind of basin and every continent worldwide: their role as dynamic components of the sedimentary basin evolution has been recently pointed out (Huuse et al., 2010, and ref. therein).

The relation between the upper Messinian breccias and fluid migration, to date only speculated (Ryan, 2009), is tested in the present study using a suite of sedimentary and geochemical techniques. Special emphasis is placed on the fabric-and-facies analyses approach, based on the comparison of the scales of observation.

The overall challenge is to validate the role of investigating brecciated fabric as:

1) *A sedimentological tool for detecting ancient cold seeps*, within the "paleo-seep search strategy".

Peculiar fabrics, accounting for the complex rheological behaviour shown by seeps carbonates remarkably received scarce attention in the last decade research papers, mainly devoted to define carbon cycling at ancient methane seeps through a geochemical/biogeochemical approach. In situ brecciation and fluid migration pathways can provide useful proxies for a readily identification of ancient cold seeps directly in the field.

2) *An opportunity to achieve an outstanding insight into the processes taking place below the seafloor in modern seepage settings.*

Little is known about the role of overpressure within the sedimentary column and how brecciation occurs in present day seep settings: investigating distinctive brecciated textures can be considered a precious way to understanding processes occurring below the sea-water interface in active seepage settings.

2 - BACKGROUND

2.1 - Hydrocarbon seeps: processes, structures and the geological record

Modern hydrocarbon seeps (especially methane-seeps) occur in a variety of different marine geotectonic settings (Campbell et al., 2002). They are typical features of ocean margins, where there's maximum availability of organic carbon.

Cold seeps occur at ambient temperatures and are caused by different geological phenomena, like compression of the sediments and differences in the hydrostatic pressure or hydrocarbon migration.
Blowouts or seeps (calm fluxes) at the seafloor, sometimes linked to shallow gas hydrate occurrences, are common and usually sustain chemosymbiontic invertebrate communities (Sibuet & Olu, 1998).

In such environments, a major sink of methane and non-methane hydrocarbons is the precipitation of authigenic carbonates on the ocean-floor or in the sediments, which are closely coupled to the activity of microbial communities in the hydrate/seep environments (Zhang & Lanoil, 2004). Methane-derived carbonates preferentially form within the sediment (Paull et al. 1992; Gaillard et al., 1992), where penecontemporaneous sulphide and sulphate mineralization can be common.

Phenomena and products related to hydrocarbon migration and gas/fluid seepage have been recognized and studied worldwide in both recent active settings and fossil seep sites in various sedimentological and geodynamic settings: an overview is proposed in the next paragraphs.

2.1.1 - *Hydrocarbon seeps: processes and products*

2.1.1.a - Seafloor structures derived from fluid escape

Peculiar seafloor structures testify fluid escape phenomena (e.g. mud volcanoes, mud ridges, pockmarks; Fig. 2.1.1).

Mud extrusions are signs of active fluid seepage and are related to mud diapirism occurring from below. Their most spectacular expression is represented by mud volcanoes (MV), surface edifices formed by the eruption of fine grained sediment, oil and gases (dominantly CO_2 and methane) from the subsurface. Fragments of country rock are also sometimes entrained. They range in size from <1 m - typical of mud volcanoes formed by liquefaction at shallow depths - to edifices that are a few hundred meters high or extend laterally for more than 1 km. The largest eruptions deliver mud to the surface from depths that exceed more than 1 km (Kopf, 2002).

Mud volcanism requires thick layers of unconsolidated sediment with high pore pressures. They are thus most common in areas with high sedimentation rates, such as sedimentary basins in accretionary prisms, where their eruption is favoured by the increase in pore pressures induced by compressional forces (Wang & Manga, 2009).

Pockmarks are on the other hand negative structures related to such phenomena: they are sea-floor craters representing the seabed expression of vertical focused fluid flow through soft, fine-grained sediments (King and MacLean, 1970; Hovland, 1982, 1984; Hovland & Judd, 1988; Judd & Hovland, 1992). They are usually circular or oval in plan view, their diameter varies between 10 and 450 m and they have a 1-25 m depth range (Pilcher & Argent, 2007). Pockmarks are thought to form preferentially in soft sediment areas, where the low permeability avoids a constant seepage (Chand et al., 2009) and the gas pressure can rise until it becomes higher than the static pressure of the overlain sediments. The following explosive release of this gas is assumed to be responsible for the formation of pockmarks.

In the major siliciclastic settings, sand volcanism and injections are commonly occurring phenomena when fluid release from below takes place.
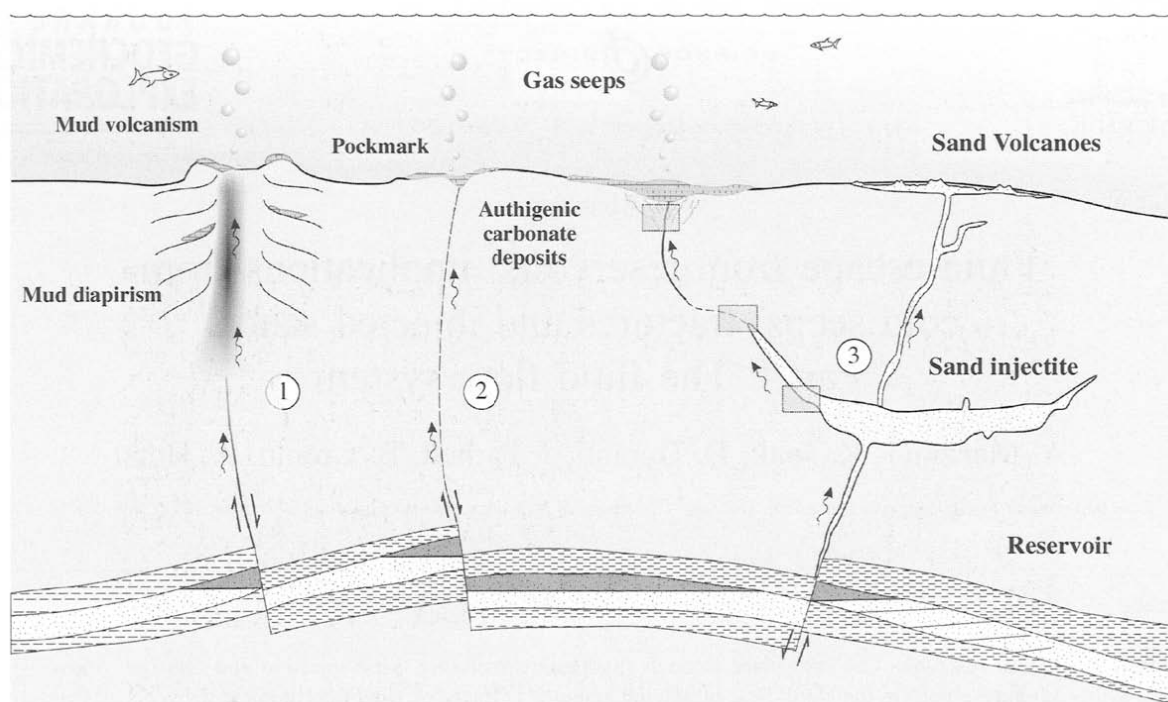
Fig. 2.1.1 – Seafloor/subseafloor structures and products associated to fluid escape phenomena. In the example, from the North Sea, the fluids from below have origin from a deep reservoir (Mazzini et al., 2003).

2.1.1.b - Gas hydrates

Gas hydrates (or clathrate hydrates) are ice-like crystalline solids formed from a mixture of water and suitably sized *guest* gas molecules (usually mostly methane). The water (*host*) molecules, upon hydrogen bonding, form lattice structures with several interstitial

cavities. The guest gas molecules can occupy the lattice cavities and, when a minimum number of cavities are filled, the crystalline structure will become stable and solid gas hydrate will form, even at temperatures well above the melting point of water ice. Gas hydrates account for methane from: biogenic production, pore water advection, deep source (biogenic deep source and/or thermogenic).

The theoretical area of clathrate stability (Fig. 2.1.2) is delineated by the transition between the solid (hydrates) and gas phases, intersected by the sea water temperature gradient above the sea floor and by the geothermal gradient below the sea floor (Dickens, 2001). The position of hydrate phase boundary is primarily a function of gas composition, but may also be controlled by pore fluid composition (e.g presence of salt), pore size, and possibly sediment mineralogy: the addition of NaCl decreases the area of the stability field, while the addition of other gases to methane increases the area of the stability field (Fig. 2.1.2).

Gas hydrates are widely distributed along continental margins (Kvenvolden, 1988, 1998; Suess et al., 2001). However, they do not form in the ocean due to the low concentration of methane. The sedimentary area of clathrate stability, also know as the Gas Hydrate Stability Zone (GHSZ) is therefore a lens, bounded landward by the point where the field of clathrate stability is no longer intersected by the geothermal gradient. It extends oceanward, with increasing water depth, but thins in

Fig. 2.1.2 - Phase diagram showing the boundary between the free methane gas and methane hydrate for a pure water and pure methane system. The different effects on the hydrates stability field induced by the presence of salts or by the addition of gases other than methane are shown (after Kvenvolden, 1998).
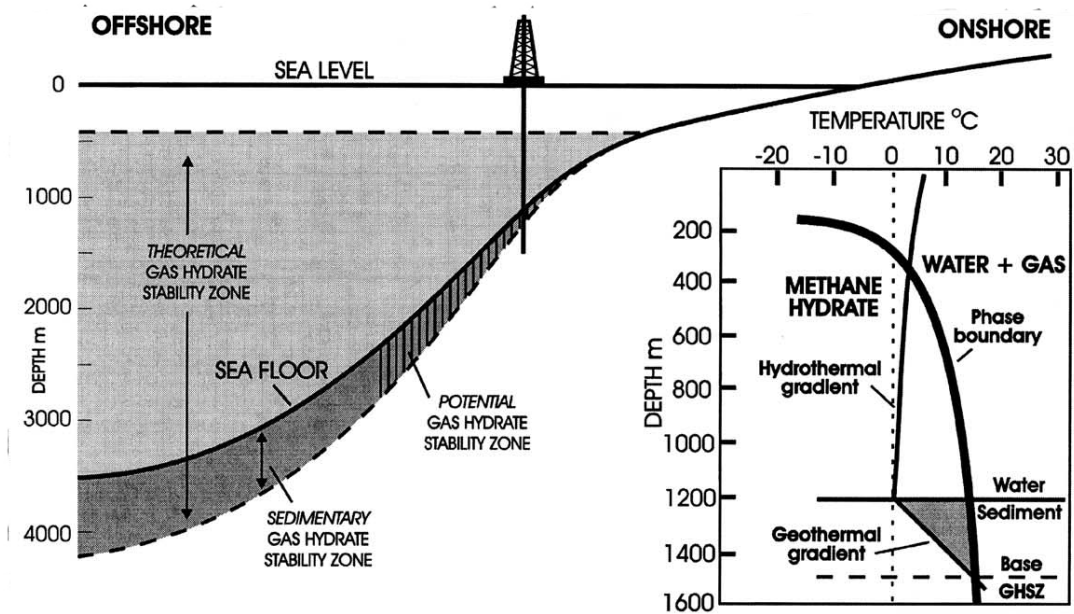
Fig. 2.1.3 - Oceanic Gas Hydrates Stability Zone (GHSZ), showing theoretical, sedimentary and potential zones of hydrate formation, with insert depicting pressure-temperature profile in wells.

those areas typified by higher geothermal gradients such mid-oceanic ridges or hot spots. However, gas hydrates do not form beyond continental wedges due to sub-critical methane concentrations within the sediments (Beauchamp, 2004; Tréhu et al., 2006). As a result, the potential area of hydrates formation is a narrow subset of the sedimentary zone of clathrate

stability that excludes both sea water and sub-abyssal sediments and lies mostly beneath continental slopes in water depth exceeding 500 m (Fig. 2.1.3). In general, GH are stable at water depth greater than 300 to 500 m and burial depth lower than 100 to 1100 m (Kvenvolden, 1993). In the permafrost areas of the northern hemisphere, the GHSZ, which lies a few hundreds of metres below the surface, is bounded by the southermost extent of the permafrost and to the north by the Arctic Ocean, which, by and large, delineates the northernmost extent of the permafrost, for the exception of a narrow band of subsea permafrost (Goldberg et al., 2000).

Dissociation of hydrates at the base of the hydrate stability zone (BHSZ) can arise through:

- an increase in temperature due to increasing burial depth (assuming continued sedimentation)
- an increase in sea bottom-water temperatures
- a decrease in pressure (e.g. lowering of sea level)

Gas hydrate dissolution takes place when pore water methane concentration is lower than solubility: it can happen within the whole GHSZ, generating water and dissolved methane, without appreciable volume increase. It differs from *gas hydrate dissociation*

whereby the latter takes place when T, P move out of stability zone. This occurs near base GHSZ and generates water and free gas, volume increase, possible overpressure.
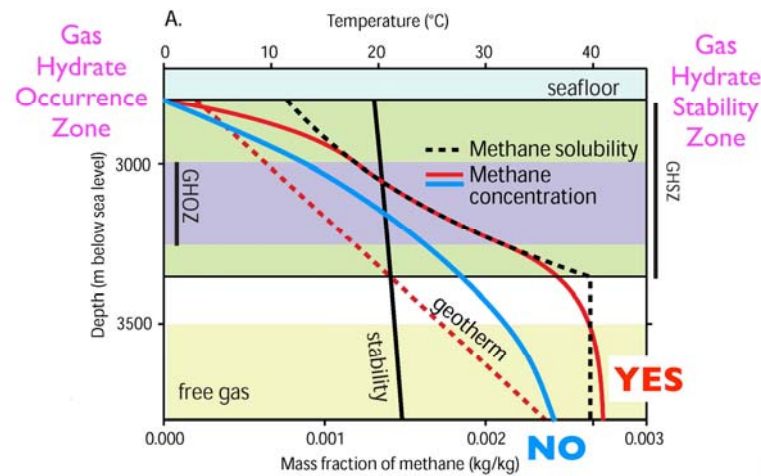
Fig. 2.1.4 - Gas hydrate formation and persistence in the GHSZ depends on the methane concentration: if it isn't higher than solubility they dissolve or not form at all. A boundary condition is represented by zero methane concentration at sulphate-methane interface.

Gas hydrate formation and persistence in the GHSZ depends on the methane concentration: if it isn't higher than solubility they dissolve or not form at all. A boundary condition is represented by zero methane concentration at sulphate-methane interface (Fig. 2.1.4).

The relevance of gas hydrates research is related to three main geologic hot topics:

1) Energy resources

The concentrations of dissolved methane in the ocean range from a few nM in seawater to about hundred mM in hydrate-bearing subsurface sediments (Reeburgh, 2007): interestingly, submarine gas hydrates bind more methane than all other reservoirs on Earth (Milkov, 2004). Conventional gas resources are trapped beneath methane hydrate layers in ocean sediments: one cubic meter of gas hydrate yields 164 m^3 of gas and 0.8 m^3 of water at standard temperature and pressure (Kvenvolden, 1993). This points to gas hydrates as a great energy resource, though difficult to be trapped due to their narrow P-T stability range.

2) Climate change

Rapid methane release is directly related to climate change issues, since methane is a greenhouse gas significantly more - c. 20 times - aggressive than CO_2, depending on the efficiency of the AOM filter (see par. 2.1.1.c).

3) Environmental impact

Gas hydrate growth and dissociation influence the physical properties of the sediments: upon dissociation, what was once solid hydrate will become liquid water and gas. This could lead to increased pore-fluid pressures in under-consolidated sediments, with a reduced cohesive strength compared to overlying sediments, thus forming a zone of weakness. This zone of weakness could act as a site of failure in the event of increased gravitational loading or seismic activity.

<u>Tracing ancient gas hydrates occurrences</u>

The water in the gas hydrate cages is enriched in ^{18}O by 2x to 3x relative to the primary pore-waters (Davidson, 1983; Ussler & Paull, 1995). Consequently, unusually high $\delta^{18}O$ values of seep carbonates have been used to trace gas hydrate destabilization (Bohrmann et al., 1998). Due to the enrichment of ^{18}O in gas hydrates, anomalously positive $\delta^{18}O$ carbonate values could argue in favour of gas hydrate destabilization at methane-seep sites. Unfortunately, oxygen isotopes are much more prone to exchange than carbon isotopes in carbonate rocks. The oxygen isotope ratio is believed to shift towards lower $\delta^{18}O$ values during rock alterations, because meteoric waters are usually significantly depleted in ^{18}O relative to marine waters. Therefore, it is possible that signatures of gas hydrate destabilization have been obscured in some ancient seep carbonates (Peckmann & Thiel, 2004, and ref. therein).

Some examples of gas hydrate occurrences inferred by the oxygen isotopic signature are nonetheless reported in the literature:

1) the significant ^{18}O-enrichment of carbonates (relative to a composition in equilibrium with ambient waters) at methane-seeps in the Mediterranean (Aloisi et al., 2000);

2) the case of the stratabound dolomites formed in Tortonian marls in the Lorca Basin (SE Spain) prior to the Messinian salinity crisis: the geochemical signature of the dolomites - high $\delta^{18}O$ values, both high and low $\delta^{13}C$ values - and is coupled with the deformation structures yielded by the Tortonian sediments (Pierre et al., 2002). The latter include slumps and faults, often associated with the breakdown of gas hydrates (Kvenvolden, 1998; Paull et al., 2003);

3) the positive $\delta^{18}O$ signal in the seep limestones of the Tertiary Piedmont Basin (Martire et al., 2010).

Some gas hydrate-sediment aggregates exhibit a globular texture. As hydrate-associated carbonates cast this globular texture, carbonate fabrics are a potential tool to track a relation of ancient seep sites with destabilising gas hydrates, even more objective than $\delta^{18}O$ signal. Important attempts to trace ancient gas-hydrate - related deposits on the basis of sedimentological and facies characterization have been recently carried out (clathrites *sensu* Bohrmann et al., 2002; Martire et al., 2010).

Gas hydrates trap preferentially ^{18}O-rich water molecules, resulting in ^{18}O depletion of the remaining pore fluids (Sample & Kopf, 1995; Aloisi et al., 2000; Ussler & Paull, 2001; Pierre & Rouchy, 2004). By contrast, the decomposition of gas hydrates liberates ^{18}O-rich freshwater, which may locally contribute to the ^{18}O enrichment of pore solutions (Kopf et al., 1995). In particular, according to Pierre & Rouchy (2004) the coupled $\delta^{18}O$ - ^{13}C signature in the diagenetic carbonates is a proxy for the formation/dissociation of gas

hydrates: a ^{18}O-depleted - ^{13}C-enriched signal is indicative of gas hydrate formation, while a ^{18}O-enriched - $\delta^{13}C$-depleted is indicative of gas hydrate dissociation.

2.1.1.c - Hydrocarbon-derived carbonates

Methane-derived carbonates are authigenic carbonates highly diffused in the cold seeps.

Carbonate precipitation at methane-seeps results from the increase in alkalinity produced by the release in HCO_3^- during the anaerobic oxidation of methane (AOM) and higher hydrocarbons

(Fig. 2.1.5; Ritger et al., 1987; Paull et al., 1992). AOM is performed in anoxic environments by consortia of methanotrophic archaea (ANME) and sulphate reducing bacteria (SRB) (Aloisi et al., 2000; Boetius et al., 2000; Orphan et al., 2001; Peckmann et al., 2001), though microbiological evidence suggests that methane may be oxidized by archaea without forming a close physical partnership with sulphate-reducing bacteria (Zhang & Lanoil, 2004). AOM generally occurs within the sulphate-reduction zone: in this reaction methane oxidation (a) is coupled to sulphate reduction (b).

(a) $CH_4 + 3 H_2O \rightarrow 4H_2 + HCO_3^- + H^+$

(b) $2[CH_2O] + SO_4^{2-} \rightarrow 2 HCO_3^- + H_2S$
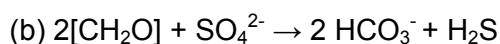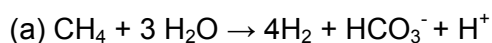
The net reaction for AOM with sulphate is:

$CH_4 + SO_4^{2-} \rightarrow HCO^{3-} + HS^- + H_2O$

Finally, the carbonate ions associate with calcium of interstitial water and authigenic carbonates precipitate. Under general conditions, in the absence of gas discharge, this processes of authigenic carbonate formation would not take place.

Both microbially mediated oxidation of organic matter by sulphate reduction and microbially mediated anaerobic methane oxidation increase alkalinity (by increasing DIC) of pore fluids, hence stimulating carbonate precipitation.
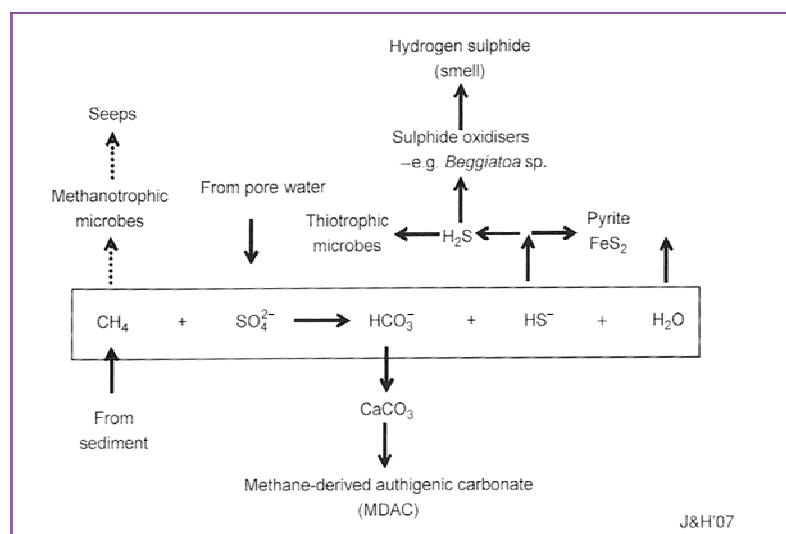
Fig. 2.1.5 - Anaerobic oxidation of methane: ingredients (methane and sulphate), products (hydrogencarbonate, hydrogen sulphide and water) and by-products (methane-derived authigenic carbonates - MDAC - and pyrite). Excess methane is available for utilization by methanotrophs (after Judd & Hovland, 2007).

Savard et al. (1996) suggested that the mineralogy of early precipitates at methane seeps is controlled by the fluctuations in ion activity ($\alpha_{carbonate}/ \alpha_{sulphate}$).

According to Roberts (2001), more extensively, the main parameters regulating the composition and development of a carbonate body in such contexts are:

- the methane pressure in interstitial sedimentary fluids

- the flux discharge and rate in the venting zone

- the evolutionary path of the rising fluids

Where iron reduction: $CH_2O + 4FeOOH + 7H^+ \rightarrow HCO^{-3} + 4Fe^{2+} + 6H_2O$ and sulphate reduction occurred contemporaneously, alkalinity would have been even increased by the consumption of protons and the production of bicarbonate ions (c):

(c) $4CH_4 + CH_2O + 4SO_4^{2-} + 4FeOOH + 3H^+ \rightarrow 5HCO^{-3} + 4FeS + 10H_2O$

This scenario (Peckmann et al., 2003) does not necessarily imply that AOM by sulphate and iron reduction are coupled, but if these processes occur in close proximity, carbonate formation is even more favoured than by AOM alone.

Sulphide removal in such environments is regulated by: oxidation by microbial communities; Fe-sulphide formation; ebullition (bubble stripping). Activity of sulphate reduction is enhanced in such environments (Zhang & Lanoil, 2004): pyrite, celestite and/or barite are indicative of sulphate reduction conditions. Pyrites enclosed in the seep limestones generally show low $\delta^{34}S$ values and a significant variability of their isotopic composition on a small scale, both pointing to bacterial sulphate reduction as the sulphide-supplying process.

In these unique marine environments constituted by sediments associated with gas hydrates and hydrocarbon seeps, AOM is a major sink for methane on Earth and dominates the carbon and sulphur cycles, thus playing a major role in the regulation of global methane fluxes (Hinrichs & Boetius, 2002; and ref. therein). It represents an effective filter against this potential greenhouse gas (Reeburgh, 1996, 2007): methane emission from the ocean contributes an estimated 3 to 5% of the atmospheric methane budget. The efficiency of the microbial filter against methane in the seabed depend on the methane flux rates.

The bacterial oxidation of methane produces ^{13}C-depleted bicarbonates, inheriting an isotopic signature often similar to that of the parent methane: the resulting carbonate minerals will basically reflect the isotopic signature of the dissolved inorganic carbon (DIC) pool in which they formed (Rodriguez et al., 2000). It must be considered that actually the $\delta^{13}C$ value of the methane source is usually significantly lower than $\delta^{13}C$ carbonate values, testifying additional carbon sources involved in the carbonate formation. Due to variable degrees of mixing, an evaluation of the carbon source based on $\delta^{13}C$ values alone is problematic.

The sources to be considered are:

- DIC (pool or pore water; from methane or higher HC);

- water from GH dissociation;

- water from clay dehydratation;

- seawater.

An additional complication is represented by the hydrocarbons nature itself, according to which the following correspondent isotopic ranges can be enucleated:

- *Biogenic methane* (T<50°C) is strongly ^{13}C-depleted, exhibiting values in the range -50‰/-110‰ (Whiticar et al., 1986; Whiticar, 1999) and typically <-60‰.

- *Thermogenic methane* (T>80°C) exhibits typical values ranging from -30‰ to -50‰ (Sackett, 1978).

- *Hydrothermal fluids* show values even higher than -20‰ (Botz et al., 2002, and ref. therein).

- *Petroleum* usually yields δ^{13}C values in the range from -25‰/-35‰ (Roberts & Aharon, 1994).

This problem is even more complex in ancient seep limestones, often yielding also later diagenetic ^{13}C-enriched phases that apparently formed in the zone of archaeal methanogenesis. This reveals that methane oxidation and formation may have successively occurred in the same deposit as a function of increasing burial. In such cases it is essential to detect first the early diagenetic carbonate phases, predominantly derived from the supposed oxidation of methane and thus yielding low δ^{13}C values.

Microbial mats and oligotypic chemosynthesis-based communities are commonly associated to seafloor hydrocarbon-derived carbonates. They are sustained by hydrocarbon-charged fluids: by oxidizing H_2S and CH_4 they provide energy for a food web in such harsh physicochemical conditions (Campbell et al., 2008 and references therein), similarly to the comparable biota of submarine hydrothermal vents and whale/wood-falls worldwide (Van Dover, 2000; Distel et al., 2002; Baco & Smith, 2003).

Seep limestones facies are well documented in the literature (Judd & Hovland, 2007 and ref. therein) and chiefly include: chemoherms, concretions, boulder fields, chimneys, pavements, mounds and breccias.

2.1.1.d - Fluid escape structures

According to methane (or general fluid) flux rates, three main systems can be outlined (Wegener & Boetius, 2009, and ref. therein):

- *Diffusive systems*: methane is consumed within narrow sulphate methane transition zones (SMTZ) in the seabed (here the efficiency of the microbial filter against methane is 100%).

- *Advective systems (cold seeps)*: with higher methane concentrations and flow velocities of <0.1myr^{-1}, AOM rates increase to hundreds of nmol cm^{-3} day^{-1}.

- *Cold vents*: sulphate-depleted subsurface fluids are transported upwards at high velocity (>0.4myr^{-1}) and AOM becomes sulphate-limited (Niemann et al., 2006). Flow velocities above 2.5myr^{-1} of sulphate-depleted geofluids can even prevent the flux of sulphate into the sediment and completely inhibit AOM activity (De Beer et al., 2006), with consequent high methane efflux to the hydrosphere.

It must be pointed out that constraining budgets of methane emission at active cold seeps is not easy: cold seeps show an extreme spatial and temporal variation in gas ebullition and fluid flow which is difficult to record (Tryon et al., 2002; Sauter et al., 2006).

In the Goliat hydrocarbon field of the Barents Sea in areas of consolidated sediments the upward flow is limited to open fault locations, while soft sediment areas allow diffused flow of fluids and hence the formation of pockmarks over a wide region, through removal of fine-grained material (Chand et al. 2009): disharmonic diagenesis and compaction can lead to extremely complex lateral variations.

Seafloor carbonate mounds are often associated to carbonate chimneys that likely fuelled their growth (Judd & Hovland, 2007). Less understood are the subsurface plumbing features of such structures, thought to be represented in ancient outcrops by pipe-like and other linear concretionary features (Nyman et al., 2010; Pearson et al., 2010; Dela Pierre et al., 2010).
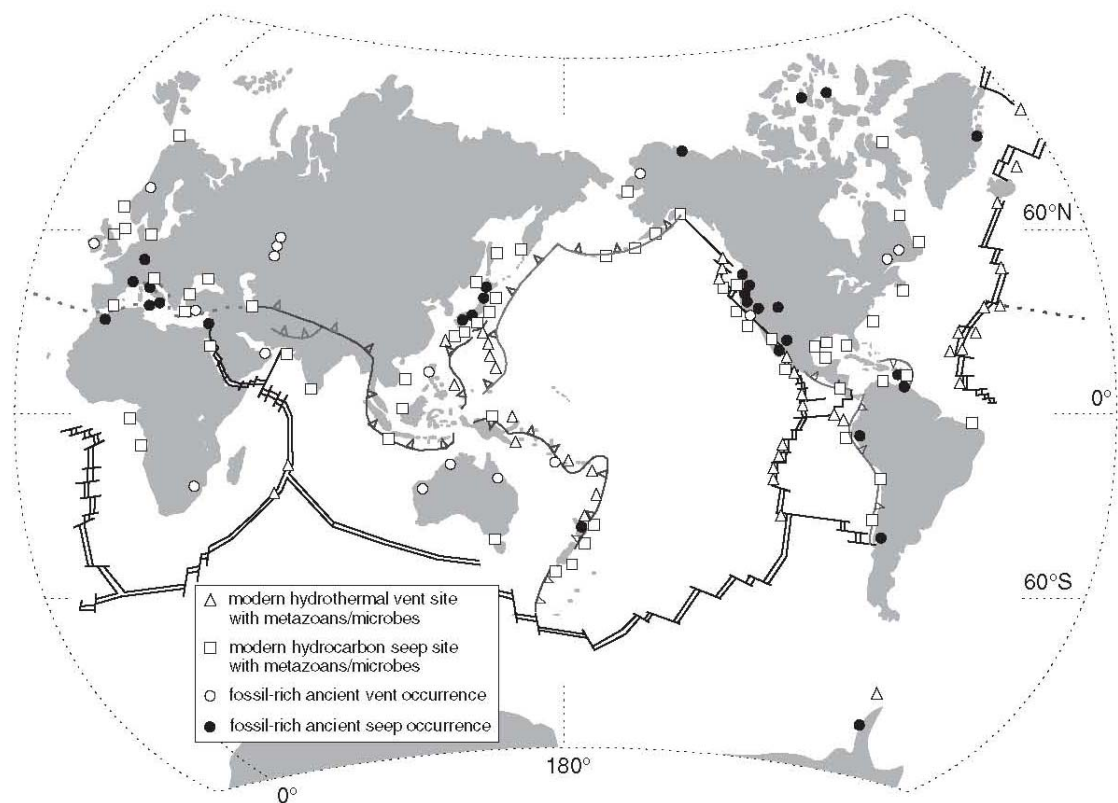
Fig. 2.1.6 - Distribution map of chemosynthesis-based settings, illustrating those Archean to Recent hydrothermal vents and hydrocarbon seeps with associated metazoan and/or microbial signatures (after Campbell, 2006).

2.1.2 - *Brecciation processes at hydrocarbon seeps*

Many methane-seep limestones are intensively fractured (Beauchamp and Savard, 1992; Kelly et al., 1995; Peckmann et al., 1999b): in situ brecciation is a phenomenon related to hydrocarbon migration and fluid seepage recognized worldwide in both recent active settings and fossil seep sites.

Although the primary cause of such brecciation hasn't been clarified yet, four mechanisms have been proposed:

1) *rise in pressure*: fracturing of carbonate deposits in pockmarks of the North Sea has been interpreted to result from a rise in pressure due to the accumulation of methane gas below the limestone crusts and the subsequent vigorous gas release causing the crusts to break (Hovland et al., 1987). Similarly, overpressure phenomena inducing gas-explosion are thought to have occurred, among other cases, in the Miocene mud volcano plumbing system of the Chaotic Complex of the Tertiary Piedmont Basin (Clari et al., 2004) and in the Miocenic seep carbonate breccias of New Zealand (Campbell et al., 2008).

2) *formation and dissociation of gas hydrate*: they are the main processes that cause short-term and small-scale disruption of the seafloor at shallow seeps in the Gulf of Mexico (MacDonald et al., 2003).

3) *growth of gas hydrates*, commonly occurring in cold seeps setting: i.e. in modern sediments of the Cascadia margin, offshore Oregon, brecciation-like deformation is caused by the growth of gas hydrates and subsequent fracturing (Bohrmann et al., 1998).

4) *episodic release of gas hydrates*, when their buoyancy exceeds the loading of the overlying sediments: it has been shown that a porous gas hydrate variety from the Cascadia margin has a low bulk density, which may cause episodic release of large hydrate aggregates from the sea floor (Suess et al., 2001). When the buoyancy of the hydrates exceeds the loading of the overlying sediments, chunks of hydrate detach and float to the sea surface. Chunks of up to a cubic metre in size have been observed (Suess et al., 2001). The resulting sedimentary fabric might well resemble early in situ brecciation, as the carbonate layers associated with the hydrate will be fractured by this process.

2.1.3 - *Fossil hydrocarbon seeps*

The ongoing discover of active cold seeps settings, has led to the reinterpretation of many enigmatic sedimentary records over the geological time (Fig. 2.1.6; Campbell, 2006, and ref. therein).

The lively research of active cold seeps, studied with highly advanced analytical techniques, is revealing always more detailed insights on near-seabed processes, on one

hand. On the other hand, processes like brecciation and the resulting geological products cannot be directly observed, thus remaining still obscure.

Past cold seeps potentially provide a unique understanding of their modern counterparts: logistically easily accessible spots, they allow a detailed study of the subsurface seep plumbing systems and an outstandind insight into the heterogeneity of complex seep processes in space and time.

2.1.4 - Identifying fossil cold seeps: ancient seep search strategy and the sedimentological tool

To locate ancient seep deposits, a 'seep-search strategy' was proposed by Campbell and Bottjer (1993). Similarly, Kelly et al. (1995) listed typical features to recognize seep-related limestones, and several studies using lipid biomarkers to track microbial methane oxidation in ancient seep environments, endorsed this research (e.g. Thiel et al., 1999; Burhan et al., 2002; Peckmann et al., 2002).

The strategy, reviewed by Peckmann and Thiel (2004), contemplate the following main points:

  1) the geological setting and structural features, as a basic background to approach the problem;

  2) the occurrence of chemosymbiontic oligotypic taxa (sometimes absent);

  3) the identification of specific carbonate fabrics and microfabrics;

  4) the geochemical and biogeochemical signals: low $\delta^{13}C$ values of early diagenetic carbonate phases and of lipid biomarkers.

The research papers published in the last decade were mainly devoted to define carbon cycling at ancient methane seeps (geochemical/biogeochemical approach). Compared to other methods, the particular strength of the biomarker concept lays in its potential to evaluate the persistence of distinctive methane-utilizing taxa on a geological time scale. As methane is strongly depleted in ^{13}C, the isotopic signatures of specific lipids can testify the biological uptake of methane carbon and differentiate indigenous substances from allochthonous compounds and contaminants (Peckmann & Thiel, 2004).

Notwithstanding, investigations of peculiar fabric, accounting for the complex rheologic behaviour shown by seeps carbonates, remarkably received less attention.

Typification of microfacies is not always easy in such environments due to the small-scale heterogenities often occurring. Peculiar facies and textural characters in the carbonates include (Peckmann & Thiel, 2004; Cavagna et al., 1999):

• Massive carbonates of limited lateral extent, often transitional to very fine grained sediments;

• Paleoconduits;

• Fractures;

- Globular fabric (GH-resembling fabric);
- Botroydal aragonite cements;
- Micritic nodules;
- Inverted stromatoctoid cavities and upside-down stromatolites (stromatolitic fabric);
- Microbial mats;
- Clotted micrites, pyrite-bearing clotted microbialites;
- Constructive seams representing biofilms (fossilized biofilms);
- Microbreccias;
- Pyrite, celestite and/or barite; pyritiferous carbonate nodules and pyrite rims may also occur.

2.2 – The Messinian Salinity Crisis of the Mediterranean Sea and brecciation processes

2.2.1 - The Messinian Salinity Crisis (MSC)

The Messinian salinity crisis of the Mediterranean Sea (MSC) refers to an outstanding basin scale concentration event. The concept of a Messinian salinity crisis in the Mediterranean region dates back to the seventies (Hsü et al., 1973 a,b), after coring in the deep basins (DSDP Leg 13) the top of a thick Messinian evaporitic layer that was suggested by Ryan (1969) based on the observation of seismic profiles. Immediately, this catastrophic event was considered at its true scale and the large evaporitic deposits already known onland, were understood as uplifted segments of the evaporite formations in regions of active Plio-Pleistocene tectonics. The MSC is considered among the greatest evaporitic events of the Earth's history: 106 km^3 of evaporites (Ryan, 1973) were deposited over a surface of 2 millions km^2 (Fig. 2.2.1) in only 640 ka (Krijgsman et al., 1999, a, b). In such a short time span, the Mediterranean Basin experienced exceptional but ephemeral palaeoceanographic changes.

The Messinian salinity crisis occurred after the end of the late-orogenic extension in the Alboran domain and the onset of a new stage of N–S compression in the westernmost Mediterranean (Jolivet et al., 2006). The partial tectonic isolation and the subsequent hydrologic deficit experienced by the Mediterranean Basin during upper Messinian, have been related to the reduced width of the gates of Gibraltar. This phenomenon possibly resulted from this N–S shortening being active throughout the Tertiary (Jolivet et al., 2006): it can be held responsible for the shortening and the final closure of the Betic and Rifian corridors shortly before the salinity crisis, respectively between 7.6 Ma and 6.8 Ma and between at least 6.0 Ma and 5.65–5.4 Ma (Benson & Rakic-El Bied, 1991). The pre-crisis Messinian environment (pre-evaporitic phase, 7.251-5.96 Ma) recorded this progressive closure and was characterized by sea-bottom low-oxygen conditions, testified by the Tripoli Fm *Auctt.* (Tr). Tripoli consists of a cyclic repetition of homogeneous grey marls, red laminated marls and white diatomites (Bellanca et al., 2001, and ref. therein). The upper portion of the Tr and the transition to a calcareous unit (Calcare di Base Fm *Auctt.*, CdB), are key to understanding the onset of the MSC.

The hydrologic regime during the crisis changed as a function of the communication with both the Atlantic Ocean - regulated by the paleo-Gibraltar Strait - and the Parathetys. These two principal factors, together with the regime of the major rivers draining into the Mediterranean Sea, controlled the development of the crisis regulating the partial and temporary isolation of the basin and the switch between hypersaline and hyposaline conditions (switch between step 1 and step 2, sensu CIESM 2008, Fig. 2.2.2).

In the 70s the *deep desiccated basin model* proposed by Hsü et al. (1973), involving the deposition of evaporites in a relatively deep basin and shallow water conditions, was widely accepted. Twenty years later a new renovated debate started to develop and in the last decades many attempts to obtain a basin-scale scenario model have been made. The main scenarios proposed variously claim synchronous, diachronous or slightly diachronous occurrence of the main phases throughout the basin (Rouchy & Caruso, 2006 and ref. therein).

A new consensus model on the main evolutionary stages of the MSC has been recently achieved (CIESM, 2008; Fig. 2.2.2): it is based on the interpretation of the Sicilian stratigraphy proposed by Roveri et al. (2008) and combines the two-step model of Clauzon et al. (1996) and the well-established chronology of the Messinian events (Krijgsman et al., 1999a). According to this model, though still highly debated, the MSC developed in two evolutionary steps, the second of which further subdivided into two steps (two step-three stages model). In this scenario the classical basal position of the CdB is revisited.

The new consensus model can be summarized as follows:

(1) Lower Evaporites (Step 1; *Primary Lower Gypsum, PLG, 5.96–5.60 Ma*)

This step represents the acme of the crisis, with the deposition of selenites in shallow basins and euxinic shales in deep basins.

(2.1) Resedimented Evaporites (Resedimented Lower Gypsum, RLG, 5.61–5.53 Ma)

In this substep is envisaged the deposition, just above the Messinian Erosional Surface (MES), of the Calcare di Base Fm. in marginal settings, and of clastics and salt in the deepest basins.
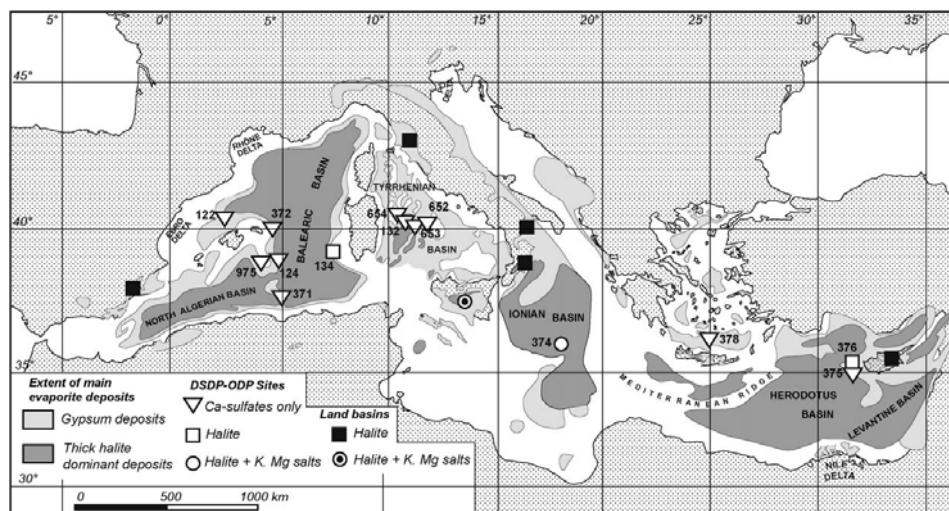
Fig. 2.2.1 - Map showing the distribution and the extent of the Messinian evaporites in the Mediterranean with location of the DSDP-ODP sites that recovered evaporitic deposits (Rouchy & Caruso, 2006 and ref. therein)

(2.2) Upper Evaporites (5.53–5.33 Ma)

Deposition of primary upper evaporites s.s. is reported only at places (Fig. 2.2.2), while a general increase in continental water influxes and the diffusion of Lago-Mare biofacies interested the whole Mediterranean area: this phase records the progressive refill of the basin. The distribution of the upper gypsum and the Lago-Mare facies, as well as the conditions under which they were deposited, is nonetheless still discussed (Rouchy and Caruso, 2006; Roveri et al., 2008; Manzi et al., 2009).

The end of the MSC is marked by the return of normal marine conditions at the base of the Pliocene (Iaccarino et al., 1999).

<u>The post-evaporitic phase (step 2, sensu CIESM 2008)</u>:

The deposition after the development of the MES belongs to the post-evaporitic phase (p-ev; 5.61-5.33 Ma), dominated by humid conditions from a climatic point of view.

The post evaporitic phase, in the past often inappropriately called "Lago-Mare" *l.s.* has been further splitted into two steps:

- *p-ev1, early post evaporitic phase, 2.1 step and lower 2.2 step sensu CIESM 2008 ("Resedimented Evaporites" and early "Upper Evaporites")*

The paleoenvironment of p-ev1 deposits, mostly represented by resedimented evaporitic deposits or barren laminated sediments, hasn't been deeply investigated. Nonetheless the early p-ev phase represents the important switch between hypersaline and hyposaline conditions: its basin-scale palaeoenvironmental meaning has been recently clarified (Sampalmieri et al., 2010) and has been object of study in this thesis (see par. 4.1.5.a). A volcaniclastic event (Odin, 1997) represents an important stratigraphic marker of this substep in the Apennines.

- *p-ev2, late post evaporitic phase, Lago-Mare, upper 2.2 step, sensu CIESM 2008 (late "Upper Evaporites")*

Many works over decades were focused on pev2 phase, which is interpreted to represent the establishment of the brackish water conditions that allowed the flourish of the Lago-Mare biofacies (Grossi et al., 2008 and ref. therein). From a stratigraphic point of view, this events lays atop the second recognized important unconformity.

In this thesis the numeric nomenclature introduced by the CIESM model for the post-evaporitic phase will be avoided; the terms early post-evaporitic phase (or p-ev1) and late post-evaporitic phase (or p-ev2) will be preferred.

<u>The Messinian Erosional Surface</u>

The Messinian Erosional Surface (MES) is a polyphased erosional surface that affected the Mediterranean margins during the MSC with several critical episodes (Fig. 2.2.2). *Strictu sensu*, the MES refers to the major episode related to the greatest water level fall: more than 1000 m (up to 1500 m) occurred during the deposition of the lower evaporites,

from the onset of the evaporite deposition till the end of the first stage (Rouchy & Caruso, 2006 and ref. therein). Erosional processes remained active during the second evaporitic stage, especially whenever the basin dried-up, and also a second great unconformity (MES2) marks the upper Messinian events within the post-evaporitic phase (Fig. 2.2; CIESM, 2008; Cosentino et al., 2010).

The MES has been recognized throughout the Mediterranean Basin in both offshore (Escutia & Maldonado, 1992; Guennoc et al., 2000; Lofi et al., 2005; Maillard et al., 2006) and on land sections (Guillemin & Honzay, 1982; Costa et al., 1986; Cita & Corselli, 1990; Riding et al., 1999; Roveri et al., 2001; Rouchy et al., 2003; Soria et al., 2005; Cornée et al., 2006).
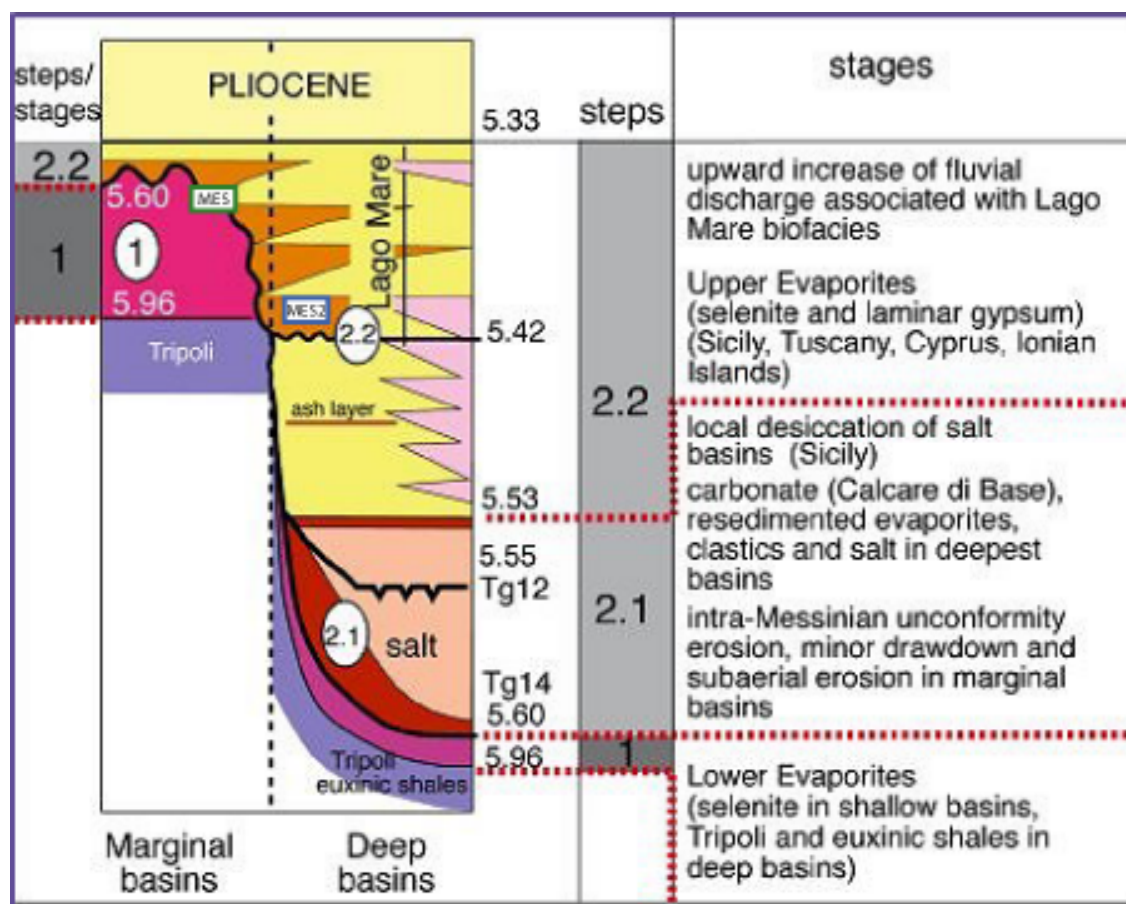
Fig. 2.2.2 - The new MSC scenario (CIESM, 2008), see text for explanation.

2.2.2 - Upper Messinian brecciated limestones and the "Calcare di Base" Auctt.

Within the Messinian debate, the origin of the Calcare di Base Fm *Auctt.* (CdB) has long been discussed. The facies variability of the CdB has been often pointed out, but so far it is still poorly understood.

The transition from the pre-evaporitic diatomite formation (Tripoli Formation) to the overlying evaporites is marked by two types of limestone:

1) The first type - more common and diffused - is named 'Calcare di Base' (basal limestone). This unit is formed of massive limestone beds (Ogniben, 1957, 1963; Decima & Wezel, 1973; Decima et al., 1988), separated by layers of laminar limestone, dolomite, calcareous marl, or rarely gypsum. At some places stromatolites occur at the transition from the Tripoli Formation to the Calcare di Base (Oliveri et al., 2010 and ref. therein) or at the top of massive Calcare di Base limestone beds (Decima et al., 1988).

The total thickness of this unit is quite variable, ranging from 20 to 60 m. The Calcare di Base was classically interpreted as evaporitic limestone (Decima et al., 1988). According to this interpretation, diagenetic alteration resulted in pseudomorphs after gypsum and mouldic pores, that were primarily filled with halite crystals, while the peloidal microfabric has been linked to bacterial activity in evaporitic environment (Tamajo, 1961; Ogniben, 1963; Decima et al., 1988). Its bacterial-induced precipitation in a normal marine setting has finally been defined (Guido et al., 2007), but the nature of the brecciated fabric is still matter of controversy.

Two triggers for brecciation have been already invoked: a) in situ collapse brecciation produced by halite dissolution (autobreccia sensu Pedley & Grasso, 1993, and references therein); b) penecontemporanoeus dismantling of carbonates and evaporites previously deposited during the MSC, thus consistent with mass wasting processes (CdB of the Caltanissetta Basin, Roveri et al., 2008; Manzi et al., 2010). To date, the relationship between the upper Messinian breccias and fluid migration has only been speculated (Ryan, 2009).

2) The second type is the 'Calcare Solfifero' (sulphur-bearing limestone), representing a local subunit, which is intercalated in the upper part of the Calcare di Base or is found on top of it (Decima et al., 1988). Sometimes, the Calcare Solfifero is described as an independent unit resting on the Calcare di Base or directly on the diatomite unit, where the basal limestone is missing (Dessau et al., 1962).

The Calcare Solfifero is a diagenetic limestone. On the basis of very negative carbon isotope signatures in this unit, McKenzie et al. (1979–1980) and Bellanca et al. (1983, 1986) ascribed the precipitation of early diagenetic carbonate to the action of sulphate reducing bacteria.

According to many authors (McKenzie, 1985; Bellanca & Neri, 1986; Decima et al., 1988; Caruso et al., 1997; Bellanca et al., 2001; Rouchy & Caruso, 2006) both types of limestone, the Calcare di Base and the Calcare Solfifero, pass basinwards into the lower gypsum and salt units and are overlain by the upper gypsum units. This stratigraphic relationship, however, is still under discussion and, taking the view that the Calcare di Base is mostly a non in situ brecciated limestone, Roveri et al. (2008) argue that its base represents a regional-scale unconformity and that it does not mark the onset of the MSC; this stratigraphic interpretation is reported in the new consensus model (CIESM, 2008). Roveri et al. (2008) support Hilgen & Krijgsman (1999) in recognizing the dolostones above the Tripoli Formation as the only part of the Calcare di Base that is the lateral equivalent of the primary Lower Gypsum.

3 - METHODOLOGY

3.1 - Methodological approach

In order to refine the puzzling context of the Messinian brecciated limestones of the Mediterranean Sea in terms of stratigraphy and origin, sedimentological techniques (outcrop facies analysis, natural radioactive measurements, facies and fabric investigations; par. 3.3) have been integrated with compositional and geochemical techniques (XRD and EDS analyses, stable isotopes $\delta^{18}O$ and $\delta^{13}C$, organic geochemistry; par. 3.4).

The methodological approach of this thesis has been mainly focused on sedimentological and fabric observations carried out at different scales, supported by natural radioactivity and stable isotopes data. Fabric was therefore investigated from the outcrop- to the thin section-scale, using optical, electronic and cathodoluminescence microscope techniques.

The facies analysis was mainly focused on:

• the variation of the fabric with the scale,

• the framework of microfacies, peculiar carbonate fabric and phases characterization, with special emphasis placed on the identification of the primary vs. the post-depositional signals (breccias, concretions, cements).

• the type of brecciation.

The facies investigation represents therefore the core analysis: carried out in any study area (Fig. 3.1), it has been a guide for the sampling for geochemical purposes (see par. 3.4.2-3).

3.2 - Sampling

Detailed stratigraphic investigations were performed and contextual outcrop gamma ray profiles were acquired in correspondence to key sections.

Different sampling techniques (Flügel, 2004) have been chosen:

• <u>stratified sampling</u> has been performed where detailed stratigraphy was obtained, often accompanied by the acquisition of gamma-ray log profiles;

• <u>cluster sampling</u> has been the most used sampling method, since it is the most suitable for facies yielding high lateral variability like this one;

• <u>search sampling</u> (preferentially samples collected for their noticeable structures) and <u>pilot sampling</u>, aiming to a first overall picture of the studied section. These methods heve been mostly applied to minor study areas (Fig. 3.1), visited in order to gain a more exhaustive and wider spectrum of facies and give a regional relief to the approached problem.

Fig. 3.1 - Location of the main study areas in the context of the Mediterranean Basin

Maiella Mts

Maiella basin (Figs. 3.1, 3.2) yields an unequivocal MSC stratigraphy, so it has been considered the reference study area in this work. The initial results in this area were encouraging and revealed a noticeable facies inventory in the brecciated limestones unit. Since Maiella area soon showed interesting clues of an outstanding ancient oil field, 15 samples were chosen also for organic geochemistry analyses.

Calabrian Arc

The Calcare di Base unit crops out in the Rossano Basin and in the Crotone Basin, both located on the Ionian side of the Calabrian Arc (Figs. 3.1, 3.2). The two basins experienced a similar evolution in Messinian times. In the Rossano Basin two sections (CROP and CROP3) in the vicinity of Cropalati (CS), were studied and sampled in correspondence to the Calcare di Base (CdB) outcrops. A correlation between the two studied sections is not possible, due to the inhomogeneous distribution and degree of brecciation.

In the Verzino area (Crotone Basin) spot samples were collected with the aim of search/pilot studies, in order to compare them to the samples of Rossano.

Additionally, some outcrops were visited in the nearby of Briatico (VV, Cessaniti Basin, central Calabria; Figs. 3.1, 3.2) in order to observe the main mesoscopic fabrics in the CdB.

Sicily

In the Caltanissetta Basin in Sicily (Figs. 3.1, 3.2), two locations representative of the CdB and its sulphur bearing facies - Centuripe and Capodarso, respectively - were sampled for pilot studies and investigated with the main aim of tracing the occurrence of fluid migration markers and define the type of brecciation. They were eventually compared to the more deeply investigated analogous features in the Maiella and Rossano Basins.

Fig. 3.2 - Distribution of the Messinian deposits within the Apennine-Maghrebian foredeep and surrounding area (modified after Selli, 1973)

3.3 - Sedimentological techniques

3.3.1 - Outcrop facies distribution

Stratigraphic reconstructions were accompanied by lithofacies analyses in the field, mainly devoted to investigate the lateral variability of the geobodies.

In the NW-Maiella area particular attention was placed on the identification of paleo-fluid migration conduits (Fig. 4.1.3). The inventory of the lithofacies detected can be gathered to three main typologies: 1) carbonate breccias and authigenic concretions (brecciated massive limestones *strictu sensu*, BL); 2) patchy limestones embedded in the host sediment (PL); 3) fluidized sediments with minor carbonatic fraction (FS).

3.3.2 - Natural radioactivity (NRD) measurements

Natural radioactivity (NRD) is acquired in sedimentary environments to determine the shaliness, the clay content and the presence of organic matter in the rocks.

Along the sections where detailed stratigraphy was performed, the γ-ray values were measured every 20 cm with count times of 120 s. The NRD measurements were performed using an integral 2" 2" NaI (Tl) Gamma Scintillator equipped with a field spectrometer that qualitatively detects the contribution of each natural radioactive element (^{238}U, ^{232}Th and ^{40}K).

Field spectra were obtained, with a count time of 20 min, in correspondence to high or anomalous values of radioactivity. This field spectrometry technique has been efficiently compared to laboratory analyses performed by a HPGe γ - spectrometer, rendering the radioelements concentrations and more accurate radioactivity measurements (Sampalmieri, 2006; Sampalmieri et al., 2008).

NRD spectrometry is a paleoenvironmental tool used in the sedimentary successions to evaluate: 1) the amount of the detrital fraction; 2) the presence of authigenic ^{238}U, catalyzed in the sediments by organic matter; 3) the occurrence of volcaniclastic events. In general, the co-occurrence of the three main radioelements (^{40}K, ^{238}U and ^{232}Th) testifies a detritic origin of sediment, while a ^{238}U-dominant radioactivity is referable to an authigenic origin.

Natural radioactivity (NRD) characterization is particularly efficient to define the paleoenvironment in successions that are barren in biofacies. Laminated sediments devoid of benthic fauna are generally indicative of anaerobic/dysaerobic conditions: gamma-ray techniques furnish precious indirect proxies for characterization of suboxic/anoxic environments and for the detection of organic matter (authigenic uranium values and Th/U ratios).

Authigenic ^{238}U is catalyzed by organic matter in the sediment. Th/U ratio is a proxy for redox conditions in sedimentary environments (Jones and Manning, 1994; Wignall, 1994) and is also sensitive to the input of detrital grains. The ^{238}U content is primarily related to processes of organic matter enrichment (authigenic uranium, U_{aut}) and secondarily to the input of detrital grains (U_{det}). In contrast, ^{40}K and ^{232}Th are ascribed entirely to the clastic fraction. Th/U ratio provides a measure of the oxygen conditions in the depositional environment: Th/U<<1 indicates anoxic conditions; Th/U>>1 indicates oxic conditions; the ranges 1<Th/U>1 point to dysoxic conditions. Carbonate anions are powerful complexing agents for U (VI). The U_{aut} was calculated using the formula $U_{aut} = U_{tot}$) U_{det} (Wignall, 1994), where U_{det} is Th/3 because in the sedimentary rocks U_{det} is 1/3 of Th content.

These proxies have been used here to define the palaeoenvironment at the hypersaline/hyposaline transition of the MSC (Sampalmieri et al., 2010).

3.3.3 - Facies and fabric investigations

Observations and facies analysis have been carried out at first on the fresh cut of the hand samples, on thick sections and on polished thin sections, using optical devices.

Cathodololuminescence and electronic microscopes were used for the observation of selected samples, yielding some of the most representative microfacies.

Since the many scale invariant geological phenomena include fluid assisted brecciation and oil fields, scale invariant fabrics have been evaluated.

The observation of the fresh cut of the hand samples guided both the choice of the most interesting areas for thin sections and the identification of the most important microfacies, further separated, where necessary, for geochemical analyses.

Thin sections were observed under polarized and cross-polarized light microscopy for fabric and facies characterization, using a Stereoscopic microscope Zeiss 2000-C, with transmitted light stage and polarization, equipped with digital camera Nikon Coolpix 990.

Cathodoluminescence (CL) analyses were performed by a CITL 8200 MK3 equipped with a ZEISS "Amplival" Microscope (University of Postdam, Institut für Erd- und Umweltwissenschaften; GFZ, Deutsches GeoForschungs Zentrum, Potsdam). CL analyses provide: 1) exalted textural features, offering a contribute to the definition of the rheologic behaviour of seep limestones (hidden fabrics); 2) an insight in the stages of cementation and their relative timing (early-stage vs. late-stage phases). 53 sections were analyzed in CL view: 25 from the Maiella area, 20 from the Calabrian Arc and 8 from Sicily.

SEM-based analyses were performed using the device XL30 LaB6 Analytical Scanning Electron Microscope equipped with EDAX 134 eV for semi-quantitative microprobe analysis (Roma Tre University, LIME Laboratories). This kind of investigation was mainly devoted to the detection of microtextural patterns and to refine the microfacies. 26 samples/subsamples were analyzed in SEM view: a) 16 from the Maiella area: 12 from carbonates, 4 from the host sediment (microtubes; botryoidal coated grains; microfractured grains; scraped grains); b) 8 from the Calabrian Arc (6 from Rossano Basin, 2 from Crotone Basin); c) 2 from Sicily.

3.4 - Compositional and geochemical techniques

3.4.1 - Compositional analyses: XRD and EDS

Basic compositional characterization was obtained performing:

- petrographic observations (par. 3.3.3)
- mineralogical analyses on bulk samples were performed with a Scintag model X1 diffractometer, using the standard X-ray Diffraction (XRD) techniques (Giampaolo & Lo Mastro, 2000).
- Energy Dispersive X-ray microprobe (EDAX Inc., Mahway, NJ, USA)

The mineralogical and chemical results will be exposed within the facies analyses data (pars. 4.1.3, 4.2.3, 4.3.3).

3.4.2 - Stable isotopes analyses ($\delta^{18}O$ and $\delta^{13}C$)

Analyses of the C and O stable isotopes were performed on the major part of the collected samples.

Moreover, on the basis of the main results achieved through different scale facies analysis, microfacies were sub-sampled for $\delta^{13}C$ and $\delta^{18}O$ characterization. The subsamples were manually separated.

In the Maiella area 123 samples were collected for stable isotope analyses; 32 of them were subsampled (Appendix 3).

In Calabria 80 samples were collected from the CdB for isotopic studies; 8 of them were subsampled (Appendix 4).

In Sicily 72 samples from CdB Fm. were collected for isotopic studies, 19 of them were subsampled (Appendix 5).

The analytic procedure on the samples was performed at the research institute CNR-IGAG of Rome. Oxygen- and carbon-isotope data have been obtained from powder rock samples. Roasting of samples for 40 min at 430°C in high-vacuum glass tubes was followed by dissolution in 100% phosphoric acid at 25°C under high vacuum for about 12 h. The obtained CO_2 was cryogenically separated from other gases and measured with a Finnigan Delta S mass spectrometer. The isotopic results are expressed in δ‰ units and reported against the PDB-1 standard. The measure was then repeated a second time: the average values obtained from two measures are reported in the results tables (Appendices 2, 3, 4).

Basically, methane-C and altered water-O propagate through a series of equilibrium reactions and are incorporated into authigenic carbonate phases. Oxygen isotopes are exchanged between the dissolved inorganic carbon pool and water derived from hydrate dissociation, clay dehydration or seawater.

Methane-seep carbonates are typified by low $\delta^{13}C$ values, as they inherit the stable isotope signature from their carbon source (^{13}C-depleted methane); nonetheless, the $\delta^{13}C$ value of the methane source is usually significantly lower than $\delta^{13}C$ carbonate values, indicating additional carbon sources involved in carbonate formation (Peckmann & Thiel, 2004; Formolo et al., 2004). The interpretation is commonly further complicated by the complex framework of microfacies. The sub-sampling hence provides a less biased chemical and geochemical signal in seep-limestones. More sophisticated techniques of subsampling - such as microdrilling and micromilling - are nonetheless advised for future investigations to obtain a more accurate signal, as recently shown by Natalicchio (2010).

3.4.3 - Organic geochemistry

Organic geochemistry analyses on 15 selected samples from the Maiella area (Appendix 6) were performed at the ENI research laboratories in San Donato Milanese (MI, Italy).

Characterization of both rock (TOC and RE) and bitumen (GC-MS, carbon isotopes) was obtained with the standard techniques (Scotti et al., 1998 and ref. therein).

Rock characterization was articulated into two kind of analyses:

1) TOC (Total organic carbon, or "organic matter OM content"): performed on all samples, is given both by the kerogen fraction (in situ OM) and the bitumen fraction (migrated OM).

2) RE (Rock-Eval pyrolisis) or source rock evaluation: performed on un-washed and washed samples yielding a TOC>0.2%; it gives the quantity of "Organic" extractable vs. "Organic" unsoluble.

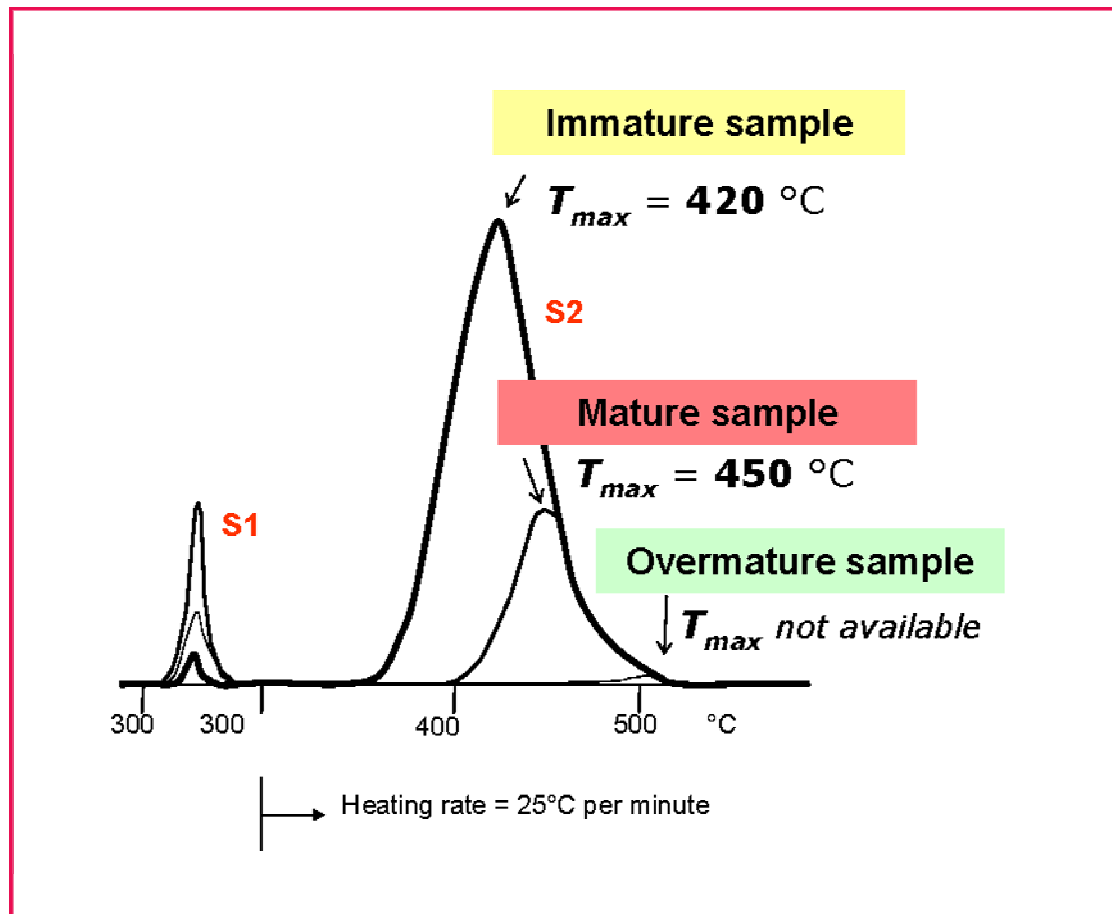Fig. 3.3 - T_{max} from Rock-Eval pyrolysis and relative maturity of the samples (after Scotti et al., 1998)

The parameters obtained from this analysis (Appendix 5) are:

*   **S1**: indicates the free hydrocarbons, i.e. the hydrocarbons generated but not yet expelled from the rock sample.

*   **S2**: the residual petroleum potential, representing the generation of hydrocarbons not yet produced in a natural way.

- **T_{max}**: the temperature at which the maximum of residual petroleum potential - after kerogen pyrolysis occurs (peak of S2). It must not be confused with the maximum temperature (very lower) reached by samples during their burial history. T_{max} increases as a function of the temperature of the sample and therefore is commonly used to define its degree of maturity (overmature-mature-immature; Fig. 3.3)

- **HI**: a kerogen quality parameter (for immature samples); the higher is HI, the more is the quantity of oil that can be generated compared to gas.

The source rock (<u>bitumen</u>) characterization is defined through oil-source correlation, obtained by 1) detailed molecular analyses (GC-MS, gas chromatography-mass spectrometry: biomarker analysis) and 2) isotopic characterization ($\delta^{13}C$ of bitumen, extracted by means of an organic solvent). Bitumen characterization was performed on the samples yielding high HI values.

Biomarkers analyses supply information on the source rock in terms of: lithology, depositional environment, rock maturity, age.

4 - RESULTS

4.1 - The Brecciated Limestones of the Maiella Mountains

4.1.1 - Geological setting and the Messinian record in the area

The Maiella Mountain represents the outermost and youngest portion of the outcropping central Apennine chain (Fig. 4.1.1; Bigi et al., 1989; Patacca et al., 1992; Cipollari et al., 1995). Maiella Mountain is a thrust-related, asymmetric, roughly NS oriented box-shaped anticline, with a steep E-dipping forelimb and an arc-shaped trend with eastward convexity (Scisciani et al., 2000).

Maiella represents the culmination of an antiformal stack, composed by two major units (Mt. Maiella on top and Casoli on bottom), which overrides the Adriatic foreland in the subsurface. This system of imbricates is in turn overthrust by the Mt. Morrone unit to the west, and by the Molise and Sicilide allochton to the east (Vezzani & Ghisetti, 1998).

During the Messinian stage, Maiella basin was part of the unflexured Adriatic foreland domain of the Apennine orogenic system. Westward of the present Maiella Mts a W-dipping ramp (Queglia-Morrone-Alfedena) characterized the connection between the Apennine foredeep basin (Marsica–Laga Mts basin), to the west, and the Adriatic foreland domain, to the east (Maiella Mts). The Maiella area was affected by the Apennine orogeny only starting from the Early Pliocene (Cipollari et al., 1995). To SE of the Maiella area, the Molise allochthonous Unit, consisting of upper Oligocene-upper Miocene basinal deposits, was affected by northward orogenic transport during late Messinian-early Pliocene times (Fig. 4.1.1). The pre-orogenic sequence within the moderately WSW-dipping backlimb is truncated by the Caramanico Fault Auctt., a steeply N-S oriented west-dipping normal fault (Scisciani et al. 2000, and ref. therein).

Two main sedimentary domains developed in Mesozoic times: an inner platform - platform margin-slope to basin system affected the Southern sector, while transitional to open marine Upper Trias-Cretaceous deposition took place in the Northern sector (Eberli et al., 1993; Lampert et al., 1997). With the prograding phase of the carbonate system recorded by the Orfento Fm Auctt., the platform margin ceased to be active and, from late Cretaceous times a carbonate ramp system was established. The carbonate

Fig. 4.1.1 - Location of the study area

ramps were first distal and tropical (Santo Spirito Fm Auctt.; Upper Cretaceous-Middle Miocene) and then shallow and temperate (Bolognano Fm Auctt.; Middle-Late Miocene). This latest carbonate ramp is articulated in four members: 1) Briozoi Limestones mb.; 2) Orbulina Marls mb.; 3) Lithotamnium Limestones mb.; 4) G. Multiloba Marls mb, recorded only at places. The topmost member of the Bolognano Fm is thus generally constituted by Lithotamnium Limestones, commonly affected by tar impregnations in their discontinuities and primary porosity (Marchegiani et al., 2006; Agosta et al., 2009; 2010).

The following deposits, related to the Messinian Salinity Crisis, conformably rest above the Bolognano Fm (see next subparagraph). Finally, during the late Pliocene-early Pleistocene, a new sedimentary cycle was deposited with marked angular unconformity all along the Adriatic border of the Apennine chain. This sequence starts with basal deltaic conglomerates (Turrivalignani Fm), is transitional upwards to marine clays (Mutignano Fm) and is finally closed by regressive sands and conglomerates (Ghisetti & Vezzani, 2002).

<u>The record of the Messinian Salinity Crisis in the Maiella area</u>

The record of the Messinian salinity crisis in the Maiella area is known from well data and outcropping record both in the NW and SE Maiella areas (Di Napoli, 1964; Crescenti et al., 1969; Crescenti et al., 1975; Patacca et al. , 1992).

The upper Messinian deposits connected to the major phases of the Messinian Salinity Crisis widely crop out in the northwestern Maiella sector (Fig. 4.1.1), where the MSC has been recorded in a marginal and shallow basin. The onset of the crisis is exposed in some sections in the Valle dell'Orte (Fig. 4.1.3; Madonna della Croce, Madonna del Monte sections) where, according to the previous literature (Di Napoli, 1964), dolomitic oolitic mudstones resting atop Lithotamnium Limestones, pass upward to vacuolar gyspiferous limestones or directly to gypsum. The gypsum unit is referable to the Lower Evaporites (or Primary Lower Gypsum, PLG), passing up-section, above a spectacular erosional surface (the Messinian erosional surface, MES) to barren shales and brecciated and concretioned carbonates (early post-evaporitic deposits; Colle di Votta section, Sampalmieri et al., 2008).

Above a younger erosional surface (MES 2), marls and clays with Parathetyan ostracofauna (late post-evaporitic deposits) testify in the Maiella area the occurrence of the well-known oligohaline Lago-Mare event (Cipollari et al., 1999; Gliozzi et al., 2002; Crescenti et al., 2002; Cosentino et al., 2005), correlatable to the Loxocorniculina djaffarovi zone (Carbonnel, 1978).

In the south-eastern Maiella area the exposed MSC succession is mostly represented by the post-evaporitic phase, yielding both resedimented evaporites and Lago-Mare deposits (Taranta Peligna and Fonte dei Pulcini sections; Catenacci, 1974 and Cipollari et al., 2003 and references therein).

Lago-Mare deposits predate the early Pliocene flooding of the Mediterranean area, responsible for the deposition of bathyal clays (Cigno Clays Auctt., NW Maiella; Taranta Peligna clays Auctt., SE Maiella). The Mio-Pliocene boundary in the Maiella area is approximated by a neritic conglomerate (San Valentino Conglomerate Auctt.), which rests in angular unconformity on the eroded terms of the upper Messinian succession (Cipollari et al., 2003; Centamore & Nisio, 2003).

<u>Previous studies of the brecciated limestones in the area</u>

The previous works offer an unclear idea concerning the stratigraphic position of the Brecciated Limestones (Bcl). The following two interpretations have been proposed:

1) Bcl, yielding evaporitic intertidal facies (Centamore & Nisio, 2003), lay at the base of the gypsum succession (Crescenti et al., 2002; Centamore & Nisio, 2003; Apat, 2005) or substitute primary gypsum in the more elevated areas.;

2) According to the former official Italian geological mapping (Catenacci, 1974), Bcl occur indifferently at the base, laterally or atop the gypsum deposits. Notwithstanding, the author doesn't suggest the occurrence of an erosional surface at the base of the unit. He describes the Bcl as massive limestones, distinguishing them in two units, according to their co-occurrence, or not, with the upper Messinian clays.

Though their facies variations have never been deeply investigated, on the basis of their similarities to the Calcare di Base Fm Auctt (CdB), the Bcl have been traditionally considered evaporitic/sulphur-bearing limestones, possibly even karstified (Centamore & Nisio, 2003; APAT, 2005). A hypothesis relating these carbonates to fluid-induced processes astonishingly dates back to 1901: "*Io ritengo che il fatto sia dovuto (se mi si permette le frase) ad un fenomeno carsico a rovescio. Ossia non determinato da erosioni di acque agenti dall'esterno all'interno, sebbene di acque mineralizzate provenienti dal basso. […] E che durante il Miocene superiore si sprigionassero, in queste località sorgenti mineralizzate, ce lo testimonia anche la presenza della celestina, la cui quantità è tale da farmi ritenere che un giacimento così importante ed anche così localizzato, non possa avere che un'origine crenogenica.*" (Giattini, 1901).

4.1.2 - *Field data: stratigraphy, NRD signal and main lithofacies*

In the NW Maiella area (PE, Abruzzi Region), the MSC stratigraphy has been successfully reconstructed through a continuous composite log (Fig. 4.1.2) obtained from the detailed stratigraphic study of three quarries located in the Trovigliano-Colle di Votta area (Fig. 4.1.3). This composite section (Fig. 4.1.4) clearly shows that the Brecciated Limestones unit (Bcl) in the Maiella area rests above the Messinian erosional unconformity cutting the Primary Lower Gypsum (PLG).
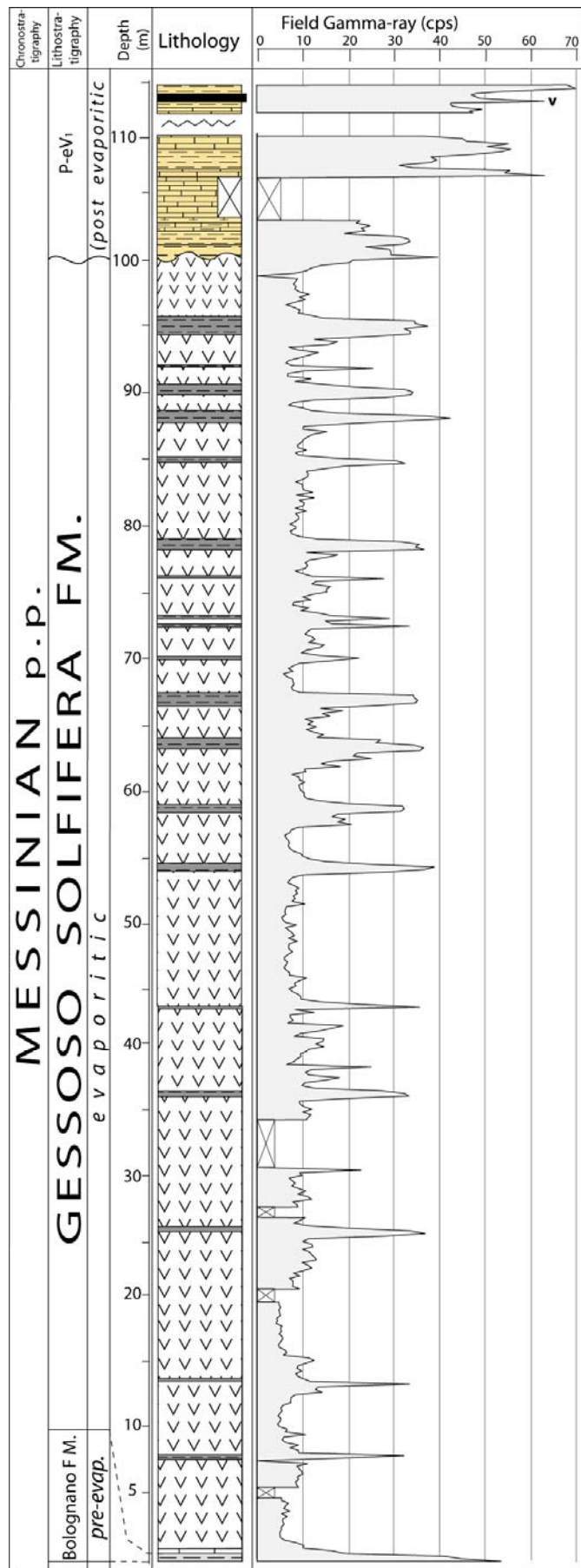
Fig. 4.1.2 - Lithologic and gamma-ray composite log profile of the Trovigliano-Colle di Votta section

Once clarified the stratigraphic relationships, detailed facies analysis and sampling were performed in the northern sector of the NW Maiella Mts (Fig. 4.1.3). This work revealed that in

the study area the MES is an articulated surface and cuts the succession at different stratigraphic levels of the PLG and of the Bolognano Fm (Figs. 4.1.4, 4.1.6, 4.1.15, 4.1.23).

Within the Bcl three main lithofacies have been enucleated, on the basis of the outcrop-scale fabric (Fig. 4.1.5):

1) Lithofacies **a** - Brecciated Limestones (BL): Massive cemented limestones, yielding tar and microtar (Fig. 4.1.5.a).

2) Lithofacies **b** - Patchy Limestones (PL): patchy concretions and breccias (guest carbonates) within a marly-pelitic succession (host sediment) (Fig. 4.1.5.b).

3) Lithofacies **c** - Fluidized Sediments (FS): fluidized dark brown pelites with minor carbonate concretions and botryoidal aragonite (Fig. 4.1.5.c).

In the following subparagraphs, Trovigliano-Colle di Votta composite section and Decontra section (Fig. 4.1.3), where detailed stratigraphy was reconstructed, will be described. The three main lithofacies will be eventually threaten .

<u>Colle di Votta-Trovigliano composite section</u>

The Trovigliano-Colle di Votta section is a reference composite section for the MSC stratigraphy of the NW-Maiella area and in general of the Adriatic foreland (Sampalmieri et al., 2010): the field gamma-ray profile acquired along this section has been successfully compared with the gamma-ray log of the wells drilled at the Adriatic side of the central Apennines (S-Eastern of the Maiella Mts) for hydrocarbon exploration (Sampalmieri et al., 2009).

The Trovigliano-Colle di Votta section (Fig. 4.1.2) exhibits the Messinian record from the pre-evaporitic phase to the early post-evaporitic phase. In detail, the Messinian interval of the Maiella succession is characterized by:

1) <u>pre-evaporitic</u> deposits (Fig. 4.1.2): marine bluish clays with echinoderms, fish remains and oligotypic benthic foraminifers (*Elphidium* spp., *Lagena* spp., *Bolivina* spp., *Planulina* spp., *Bulimina* gr.; Smedile & Faranda, pers. comm.) passing upward to dolomicritic muds (Di Napoli, 1964) and nodular limestones with ostracods (*Aurila* sp.). Shallow-water (40-50 m depth) suboxic conditions characterized the pre-crisis environment in the Maiella Basin, as evidenced by both the biofacies association (Di Napoli, 194; Smedile & Faranda, pers. comm.) and the gamma-ray signal (Sampalmieri et al., 2008).

2) Atop, a fenestral laminated stromatolitic limestone marks the <u>onset of the crisis</u>.

3) The <u>Primary Lower Gypsum</u> unit (PLG, evaporitic deposits) conformably rests above the pre-evaporitic succession. The PLG is about 100 m-thick and is arranged in 19 precessional-forced sapropel/gypsum cycles (Fig. 4.1.2). The sapropel layers yield rare otoliths and fish teeth. The gypsum facies associations can be grouped as follows: a) selenite and banded selenite, in the a lower portion (cycles I-V); b) *branching-selenites* and associated gypsum laminites, in the middle-upper portion (cycles VI-XIII); c) primary selenites accompanied by gypsarenite, graded gypsum laminites and scattered reworked selenites, in the uppermost portion (XIII-XIX cycles). In the Trovigliano area the PLG is cut by fluid flow mesostructures (FS, see next suparagraphs; Fig. 4.1.5.c). Microbial limestones characterize the carbonate fraction of the lower and middle portions. Evaporitic sediments pass, through the MES (Figs. 4.1.6, 4.1.7), to post-evaporitic deposits.

4) <u>early post-evaporitic</u> deposits (p-ev1; stages 2.1 and lower 2.2 sensu CIESM, 2008), characterized by brown laminated barren silty shales sediments and brecciated limestones and concretions. The detection of the regional-scale volcaniclastic event (see Ch. 2.2.1) undoubtedly constraints this portion to this Messinian phase (Sampalmieri et al., 2010).

5) Finally, the <u>late post-evaporitic</u> deposits (p-ev2, upper stage 2.2 sensu CIESM 2008), consisting of marls with Parathetyan ostracofauna predating the early Pliocene flooding, crop out in the
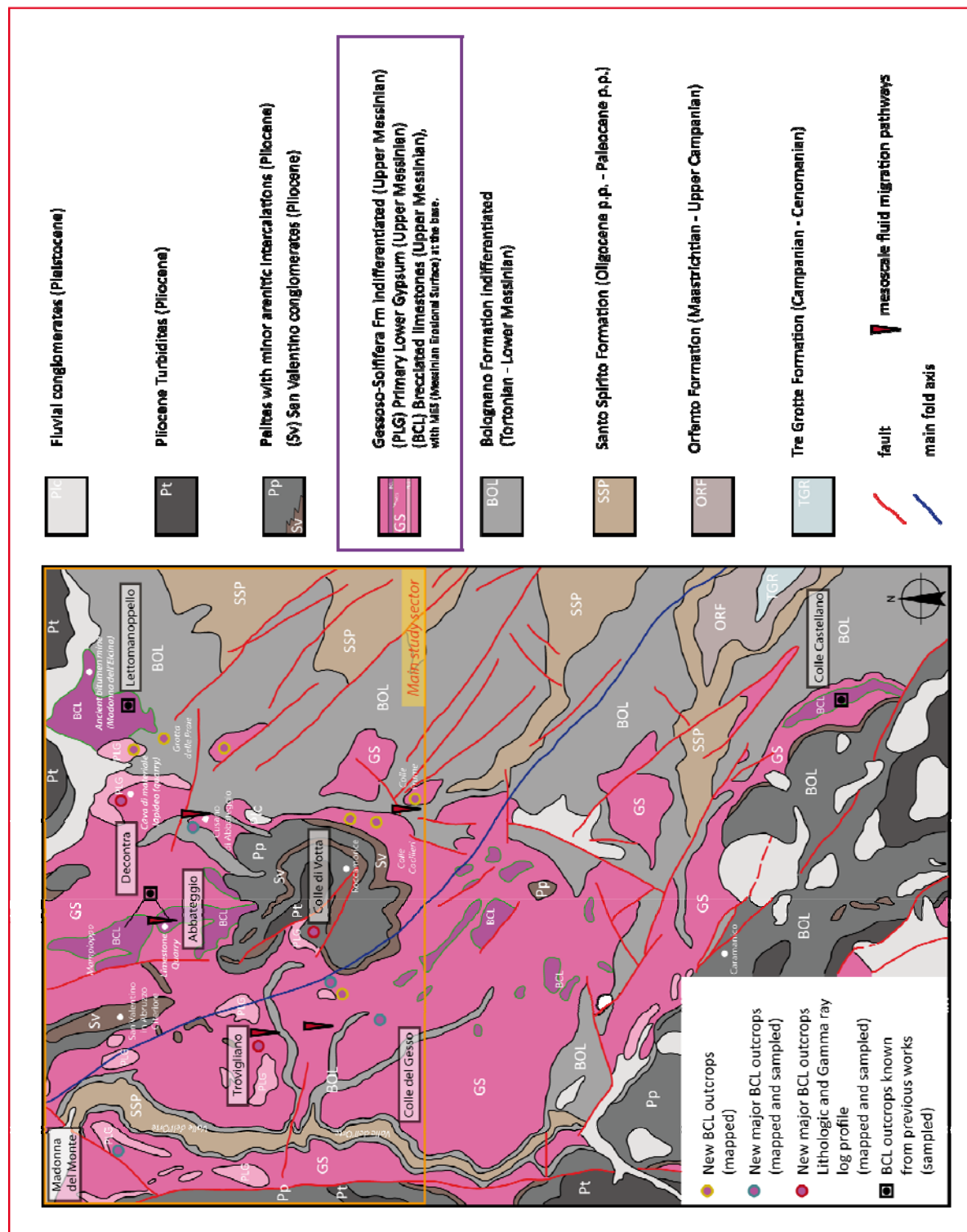
Fig. 4.1.3 - Simplified geological map of the nortwestern Maiella area (modified after Vezzani & Ghisetti, 1998; scale: 1:100,000)

nearby of San Valentino (Patacca et al., 1992; Cipollari et a. 1999). This represents the only subunit not directly cropping out in the Trovigliano-Colle di Votta composite section.

The 25-m-thick p-ev1 succession (Fig. 4.1.7) from the Colle di Votta quarry consists of barren shales, siltstones and marls (*host sediment*), enclosing patches of yellow-brownish brecciated and concretionary limestones (Fig. 4.1.5.b) or alternated to more cemented vuggy brecciated limestones (*guest carbonates*). The limestone beds are typically discontinuous and pinching out. They are thus ascribed to the PL lithofacies, representing the best example of exposed PL all over the study area.

The topmost part of the section (Fig. 4.1.8), is defined by an alternation of laminated and bioturbated marls (Fig. 4.1.7, samples CV 1 - CV 12), yielding plant remains and rare ostracods of Parathetyan affinity (Grossi, pers. comm.). This portion contains the volcaniclastic horizon, representing the regional marker for the early post-evaporitic phase.

The gamma-ray log of the evaporitic phase exhibits the typical cyclic profile perfectly resembling the alternation of primary gypsum beds and sapropelitic layers (Fig. 4.1.2). The NRD is characterized by low emission from the evaporitic beds, whereas the sapropel-NRD is dominated by ^{40}K and ^{238}U (Sampalmieri et al., 2008). Strong differences between the evaporitic and the post-evaporitic deposits were detected, both in terms of NRD intensity and gamma-ray profile. An abrupt shift in the NRD background value (from 10 Cps to 20-30 Cps) and an increase in the peak values co-occur above the Messinian unconformity (Fig. 4.1.2). In the p-ev portion high values of radioactivity have been recorded both in carbonates (20–63 Cps) and in terrigenous sediments (21–70 Cps). yet, field NRD spectrometry (Fig. 4.1.9) unravelled different patterns of radioelements contributions: the carbonate facies radioactivity is ^{238}U-dominated (up to 5.49 ppm, see Appendix 2); conversely, the γ-signal of the terrigenous deposits comes from all the three radioelements ^{40}K, ^{232}Th and ^{238}U. (Appendix 1).

See appendix 3 for a description of the samples/subsamples, named under the abbreviations RM, RM1, CV.

Decontra section

At a gypsum quarry in the vicinity of the village of Decontra (Cava di Materiale Lapideo; Fig. 4.1.3), the lower and middle portions of the PLG crop out and are truncated on top by the MES. The lithologic gamma-ray log profile (Fig. 4.1.10) has been focused on the topmost part of the section. It is typified by a mostly terrigenous succession, representing the post-evaporitic phase resting above the erosional surface. At this site the post-evaporitic record can be splitted in the following intervals (Fig. 4.1.10):
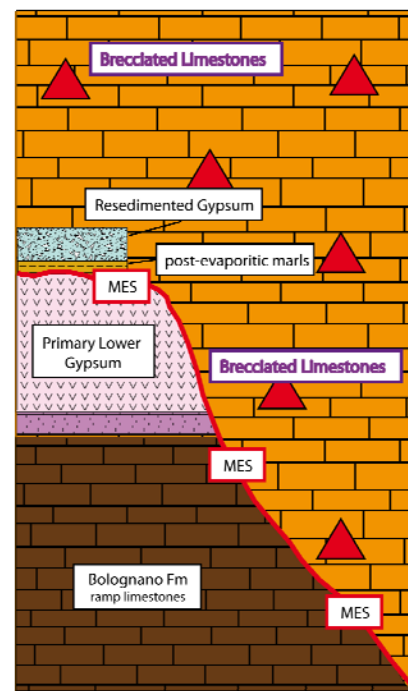

Fig. 4.1.4 - Exemplified stratigraphy of the brecciated limestones in the NW Maiella area

- 38 -

1) 0-9 m: a barren laminated marly-pelitic succession, containing gypsarenitic horizons. It must be stressed out that resedimented evaporites in the north-western Maiella area have never been mentioned before, though they widely crop out in the south-eastern Maiella flank (Cosentino et al., 2005);

2) tenth meter: a one meter thick fluidized portion (FS) interrupts the continuity of the well stratified gypsum-terrigenous succession, the carbonatic fraction is negligible to completely absent;

3) 10-17 m: a marly-pelitic succession, devoid of gypsum intervals and showing mostly homogeneous textures. On the basis of preliminary micropaleontological analyses, this portion yields ostracods and small lamellibranches of Parathetyan affinity (Grossi & Gliozzi, pers. comm.), thus suggesting the up-section transition from the early to the late post-evaporitic phase, separated by the occurrence of a second regional erosional surface (MES2); this hypothesis needs nonetheless further analyses to be confirmed.

The gamma ray signal shows values broadly comprised in the range 25-45 Cps, with a decrease in the late post-evaporitic succession (20-30 Cps) and negative spikes (lower values) in correspondence to the gypsarenite layers of the basal portion. If compared to the one of Colle di Votta section, the p-ev total NRD at Decontra section is much lower. Remarkably, the strongest difference in terms of p-ev1 lithofacies between the two sections, lays in the presence of carbonatic facies at Colle di Votta section and their absence at Decontra section.
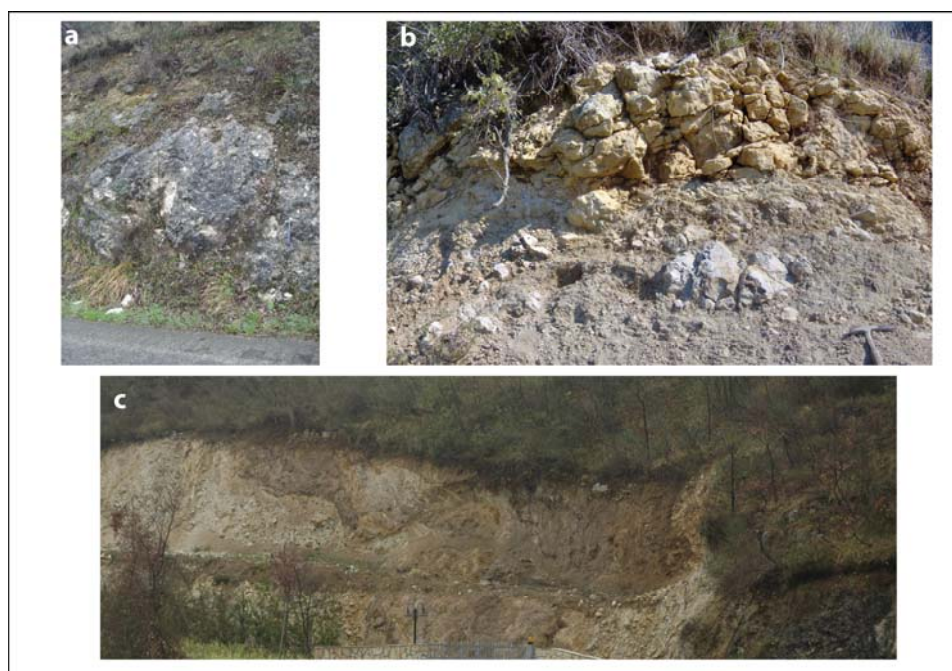

Fig. 4.1.5 - Main lithofacies of the brecciated limestones unit: a - massive brecciated limestones strictu sensu (BL); b - patchy limestones (PL); c - fluidized sediments (FS)
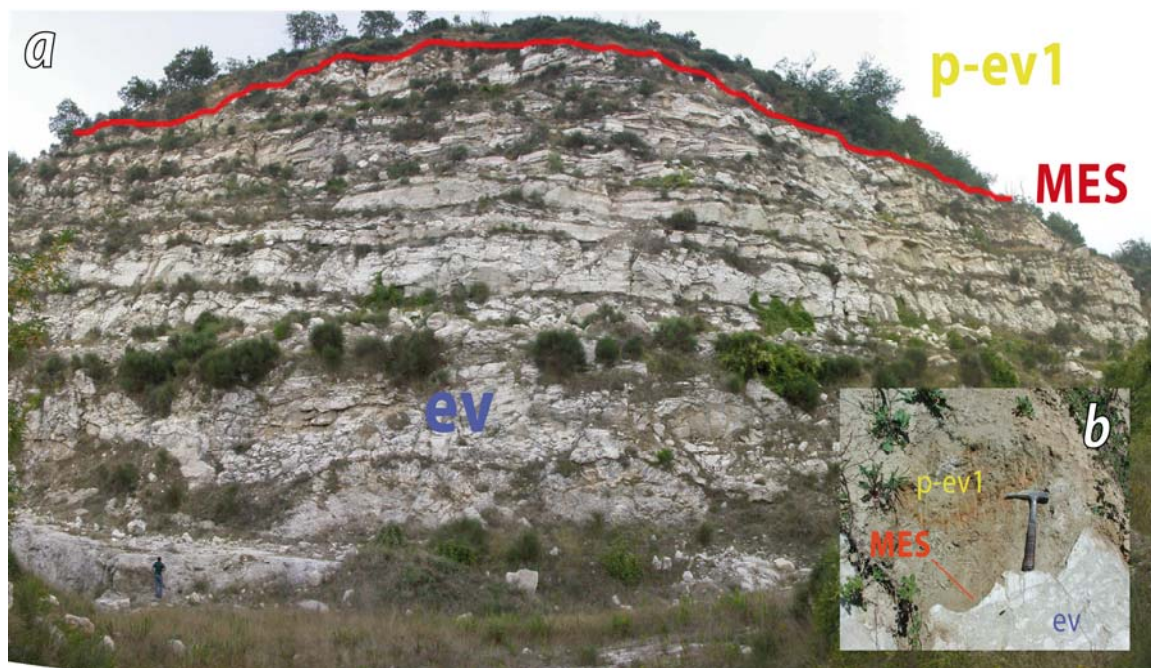
Fig. 4.1.6 - The Messinian Erosional Surface (MES at Colle di Votta section (a, closer view in b), separating the Primary Lower Gypsum (ev) from the brecciated limestones unit (p-ev1).

This stresses even more the contribution of the authigenic uranium contained in the carbonate facies of the Bcl, to the total NRD signal.

Lithofacies **a** (BL) - Brecciated limestones

The brecciated limestone lithofacies (BL) represents the typical aspect of the studied unit (Fig. 4.1.11) and is by far the most diffused type: indeed, it was the only recognized lithofacies in previous works and maps in the area (Fig. 4.1.3).

The BL are typified by massive highly cemented bodies, brecciated to different degrees and represented by vuggy limestones associated to minor pelites, trapped in at locations (Figs. 4.1.12 d, 4.1.14 c). In some cases they crop out as scattered boulder-like bodies, witnesses of former huger structures.

Breccias are clast-supported, with mostly subangular and minor subrounded clasts exhibiting a random distribution, devoid of gravity segregation (Figs. 4.1.11-12). Though brecciation is mostly pervasive, the primary stratification is generally easily recognizable (Figs. 4.1.11; 4.1.14.d).

At places the brecciated limestones show a higher fragmentation accompanied by: higher matrix content, chaoticized pelites and fluidification structures (Fig. 4.1.13). Though mesoscale fluidification features are generally less evident in this lithofacies if compared to the FS lithofacies, a relevant exception is represented by the Limestone Quarry in Abbateggio (Fig. 4.1.3), where dark-brown coloured impregnation fronts trace flow trajectories in outcrop (Fig. 4.1.14). Tar-bearing facies are common at Madonna del Monte, Grotta delle Praie and Lettomanoppello (Fig. 4.1.3).
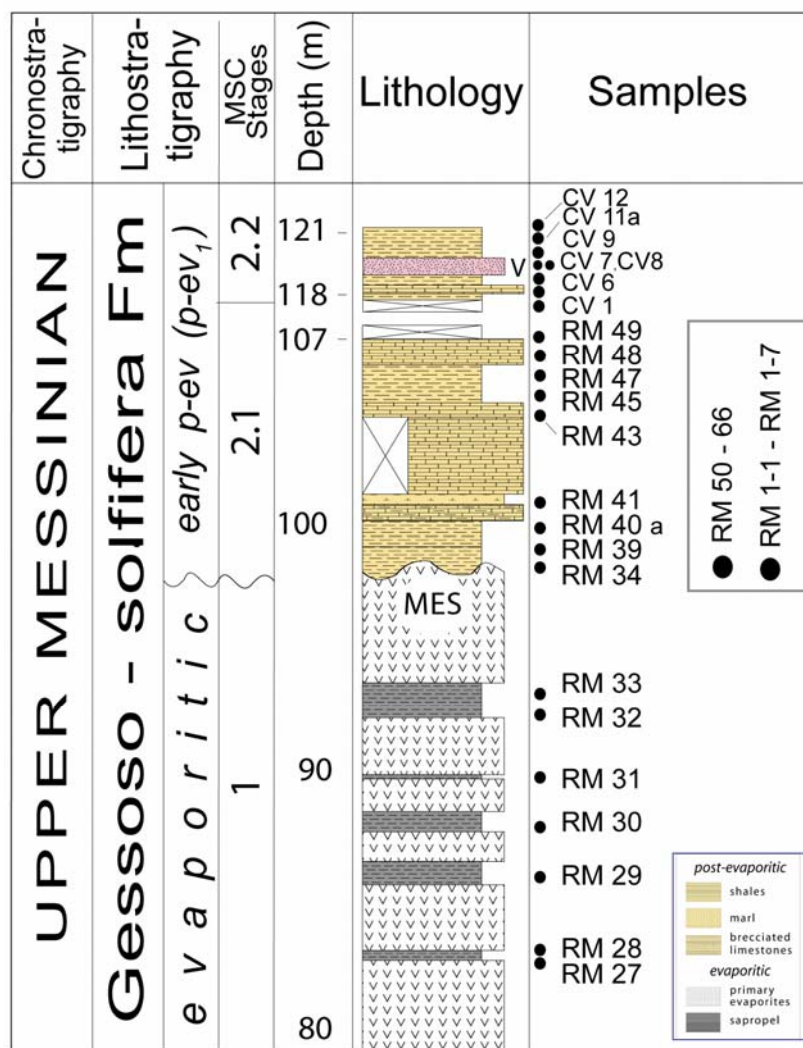
Fig. 4.1.7 - Trovigliano-Colle di Votta composite section: detail of the transition between the evaporitic and the early post-evaporitic phase (cf. p-ev1 portion in Fig. 4.1.2). The lithofacies PL defines the p-ev1 portion (samples RM 34-66; CV 1-12).

The most spectacular expression of this sublithofacies crops out at the ancient bitumen mine of Lettomanoppello, where tar plugs and patches represent relics of asphalt volcanism phenomena (Figs. 4.1.11 b, 4.1.12 e).

At Colle Castellano area (Figs. 4.1.3; 4.1.15), a great extent of massive brecciated limestones gives rise to a mound-like geometry of the geobodies. Here the Bcl - at least 30 m thick - directly lie above the topmost member of the Bolognano Fm through the MES, and are in turn topped by the late post-evaporitic deposits through the younger major Messinian unconformity (MES2, Cosentino et al., 2010).

The sampled areas where this lithofacies crops out are: Abbateggio (ABB), Mampioppo (MP), Madonna del Monte (MM), Lettomanoppello (LET) and Colle Castellano (CC) (abbreviations of the samples in brackets; see Fig. 4.1.3 to locate the cited sites; see Appendix 3 for a description of the samples/subsamples).

Lithofacies **b** (PL) - Patchy limestone: concretions and breccias within a marly-pelitic dominated succession

The patchy limestones (PL) constitute a less diffused lithofacies. On rock slabs, PL samples show facies comparable to the BL ones, but the outcrop-scale fabric is pretty different. They never constitute massive bodies, but rather lenses or cemented horizons (guest carbonates) embedded within the host sediment, representing the primary laminated marly-pelitic early post-evaporitic succession (Figs. 4.1.16 a, 4.1.17 a).

The host sediment, at locations affected by fluidification features (Fig. 4.1.16 d-e), contains peculiar carbonate grain types: microbrecciated, microtubular and botryoidal (Fig. 4.1.17 c).

The concretions are made up by centimetric to submetric isolated bodies, laterally passing into cemented laminites (Figs. 4.1.17 a, 4.1.18 e).On rock slabs they show weakly to highly cemented dark brown textures (Figs. 4.1.17 b and 4.1.17 f, respectively).

At the outcrop scale breccias constitute buildups or discontinuous strata typified by subangular centimetric-subcentimetric clasts showing no preferential orientation. They exhibit both cemented clast-supported fabrics (Figs. 4.1.16 b; 4.1.18 a) and matrix-supported fabrics (Fig. 4.1.16 c). In the latter case the higher matrix/clasts ratio is accompanied by the presence of subrounded clasts associated with the subangular ones, generally more diffused in the guest brecciated carbonates. On rock slabs they unravel a dark brown texture, cemented and brecciated to different extents (Fig. 4.1.18 a-d) or, even more commonly, extremely chaoticized facies, likely accounting for fluidification processes (Fig. 4.1.19)

Colle di Votta section (Fig. 4.1.3) is the most representative site of the PL lithofacies. A more specific case is by contrast represented by Colle del Gesso area (Fig. 4.1.3), where only few patches

Fig. 4.1.8 - Topmost part of the Colle di Votta composite section (a): this portion yields rare ostracods of Parathetyan affinity and the volcaniclastic layer that constraints this part of the succession to the early post-evaporitic phase. Brecciated limestones occur in this portion only to a lesser extent, the dominating facies is characterized by alternating laminated (b) and homogeneous (bioturbated) marls and pelites.
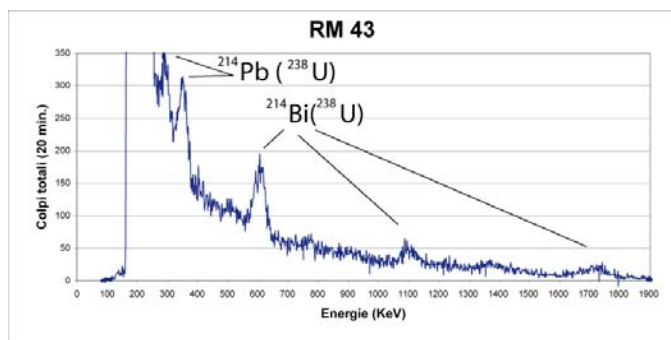
Fig. 4.1.9 - Example of a field spectrum obtained in the brecciated limestones: the natural radioactivity is mostly related to authigenic uranium, since the detrital fraction (represented by K and Th) is negligible.

of concretioned limestones are associated to the basal portion of the PLG: their highly recrystallized texture doesn't allow to ascribe them to the Bcl unit in a definitive way.

Lithofacies **c** (FS) - Fluidized sediment

This lithofacies represents the most localized expression in the field of the Brecciated Limestone unit (Bcl) and definitely contains only a subordinate carbonatic fraction. Notwithstanding, it constitutes a key lithofacies to understanding the trigger of brecciation in the studied unit: it yields the most spectacular mesoscale fluid migration pathways, cutting the PLG throughout (Fig. 4.1.20). The main lithology is made up by dark brown to black folded and wispy-microfolded pelites (Figs. 4.1.20 c-d, 4.1.21), associated to whitish and ocraceous flames resulting in a general chaotic texture. The peculiar carbonatic facies association that typifies the channels contemplates: centimetric homogeneous calcitic nodules (Figs. 4.1.20 b; 4.1.22 a, e); fibrous aragonitic botryoids (Fig. 4.1.22 c-d); vuggy limestones (Fig. 4.1.22 b), at places showing scoria-like textures; minor carbonatic pale blue micronodules.

The sampled areas where this lithofacies crops out are: Trovigliano (BUN, CBU 3), Cusano di Abbateggio (CT) and Decontra (DEC) (abbreviations of the samples in brackets; see Fig. 4.1.3 to locate the cited sites; see Appendix 3 for a description of the samples/subsamples).

The lithofacies distribution

The distribution of the Messinian brecciated limestones, and of their single lithofacies as well, doesn't appear to be relatable to the principal tectonic elements: this is consistent with the fact that the main compressive phase affecting the area is referable to the early Pliocene (Cipollari et al., 1995). Beside that, the area is interested only by minor deformations, mostly related to the development of the main fold and to the following extensional phase, the latter being expressed by normal faults generally WSW dipping, with a broad NW-SE trend.

The BL is the most diffused lithofacies and yields mesoscale tar injections at the Lettomanoppello former mine and at Madonna del Monte (Fig. 4.1.3). The PL distribution is subordinated. The flow trajectories in the field can be mostly observed associated to FS lithofacies (Trovigliano; Colle Frume and Cusano di Abbateggio areas; Fig. 4.1.3), where they cut the PLG or the ramp carbonates of the Bolognano Fm. An exception is represented by Abbateggio Limestone Quarry (Fig. 4.1.3),

where an impregnation front affecting the BL and traceable in outcrop, draws the fluid flow trajectories (Fig. 4.1.14).
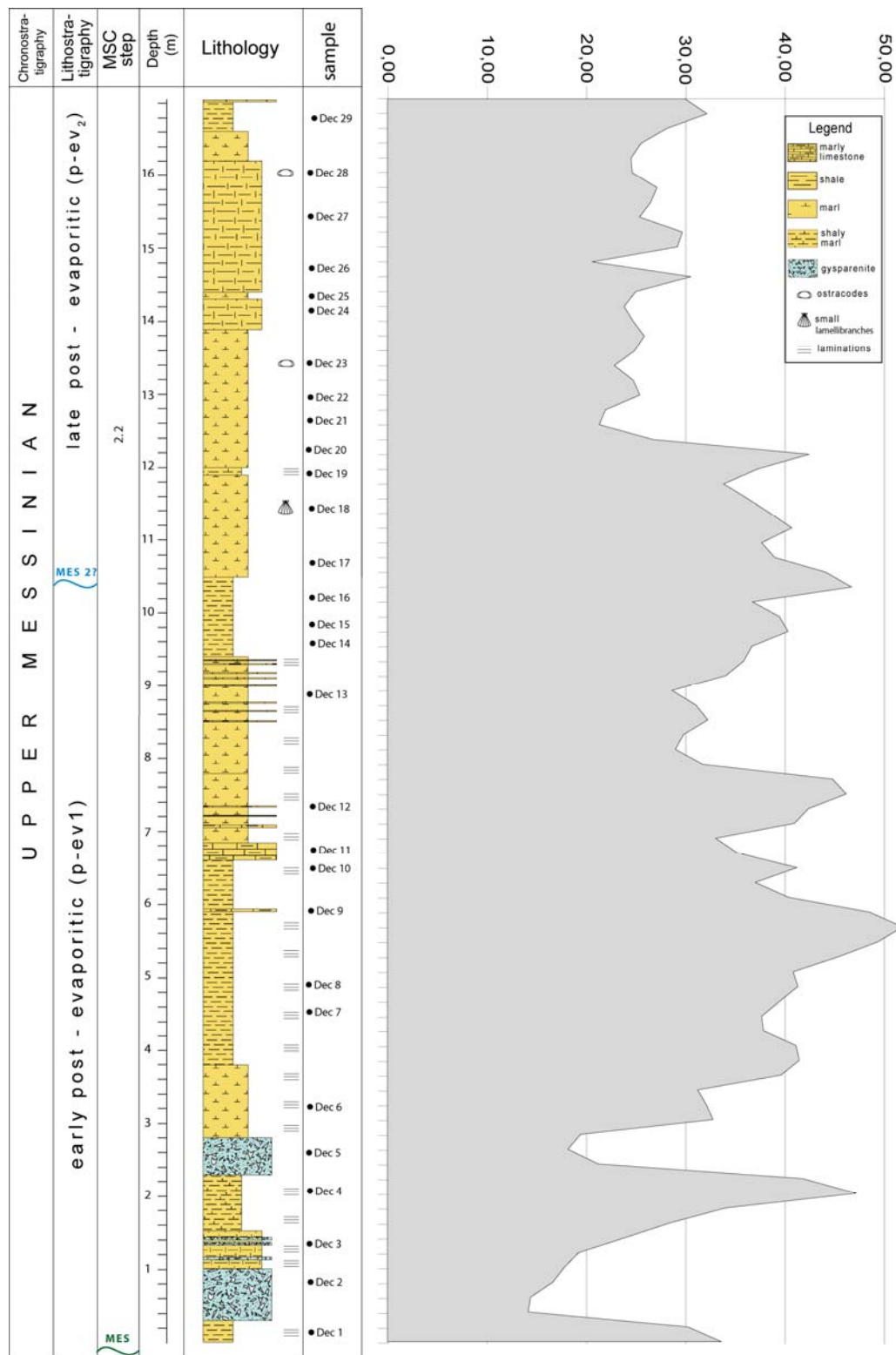

Fig. 4.1.10 - Decontra section: lithologic and gamma-ray log profile of the post-evaporitic portion of the Gypsum Quarry, in the vicinity of the village of Decontra.

Fig. 4.1.11 - BL lithofacies, mesoscopic view. They are massive, brecciated to different degrees, but fabric retentive (bed planes in dashed lines): moderately brecciated (**a**, **c**), more intensively (**b**) up to highly brecciated (**d**). Notice the presence of exposed tar (**b**) in the Lettomanoppello area.

The Messinian Erosional Surface is irregular and extremely articulated, cutting the older deposits at different stratigraphic levels (Fig. 4.1.4):

- The upper portion of the PLG (e.g. Colle di Votta section, gypsum quarry; Fig. 4.1.6)
- The middle portion of the PLG (e.g. Decontra section, gypsum quarry)
- The lower portion of the PLG (e.g.: Madonna del Monte, Fig. 4.1.23 c; Colle del Gesso)
- The ramp carbonates of the Bolognano Formation (e.g.: Abbateggio area, Fig. 4.1.23 a; Lettomanoppello mine, Fig. 4.1.23 b; Colle Castellano, Fig. 4.1.15)

The high articulation of the surface is particularly evident in the surroundings of Colle di Votta and at Madonna del Monte (Fig. 4.1.3), where it cuts the 5th-6th cycles of the PLG down to the Bolognano Fm, within a few hundreds meters radius.

The MES is responsible for the relative scarce preservation of the PLG in the area: they crop out only in correspondence to some small hills and generally yield an incomplete record, except for the Trovigliano-Colle di Votta composite section, where 19 gypsum-sapropel cycles are preserved (Fig. 4.1.2). In addition, their volumes have been extensively exploited in the many quarries of the area.
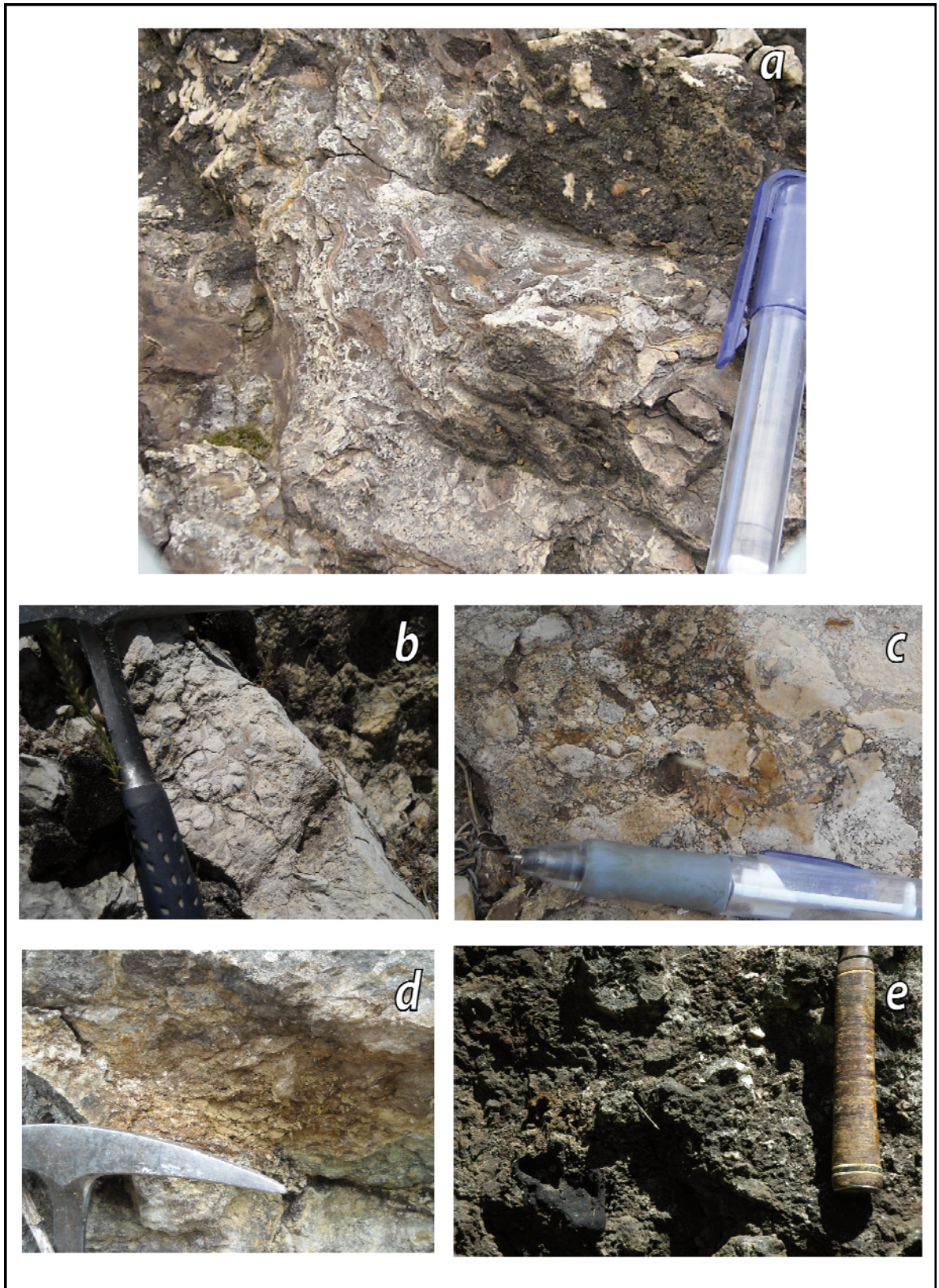
Fig. 4.1.12 - Mesoscopic facies of the BL - details. The fabric of the breccias is constituted by variously sized cemented subangular (**a**, **c**), and minor subrounded clasts too (**b**). At places dark-brown impregnated microbreccias occur (**a**), or even tar plugs, commonly occurring at Lettomanoppello area (**e**). Pelitic lenses are entrained at locations (**d**).
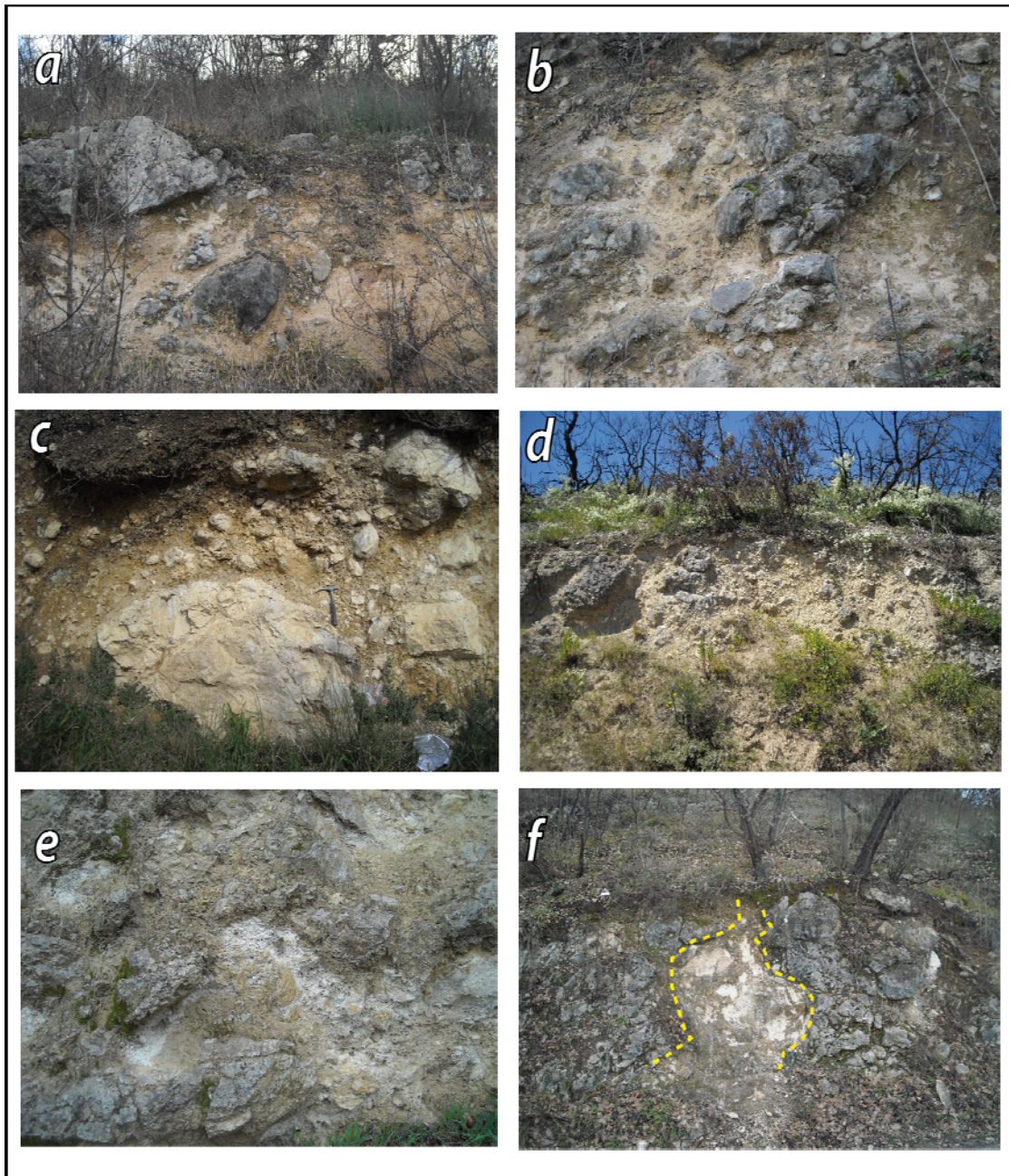
Fig. 4.1.13 - BL sublithofacies in correspondence to possibly higher flux rates and/or more focused fluid flow, resulting in higher fragmentation degree accompanied by: higher matrix/clasts ratios respect to the standard lithofacies (**a**-**d**), fluidized chaoticized pelites (**e**), mesoscale fluid migration pathways (**f**).
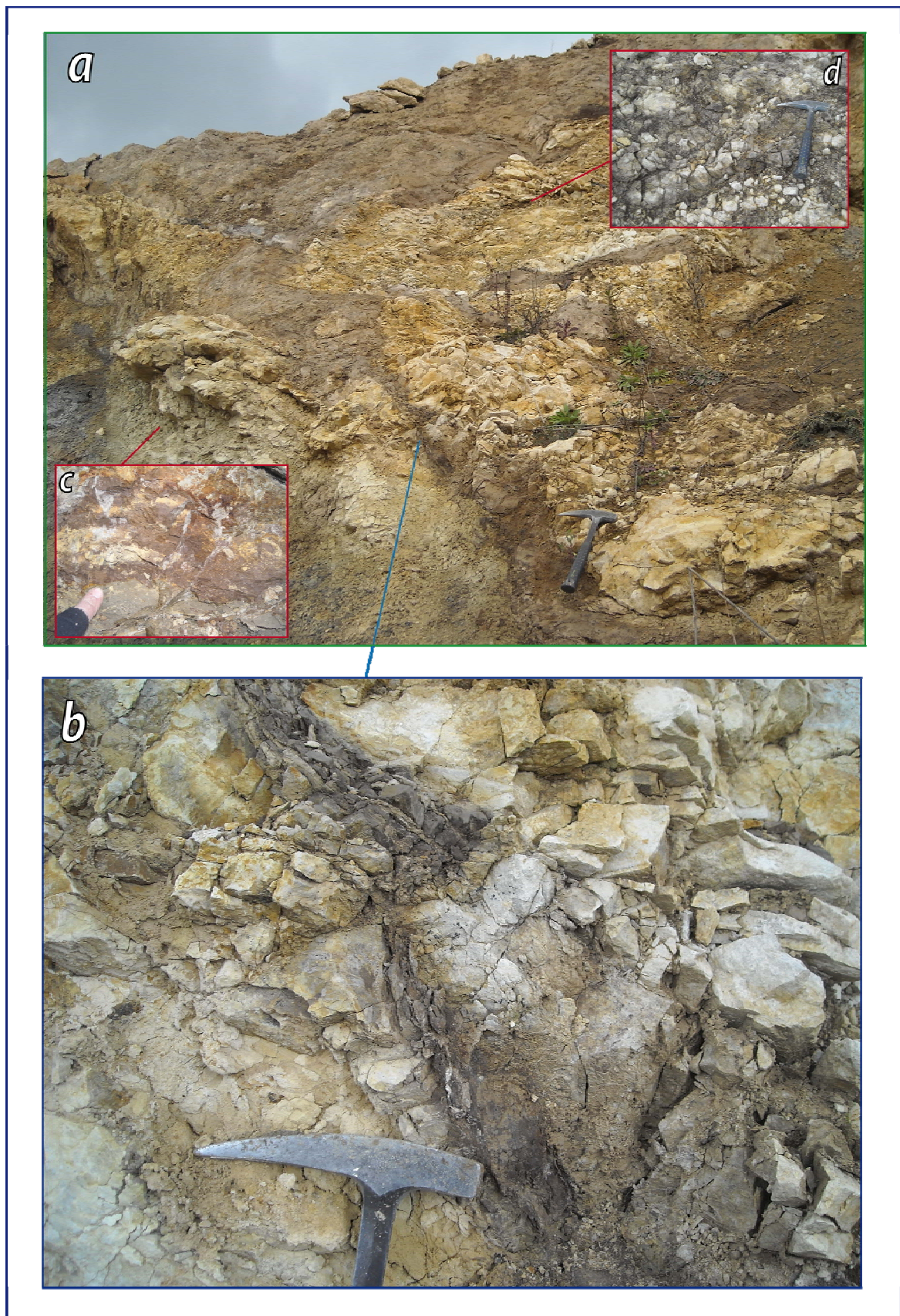
Fig. 4.1.14 - Outcrop scale fluid migration pathways at Abbateggio Quarry (**a**; **b**, closer view). Notice the entrained pelites (**c**) and the bedding retentive horizons (**d**).
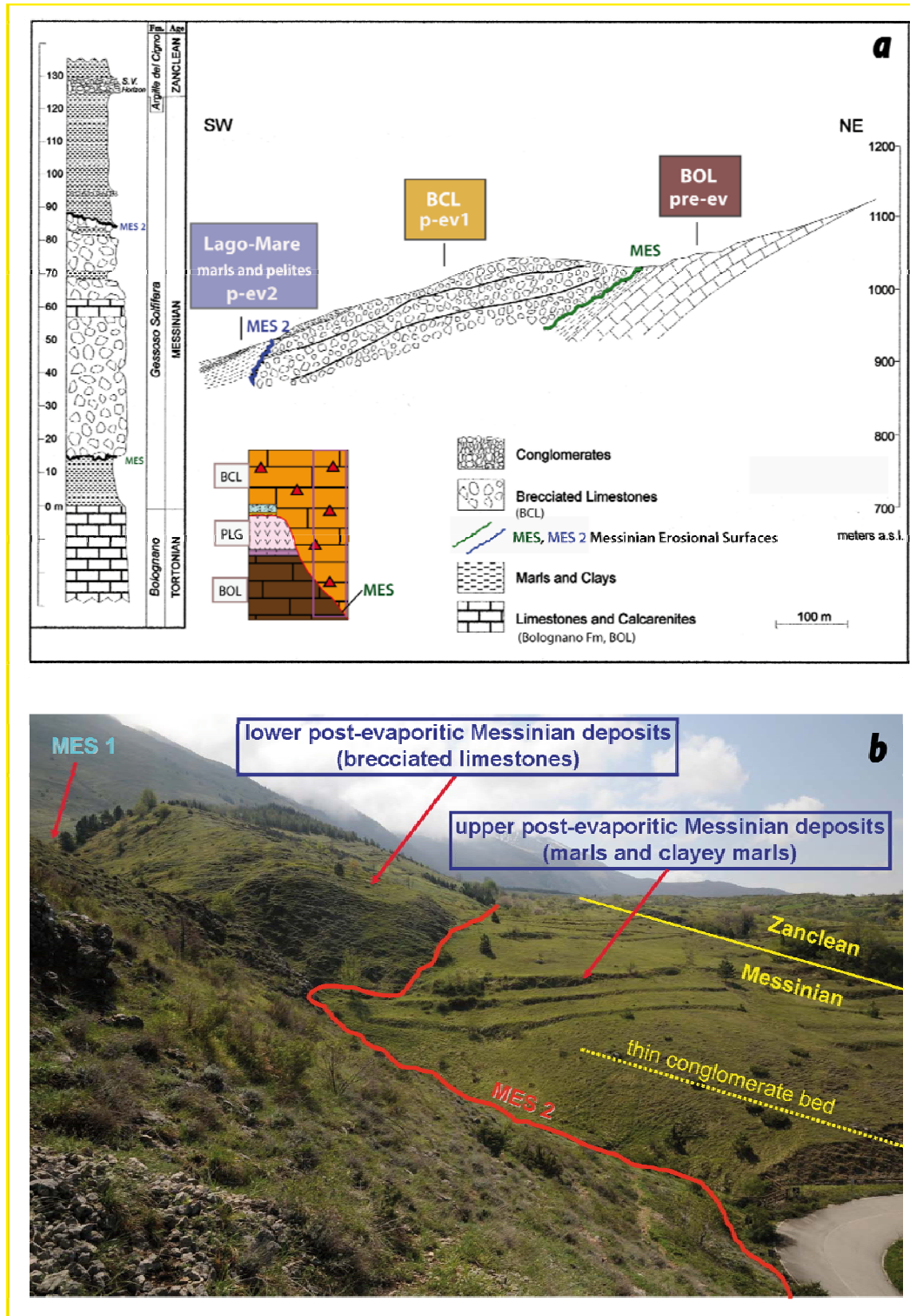
Fig. 4.1.15 - Colle Castellano section: **a** - simplified stratigraphy (modified after Crescenti et al., 2002) and **b** - panoramic view of the outcrop yielding the brecciated limestones. This area represents one of the rare sites in the Maiella area where it is possible to detect both the unconformities marking the post-evaporitic stratigraphy in the whole Mediterranean area (MES1 and MES2).
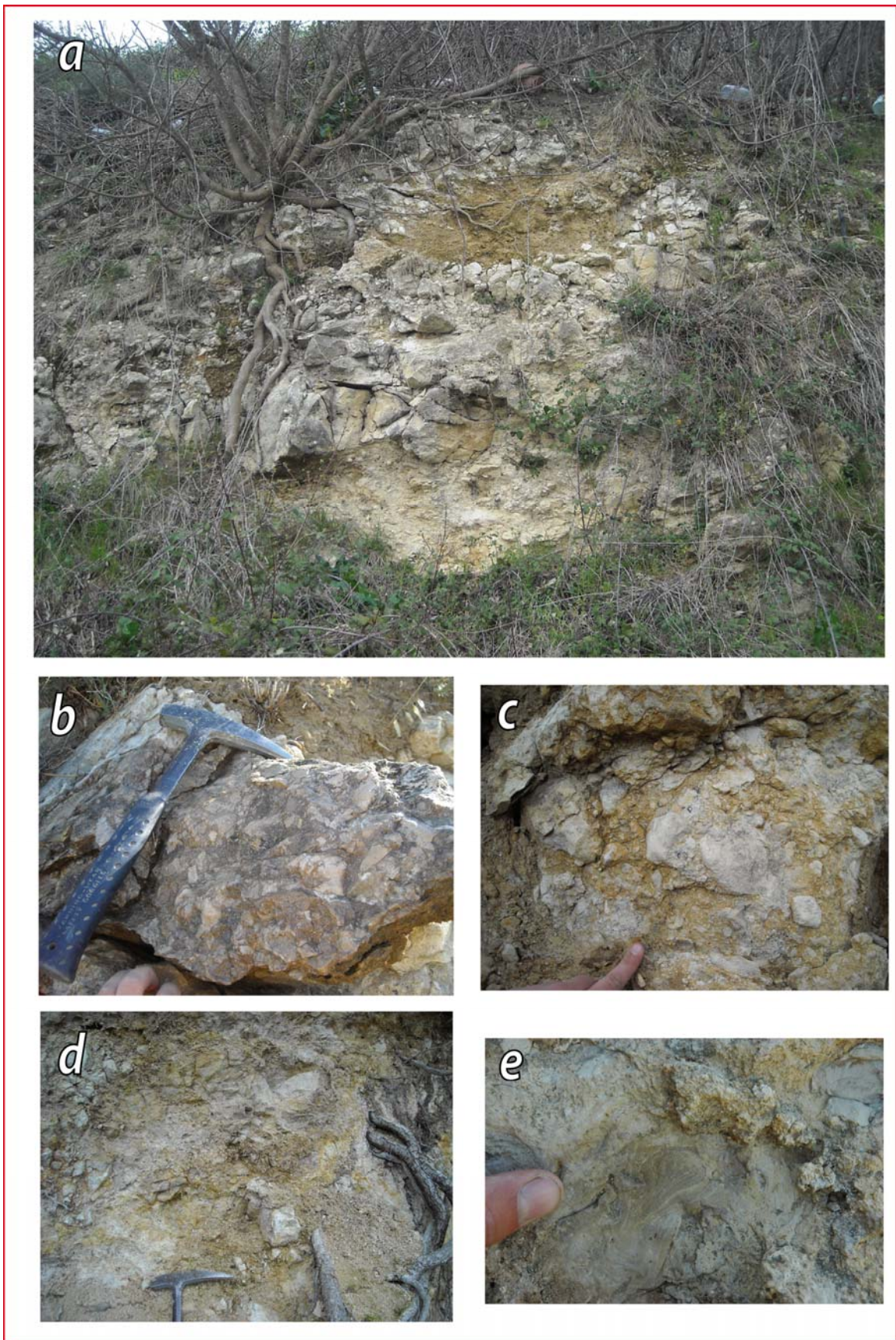
Fig. 4.1.16 - PL lithofacies - mesoscopic view.
Discontinuous mostly brecciated bodies and horizons (**a**) within the locally fluidized host sediment (**d-e**). Two main mescoscale breccia types: cement-supported, with mostly subangular clasts (**b**), and matrix-supported, with more subrounded clasts (**c**).
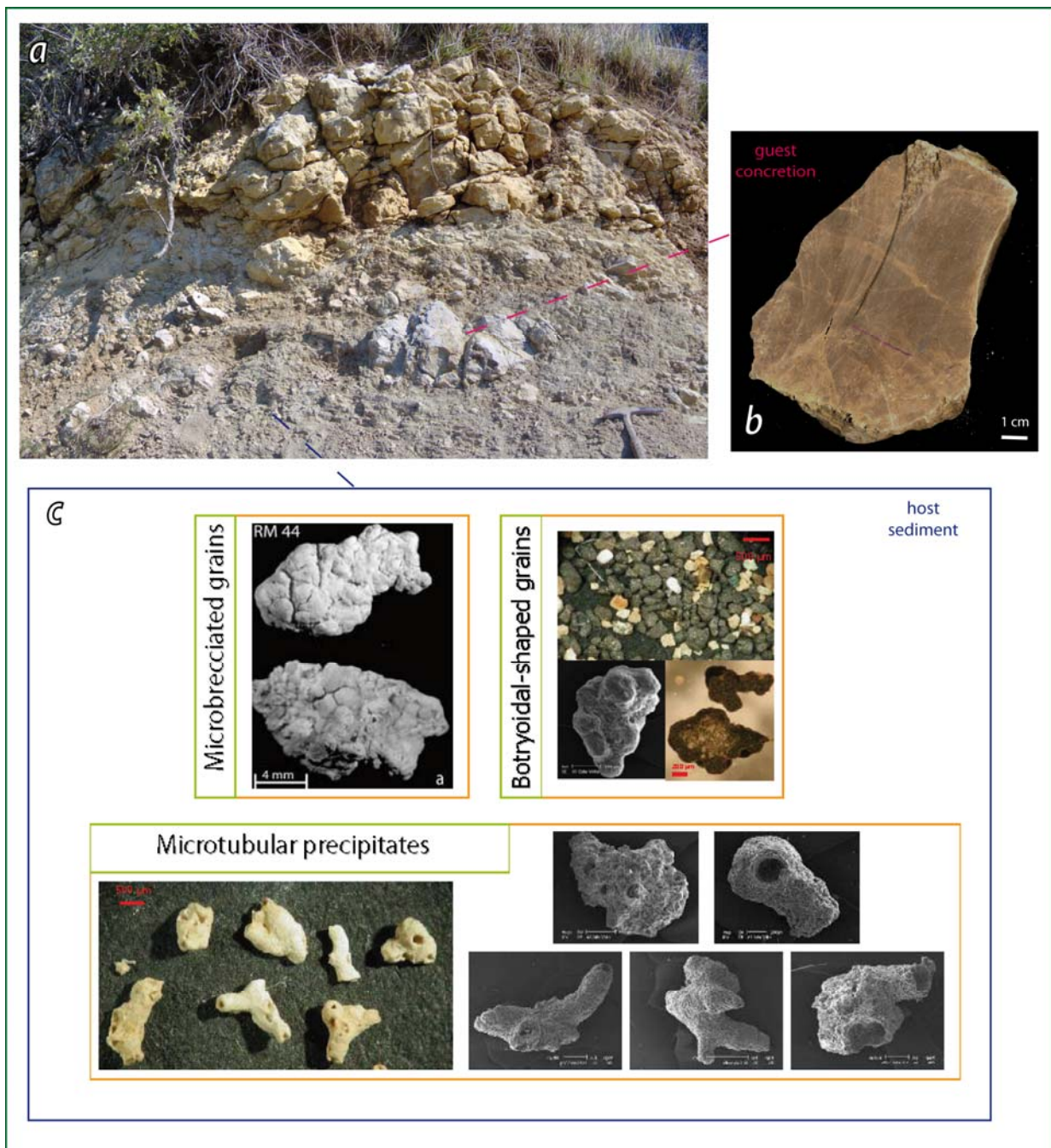
Fig. 4.1.17 - PL lithofacies: isolated carbonate concretions and buildups embedded in the host sediment (**a**).
 The guest concretions are dark-brown finely impregnated carbonates (**b**).
 The carbonate fraction of the host sediment (**c**) is made up of: microbrecciated grains; botryoidal shaped grain with a calcitic core and a rim made up of cryptocrystalline Fe-Mn-Ni oxides; microtubular precipitates.
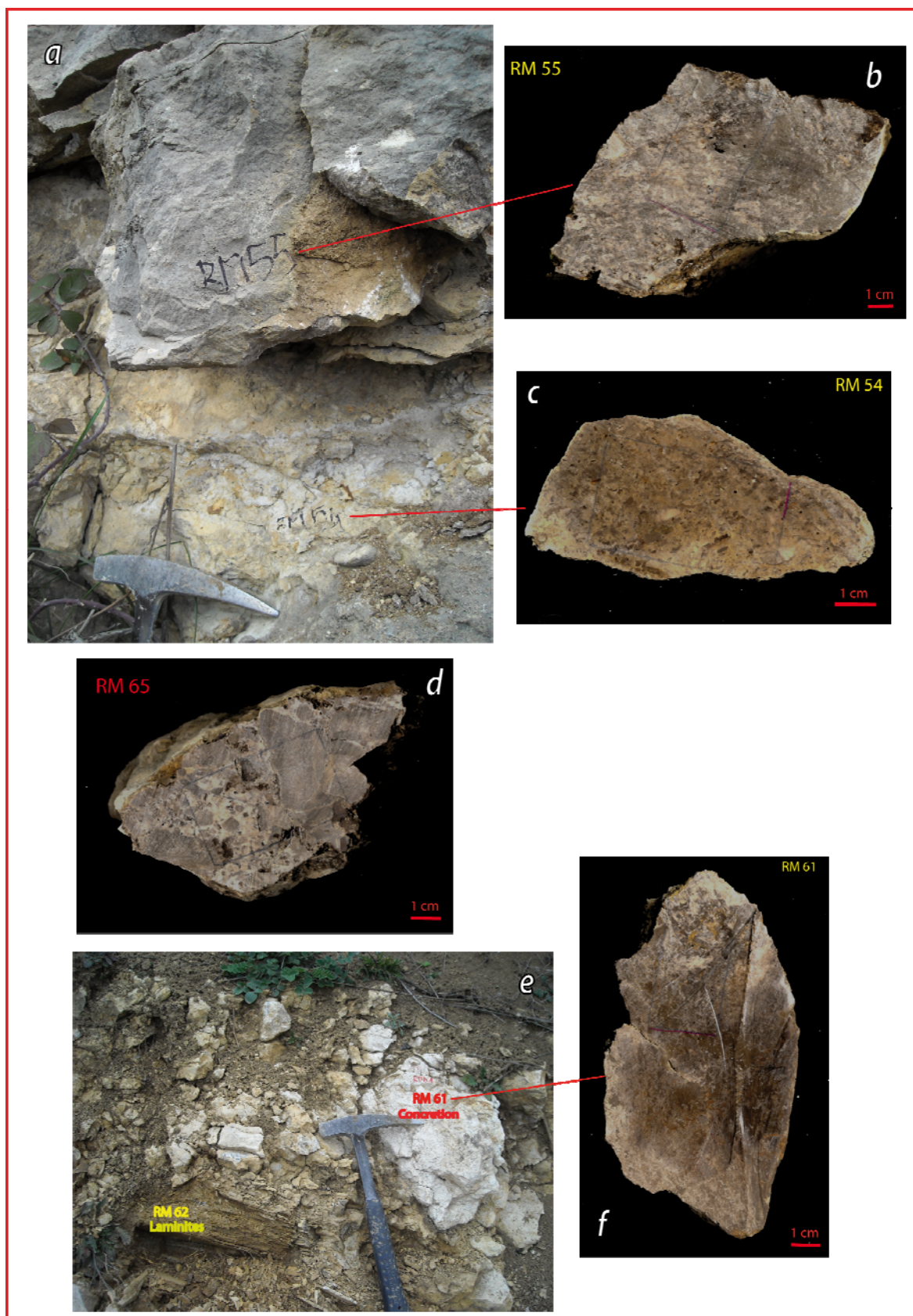
Fig. 4.1.18: PL lithofacies - Guest carbonates: tar impregnated cemented breccias (**a**-**d**) and concretions (**e**-**f**).
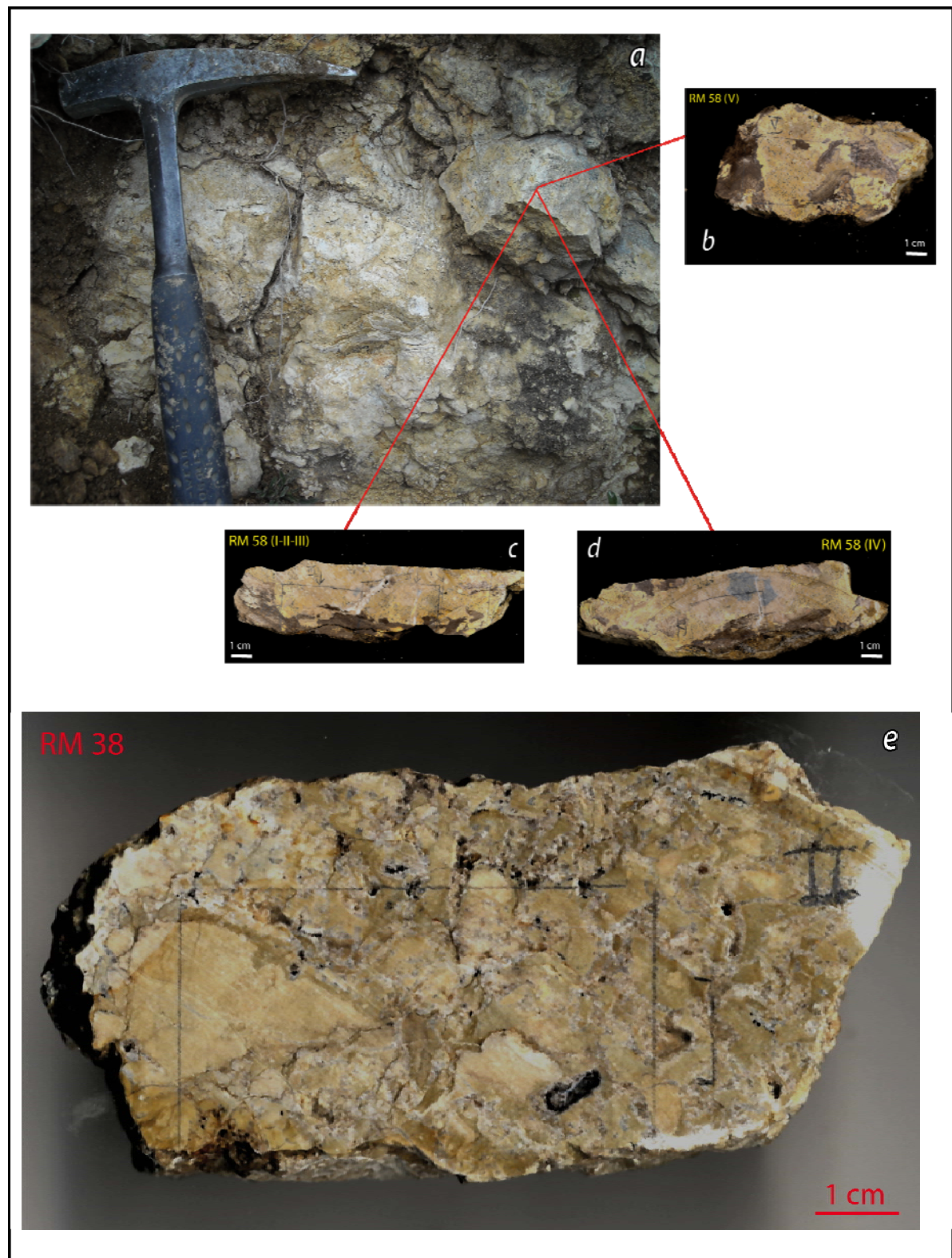
Fig. 4.1.19 - PL lithofacies - Guest carbonates: chaotic fluidized textures. Notice the presence of dark-brown pelites in some samples (**b**-**d**).
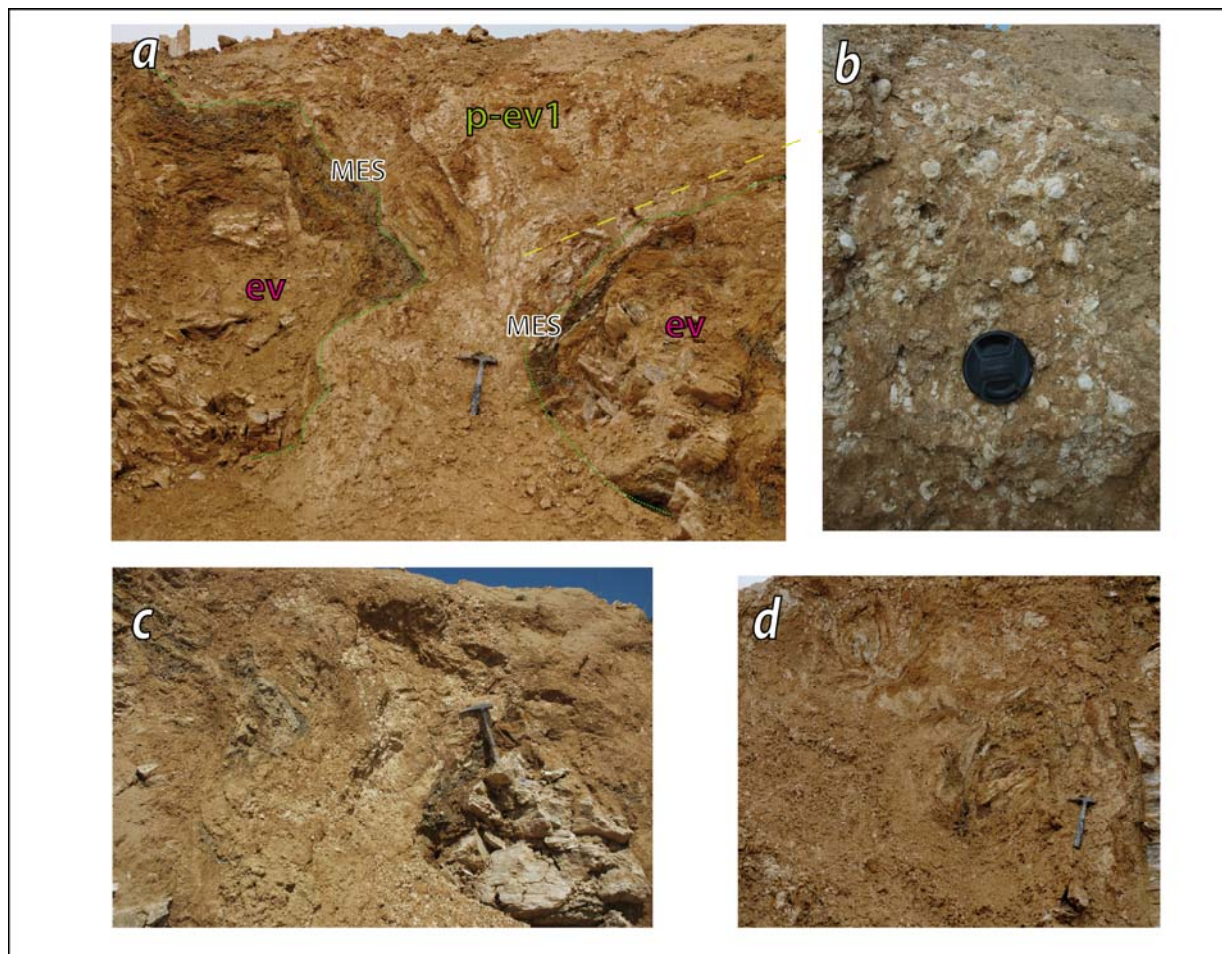
Fig. 4.1.20 - FS lithofacies - Fluid migration pathways cutting the evaporitic succession throughout (**a**). Fluidized pelites yielding carbonate concretions (**b**) and showing mesoscale folds (**c-d**). *Trovigliano area*.

4.1.3 - Facies analysis

Lithofacies **a** (BL) - Brecciated limestones

   Breccias exhibit a fabric that is traceable at any scale of observation and are mostly typified by subangular clasts (Figs. 4.1.24-4.1.25).

Two breccia-types have been defined through facies analysis:

A.   matrix-supported cemented breccias (Figs. 4.1.25 a-f; 4.1.26):

made up of subcentimetric - mostly subangular and minor subrounded - microsparitized microbial clasts, within a reddish microbial carbonate matrix. The matrix, in turn yielding millimetric to micrometric clasts (Fig. 4.1.25 c-d) and concretioned microtextures (Fig. 4.1.26 c-d), draws microscale fluid migration pathways coupled to intense microbrecciation (Fig. 4.1.26 a-b).

B.   dark brown cement-supported breccias (Figs. 4.1.25 g-h, 4.1.27 a-d):

finely tar-impregnated (Fig. 4.1.26 c-d) microbial microbreccia, yielding lenticular pseudomorphs after gypsum (Fig. 4.1.25 h).
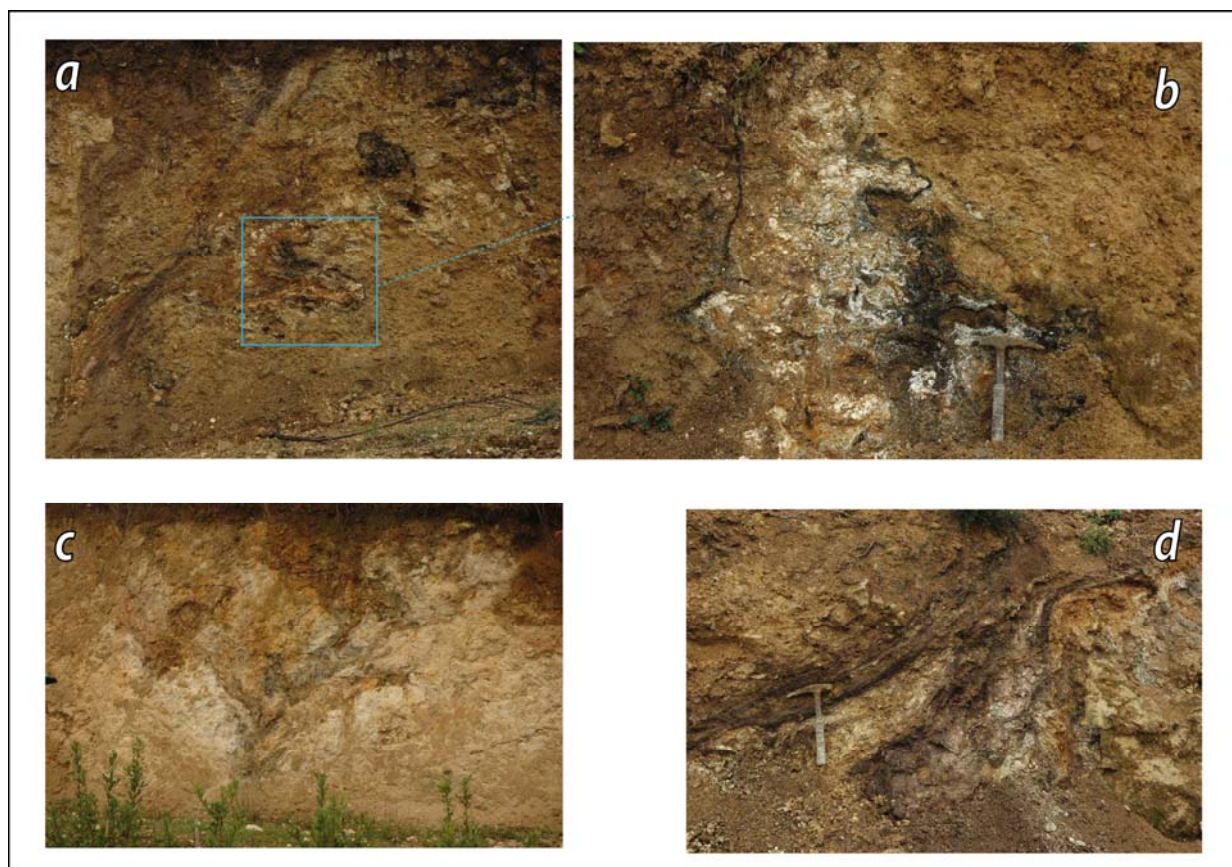
Fig. 4.1.21 - FS lithofacies -Fluid migration pathways (**a**, **c**), represented by fluidized pelites, variously ocraceous, dark brown and black (**b**, **d**). *Cusano di Abbateggio area*.

Tar therefore occurs in microbreccias, bubbles (Figs. 4.1.27 e), pores (Figs. 4.1.27 f-h, 4.1.28, 4.1.29), and is even associated to native sulphur (Lettomanoppello; Fig. 4.1.27 f). When pore-filling, it is contoured by an extremely thin fringing cement, presumably formed in interplay with hydrocarbons (Figs. 4.1.27 g, 4.1.28 d, 4.1.29 d). Commonly occurring in the chaotic subfacies (Figs. 4.1.28-29), it is associated to aragonitic fans (Fig. 4.1.28 c) and fluidized clotted microbialite (Figs. 4.1.28 d; 4.1.29 c, 2-4). The chaotic facies is depicted in fact by the occurrence of extremely fluidized, locally microbrecciated microbialite (Figs. 4.1.29 b, 1): this co-occurrence constitutes an important rheological implication, highlighting the co-existence of brittle and plastic behaviour at a very small scale and within the same microfacies. This accounts for complex spatial variations in the fluidification phenomena and fluid-rock interaction (FRI), that presumably acted in an early diagenized sediment. This consideration in turn leads to a major timing implication: the investigated post-depositional events are constrained to the early post-evaporitic phase of the MSC. The relation between the two kind of breccias (A and B) has been established through the facies analysis of two partially-impregnated samples collected in the Abbateggio area (ABB 4, Fig. 4.1.30; ABB, Fig. 4.1.31). They both show that the contact between the finely impregnated portion

and the pale cream portion is marked by a milling impregnation front, completely isolating a pale cream core in the case of the sample ABB.
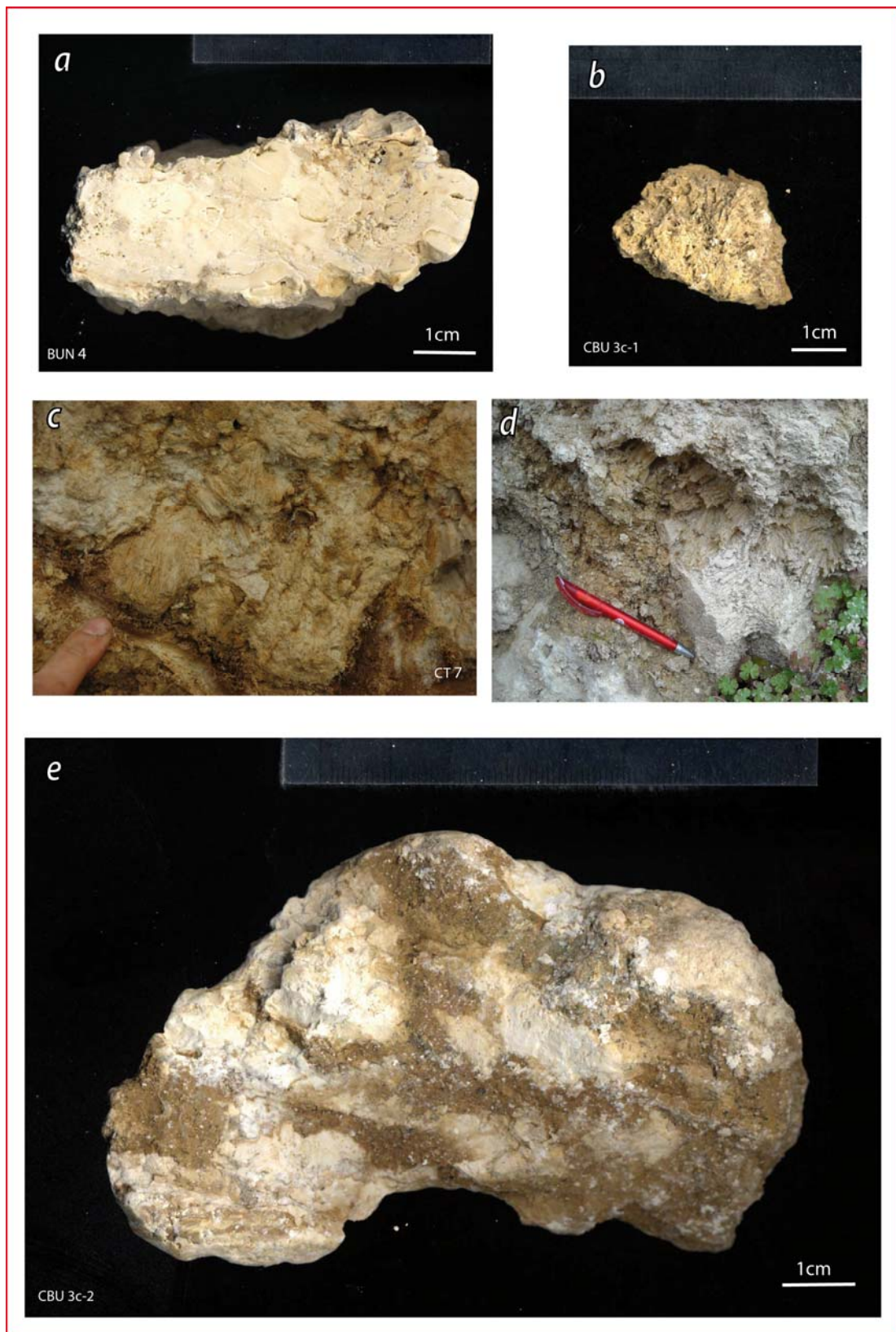
Fig. 4.1.22 - FS carbonate facies association: homogeneous white concretion (**a**), vuggy carbonate (**b**), botryoidal aragonite fans (**c**-**d**), chaotic admixed texture of concretions and pelites (**e**).
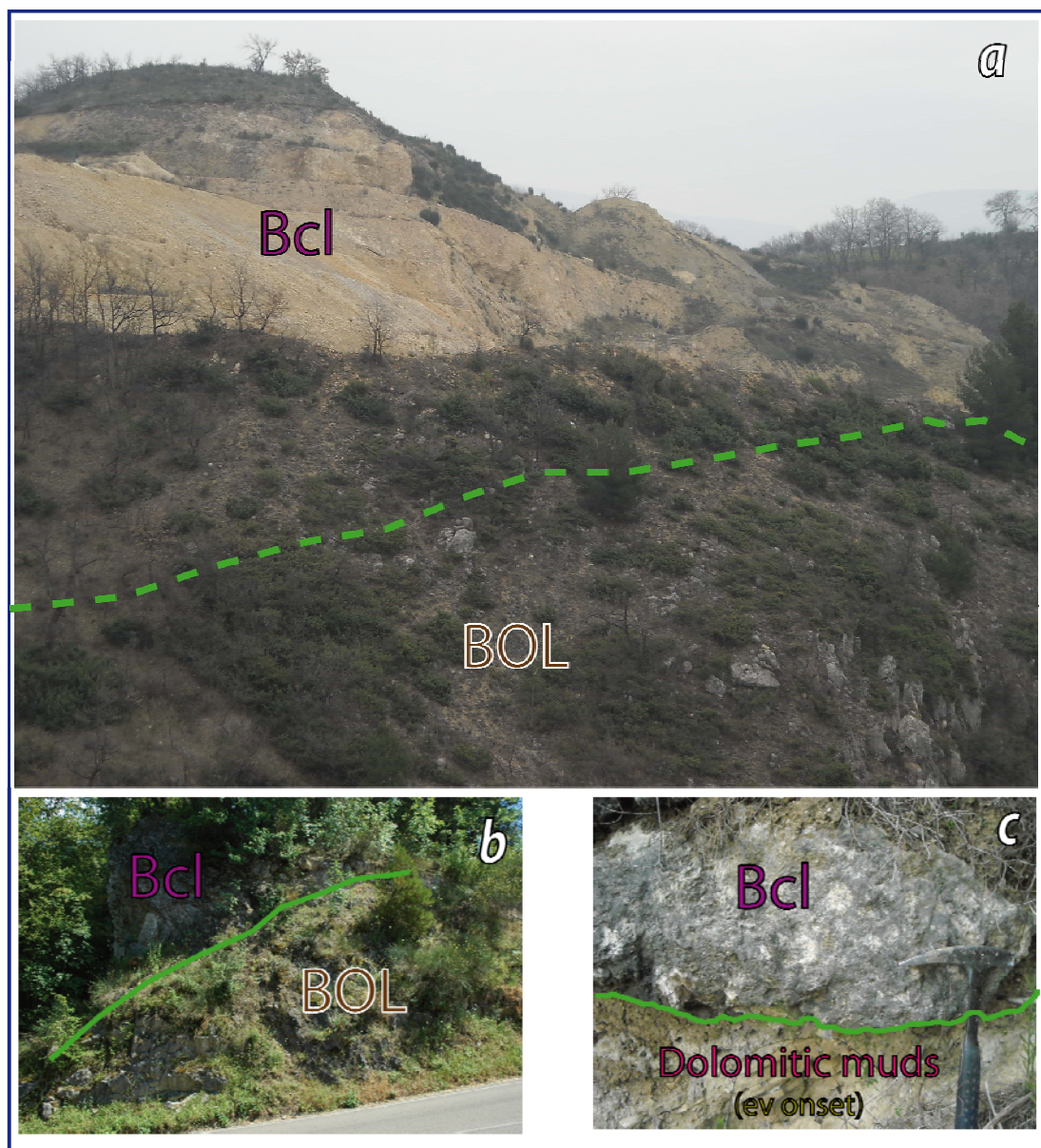
Fig. 4.1.23 - Messinian Erosional Surface (green line) - Brecciated Limestones unconformably overlying Bolognano Fm (**a**, Abbateggio Limestones Quarry; **b**, Lettomanoppello ancient bitumen mine) and basal terms of the Primary Lower Gypsum (**c**, Madonna del Monte).

The pale cream portion yields in turn a complex history of cementation and localized microbrecciation, experienced by the pseudomorphs after gypsum as well. Since the Bcl were afterwards partially impregnated, it must have not been lithified yet by that time. Yet, the fragmentation pattern testifies the co-occurrence of a brittle behaviour as well. As stated before, this accounts for small scale variations in the energy of the fluidification phenomena, but possibly also for differential early cementation within the sediment. As a whole, this results in remarkable microscale heterogenities. The pale cream facies association yields type A microbreccia, but contains also microbrecciated microbial fragments, common constituents of the type B microbreccia, fully finely impregnated s.s. (Fig. 4.1.31 d-5).

A relative timing of the post-depositional events affecting the Bcl in the Maiella area can be thus established: an earlier brecciation event accompanied by fluidification affected a partially microsparitized primary microbial sediment; soon after, a second brecciation event, locally affecting the microbial sediment and accompanied by tar impregnation, took place.

The common occurrence of barite-celestite (sometimes coupled to strontianite) and framboidal pyrite is consistent with sulphate-reducing conditions (Figs. 4.1.25 d, 4.1.32). Likely, these conditions were not constant, as two main fluidification-brecciation events affected the sedimentary pile. The possible variations in Ph experienced by the microenvironment are testified, among the others, by the occurrence of: ghost framboidal structures (Fig. 4.1.31); intensively leached native sulphur crystals (Fig. 4.1.27 f); corroded microbial fragments (Fig. 4.1.31 - 5).

Lithofacies **b** (PL) - Patchy limestone: concretions and breccias within a marly-pelitic dominated succession

The patchy limestones were sampled only at Colle di Votta section (Figs. 4.1.3, 4.1.17).

The terrigenous sediments represent the host sediment: they are barren, dominated by calcite, aragonite and quartz, with subordinate quantities of clay minerals (mainly illite and smectite), plagioclase and Fe-dolomite. Enigmatic carbonatic grains occur in the microfacies: botryoidal-shaped
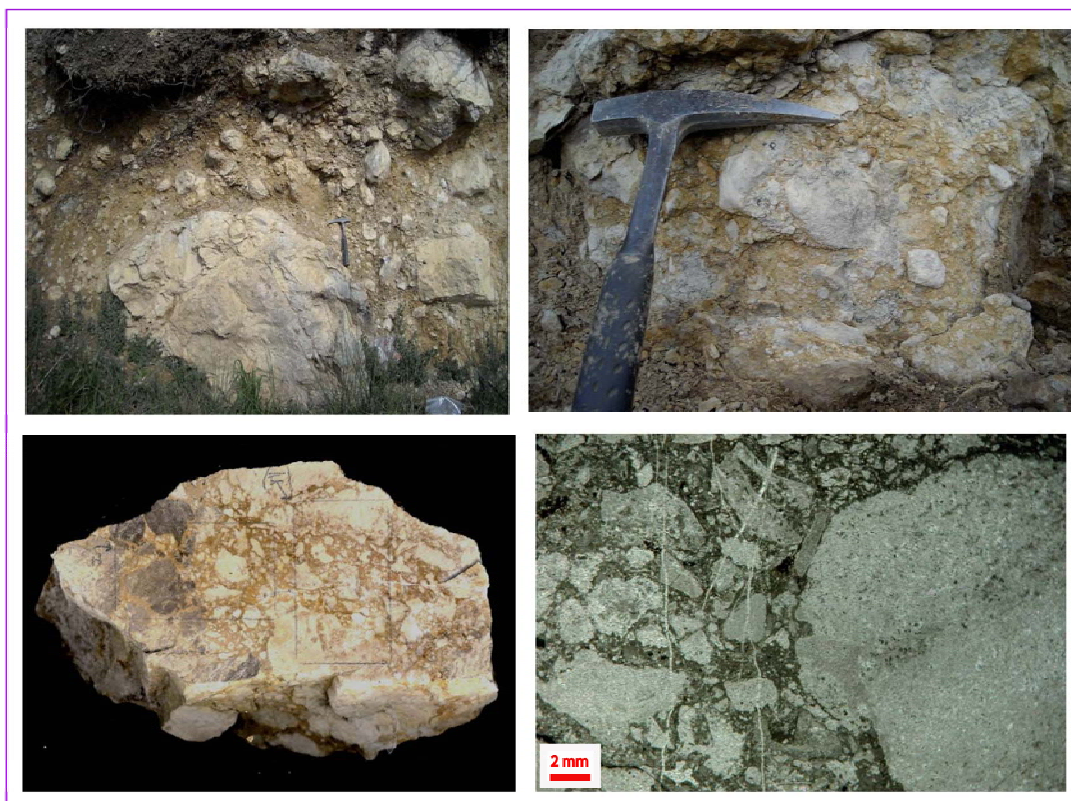
Fig. 4.1.24 - Scale independent pattern in the brecciated fabric.
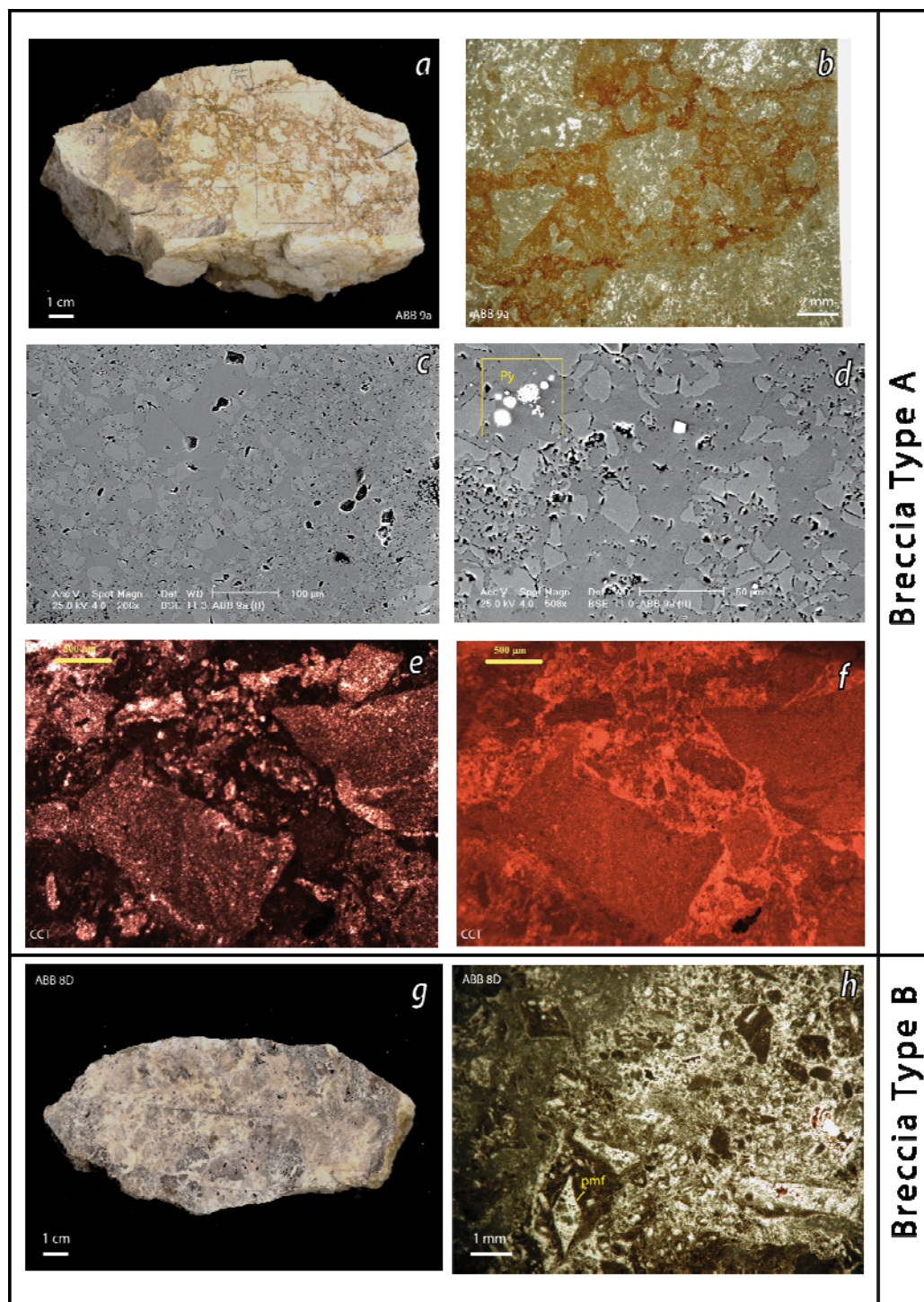
Fig. 4.1.25 - Brecciation occurring at different scales.
Breccia Type A. Matrix-supported breccia (**a**-**f**): dull microsparitized microbial clasts in a reddish microbial bright luminescent matrix, yielding framboidal pyrite (Py, **d**) and millimetric to micrometric-sized clats (**a**, sample slab; **b**, trasmited light; **c**-**d**: SEM view; **e**-**f**: coupled transmitted light - CL view).
Breccia Type B - Dark cement-supported breccia (**g**, sample slab): microbial fragments yielding lenticular pseudomorphs after gypsum (pmf, **h**, transmitted light).
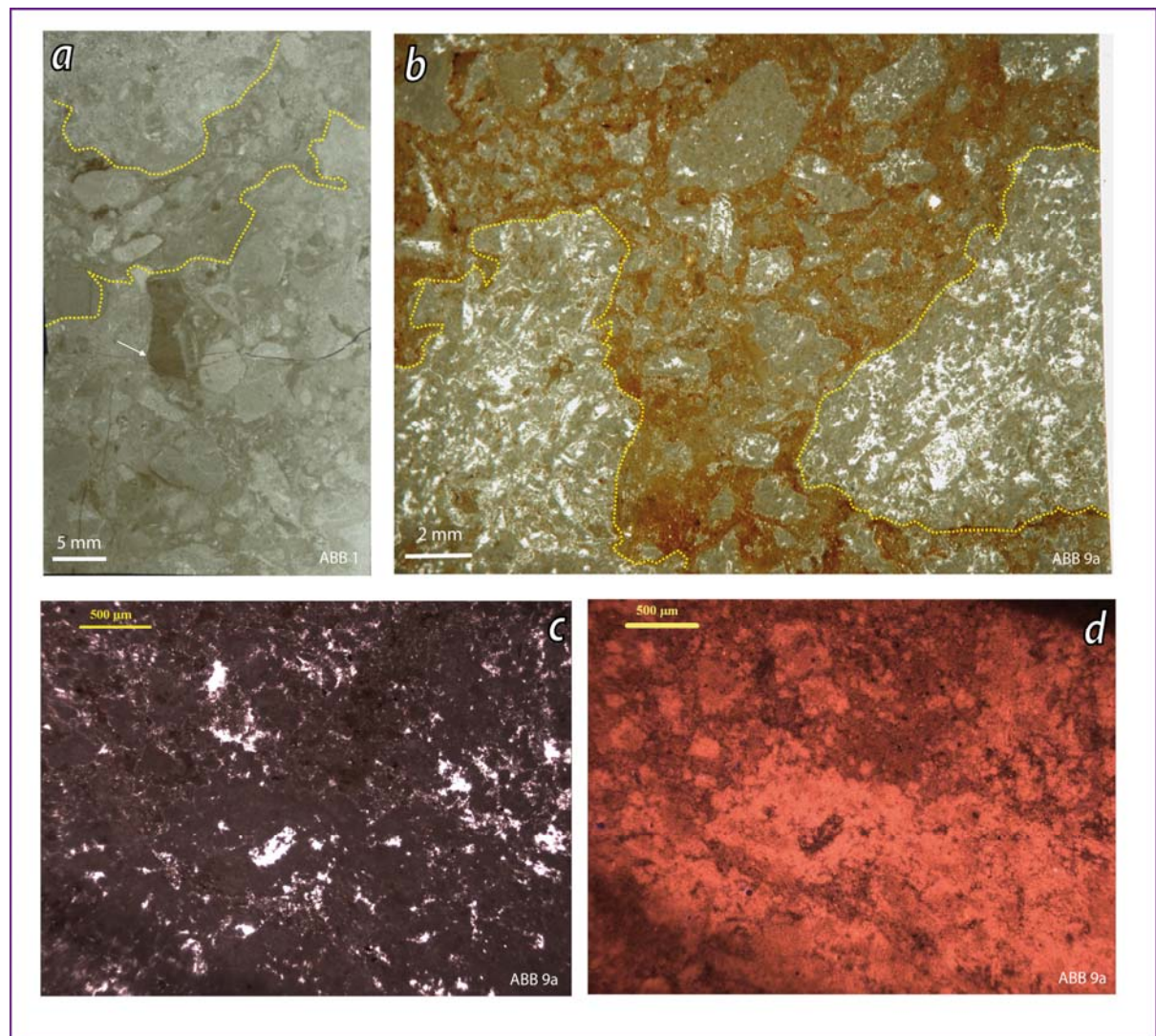
Fig. 4.1.26 - Matrix-supported breccia (Breccia Type A) - Microscale fluid migration pathways (**a-b**; dotted lines, optical view), yielding allochthonous clasts (**a**, white arrow pointing to a thrombolytic clast). Concretioned hidden microtexture associated to the matrix microbial-bearing portion (**c-d**, coupled transmitted light - CL view).

particles with a calcitic core and a rim made up of cryptocrystalline Fe-Mn-Ni oxides; microtubular precipitates; microbrecciated clasts; porous grains (Fig. 4.1.17 c).

The carbonatic guest of the PL lithofacies exhibits only a fragmentary record of the complex history of the brecciated limestones, previously deciphered in the BL lithofacies. Nonetheless, many clues actually point to similar histories to a major extent, thus highlighting the correct stratigraphic correlation between the two lithofacies.

The most common microfabrics are represented by impregnated concretions and by chaoticized breccias (Fig. 4.1.33). The latter show a puzzling arrangement of microfacies yielding:

- locally microbrecciated microbial fragments (Fig. 4.1.34).
- pseudomorphs after gypsum, both prismatic and lenticular, showing an intricate history (Fig. 4.1.35) of: microspar cementation, corrosion, sediment and tar infillings (Fig. 4.1.36 c-d).
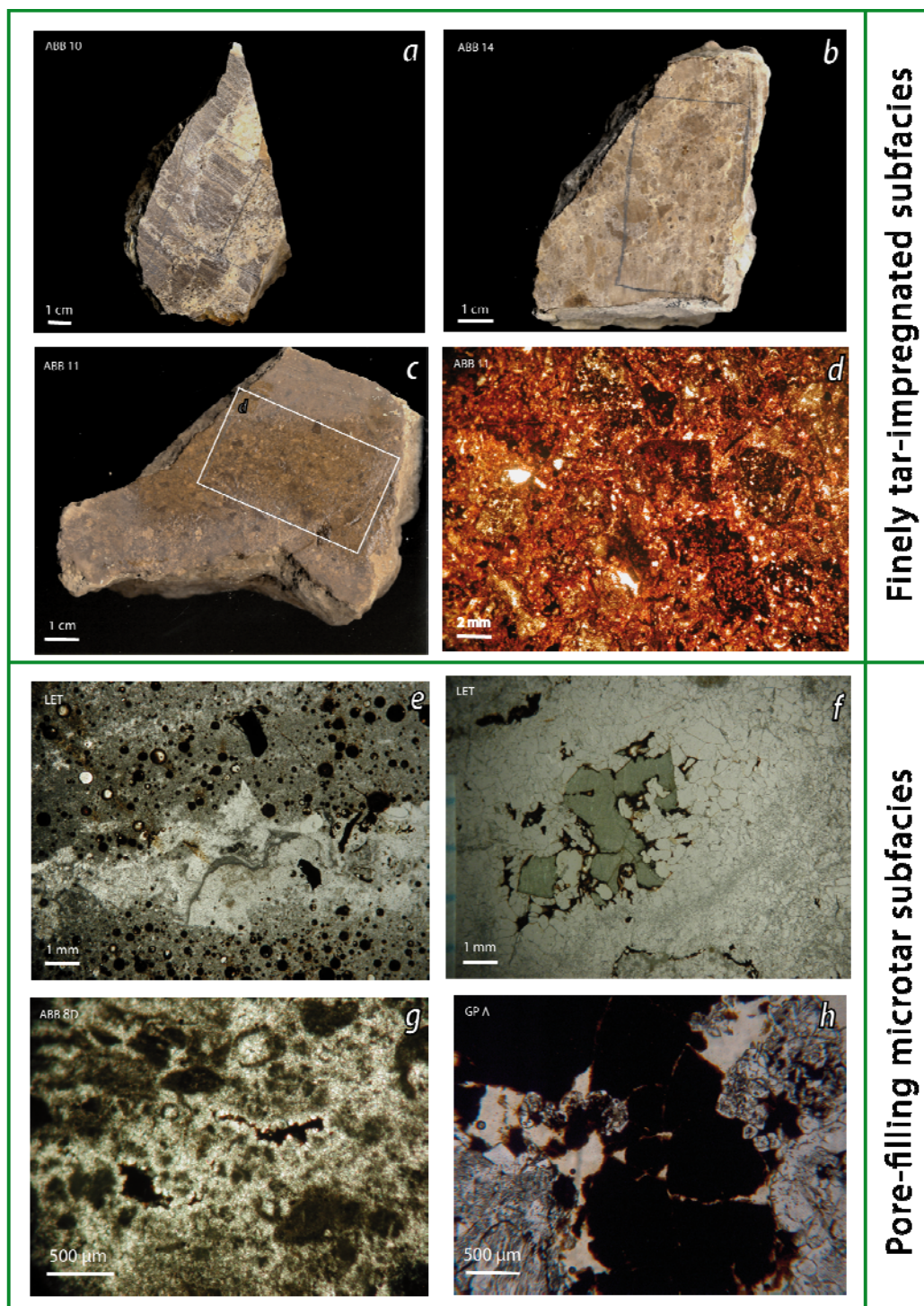
Fig. 4.1.27 - *Finely tar-impregnated* subfacies (**a-d**), samples slabs, brecciated to different degrees (**a-c**) and optical view (**d**).
Pore-filling microtar subfacies, tar bearing facies s.s. (**e-h,** optical view): bubble tar (**e**), microtar associated to native sulphur (**f**), pore filling microtar rimmed by thin fringing fibrous cement (circles, **g**) and associated to aragonite cements (**h**).
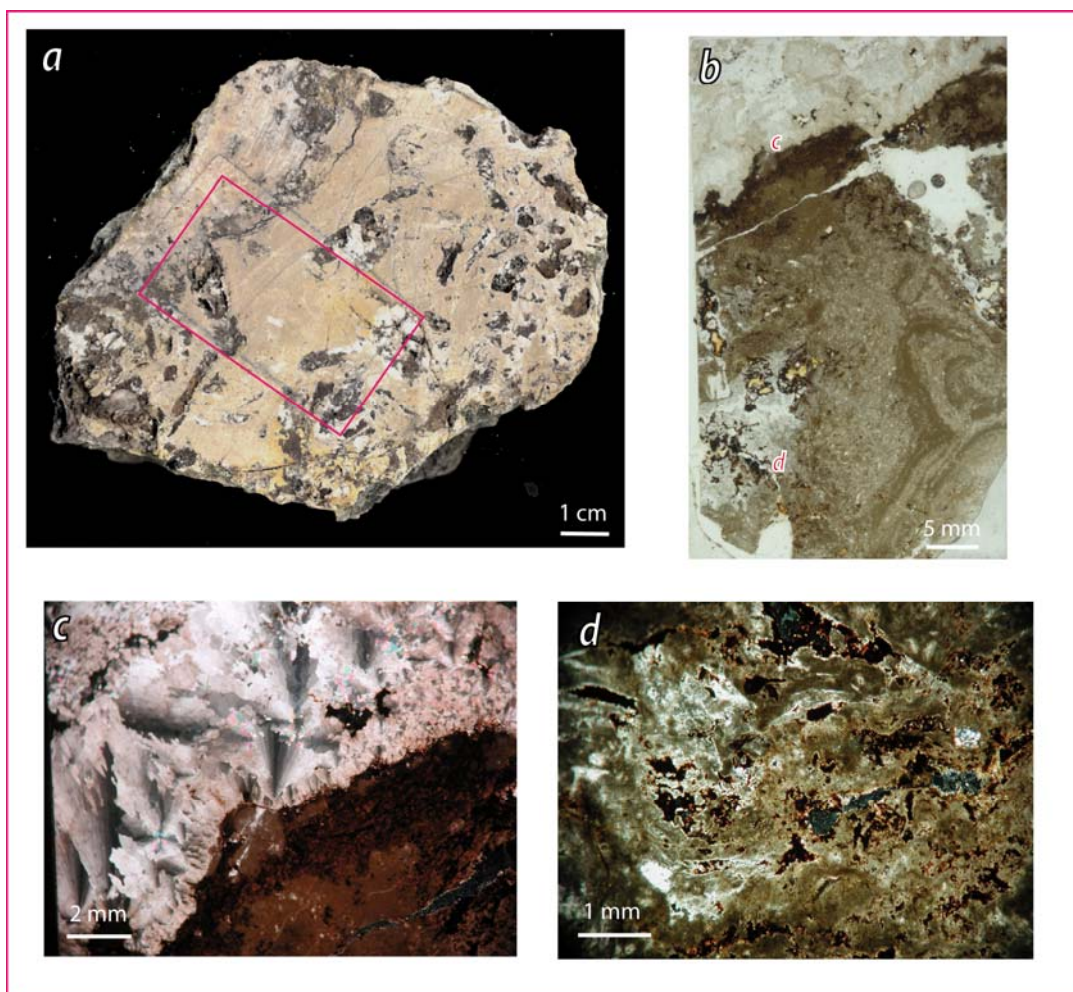
Fig. 4.1.28 - Tar-bearing brecciated limestone - chaotic subfacies; sample MM/b1, *Madonna del Monte area* (**a**, sample slab) Fluidized clotted microbial texture (**b**, **d**) with pore-filling microtar associated to aragonite fans (**c**, **d**). (**b**, transmitted light; **c-d**, crossed polars)

At the corrosion border, rod and needle shaped Fe oxides and hydroxides are present (Fig. 4.1.35 c-d). Fragments of pseudomorphs infilled by sediment have been eventually microbrecciated. The pseudomorphs definitely recorded, at a small scale, the complex history of the Bcl unit, even in terms of alternating oxidizing and reducing conditions (e.g., lenticular gypsum typically forms in high OM-content reducing microenvironments; Cody & Cody, 1988).

- finely impregnating and pore-filling microtar resembling structures (Fig. 4.1.36);

- interparticle barite-celestite and Ni-Co-Mn-Fe microveins (reducing proxies; Fig. 4.1.32 a);

- framboids of pyrite, occurring either as single isolated elements and as composite framboids (reducing proxies; Fig. 4.1.32 c).

From a compositional point of view, the limestones are mostly characterized by low-magnesium calcite, minor aragonite and pore filling chalcedony. Celestite is sometimes abundant (also in the carbonate samples from FS lithofacies), but in general has been detected only by EDS.

Proxies for both the early post-depositional event (microfluidized primary sediment) and of the late post-depositional event (tar impregnation; microbial microbrecciation) are present in the PL.

- 62 -
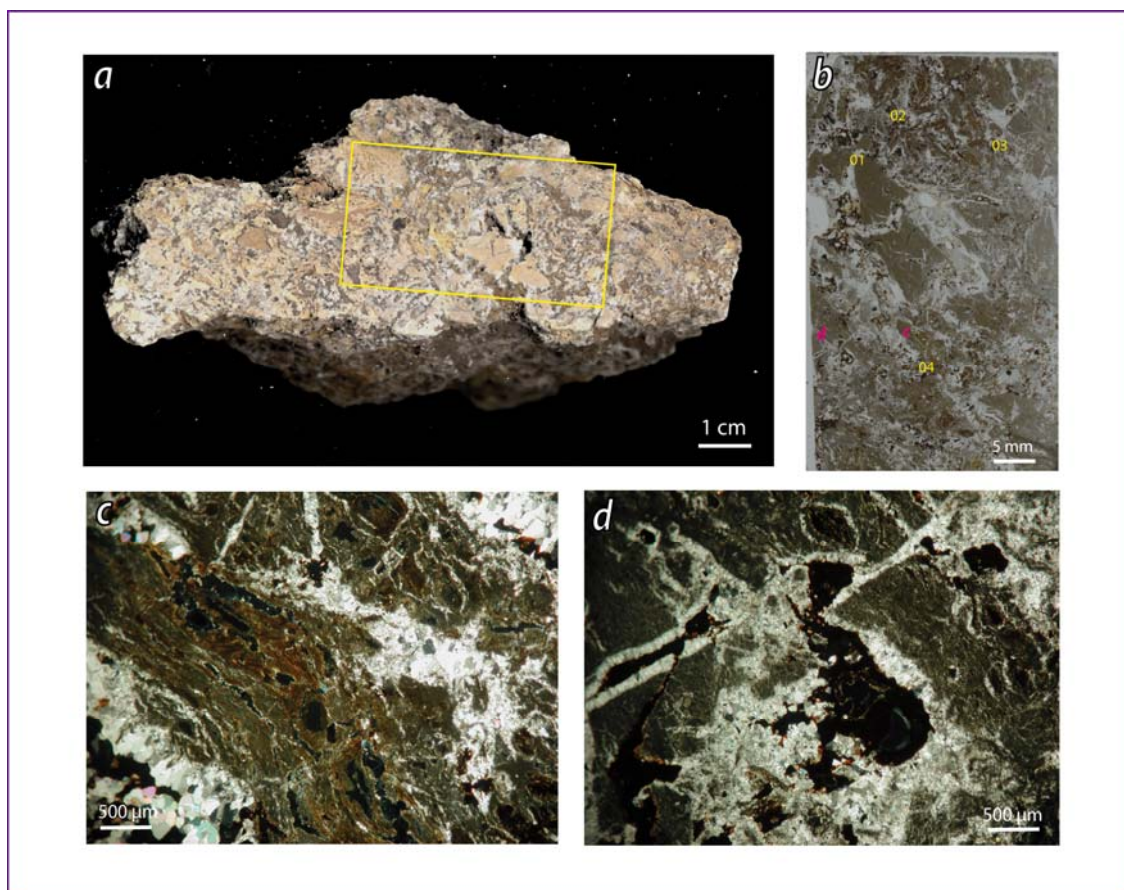
Fig. 4.1.29 - Tar-bearing vuggy limestone - chaotic subfacies; sample MM/e2, *Madonna del Monte area*
Chaotic texture (**a**, **b**) resulting from a complex rheological behaviour, both brittle and plastic.
The *brittle behaviour* is testified by:
local microbrecciation (**b 01**; **01a**-**01b**, coupled crossed polar - CL view), earlier fluidized bright orange microbial clasts, dull cement; microtar injection rimmed by fringing cement (**d**).
The *plastic behaviour* is testified by: fluidized microbial (**c**), yielding a radial texture (**b 02**, **02a**-**02b**, coupled crossed polar - CL view) or completely contorted texture (**b 03-04**; **03-04 a, 03-04 b**, coupled transmitted light - CL view), where the originally bright orange clotted microbialite, microsparitized to different extents, is mixed to dull sparry cement and moderately bright microspar.
Notice a fluid micro-channel (white dotted line **03b**).
(Continue to the next page)

In view of the hypothesis proposed herein, single elements contain independently traces of the post-depositional history of the Bcl. Beside the aforementioned example of the pseudomorphs, even the microbial fragments, a product of the late brecciation event, yield in their single elements fluidized microtextures (Fig. 4.1.34 e-f), inherited from the early fluidification event. During the second fluidification event, accompanied by oil migration, it was possibly the little more advanced diagenesis to induce in the microbial sediment a localized brittle behaviour, that by contrast affected only the microsparitized portions during the first fluidification event (Fig. 4.1.25 e-f).
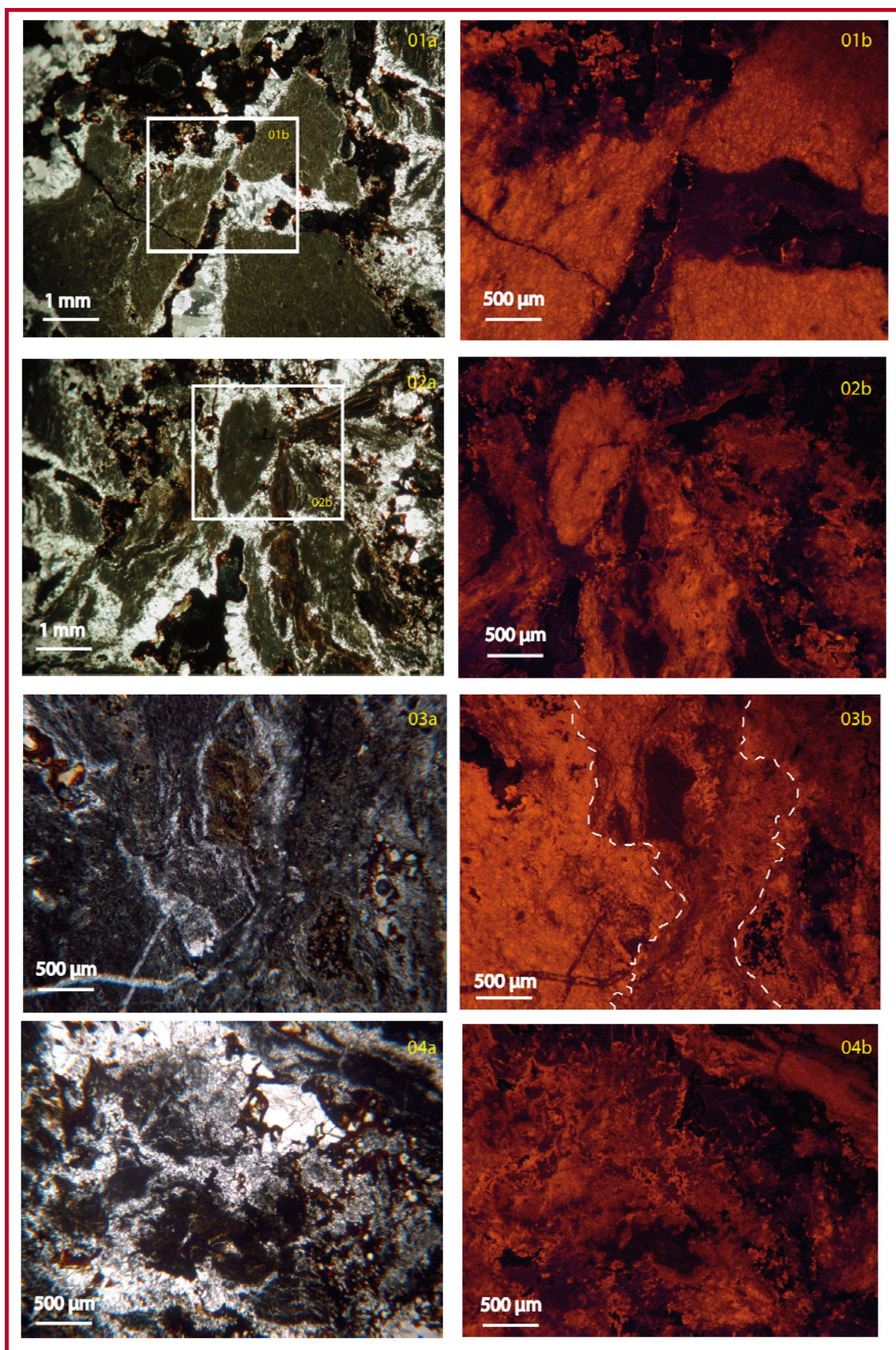
Fig. 4.1.29 - (caption in the previous page)
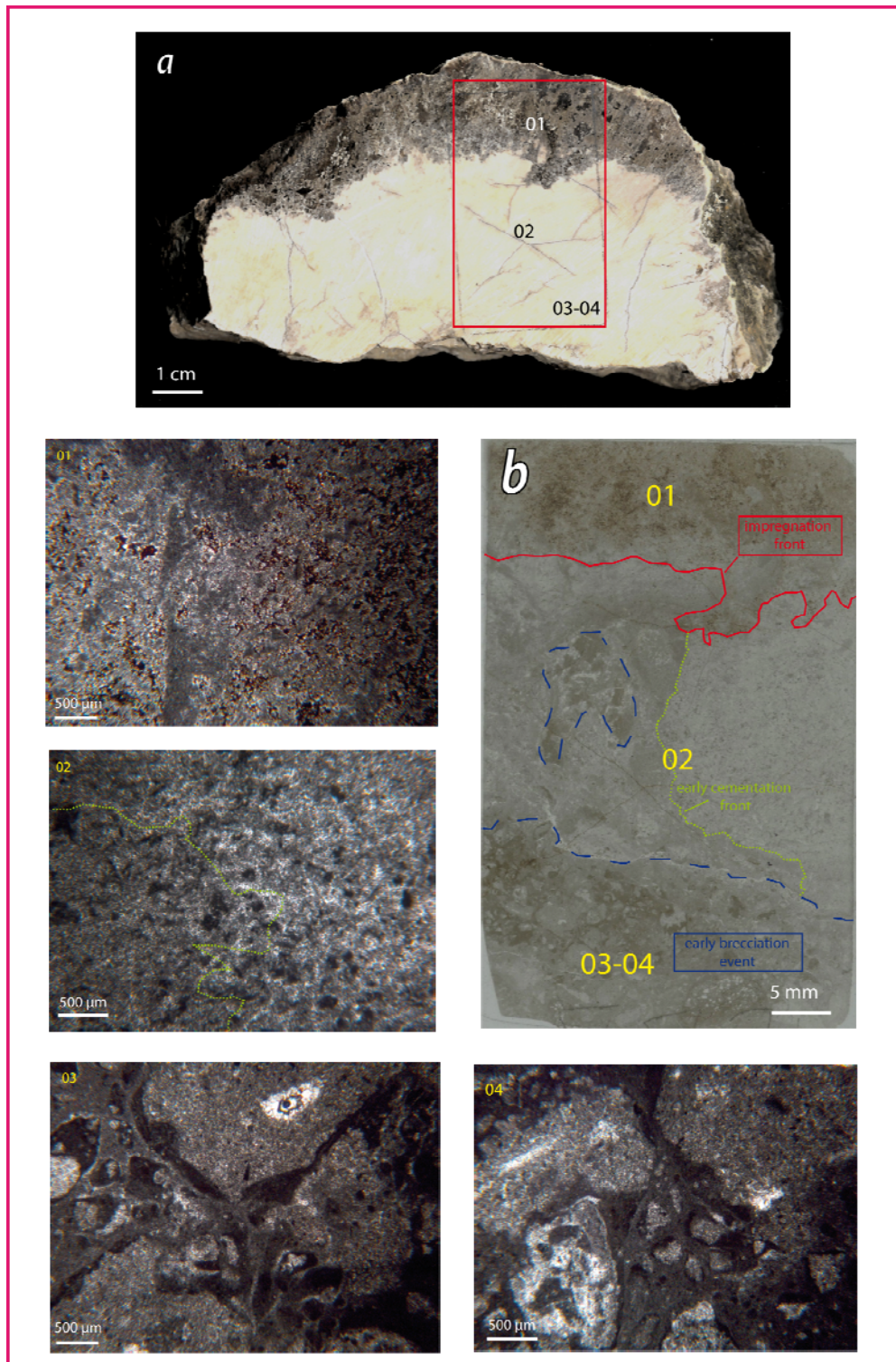
Fig. 4.1.30 - Brecciated limestone; sample ABB 4, *Abbateggio* area (**a**, **b**) - Finely impregnated microbrecciated front (**01**), representing the later brecciation event; primary pale cream microsparitized peloidal microbial microfacies (**02**), microbrecciated at locations (**03**-**04**) during the earlier brecciation event (microsparite representing the clast and microbialite representing the matrix).
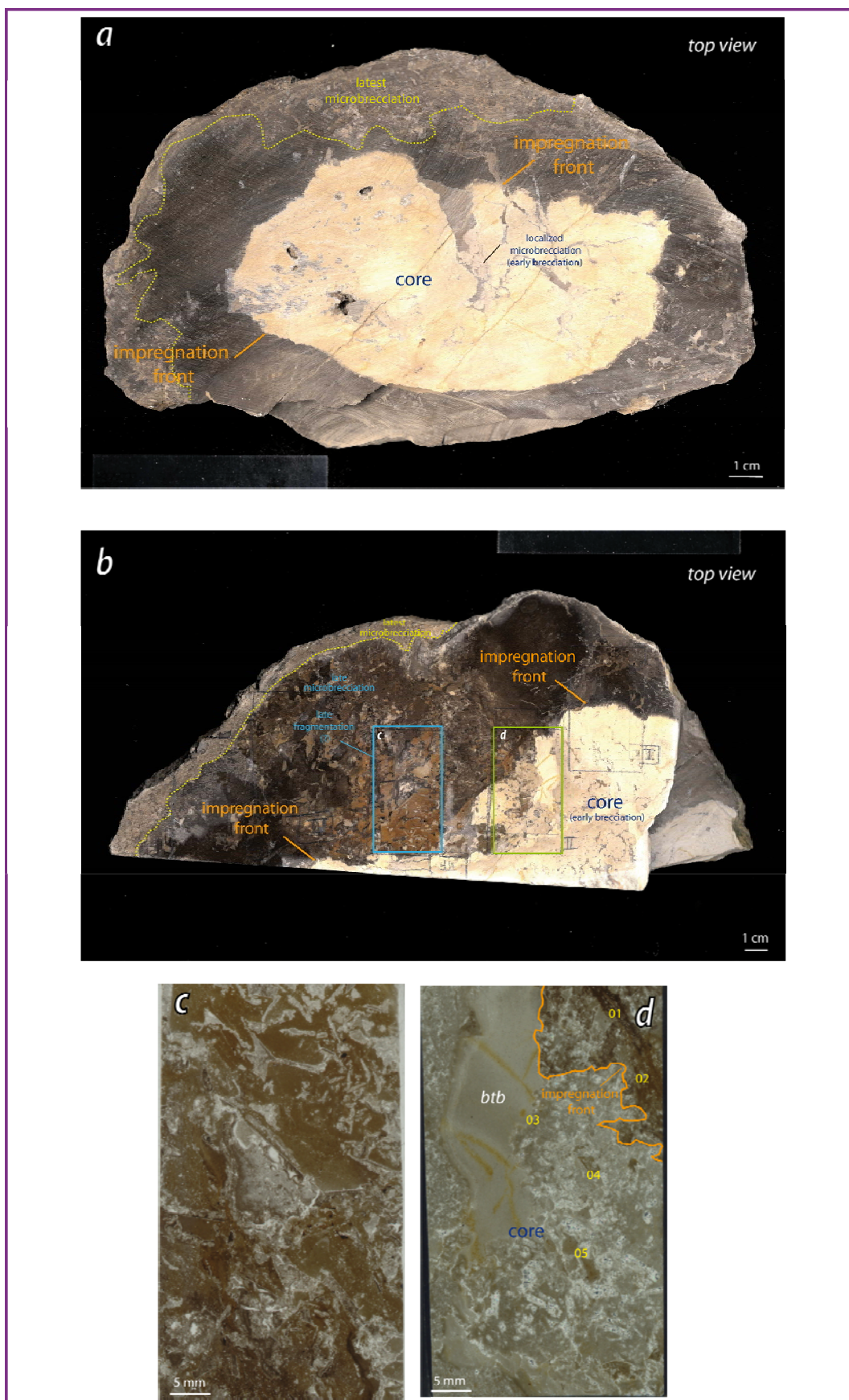
Fig. 4.1.31 - caption in the next page
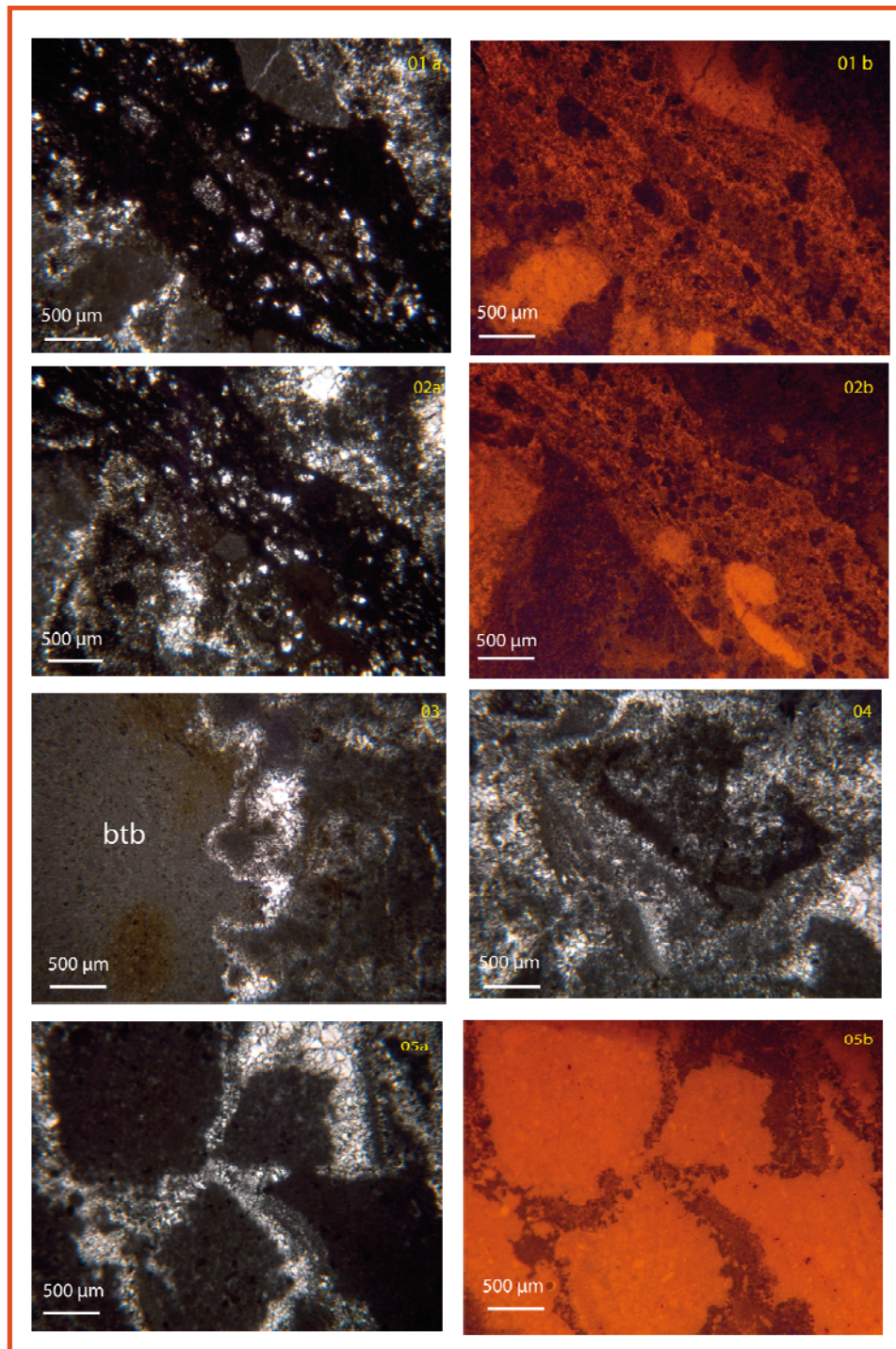
Fig. 4.1.31 - Cylindrical concretion; sample ABB, *Abbateggio Limestones Quarry*.
The late brecciation event accompanied by impregnation is recorded in this sample. The impregnation front is affected by the previous, presumably not yet completely lithified pale cream microbial facies, constituting the core of the sample (**a**). The facies variability with space is evidenced by a parallel cut (**b**), where disrupted and fragmented prismatic pseudomorphs after gypsum are contained both in the impregnated subfacies and in the pale cream subfacies (**b,c, d, 04**). In the pale cream subfacies there is also a possible relic of a bioturbation (btb; **b, d, 03**).
Microscale fluid-migration pathways in the impregnated subfacies (**01-02 a-b**, coupled transmitted light - CL view): exalted cross-cut relationship in CL view: bright yellow microbial fragments and moderately bright fluid microchannel, showing a mixed luminescence pattern, evidenced by the mostly dull microsparitized background.
Microbial microbrecciation in the pale cream subfacies: bright yellow microbial fragments, highly corroded (**05 a-b**, coupled transmitted light - CL view).
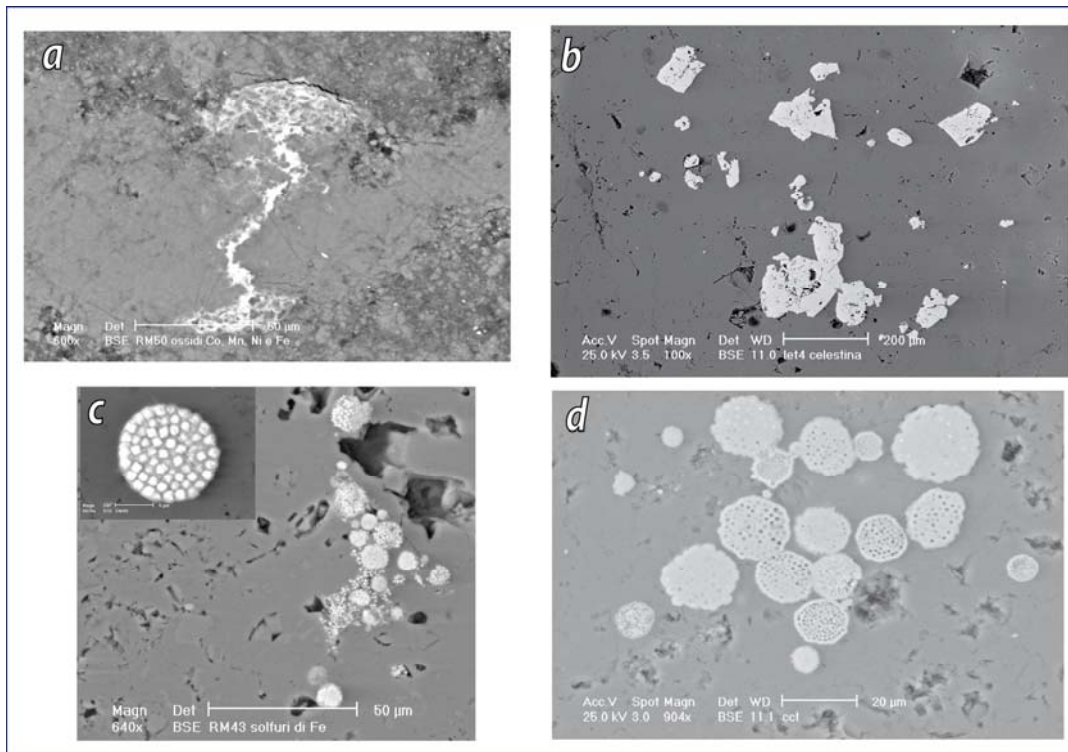
Fig. 4.1.32 - Reducing proxies in the Bcl - Ni-Co-Mn-Fe microveins (**a**); Celestite (**b**); Single and composite pyrite framboids (**c**); Ghost framboidal pyrite structure, without sulphur (**d**).

4.1.4 - *Geochemical dataset*

4.1.4.a - *Oxygen and Carbon stable isotopes*

The geochemical dataset from the Maiella area (Appendix 2; Fig. 37) is complex and shows wide ranges both in $\delta^{18}O$ (~ +5 down to -10 ‰ PDB) and $\delta^{13}C$ values (~ +5 down to -40 ‰ PDB). The major results will be first reported for each single lithofacies (BL, PL, FS) and then briefly discussed.

1) The isotopic signature of the BL (brecciated limestones lithofacies) can be clustered into three major groups (Fig. 37; Appendix 2):

- tar bearing limestones sampled at Madonna del Monte section (Fig. 4.1.3): typified by negative $\delta^{18}O$ and $\delta^{13}C$ signals (~ -6 down to -9 ‰ PDB and ~ -5 down to -15 ‰ PDB, respectively);

- tar bearing limestones sampled at Lettomanoppello section (Fig. 4.1.3): showing negative $\delta^{18}O$ values (down to -5 ‰ PDB) and $\delta^{13}C$ values concentrated in a very narrow range oscillating around the value of -25 ‰ PDB;

- brecciated limestones from Abbateggio-Mampioppo and Colle Castellano areas (Fig. 4.1.3): the $\delta^{18}O$ signal spans from positive to negative values (~ +4 down to -3 ‰ PDB), while the $\delta^{13}C$ values are generally slightly positive or approximate zero.
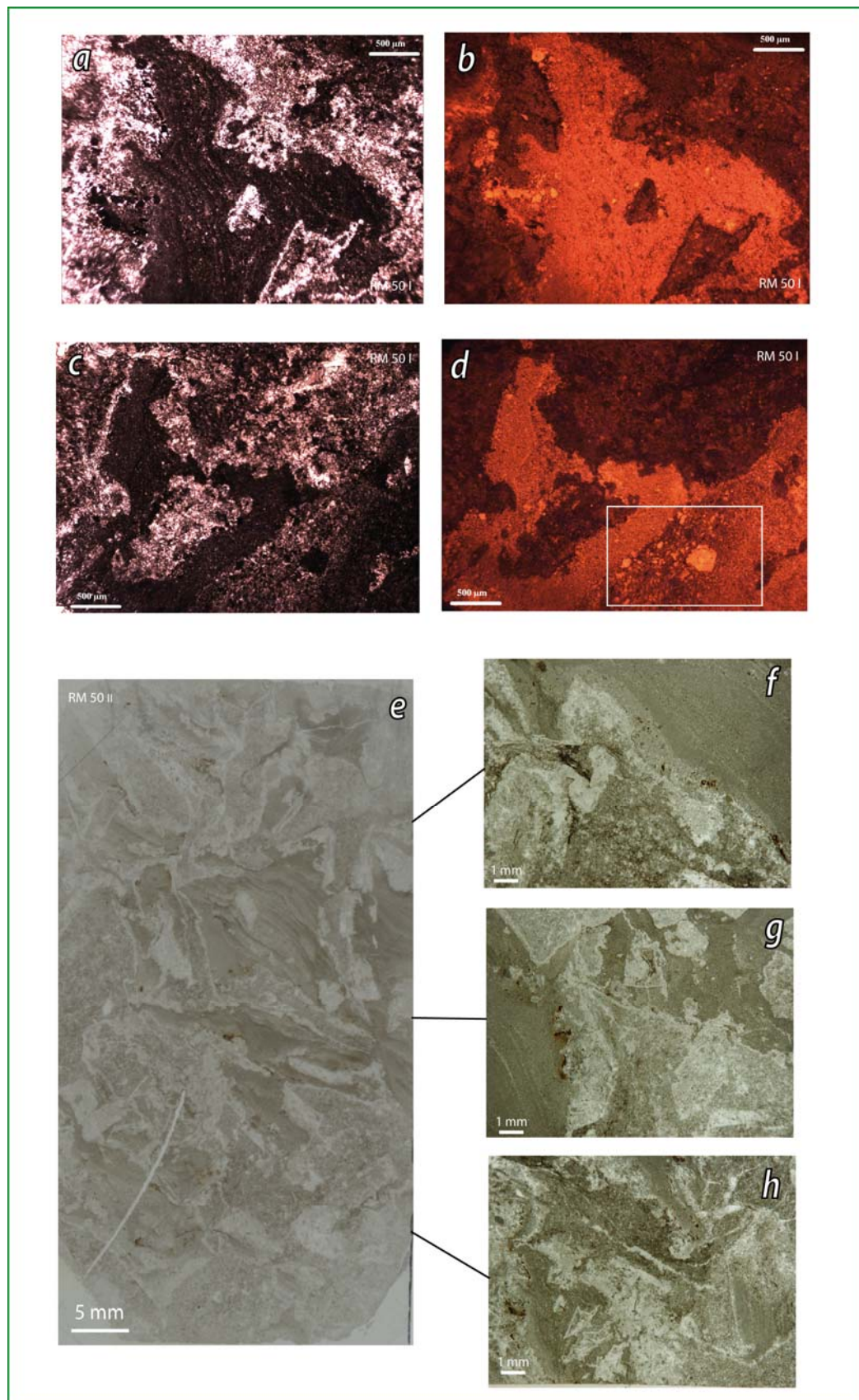
Fig. 4.1.33 - PL - Chaoticized fluidized facies (optical view, **e-h**). The microfabric is particularly exalted in CL view (**b**, **d**; transmitted light counterparts **a**, **c**): dull cemented microbialite, bright orange fluidized microbialite (weakly cemented) and the very bright orange microbial fragments (**d**, box).
Notice the corrosion contacts in any image.
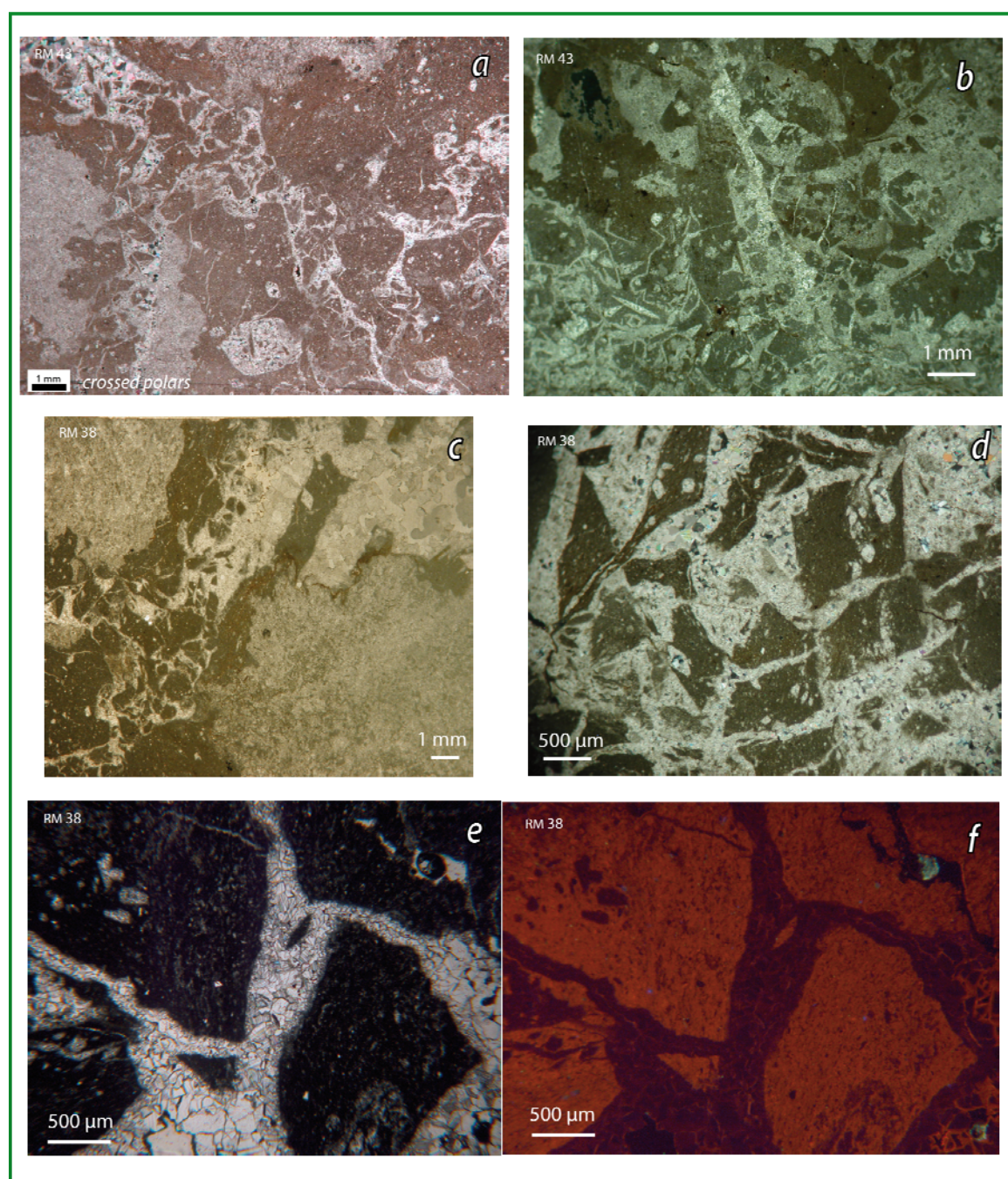
Fig. 4.1.34 - PL - Localized microbrecciation: sparry calcite cement supported-microbreccias. The CL view exalts the fluidized microtexture of the bright orange microbial clasts and the dull sparry cement (**f**; **e** is the transmitted light counterpart).
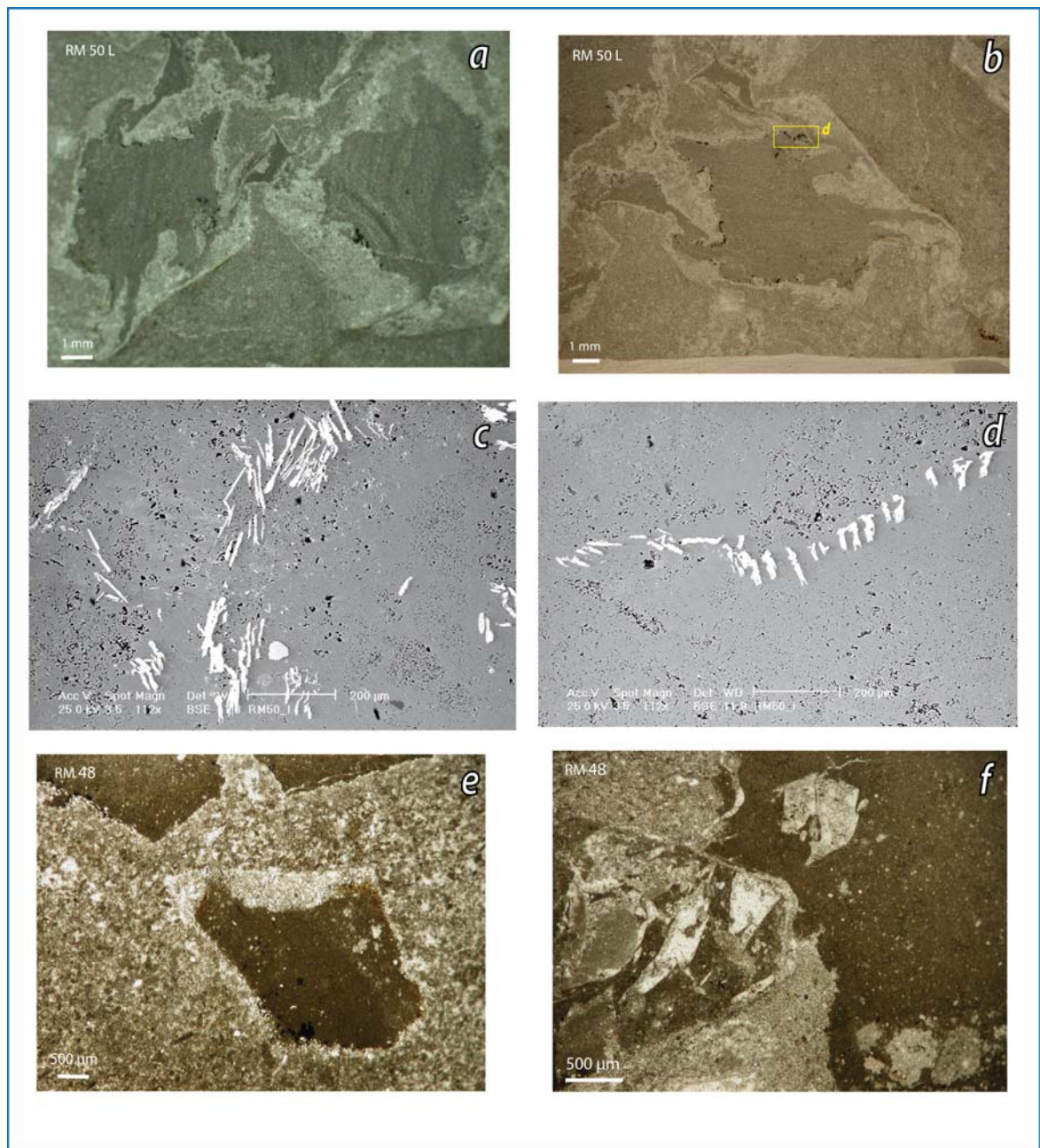
Fig. 4.1.35 - Pseudomorphs after gypsum reproducing at a small scale the complex history of these rocks. The pseudomorphs 1) were in origin gypsum crystals, growing in a mostly reducing environment which favoured microbial activity; 2) they were afterwards substituted by sparry and microsparry calcite, 3) later on experiencing in turn a polyphased corrosion by aggressive fluids. The fluidification events are the most probable responsible for the injected sediment that now fills the cores of many pseudomorphs. Notice the development of nedlee (**c**) and rod (**d**) shaped Fe oxide/hydroxide features, lying along the border between the injected sediment and the latest corrosion surface (SEM view).

At a small scale, the pseudomorphs record the alternating reducing and oxidizing conditions experienced by the sedimentary pile, possibly as a response to the microenvironmental changes led by the ascending fluids.
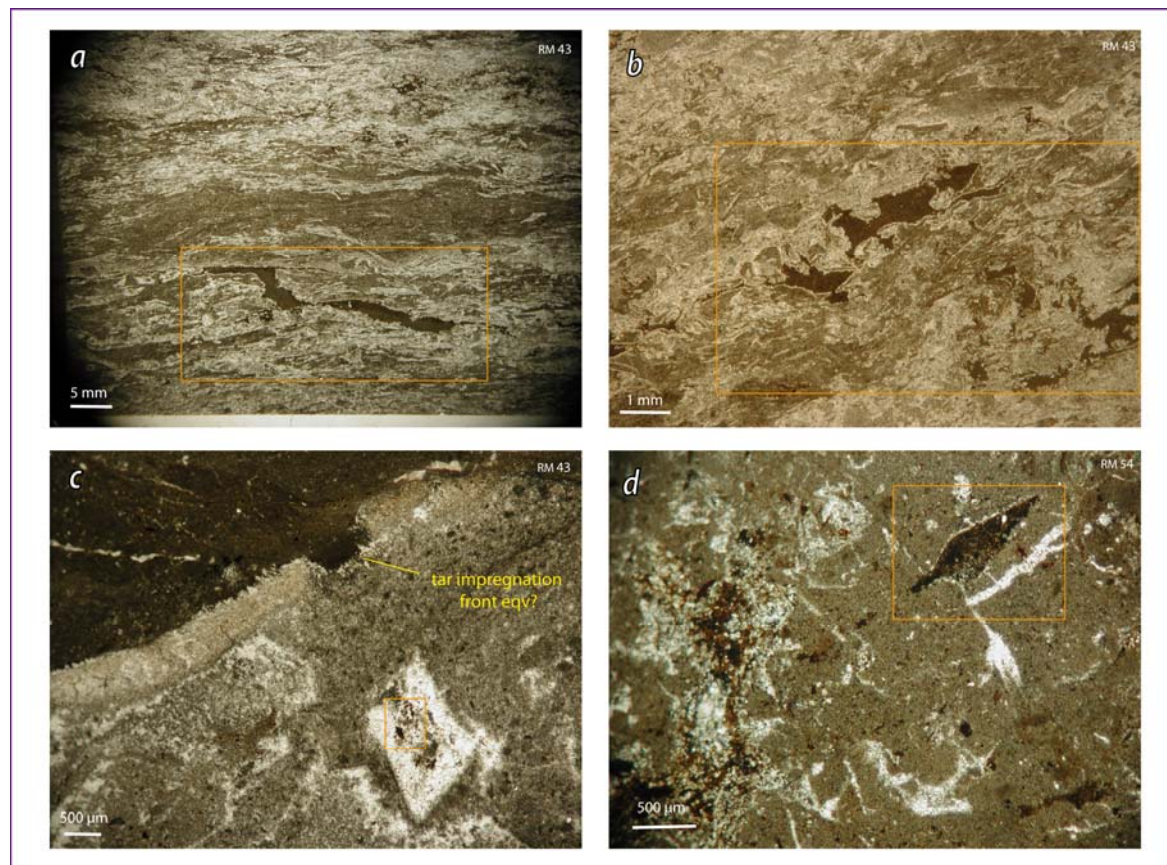
Fig. 4.1.36 - PL - Microtar and microtar equivalent structures: they perfectly resemble the microtar features occurring in the BL, even for the presence of the thin fibrous cement rim; they are represented by finely tar impregnated pelite (**a**, **b**, **d**) or tar (**c**, orange box). In **d** the impregnated pelite infills a corroded lenticular pseudomorph after gypsum (see also Fig. 4.1.34).

2) The patchy limestones (PL) mostly exhibit negative $\delta^{18}O$, concentrated between -2 and -4 ‰ PDB (Fig. 36; Appendix 2). By contrast, the wide variation yielded by their $\delta^{13}C$ signature, ranges from the positive to the negative peak of all the samples collected in the Maiella area, as clearly displayed in the stable isotopes cross plot (Fig. 4.1.37).

More specifically, three points can be highlighted:

- slightly negative $\delta^{13}C$ values have been obtained from the bulk analyses of the host sediment of Colle di Votta (-3.82‰ down to -10.89‰ -PDB).

- the carbonate grains contained in the host sediment yielded significantly more negative values: microbrecciated grains approximately show values of -11‰ PDB and the microtubular precipitates reach even more negative values, down to -39‰ PDB (Appendix 2).

- in the guest carbonates, the wide range of the signal suggests a mixing of many carbon sources. Interestingly, the most negative $\delta^{13}C$ values are yielded in the chaotic microfacies (i.e. samples RM 34a, RM 40a, RM 38; Appendix 2).

3) The carbonate samples from the fluidized sediment lithofacies (FS) exhibit a negative $\delta^{18}O$ - $\delta^{13}C$ signature (Fig. 4.1.37; Appendix 2). The botryoidal aragonite cement reaches $\delta^{13}C$ values down to
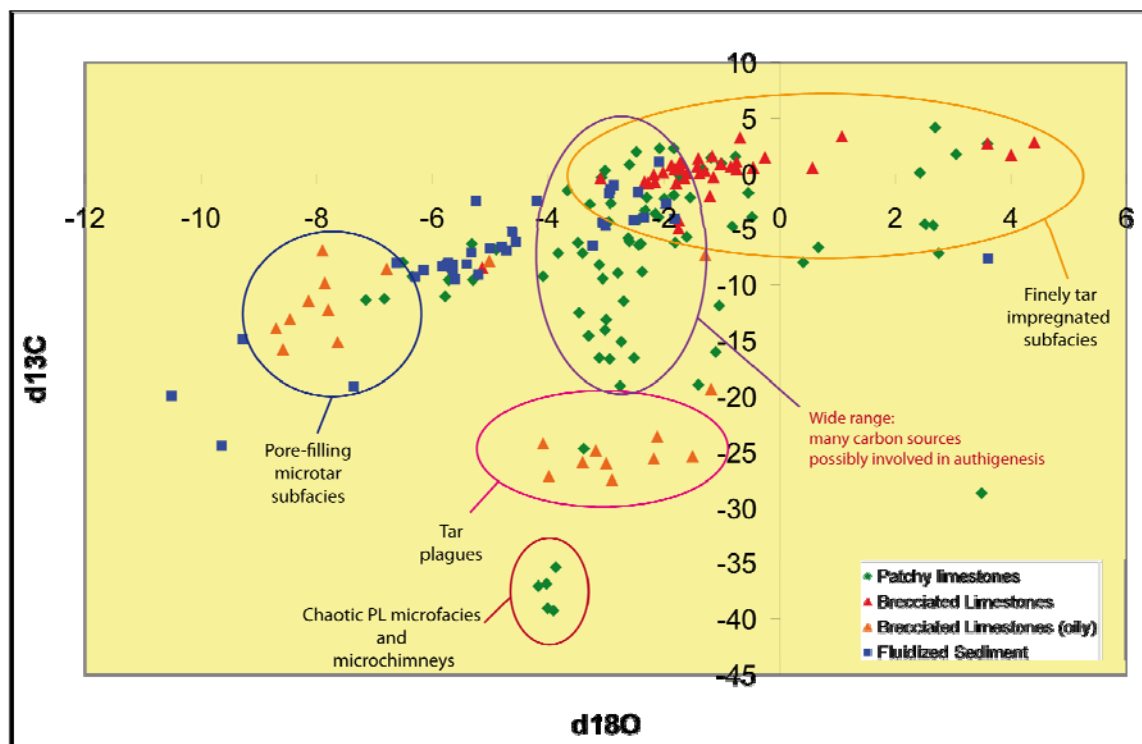
Fig. 4.1.37 - Cross plot of stable isotopes data of the Brecciated Limestones unit of the Maiella area.

-24.5 ‰ PDB, while the homogeneous white concretions are typified by δ^{13}C values within -8 and -9 ‰ PDB.

Interestingly, the high variation in both the δ^{18}O and δ^{13}C signals has been detected not only among the different samples, but also among the subsampled microfacies. Shifts of 20‰ of the δ^{13}C signal within the same sample have been recorded (Appendix 2; Fig. 4.1.38).

In sum, the isotopic signature is lithofacies-independent and seems extremely biased at a first glance. Nonetheless, taking into account the relative timing of the post-depositional events evidenced by microfacies analysis, the high variations yielded by the stable isotopes characterization can be partly explained.

The youngest event is recorded both by finely tar-impregnated facies and bubble/pore-filling microtar injections (tar bearing facies s.s.). For the finely tar-impregnated facies a direct correlation with the positive δ^{18}O record can be established, while the δ^{13}C signal is generally typified by positive or slightly negative values (down to ~ -11‰). These patterns are not exhibited by tar bearing facies s.s. (the facies containing pore-filling tar).

The facies framework predating the aforementioned event is more complex, given the commonly occurring chaoticization of the facies related to fluidification processes. A relative timing of the subevents is hardly established and the small scale heterogenities hamper the achievement of a clean geochemical signal with the sole utilized subsampling method. In this view, more refined subsampling methods are advised for detailed investigations. As a result, the

interpretation of the stable isotopes record remains obscure to a major extent. It is even difficult to isolate the primary signal, represented by the microbial/clotted peloidal facies, since all the samples are highly recrystallized and late diagenetic processes likely provided the last overprint.

The following points, regarding the $\delta^{18}O$ signal, can be enucleated:

- Once explained the positive values (finely tar impregnated facies), the $\delta^{18}O$ is concentrated to a major extent within a range oscillating around -2 and -3 ‰, whose end members reflect the isotope composition of the calcitic carbonates precipitated in equilibrium respectively with the early Messinian seawater and the brackish late Messinian seawater (Pierre & Rouchy, 1998).

- The more negative $\delta^{18}O$ values can be easily explained with freshwater dilution phenomena, that represent the commonly invoked factor to explain this kind of signature. This is consistent with the high recrystallization degree mentioned above, that could have likely provided the last overprint. Reasonably, the final $\delta^{18}O$ signal can be significantly altered respect to the original one, because of the well known T-dependence of the $\delta^{18}O$.

- On another hand, in context like the one being investigated, the occurrence of gas hydrate cannot be directly ruled out in view of the interpretation of the geochemical signal, since geochemistry of pore fluids is significantly modified by the formation/dissociation of gas hydrates.

    Gas hydrates trap preferentially ^{18}O-rich water molecules, resulting in ^{18}O depletion of the remaining pore fluids (Sample & Kopf, 1995; Aloisi et al., 2000; Ussler & Paull, 2001; Pierre & Rouchy, 2004). By contrast, the decomposition of gas hydrates liberates ^{18}O-rich freshwater, which may locally contribute to the ^{18}O enrichment of pore solutions (Kopf et al., 1995). In particular, according to Pierre & Rouchy (2004) the coupled $\delta^{18}O$ - ^{13}C signature in the diagenetic carbonates is a proxy for the formation/dissociation of gas hydrates: a ^{18}O-depleted - ^{13}C-enriched signal is indicative of gas hydrate formation, while a ^{18}O-enriched - $\delta^{13}C$-depleted is indicative of gas hydrate dissociation.

    In the Maiella area the ^{18}O-depletion is coupled to ^{13}C-depletion, thus ruling out both the hypothesis. Furthermore, to evaluate such conditions, the complex fluid-rock interaction phenomena evinced through the facies analysis should be considered.

In sum, the $\delta^{18}O$ signal in the study case can be grouped in three main clusters:

1. positive values: in correspondence to finely tar-impregnated facies/microfacies;

2. slightly negative values comprised within the range -2 and -3 ‰: accounting for the precipitation from the Messinian seawaters;

3. moderately negative values: affected by freshwater dilution and/or recrystallization phenomena.

	d^{18}O	d^{13}C
a	0,41	-7,96
b	2,7	4,14
c	0,67	-6,6
d	-1,05	-11,81
e	-1,1	-16,04

	d^{18}O	d^{13}C
a	-3,11	-0,41
b	-0,68	3,19
c	1,07	3,34
d	-1,43	0,55

	d^{18}O	d^{13}C
a	3,05	1,72
b	-2,13	-3,62
c	-2,43	-6,37
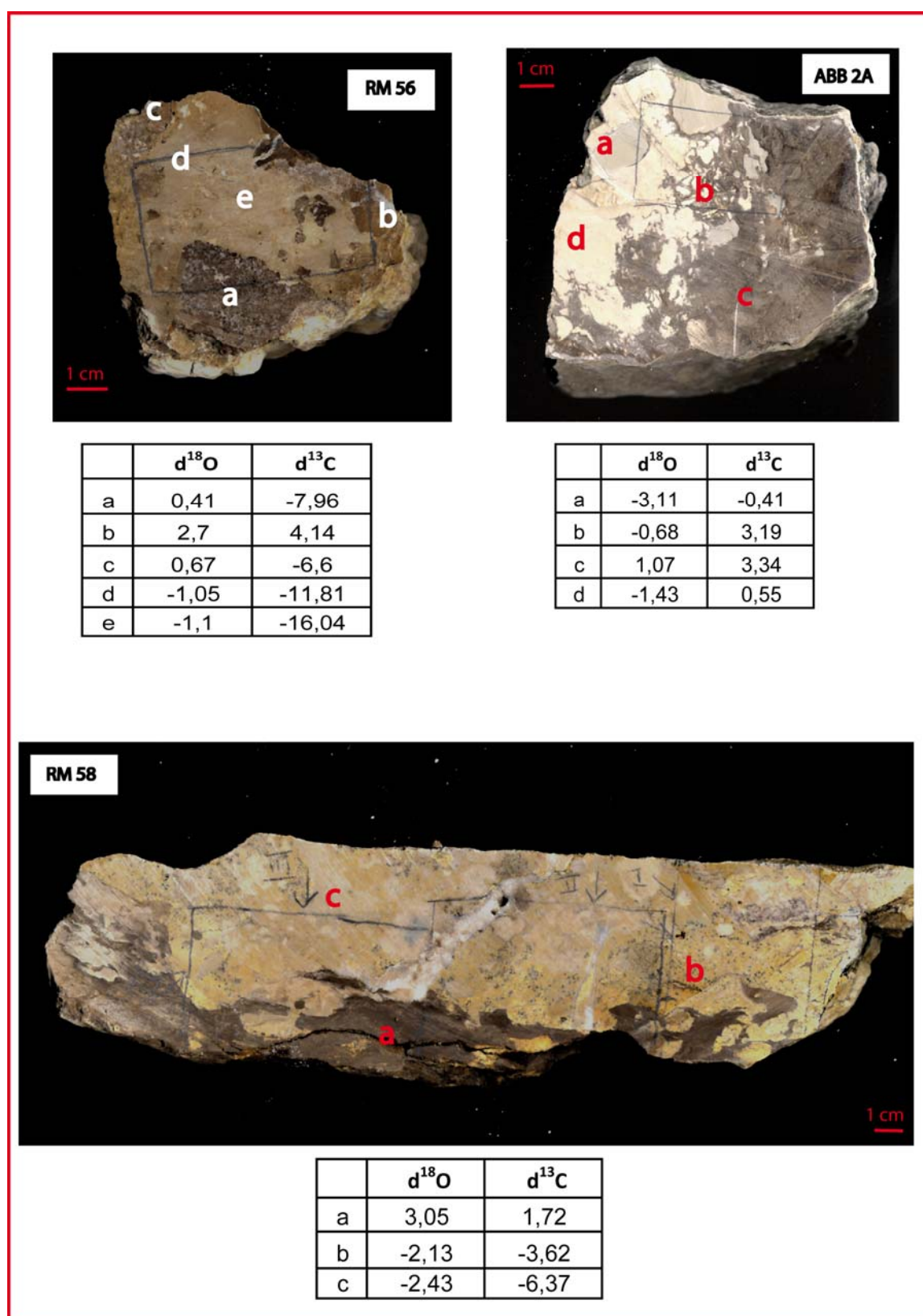
Fig. 4.1.38 - Subsampled facies yielding high variation in the isotopic signal. The positive δ^{18}O signal is shown by the dark brown, finely impregnated portions, typified on the other hand by positive to slightly negative δ^{13}C values. In the other subfacies the signal is more complex (see text for explanation, Par. 4.1.4.a).

With respect to the δ¹³C signal, the results can be summarized as follows:

- The $\delta^{13}C$ record reaches values down to -40 ‰ PDB, testifying the contribution, at least to some extent, of the anaerobic oxidation of methane to the isotopic signature. Specifically, within the range -25/-40‰ PDB, that is by far considered the indisputable proof of the role played by methane (Clari et al., 2009 and ref. therein), only a minor number of samples is enclosed, mostly ascribed to the oily sublithofacies of the BL from Lettomanoppello (Fig. 4.1.37). The few others samples belonging to this isotopic range are represent chaoticized PL and microtubular precipitates (Appendix 2). Both their negative peak, reaching a moderately high depletion, and the facies analysis, testifying the occurrence of heavy hydrocarbon-rich fluids interacting with the sediment, point to a thermogenic nature of the parent methane involved in authigenesis.

- Beside the most depleted and the aforementioned finely impregnated facies/microfacies typified by $\delta^{13}C$ values generally higher than - 5 ‰ PDB and even positive, the rest of the samples yields a general negative $\delta^{13}C$ signature, spanning from ~ -5 and -20‰. In seep environments this range represents one of the most puzzling research issue, since these values can be explained by the mixing of different carbon sources, that can envisage in turn many possible scenarios (see Ch. 2.1.2 for details), and/or by the occurrence of other diagenetic processes, like decaying organic matter, coupled or not to sulphate reduction (Raiswell, 1987; Mozley & Burns, 1993).

In the study case, in which the occurrence of hydrocarbon-rich fluids through the sedimentary pile is independently proved by facies analysis and by organic geochemistry data (Ch. 4.1.4 b), beside this background considerations accounting for the nature of the fluids and for the occurrence of other diagenetic processes experienced by carbonates, I would stress the importance of the following additional points that even enhance a biased geochemical signal:

o the small scale chaoticization of the microfacies;

o the fluid-rock interaction: the chemical exchange between ascending fluids, whatever their nature, and the sedimentary pile passed through, is in general an obscure matter; in this specific case, the commonly occurring small scale heterogenities must be taken into account when analyzing the geochemical dataset.

These points, commonly not put in evidence, are of primary importance in the case of the Bcl unit. Herein they are not deeply discussed and debated, but represent key-points and guidelines to set forthcoming investigations.

In conclusion, the possible explanation of this middle-spanning subset of data lays in a complex interplay of:

1) an original mixed sources signal, related to the contribution of different carbon sources, both carried by the hydrocarbon-rich ascending fluids and already present in the interacting sedimentary column. It is nonetheless likely that a certain amount of thermogenic methane contributed to the final signal;

2) a complex fluid-rock interaction, leading to high variability of the related precipitation and dissolution phenomena through space and time;

3) a variation in the fluid composition, since at least two major fluid migration events have been enucleated in the Maiella area in upper Messinian times;

4) a mixed microfacies signal, related to the sampling method, due to the extreme chaoticization of the fabric at any observation scale.

4.1.4.b - Organic geochemistry data

Fourteen samples, representative of the three main lithofacies of the Bcl (Appendix 5), were selected for organic geochemistry analyses, on the basis of the impregnation patterns revealed by facies investigations. For correlation purposes, also a tar sample from the younger Bolognano Fm (sample PIL, Appendix 5) was taken into account.

The results of the rock characterization, shown in the Appendix 5, can be summarized in the following points:

- The samples are typified by high TOC, reaching values up to 11,07 % (sample LET, tar bearing brecciated limestone; unwashed). Only the sample CBU 3c-4 (brown pelite, FS lithofacies) yields a very low organic content and therefore was not considered for the RE-pyrolisis analyses.

- TOC, S1 and S2 were soluble in organic solvent: this means that OM is mostly represented by migrated hydrocarbons and the kerogen content is negligible. As a consequence, S2 doesn't represent the kerogen, but the heavy fraction of the hydrocarbons, where S1 is the light fraction. The samples show high values of S2 if compared to S1: this points to a clear predominance of the high fraction (high HI, oil-prone type). An exception is represented by the sample CT 06 (brown mixed pelite, FS lithofacies) that, in spite of its high TOC, is characterized by a low petroleum potential (low S2) and low-kerogen HI (gas prone); as a consequence, this sample wasn't considered for bitumen characterization analyses.

- The T_{max} parameter indicates a low maturity of the samples. The maturity degree of the samples was confirmed by the independent vitrinite reflectance analysis, exhibiting R_0 values of 08-09%.
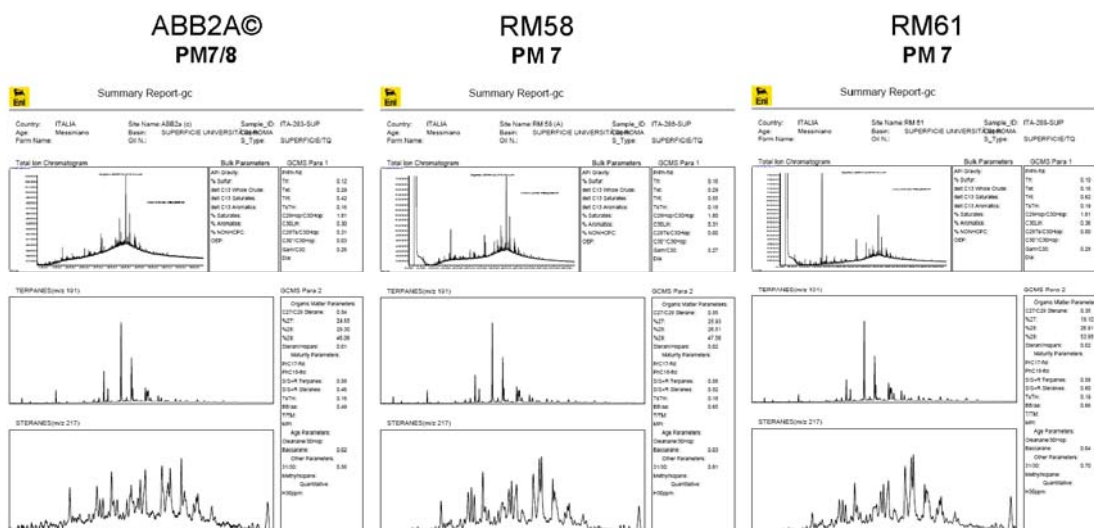
Fig. 4.1.39 - Chromatograms in the less biodegraded samples.
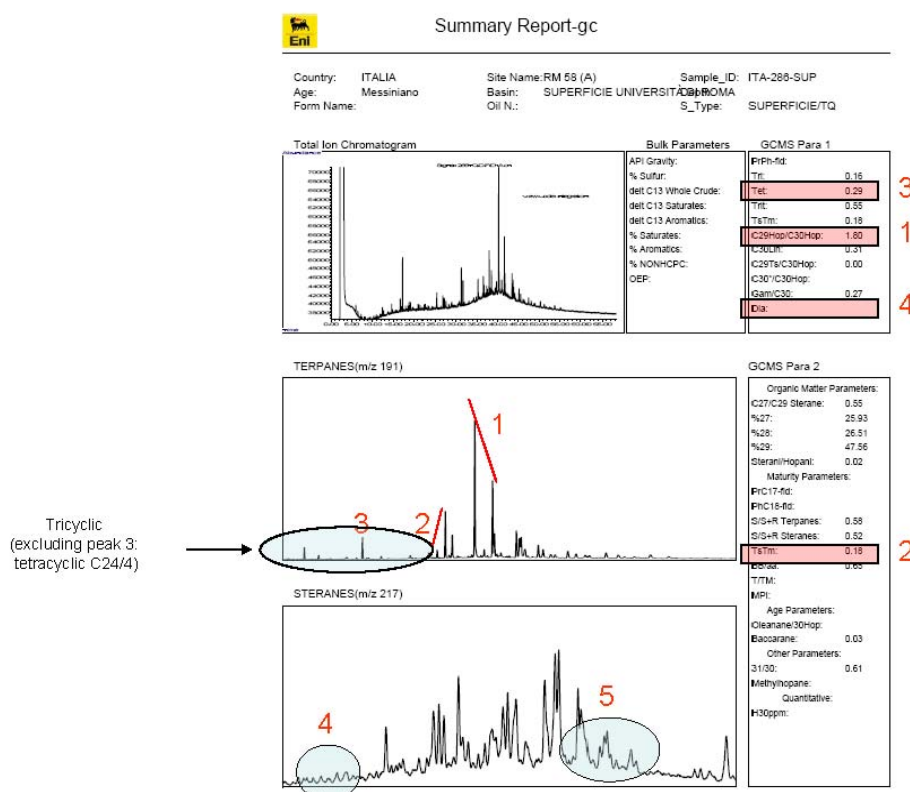
Fig. 4.1.40 - Chromatograms showing proxies for a carbonatic source rock: 1) C29/C30 hopan; 2) Ts/Tm ; 3) C24/4 abundance; 4) Diasterans absence; 5) Methilsterans occurrence.

The listed samples (Appendix 5) were analyzed for <u>bitumen characterization</u>, with the exception of the aforementioned CBU 3c-4, CT 06, MM/a1 and MM/f. The 11 analyzed samples provided biomarkers results, except for the sample DEC 1-3 (pelites and marls, incorrectly defined

bituminous). The main results coming from the bitumen characterization are summarized in the following points:

- Though the samples yielded high biodegradation index (PM 7-10; Appendix 5), it is possible to establish the affinities among them through the molecular analyses, since all the chromatograms show similarities in the tricyclic fraction (Fig. 4.1.39), more resistant to biodegradation.

- The similarities among the samples are even more highlighted by their uniform δ^{13}C signal of the bitumen, comprised in the very narrow range -26,31/- 28, 66 ‰ (Appendix 5).

- The GC-MS analyses also put in evidence peculiar patterns of presence/absence of molecular classes typical of carbonatic source rock (Fig. 4.1.40).

Since all the samples are correlatable, it is possible to state their common origin from a carbonatic source rock, reasonably Cretaceous in age (Riva, pers. comm.): indeed, combining the data of absence of the olenan - a typical Tertiary molecule - with the Messinian age of the infilled sediments, the most likely age of the source rock is older than Palaeocene.

The geochemical data definitely confirmed the macroscopic and microscopic geological evidence of oil impregnating the Messinian Brecciated Limestones. This oil is the same, presumably Cretaceous, contained in the discontinuities and in the primary porosity of the underlying Bolognano Fm. This oil clearly impregnates the BL and PL lithofacies, but doesn't seem to affect the fluidized sediments examined.

4.1.5 - Discussion

4.1.5.a - The depositional environment in the early post-evaporitic deposits

The paleoenvironment in the post-evaporitic deposits has been deciphered considering: 1) sedimentary fabric and microfacies; 2) mineralogical and compositional evidences; 3) framboidal pyrite size distribution; 4) natural radioactivity as indirect proxy for dysoxic/anoxic environment (authigenic uranium values, Th/U ratios).

Bottom redox conditions in marine and lacustrine ancient basins are often inferred by the occurrence of peculiar sedimentological structures and microfaunal assemblages. The co-occurrence, in such environments, of authigenic uranium, framboidal pyrite, barite and Fe-Mn nodules and encrustations, provides a good constraint for paleo reconstructions.

Authigenic uranium is a common constituent of hydrocarbon source rocks: it forms at the sediment-water interface under oxygen-deficient conditions and accumulates together with organic matter (OM). Its precipitation is triggered by the reduction of the soluble U^{6+} ion in seawater to insoluble U^{4+}. With respect to black shales, uranium content has even been used to estimate the TOC. In the Colle di Votta p-ev deposits, dysaerobic conditions are indicated by the co-occurrence of: fine laminations, lack of benthic biota and high U-content. Uranium

concentration in the carbonates reaches values up to 5 ppm, which are extremely high if compared to the mean values recorded in carbonate lithofacies: hydrocarbons incorporations could be responsible for such high values (see Ch. 4.1.5.e). More specifically, the NRD data are consistent with strongly anoxic environments under arid conditions (U∕Th>1.3, Appendix 1; Jones and Manning, 1994). The arid conditions of the p-ev1 phase were frequently interrupted by more humid episodes, responsible for the increase in extra-basinal detrital grains (U∕Th<1; Sampalmieri et al., 2010).

Also authigenic pyrite forms under anoxic conditions and replaces organic matter: 1) the increase in pyrite content and OM are directly correlated; 2) the size distribution of framboidal pyrite (consistent with sulphate-reducing bacterial activity) is considered a measure of redox conditions within the sediment. Pyrite is a stable phase under anoxic conditions and iron-bearing minerals are intimately associated with organic matter decomposition. The populations of framboidal pyrite shows a mean diameter of 4-8 μm, which is typical of dysaerobic conditions with anoxic bottom waters (Wilkin et al., 1996, 1997; Wilkin & Barnes, 1997; Bond et al., 2004; Wignall et al., 2005).

Barite is an authigenic mineral related to Corg content, since its organic precipitation is triggered by sulphate-reduction processes occurring in decaying OM-bearing microenvironments. Finally, also Fe-Mn oxyhydroxide are typical indicators of redox conditions. Barite and Mn–Fe oxyhydroxide: occurring within the p-ev deposits of the Colle di Votta section can form in situ by inorganic precipitation, either on the basin floor or within unconsolidated sediments. Barite can inorganically precipitate directly from the water mass in microenvironments containing decaying organic matter (Bishop, 1988).

Mineralogy definitely provides additional clues to the palaeoenvironmental conditions at the time of deposition.

As testified by U-bearing finely laminated barren deposits, yielding small authigenic framboidal pyrite and barite, anoxic conditions in a stratified water mass characterized the early post-evaporitic phase.

The correlatable fine-grained deposits from Maccarone section show analogous features in terms of mineralogy and NRD (Sampalmieri et al., 2010). They are rich in organic matter and barren in benthic biota, pointing to high organic carbon preservation in low-oxygen bottom water (Emerson and Hedges, 1988), coupled to high organic matter input from continental weathering. In addition, abundant plant remains have been observed in both analyzed sections. In particular, a rich pollen flora consisting of 130 taxa was identified in the Maccarone section (Bertini, 2006): frequent alternation between herbs and subtropical to warm arboreal taxa definitely depicts a dry early post-evaporitic phase, punctuated by wet climate episodes with strong continental runoff

(Bertini, 2006). By contrast, the p-ev1 carbonate lithofacies in the two sections yield different textures and $\delta^{18}O$ values, pointing to different genetic processes. The texture and stable isotope analysis of the carbonate facies from the Maccarone section testify an evaporative environment (Bassetti et al., 2004; Sampalmieri et al., 2010), whereas the brecciated carbonates from the Colle di Votta section - characterized by negative $\delta^{18}O$ values - are related to more complex processes most likely connected with a fluid-rich diagenetic environment with high pore-fluid pressure (see next paragraphs).

Fine-laminated deposits, generally barren in benthic biota and autochtonous biota are well known from the Messinian deposits of the whole Mediterranean Basin. This kind of deposits were recovered in several western Mediterranean ODP sites (Iaccarino & Bossio, 1999) and in the Tyrrhenian abyssal plain (ODP Site 652; Borsetti et al., 1990; Cita et al., 1990) as well as in the Mediterranean borderlands (Vismara-Schilling et al., 1976; Fortuin et al., 1995; Bassetti et al., 1994, 1998; Roveri et al., 2001; Cosentino et al., 2005). It has been shown that a precise correlation can be established among the pre-Pliocene deposits at ODPSite 652, the thick Messinian Lago-Mare succession drilled at the Mondragone 1 well (Garigliano Plain) and the Maccarone and Maiella outcropping sections (Cosentino et al., 2006, Sampalmieri et al. 2010). The possible correlation between the Maccarone section and ODP Site 652 suggests an extension to the Central Mediterranean Basin of the strongly anoxic environment and the paleoclimatic scenario reconstructed for the Messinian Adriatic sub-basin from the Maccarone and Colle di Votta sections.

The higher NRD values of p-ev1 (high U_{aut}), in comparison with the sapropelitic layers of the Primary Lower Gypsum (low U_{aut}), could be explained by the development of more restricted conditions in the circulation of the Mediterranean water mass as a consequence of the complete closure of the Gibraltar Strait at the evaporitic/post-evaporitic transition. The occurrence of post-evaporitic well laminated barren deposits also from the Maccarone section, the Mediterranean borderland sections and ODP sites suggests that these anoxic conditions extended to other sub-basins of the Mediterranean region.

The strong increase in the γ-signal at the MES of the Colle di Votta section, which in the p-ev1 deposits reaches higher values than the evaporitic sapropel layers, represents a stratigraphic marker for the recognition of the lower p-ev1 deposits in the whole Mediterranean Basin.

In the latest Messinian frame, authigenic uranium (Th/U ratio, mostly <<1), barite, ankerite, Fe-Mn oxyhydroxide and small (5-8 µm) authigenic framboidal pyrite, clearly define strongly paleoredox conditions - from dysaerobic to fully anoxic - in the Adriatic sub-basin of the Mediterranean Sea.

4.1.5.b - Fluid migration pathways and anatomy of the deposits

Two fluid migration events have been enucleated through the microfacies analysis. Nonetheless the second event did not completely overprint the first one, and gave rise mostly to oil impregnation and localized microbrecciation. As a consequence, the first event can be depicted as the major one, responsible for the creation of the principal conduits, eventually reused by the following second migration event.

Fluid migration pathways have been observed from the mesoscale to the microscale and are associated to any lithofacies type.

The FS lithofacies shows the most spectacular conduits, cutting even the pre-MSC related succession. The conduits are typified by a facies association yielding generally low ^{13}C depletion (excepts for the aragonitic botryoids) and also scarce tar impregnation content (par. 4.1.4.b). The scarce authigenic carbonate precipitation is consistent with low fluid rock interaction (low FRI), presumably related to localized high flux rates. The carbonate fraction is accompanied by fine sediments yielding extreme chaoticization and microfolding. This fabric, coupled with the anomalous brittle behaviour shown by the gypsum evaporitic unit and the geochemical signal, points to the catastrophic nature of the associated fluid migration event.

In the widespread massive brecciated limestone lithofacies (BL), fluid migration channels occur only at locations at the mesoscale. The fluid escape trajectory at the Abbateggio Limestone Quarry (Fig. 4.1.14) can be easily ascribed by converse to the latest fluid migration event, and thus better defined as an oil-impregnation front. Of major interest in the BL is by contrast the intense fragmentation pattern, accompanied by higher matrix content shown at locations in the brecciated bodies: possibly, in correspondence to those sites the fluid flow was more focused than elsewhere within the brecciated masses. Microscale cross-cutting patterns and fluid flow trajectories are commonly occurring. The general more depleted carbon isotopic signature of the BL is consistent with lower flux rates of the hydrocarbons involved in the event; nonetheless the following oil impregnation presumably provided a successive enrichment to the previous acquired signal.

In the PL lithofacies the fluid migration proxies are unrevealed by the microfacies: the microtubular precipitates associated to the host sediment, on the basis of their depleted isotopic signal and their strikingly resemblance to present-day analogues (Fig. 4.1.24), can be defined microchimneys. They possibly testify lower flux rates coupled to higher fluid-rock interactions, since some of the most ^{13}C-depleted signals are recorded in this lithofacies (Appendix 2), pointing to AOM directly involved in authigenesis. Notwithstanding, it must be pointed out that this study revealed that the sole isotopic signal is often inadequate to define seep facies, since small scale high variations commonly.

<u>An ancient oil field</u>

Hydrocarbons have long been studied in the pre-MSC carbonate rocks of the Maiella Mts: a well-known geofluid reservoir is hosted in the carbonate sequence of the Maiella anticline. Within the fractured reservoir, discontinuities affecting the Tre Grotte Fm (slope limestones, upper Cretaceous) are thought to have enhanced hydrocarbon migration, whilst the discontinuities of the Bolognano Fm (ramp carbonates, Oligo-Miocene), showing a general low connectivity, could have mostly provided conditions for their storage in the open fractures and primary pores (Marchegiani et al., 2006). Some authors, by contrast, pointed out the role of the Bolognano Fm also as a fluid migration site through its discontinuities (Agosta et al., 2009; 2010).

The organic geochemistry data (par. 4.1.4.b) testify that the same oil impregnated both the Bolognano Fm and the upper Messinian brecciated limestone unit. This can lead to two possible scenarios: 1) *From a fractured reservoir to a seeping, locally venting seep site.* In upper Messinian times, HC-rich fluids migrated from a Cretaceous reservoir and flowed along discontinuities in diagenized carbonates (Cretaceous to middle-upper Miocene in age), impregnating and interacting with the early diagenized post-evaporitic upper Messinian succession. 2) *A remobilized oil, temporarily stored in the diagenized ramp carbonates, re-activated after a major drawdown of the sea level.* According to this scenario, the Cretaceous oil could have migrated along the Maiella succession in two steps: at first before Messinian times, coming from a Cretaceous reservoir and being temporarily stored in the ramp limestones and further remobilized after the major drawdown of the sea level in the upper Messinian.

In view of that, it must be considered that leached zones below unconformities are considered among the favored settings for carbonate reservoirs (e.g. Paradox Basin, Flügel, 2004).

4.1.5.c - Primary vs. secondary processes: rheological behaviour, fluidification and brecciation

It was possible to establish a relative timing of the post-depositional events in the Bcl, on the basis of only a few samples since the microfacies are often extremely chaoticized. The impregnated samples from Abbateggio area provided the key to enucleate:

1. an earlier brecciation event, accompanied by a catastrophic fluid release focused in correspondence to mesoscale conduits and leading to an extreme fluidification of the facies at any scale. Brecciation was mostly experienced by the early cemented (microsparitized) portions and exhibits a scale invariant pattern.

2. a later brecciation event was accompanied by oil impregnation, that took place in two ways: on one hand, the portions uncemented by that time became finely impregnated, and this fluid-rock interaction provided a specific oxygen and carbon isotopic signature in the subfacies (from slightly negative $\delta^{18}O$- $\delta^{13}C$ signature); on the other hand, the presumably already

cemented carbonate portions hosted the oil in the microporosities. No impregnation occurred in correspondence to the FS lithofacies, while the BL and the PL experienced a similar history, with the aforementioned microfabrics.

The Cretaceous source rock feeding the system likely released at first the light hydrocarbons fraction, whose composition was probably accompanied by the thermogenic methane, as consistent with the isotopic signature (the most depleted values are consistent with processes of AOM, but the moderate degree of the depletion points to a thermogenic nature of the methane involved in the process).

Soon after, the upward migration of heavier hydrocarbons and oil took place, but this latest fluid migration event wasn't accompanied by great overpressures as the first one, since the major conduits fluid migrations had already been created.

In both cases, the rheological behaviour recorded in the studied unit is highly inhomogeneous, testifying possibly both localized overpressure and heterogenities in a partially lithified sedimentary pile.

In such a context, the invoked trigger for brecciation is fluid overpressure. Remarkably, this is consistent with:

o   the observed sedimentological characters, that clearly rule out both a resedimented nature and collapse-related phenomena;

o   the scale independent pattern of the breccias (Fig. 4.1.41) presumably reflects a fractal pattern, that in the breccias is commonly related to fluid-induced processes.
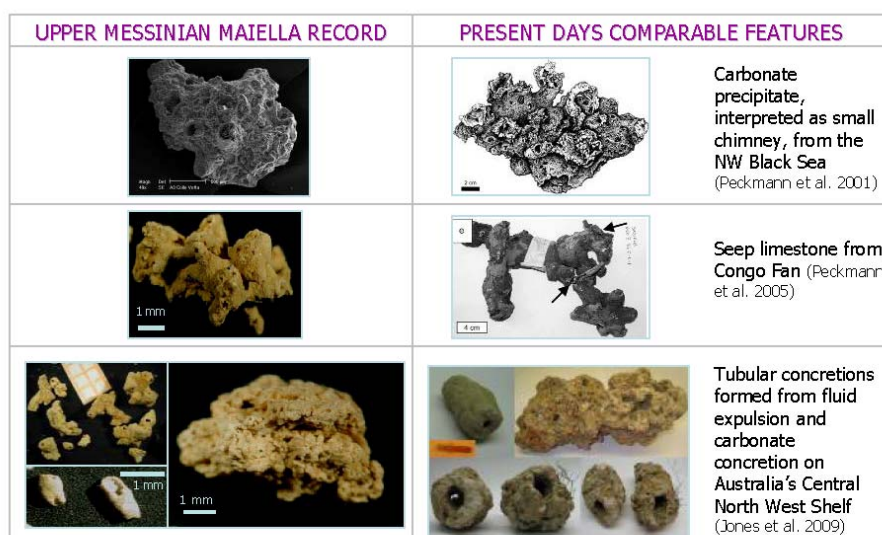
Fig, 4.1.41 - Comparison between the grains precipitated within the host sediment of the patchy limestones at Colle di Votta and features sampled in present day fluid flow sites.

4.1.5.d - Seep-limestones markers and fluid-rock interaction

In sum, some peculiar seep limestones markers were thus identified in the Bcl:

1) Chimneys and microchimneys

2) Brecciation and microbrecciation

3) Patchiness of concretions

4) Pyrite bearing clotted microbialites

5) Celestite and barite

6) Botryoidal aragonite

7) Wide ranges of negative δ^{13}C data.

Though the samples never gain extremely negative δ^{13}C values, even an unusually large isotopic heterogeneity at millimetre scale is considered consistent with methane-influenced processes.

The different fluid migration events affecting the Bcl unit also resulted in possibly alternating reducing and oxidizing phases, as evidenced by the multiple occurrence of: corrosion surfaces, microspar precipitations, sediment infillings and by the co-occurrence of both oxidizing and reducing proxies. This complex history represents the possible local response to complex fluid-rock interaction, variable through space and time. These alternating micro-environmental changes are possibly responsible for the localized presence of subrounded clasts in the brecciated bodies, whose rim was likely corroded by aggressive fluids.

4.1.5.e - The timing of the fluid migration event

The fluid migration features and the brecciated fabrics:

- are mainly developed in the early post-evaportic succession (p-ev1), resting above the Messinian Erosional Surface. In this portion, in particular after the deposition of resedimented evaporites - as shown by the Decontra succession (Fig. 4.1.10) - takes place the complex fluid-rock interaction.

- never affect the late post-evaporitic succession;

- at places cut the evaporitic (PLG) succession throughout, by means of spectacular outcrop-scale conduits. This specific phenomenon is localized and catastrophic.

The proposed Messinian fluid escape event in the Maiella area is thus clearly constrained to the early post-evaporitic phase (p-ev1), after the earlier deposition of resedimented evaporites and the development of an important erosional surface. This surface testifies a major drawdown in the basin and the resulting high depressurization could have possibly favoured the claimed fluid release.

4.1.6 - Major remarks and the proposed scenario

- In the NW-Maiella area brecciated limestones (Bcl) unconformably overlay the Primary Lower Gypsum Unit (*Gessoso-Solfifera Fm.*). The Maiella Bcl unit rests above the regional Messinian

Erosional Unconformity (MES) and its stratigraphic position can be ascribed to the early post-evaporitic phase (p-ev1, *Auctt.*).

- Three main representative lithofacies of the Bcl were enucleated: 1) massive brecciated limestones s.s. (BL), 2) patchy limestones embedded in a host sediment (PL) and 3) fluidized sediments, with minor carbonatic fraction (FS).

- The paleoenvironment was defined through the host sediment, testifying poorly oxygenated and well-stratified water masses depicting an OM-rich (anoxic) environment. Soon after its deposition, fluid migration processes took place.

- Fluid migration pathways cutting both the evaporitic and the post-evaporitic unit were recognized. Fluid flow conduits occur both at the mesoscale and at the microscale. Subcentimetric microchimneys were collected from the host sediment as well. Hydrocarbons flowed along fluid migration pathways within the partially lithified sedimentary column: the fluid migration occurred in two main steps, with a more catastrophic character of the first one.

- The fluid migration events were both accompanied by brecciation. The first one is responsible for the common occurring fluidification features in the facies, the second one led to tar impregnations according to different patterns.

- The brecciated limestones had complex rheological responses to the fluid migrations, whose variations in space, time and composition possibly led to alternated oxidizing and reducing microenvironments.

- The geochemical dataset shows wide ranges both in $\delta^{18}O$ (~ +5 down to -10 ‰ PDB) and $\delta^{13}C$ values (~ +5 down to -40 ‰ PDB); this high variation, is also shown at the scale of the single sample in some cases. The $\delta^{18}O$ signal mostly points to carbonate precipitated in equilibrium with the Messinian seawater. The $\delta^{13}C$ signal can be explained taking into account: 1) an original mixed carbon sources involved in authigenesis, testifying, at least to some extent, the implication of the AOM; 2) a complex fluid-rock interaction (FRI). Two end members are represented by: a) the carbonates associated to FS - the less depleted in $\delta^{13}C$ - pointing to focused fluid flow, high flux rates, low FRI, AOM secondarily involved in authigenesis; b) the chaoticized patchy limestones and the microchimneys - the most depleted in $\delta^{13}C$ - testifying pervasive fluid flow, low flux rates, high FRI, AOM directly involved in authigenesis.

- A number of seep limestones markers were identified in the brecciated limestones.

- Localized overpressure is the process suggested as trigger for brecciation.

The proposed scenario

A catastrophic fluid release occurred in the foreland domain of Adria (Maiella Basin) in upper Messinian times, soon after the deposition of anoxic sediments during the early post-evaporitic

pase. Most likely, the major drawdown of the Mediterranean Sea could have played a critical role in the fluid expulsion from below, given the contextual high depressurization experienced by the sedimentary column. The fluid flow meso- and micro-conduits and the brecciated facies testify that fluid-rock interaction took place in a partially lithified column. The proposed scenario for the upper Messinian Maiella Basin depicts an upward hydrocarbon-rich fluid migration through the Messinian succession, developed with major fluxes along giant neoformed chimneys and seepage through the host sediment. This event was accompanied by authigenic carbonate precipitation and brecciation.

The integrated facies analysis points to a strongly anoxic environment during the deposition of the p-ev1 unit, which further experienced - in a diagenetic context - the precipitation of authigenic carbonate phases and processes of brecciation. The independent scale-brecciation observed in the intraformational breccias suggests the occurrence of hydraulic fracturing, hence indicating overpressure of gas as the most likely trigger for brecciation. This hypothesis is consistent with the detection of traces of oil and fluidification structures. In addition, the geochemical dataset, revealing a moderate to medium ^{13}C depletion, is compatible with the incorporation of hydrocarbons - possibly even higher than methane - during the precipitation of the authigenic carbonates.

All the acquired data point to depict a feasible paleo oil-to-gas seep scenario, developed soon after the deposition of the early post-evaporitic unit in the Maiella foreland basin.

4.2 - The *Calcare di Base* of the Calabrian Arc

4.2.1 - Geological setting and the Messinian record in the area

The structural evolution of Central Calabria is related to the onset of the southeastward migration of the Calabrian Arc during the Serravallian-Tortonian (Mattei et al., 2002), and to the collision between the Calabrian fold-and-thrust belt with the Adria plate continental margin from the late Tortonian to the Pliocene. This caused general accretionary tectonics along the Ionian side and extensional tectonics in the incipient Tyrrhenian Sea back-arc region.

The main geodynamic events mentioned above led to the activation of crustal oblique transpressional fault zones - mainly dipping toward NE and characterized by left-reverse movements - that profoundly conditioned basins evolution during Middle Miocene to Middle Pleistocene times (Van Dijk et al., 2000; Tansi et al., 2007).

Rossano and Crotone basins are located along the onshore Ionian side of the Calabrian Arc (Fig. 4.2.1), and their Neogene successions constitute the filling of the wedge-top basins that represent the southern limbs of the Apennine foreland basin system (DeCelles & Giles, 1996; Critelli, 1999). The Neogene sedimentary units record similar histories in both basins and unconformably overlie an articulated basement (including the Sila Unit, a complex assemblage of Palaeozoic crystalline rocks and its Mesozoic sedimentary cover).

The Rossano Basin infill consists of a continental to marine-paralic succession (Roda, 1964). The first depositional unit, Tortonian-early Messinian in age, constitutes a transgressive system that rapidly evolved from continental (alluvial conglomerate) to deep marine sedimentation (turbiditic sandstones and pelagic clays). The marls and diatomaceous shales of the Tripoli Formation and the Calcare di Base Formation (CdB) cap the unit. The upper Messinian portion, belonging to the Gessoso-Solfifera Formation,unconformably covers previous deposits. In the Early Pliocene, deep-marine marls and turbiditic sandstones record the restoration of normal marine condition (Zecchin et al., 2004).

In the Rossano Basin the CdB conformably overlies the Tripoli Fm Auctt. (Tr) and is in turn unconformably overlain by the Gessi Fm Auctt. (typified by resedimented gypsum facies), through the MES (Fig. 4.2.2). A salt-bearing unit associated to clays (Argille marnose salifere Fm), was exploited in the last century in a mine in the nearby of Rossano. It was not found in exposure and was described by Ogniben (1963b) on the

Fig. 4.2.1 - Simplified geological map of northern Calabria (after Guido et al., 2007) and location of the major study area (Rossano Basin) and the second sampled area (Crotone Basin).

basis of well data. The stratigraphic position of the salt-bearing unit remains uncertain, since the salt could have experienced diapirism similarly to the correlatable Detritico Salina Unit cropping out in the Crotone Basin. It may possibly represent a lateral equivalent of the Resedimented Gypsum Unit.

The stratigraphy of the Crotone Basin was established by Ogniben (1955, 1962, 1973) and more extensively by Roda (1964, 1970, 1971), who recognized three major sedimentary cycles bounded by basin-wide unconformities. The Neogenic sedimentary evolution of the Crotone Basin starts with the Serravallian-Tortonian continental to shallow-marine San Nicola Fm and the offshore Ponda Clays (Roda, 1964a). The following record resembles the contemporary evolution of the Rossano Basin to a major extent: unconformably resting above the Ponda Clay, the MSC-related deposits of the first phase are represented by the Tripoli Fm, reduced in thickness or totally absent, and the Calcare di Base Fm, conformably resting on the Tr or in turn unconformable on the Argille della Ponda Fm. Panoramic views in the field reveal how this variation in thicknesses can be ascribed to an articulated paleogeography developed after the Argille della Ponda deposition. The deposits of the first phase are bounded at their top by the MES, above which gypsarenites and salt-bearing deposits occur.

The halite deposits are associated with a sedimentary chaotic complex, made up of metric blocks of limestone and alabastrine gypsum included in an argillaceous matrix (Detritico-Salina Fm). Finally, gypsarenites, sandstones and "Lago Mare" pelites (Gennari & Iaccarino, 2004) constitute a late Messinian unit that onlaps both the chaotic complex and the gypsarenite.

An erosional surface separates the latest Messinian deposits from the overlying fluvial conglomerates (Caravane conglomerates), abruptly covered in turn by the offshore Cavalieri marls (Early Pliocene). The marls grade upward into the shallow-marine Zinga Molasse deposits (Pliocene; Roda, 1964; Zecchin et al., 2004).

4.2.2. - Field data: stratigraphy, NRD signal and main lithofacies

In this study the Calcare di Base of the Calabrian Arc has been studied in detail in the Rossano Basin (Cropalati section, north-eastern Calabria, Fig. 4.2.1). Secondarily, sampling has been performed also in the Crotone Basin (Verzino area, Fig. 4.2.1) and in the Cessaniti Basin (Briatico area, central Calabria).
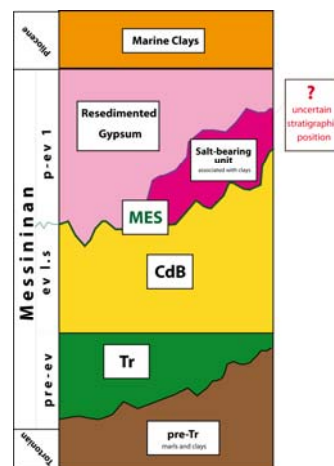
Fig. 4.2.2 - Schematic illustration of the MSC record in the Calabrian Arc (not to scale). Tr, Tripoli Fm; CdB, Calcare di Base; MES, Messinian Erosional Surface. Since the Salt-bearing unit experienced late diapirism, its stratigraphic position is still unclarified.

<u>Rossano Basin</u>

Two sections in the vicinity of Cropalati (CS), were studied and sampled (sections CROP and CROP3, Figs. 4.2.3-5). In the Rossano basin the CdB is typified by a cyclic alternation of thick-bedded massive carbonates and thin-bedded laminated pelites and marls.

CROP section (Figs. 4.2.3, 4.2.5 a) clearly shows a conformable transitional contact between the Tripoli Fm (Tr) and the Calcare di Base Fm (CdB): stromatolitic facies typify both the topmost interval of the Tr and the lower beds of the CdB. The CdB unit contains nine carbonate-pelite cycles in this section and shows a brecciation degree varying from low to absent in the basal beds, but significantly increasing up-section (Fig. 4.2.3). It must be pointed out that the estimation of the brecciation degree has been so far merely based on outcrop scale qualitative observations.

CROP3 section is constituted by eight CdB cycles, cut on top by the MES, above which resedimented gypsum facies occur (Figs. 4.2.4, 4.2.5 b-c). This possibly testifies that these cycles are the topmost portion of the CdB recorded in the area. Nonetheless, the high brecciation degree affecting this section, resulting in somehow amalgamated beds, on one hand doesn't allow a correct count of the cycles and on the other hand doesn't allow a correlation between the two studied sections. The inhomogeneous distribution and degree of brecciation also occur within single beds (Fig. 4.2.5 b-c). A lot of veins cut the succession throughout.

The gamma ray log profile exhibits upward increasing - decreasing - constant trends along CROP section (Fig. 4.2.3) and a general decreasing trend along CROP3 section (Fig. 4.2.4). The major spikes (50-61 Cps) have been recorded in the ocraceous pelites of CROP3 section, but anomalously high NRD-values also affect the limestones (32-50 Cps). Field spectra indicate a ^{238}U-dominated NRD concerning both carbonates and pelites, the latter also exhibiting a minor contribution of ^{40}K and ^{232}Th (Fig. 4.2.6). The radioelements patterns in the CdB represent indirect proxies for low detrital input in the Rossano Basin during the cyclic deposition of carbonates and pelites, pointing by contrast to processes related to authigenesis.

The CdB is basically fabric retentive: the original bedding and the depositional features are partially obliterated only in correspondence to the locally more pervasive brecciation. In such cases the primary bedding planes are traceable only laterally and the maximum degree of brecciation defines "blob-like" bodies, only apparently unconformable on the lateral bedding-retentive brecciated bodies (Fig. 4.2.5 c). In some intensively brecciated beds, relict highly-cemented marly laminae allow the recognition of the original stratification: the laminae are always concordant to the breccias bedding planes (Fig. 4.2.7).
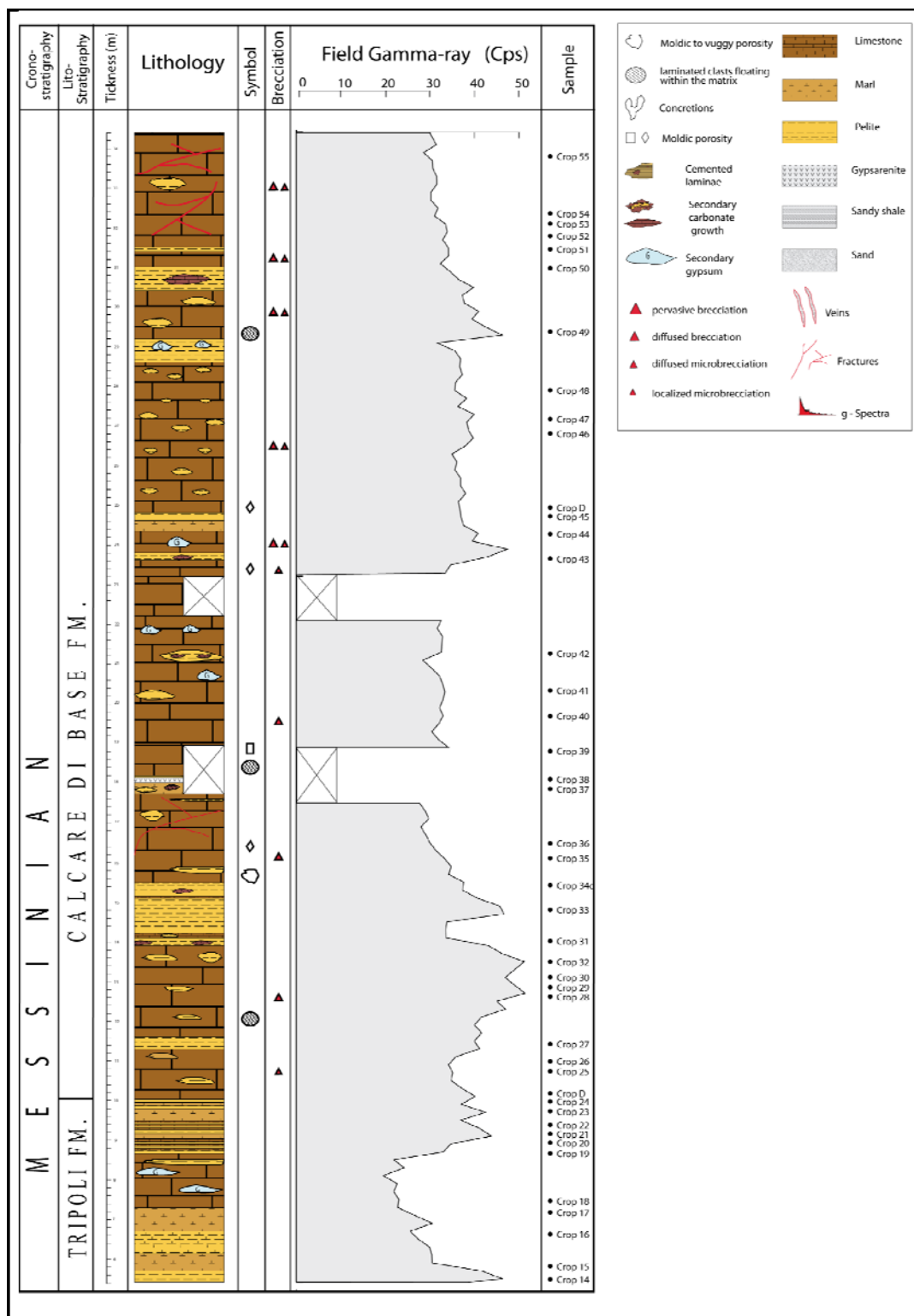
Fig. 4.2.3 - Rossano Basin - Lithologic and gamma-ray log profile of the Cropalati section "CROP", showing the transitional conformable contact between Tr and CdB. In this site the CdB is brecciated to a minor extent.

Fig. 4.2.4 - Rossano Basin - Lithologic and gamma-ray log profile of the Cropalati section "CROP3"; in this site the CdB is more intensely brecciated.
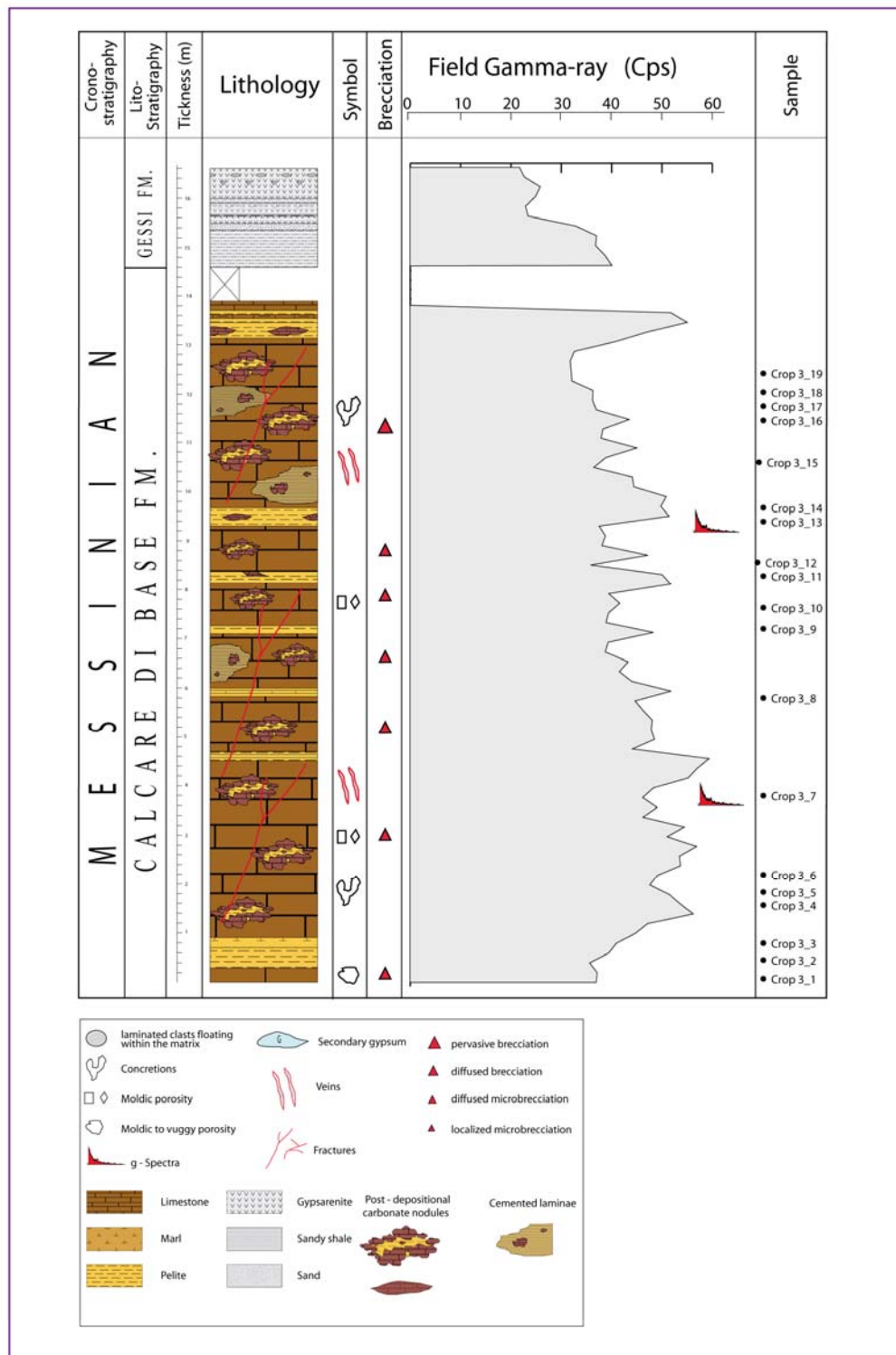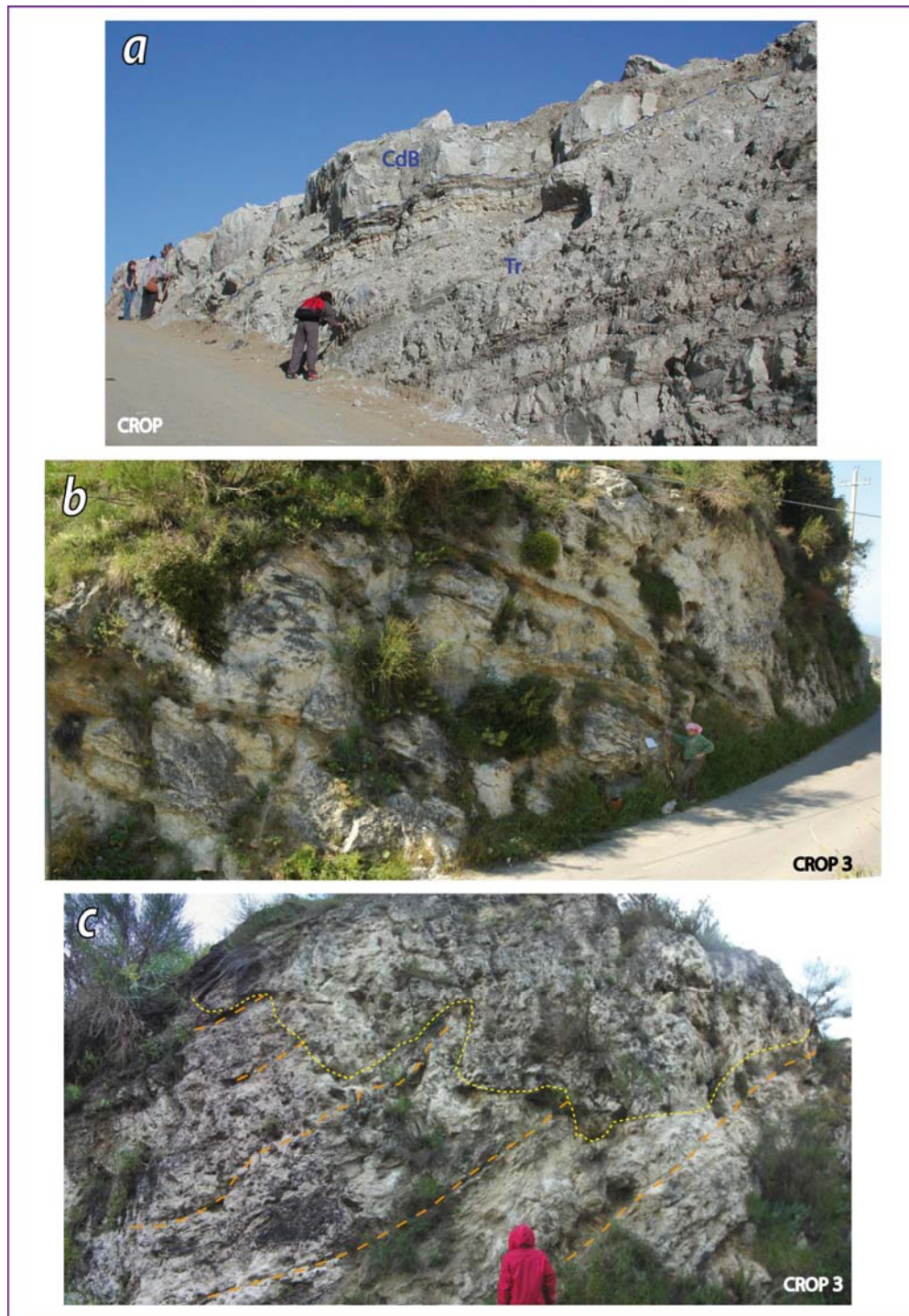
Fig. 4.2.5 - Rossano - Main outcrops.
(**a**) Basal portion of the <u>section CROP</u>, showing the transitional contact between the Tripoli Fm. (Tr) and the Calcare di Base Fm. (CdB). Slightly brecciated facies typify this section, though up-section the brecciation degree gradually increases (Fig. 4.2.3).
(**b**-**c**) The <u>section CROP3</u> generally yields a high brecciation degree, but exhibits an extreme lateral variation. This is clearly revealed by the two perfectly correlatable investigated outcrops, standing one in front of the other and separated only by a small local road. Notice how the breccias are mostly bedding-retentive (**c**, dashed orange line), but the bedding planes interrupt in correspondence to ideal surface (**c**, dotted yellow line) isolating the maximum brecciation degree zone, represented in outcrop by an isolated "blob-like" body. The facies are perfectly correlatable on both the sides of this ideal surface, but the different brecciation degree is deduced by the presence/absence of the bedding-retentive planes.
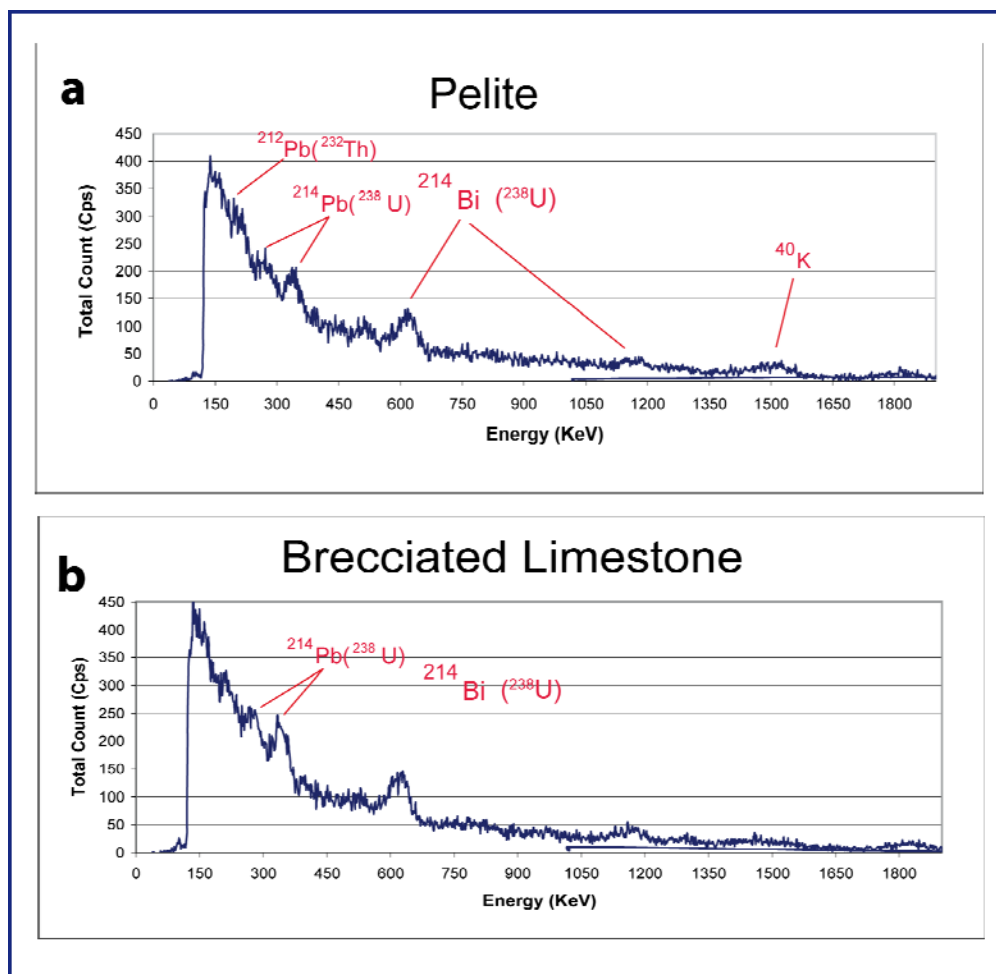
Fig. 4.2.6 - Natural gamma-ray (NRD) spectra obtained on pelites (**a**) and carbonates (**b**) of the Calcare di Base Fm.
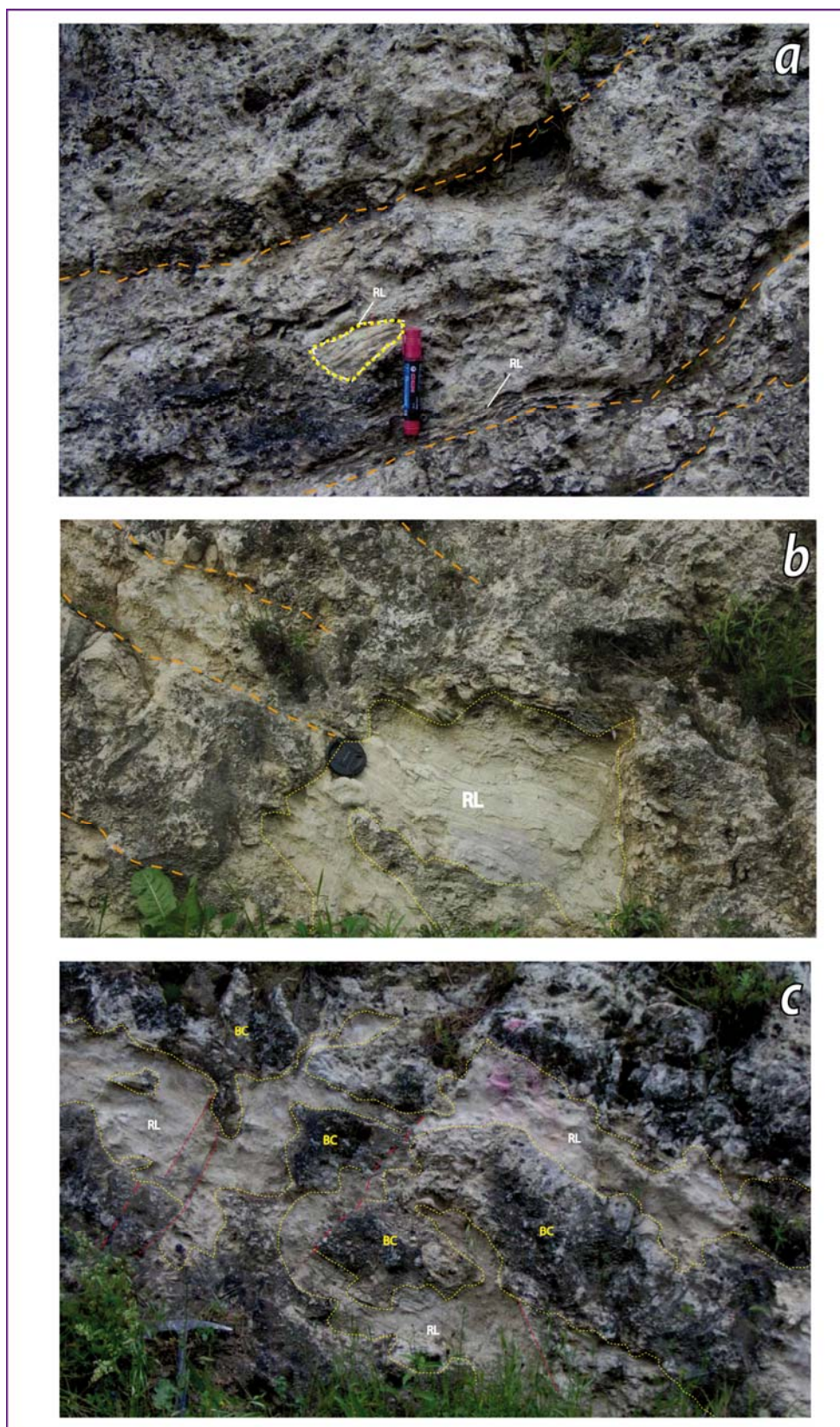
Fig. 4.2.7 - Rossano Basin - Bedding planes (orange dashed lines) and concordant relict primary lamination (RL, encircled in yellow dotted lines). The contact between breccias (BC) and laminae is abrupt (**b**) or articulated (**c**), resulting in patchiness of the geobodies, eventually dissected by faults (red dashed lines).

Fig. 4.2.8 - Rossano Basin - Main CdB lithofacies at the outcrop scale.
Concretions (CR) and breccias (BC), devoid of gravity segregation and with dominantly subangular clasts (**a**-**b**). Pelitic horizons yield carbonate cloudy-shaped concretions (**c**), giving rise to a texture resembling a peculiar facies association shown in the carbonate beds (**d**). The latter is made up of cloudy carbonate nodules (cnd) and wispy pelites exhibiting a flames-like structure (fls): this association is named cnd-fls in this work.

The facies association in the carbonatic beds consist of:

1) marly lime mudstones, locally to extensively (Fig. 4.2.8 a) brecciated. Breccias are typified by subangular irregularly-shaped clasts, devoid of gravity segregation (Fig. 4.2.8 b);

2) pervasively cemented concretions (Figs. 4.2.8 a, 4.2.12 b).

3) coupled secondary cemented cloudy nodules (cnd) and finely laminated pelitic lenses (flames-like structures, fls). In the Rossano Basin the cnd are common constituents of the CdB facies at any scale. The fls are always associated with the cnd, giving rise to a peculiar facies association, hereby termed "cnd-fls". The cnd-fls constitute thin levels, that are concordant to the primary bedding (Fig. 4.2.8 d).

The pelitic horizons are greenish-brown to ocraceous and often crop out as lenticular thin-bedded horizons. They yield cloudy carbonate concretions, thus resembling the cnd-fls facies, but with different relative proportions of carbonate and pelite (Fig. 4.2.8 c).

Fig. 4.2.9 - Crotone Basin - Bedding-retentive breccia in the CdB. Brecciated massive limestone beds with minor pelitic interbeds (**a**). Brecciation is clearly fabric-retentive (**b**) and overprints the primary lamination (**c-d**).

A diffused vuggy/fenestral porosity affects the carbonatic beds, showing mm-to-dm sized horizontally elongated pores, associated with mm-sized rhombs (possibly leached dolomite). The total porosity can be partly related to eroded pelitic lenses (major flames-shaped pelites).

Crotone Basin

In the vicinity of Verzino (KR), samples of the Calcare di Base Fm have been collected at various sites (Gabella Mortilla, Timpa del Castello, Cerenthia Vecchia, San Basile). Negligible thicknesses of Tripoli Fm (Tr) crops out, but they are sufficient to allow the proper reconstruction of the MSC-stratigraphy in the area: also in Crotone basin the CdB conformably overlies the Tr (Fig. 4.2.2).

The CdB in the Crotone Basin is represented by cemented thick-bedded limestones, with extremely thin pelitic interbeds (Fig. 4.2.9 a). Cemented laminites represent the primary facies, whose fabric, though overprinted by secondary bedding-retentive brecciation (Fig. 4.2.9 b-d), is generally easily traceable. No gradational features have been observed within the brecciated beds, constituted by dm- (Fig. 4.2.9 a) to cm-sized (Fig. 4.2.9 b) clasts.

At places the laminites are chaoticized and disrupted (Fig. 4.2.10), with associated microbrecciation (Fig. 4.2.10 b). Fluid-migration features accompanied by tear structures also occur (Fig. 4.2.10 a).

Fig. 4.2.10 - Crotone Basin - Fluidification proxies.
(**a**) fluid migration-like structures (red dashed line) associated to tear-structures (yellow dotted lines, above the hammer); (**b**) disrupted laminae and associated microbrecciation; (**c**) extremely chaoticized laminae (plain blue outline)

Siliceous flames and nodules are commonly associated to the limestones, while secondary gypsum represents the common infilling of the primary porosity and veins in the CdB in Verzino area.

Cessaniti Basin

In the Cessaniti Basin, belonging to the Tyrrhenian side of the Calabrian Arc and thus already experiencing extensional regimes in Messinian times, the site of Briatico was quickly visited in order to observe the mesofacies and compare it to the major sampled areas.

In the nearby of Briatico the Cdb unit is represented by a vuggy limestone with fenestral porosity, yielding discontinuous lenses of marly homogeneous limestones. The occurrence of post-depositional processes is revealed by secondary carbonate growths with intruding patterns (Fig. 4.2.11 b) and local brecciation. Brecciated beds interestingly represent a good example of mosaic breccia type (Fig. 4.2.11 a), that points to in situ brecciation phenomena.
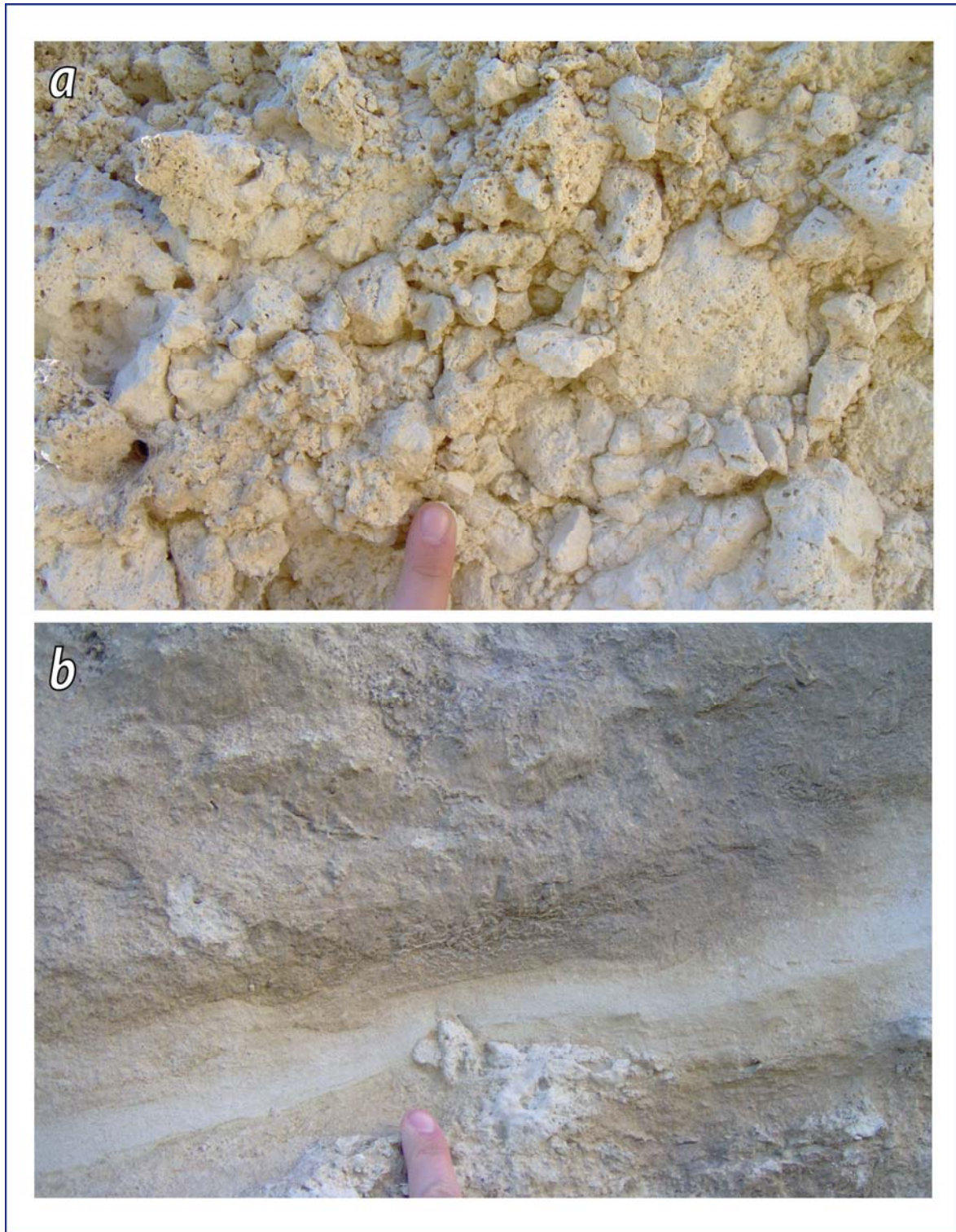
Fig. 4.2.11 - Briatico section, Calcare di Base. Mosaic breccia (**a**); detail of secondary growth concretions (**b**). They are both related to post-depositional processes affecting the CdB.

4.2.3 - Facies analysis

<u>Rossano Basin</u>

Both breccias and concretions yield peloidal clotted microbial microfacies, commonly fluidized and microbrecciated (Figs. 4.2.16-18).

The less brecciated beds, typically occurring in the basal portion, are typified by muddy matrix-dominated facies, that contains minor cemented clasts and centimetric levels of the aforementioned cnd-fls association (Fig. 4.2.12 a).

The cloudy nodules constitute microsparitic celestite-bearing carbonate growth microstructures: their cementation front encloses primary microfacies elements (Fig. 4.2.13 c-e). Reasonably, the contemporaneous growth of many nodules progressively confines the pelitic fraction, that finally results in the wispy structures of the cnd-fls (Fig. 4.1.13 a). The flames-like structures are thus interpreted to represent relict pelitic interbeds within the major carbonatic beds: this is also consistent with the concordant pattern of the cnd-fls with respect to the primary bedding (Par. 4.2.2). The cnd-fls locally underwent fluidification (Fig. 4.2.13 b), even associated to brecciation (Fig. 4.2.12 d).

Mud-supported breccias (Fig. 4.2.12 c), more common in the CROP section, show the coexistence of brittle- and plastic-related features: cemented fragments are associated to muddy portions with inception of fragmentation.

Cemented breccias (Fig. 4.2.12 e-f), more common in the CROP 3 section, show textures more likely related to brittle behaviour: they are clast-supported, constituted by subangular and minor surrounded elements of the host rock, accompanied by spar cement. The same textural relationships have been observed in localized microbrecciation occurrences (Fig. 4.2.14).

Interestingly, microbrecciation is lithology independent: it is shown by the basal stromatolitic samples and by the pelitic interbeds as well (Fig. 4.2.15).

The concretions yield a fluidized microfabric (Fig. 4.2.16 a, c): the rod-shaped peloids are variously oriented, depicting microfolds.

Aragonite represents by far the main carbonatic phase, together with variable amounts of calcite (the cement, dominant in the concretions) and negligible amounts of ankerite-dolomite. Only the stromatolitic facies revealed dolomite/HMg-calcite mineralogy. Pore-filling silica cement (chalcedony) and celestite are associated with the calcite. Celestite fills intergranular spaces in the microspar or forms veins where microdolomite rhombs occur (Fig. 4.2.19). Minor barite also occurs.

Concerning the fine-grained horizons, their non-siliciclastic fraction is mostly made up of calcite, with minor amounts of ankerite, celestite and aragonite. With regard to their carbonatic content it must be pointed out that: 1) they often contain cemented carbonatic nodules; 2) fine
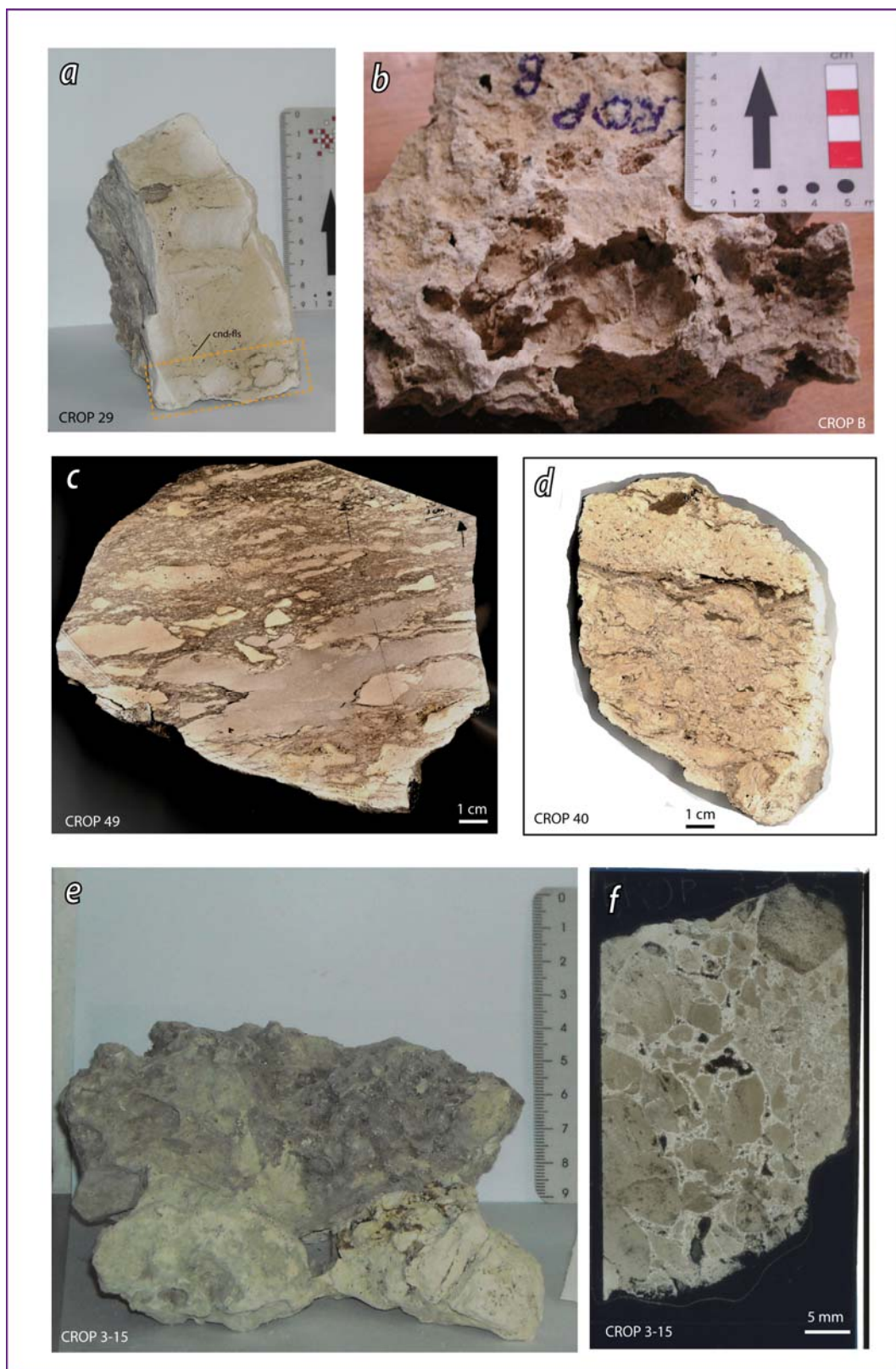
Fig. 4.2.12 - Rossano Basin - Main facies in the CdB.
Cnd-fls level (dotted box) and clasts floating in a muddy matrix (**a**, rock slab); concretion (**b**, hand sample); breccia within a muddy matrix, displaying proxies for both brittle and plastic behaviour, presumably co-occurring (**c**, polished slab); chaoticized and partly brecciated cloudy nodules (**d**, rock slab); brecciated limestone (**e**, hand sample), with microbrecciated texture in turn (**f**, polished thin section), made up of mostly subangular densely packed clasts, arranged in different granulometric classes, within a spar-cement.

granular to fine-to-medium grained blocky calcite occurs in veins and in irregular interconnected microareas (Fig. 4.2.26); 3) microbrecciation somewhere affects their microfabric.
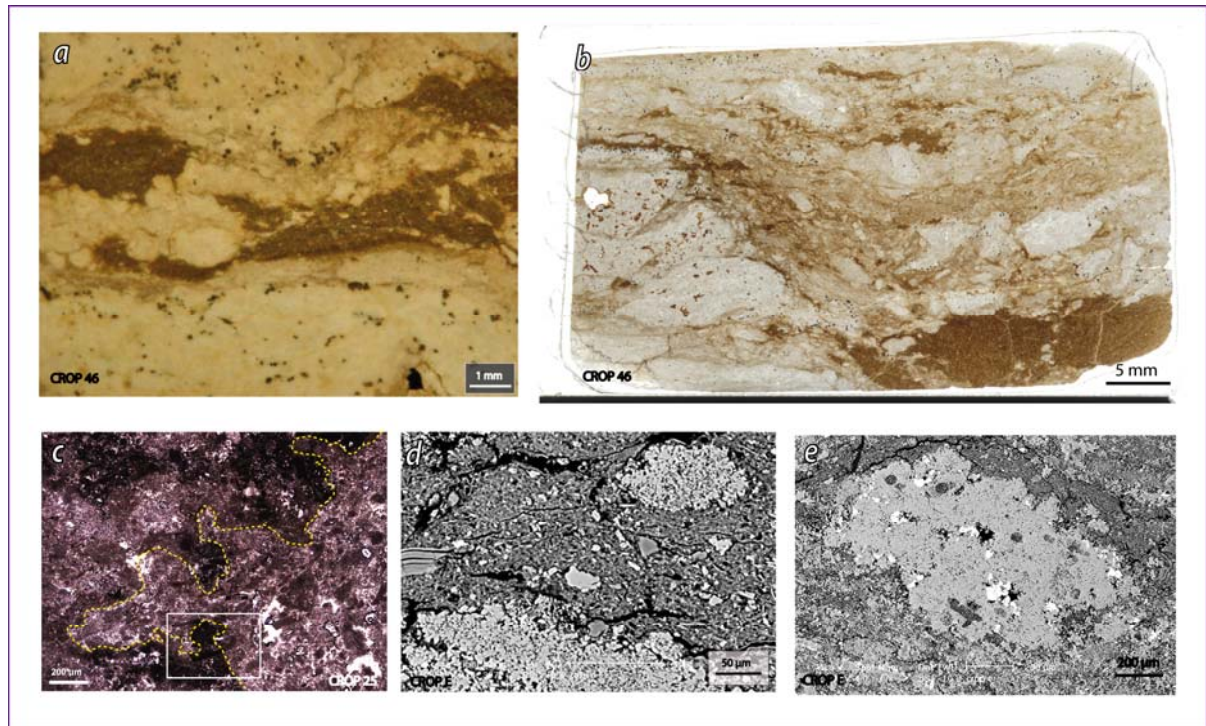
Fig. 4.2.13 - Rossano - Cloudy nodules (cnd) and flames-like structures (fls): cnd-fls facies association.
The fls result from the progressive cloudy nodules growth (**a**) and at places experience later chaoticization (**b**).
The cnd are in turn the result of microsparitization of the primary microbial-peloidal microfacies, as shown by the cementation front (**c**, dashed yellow line; in the white box a detail of this front in a single rod-shaped peloid). At the SEM-scale the cnd-fls reveals its scale independent pattern and the presence of the primary fecal pellets within the nodules (**d**-**e**).
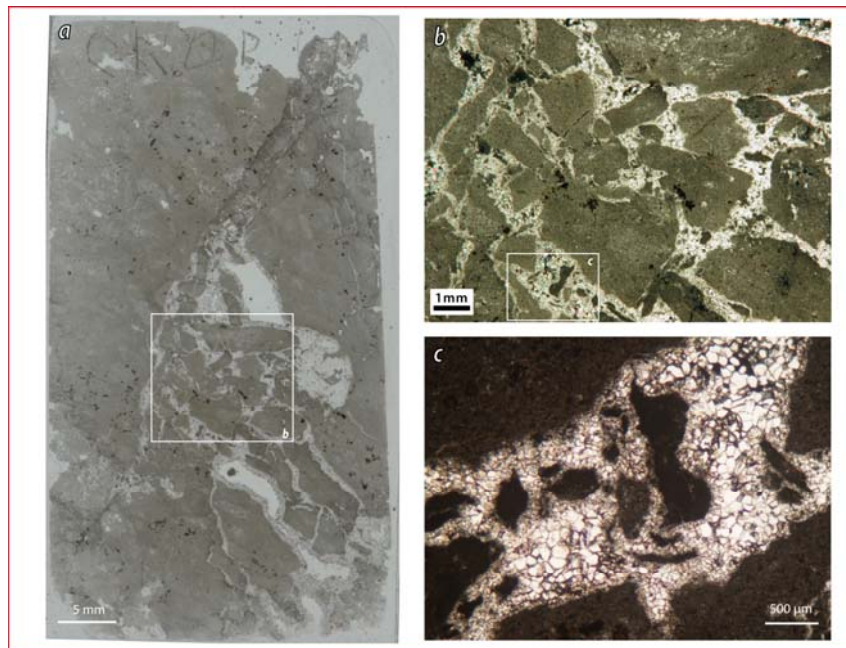
Fig. 4.2.14 - Rossano Basin - Sample CROP C (Appendix 3): microfacies. Localized microbrecciation, the nature of the breccia is the same as the host rock (**a**-**b**; possibly a small scale example of a parent bed sensu Kopf, 2002). The cement network supporting the microbreccia is typified by spar cement accompanied by variously-shaped microbial fragments (**c**).
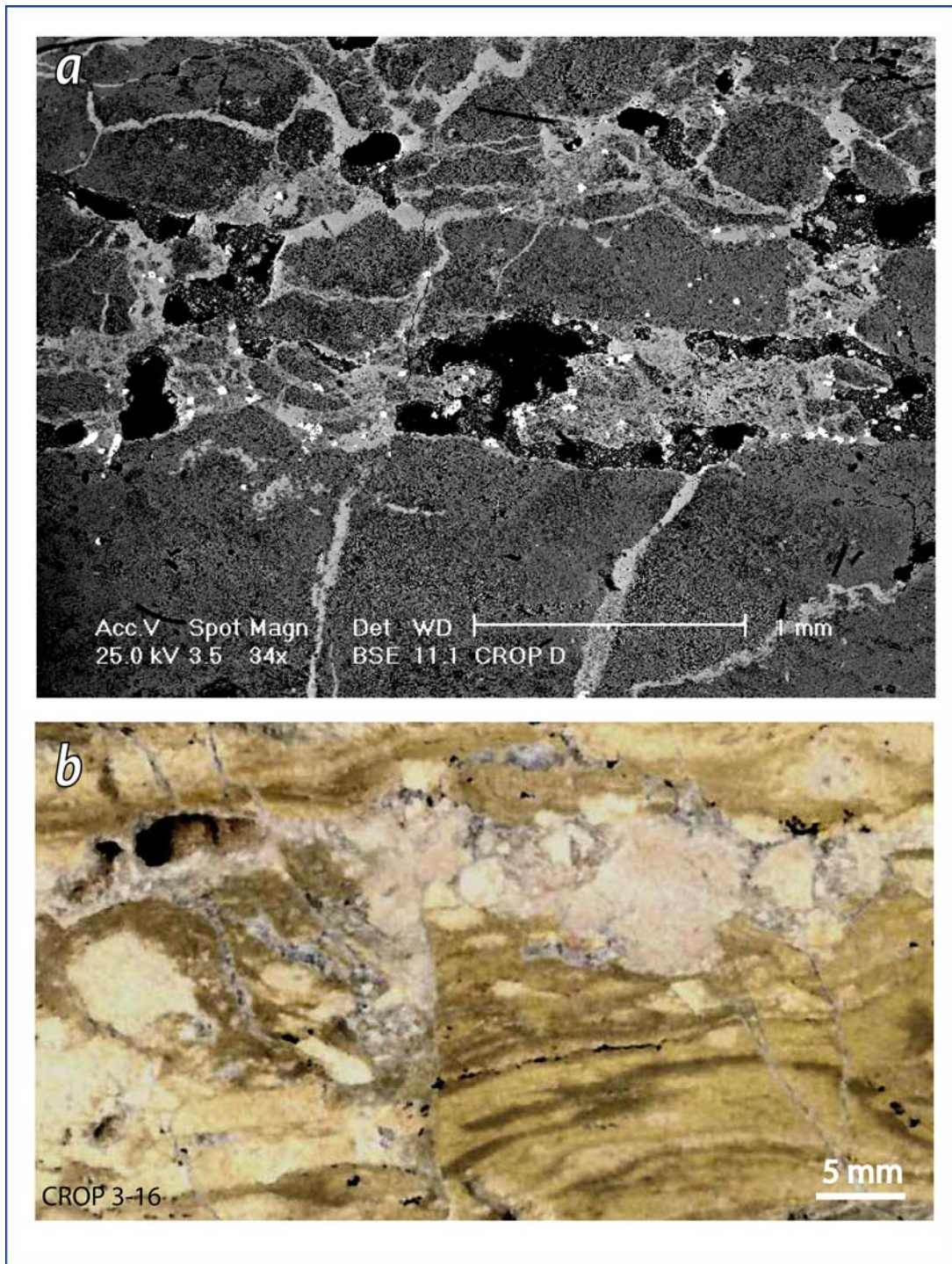
Fig. 4.2.15 - Rossano Basin - Lithology-independent brecciation. Microbrecciation affects the basal stromatolitic beds (**a**) and the major pelitic interbeds as well (**b**).
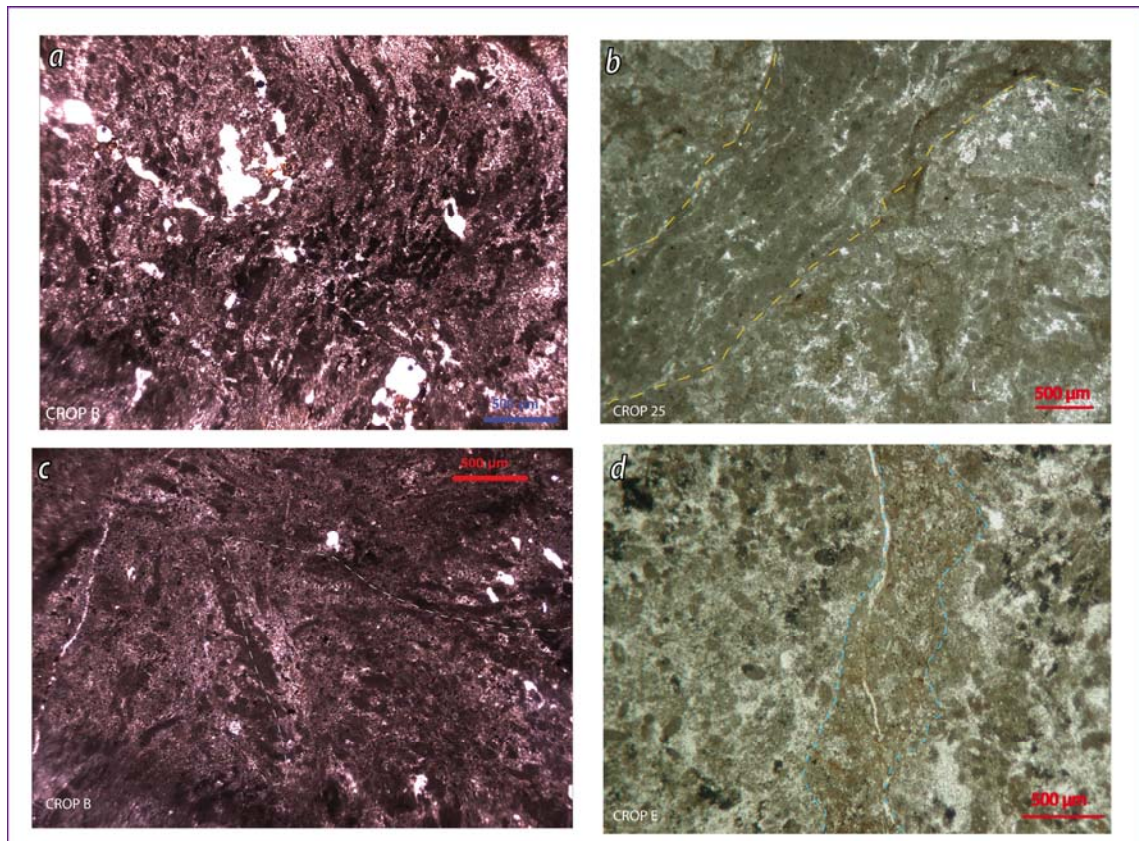
Fig. 4.2.16 - Rossano Basin - Fluidification features affecting the primary microbial-peloidal facies: microfolding (**a**, **c**) and microinjections (**b**, **d**).

Crotone Basin

In the Crotone Basin the microfacies of the CdB is mostly represented by disrupted chaoticized laminae (Figs 4.2.20), associated to local microbrecciation (Figs. 4.2.20 e, 4.2.21).

The primary facies afterwards experiencing microbrecciation is microbial, as evidenced by the microfacies represented by filamentous rod shaped peloids and clotted microbialite forming dendritic clumps and dense aggregates (Fig. 4.2.22). Secondary gypsum and associated anhydrite are common interparticle constituents.

SEM analyses revealed that the microsparitization experienced by the primary fabric resulted in celestite-bearing nodules, perfectly resembling the cnd occurring in the Rossano Basin (Fig. 4.2.23).

Siliceous nodules are associated to the CdB in the Crotone Basin. This subfacies was investigated in one sample (Fig. 4.2.24), where a K-feldspar nodule shows a vacuolar texture rimmed by a fluidized host carbonatic sediment. The carbonatic fraction is made up of celestite-bearing calcite yielding framboidal pyrite and associated to high-magnesium calcite (HMC) with a concentric microtexture. Secondary gypsum occur both in the host sediment and in the nodule.
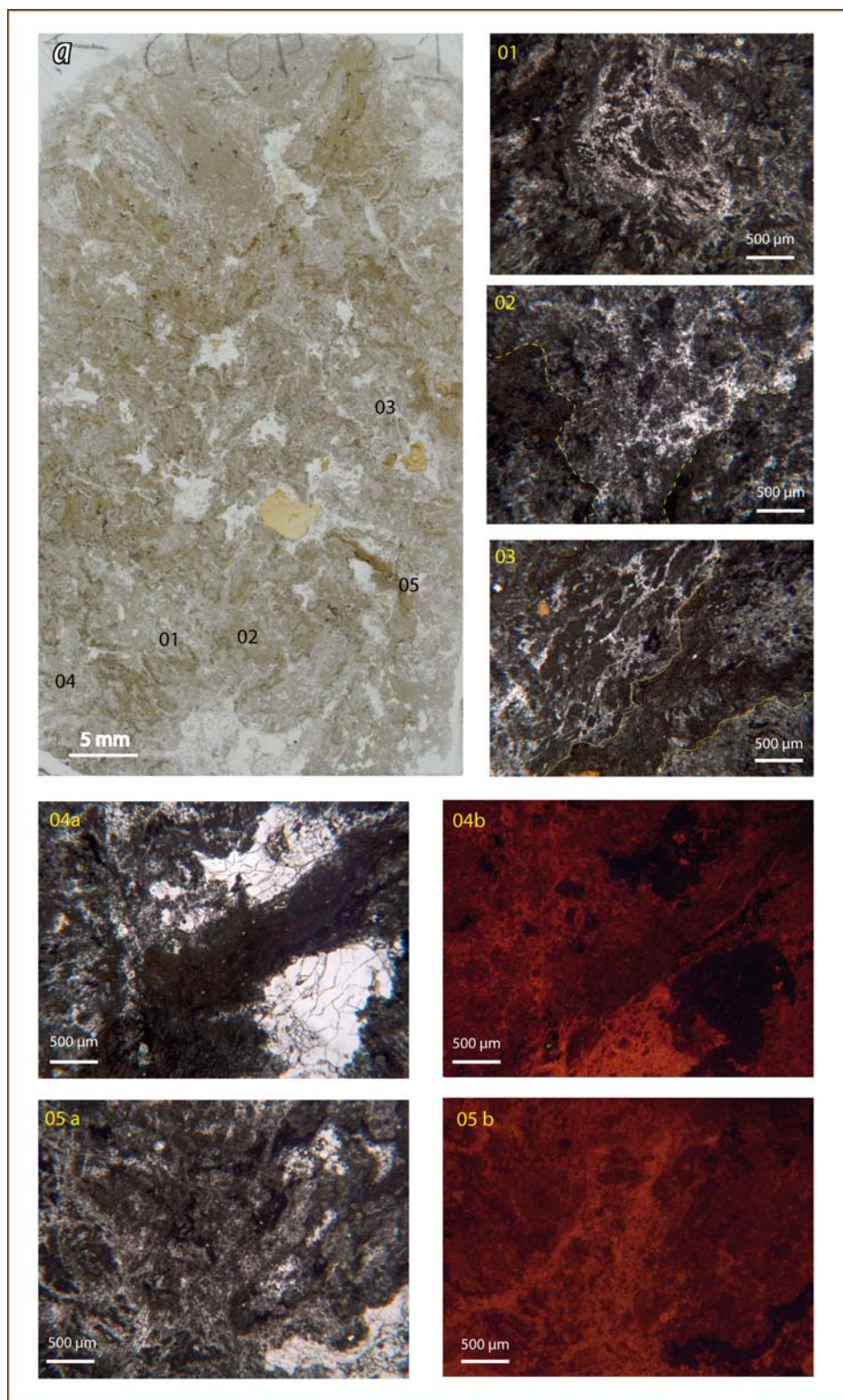
Fig. 4.2.17 - Rossano Basin - Sample CROP 3-1 (Appendix 3), microfacies (**a**).

Small scale fluidification features (**01**) and micro-channels (**02**-**03**).

Oblique pelitic injection cutting pore-filling chalcedony (**04 a**-**b**, coupled transmitted light and CL view); the CL view defines better the pelitic injection (dull), the microbial fraction (bright orange, both clean and mixed signals) and the chalcedony (non luminescent).

The fully chaoticized microbial - partly microsparitized - matrix (**05a**, transmitted light), reveals hidden microinjections in CL view (**05b**).
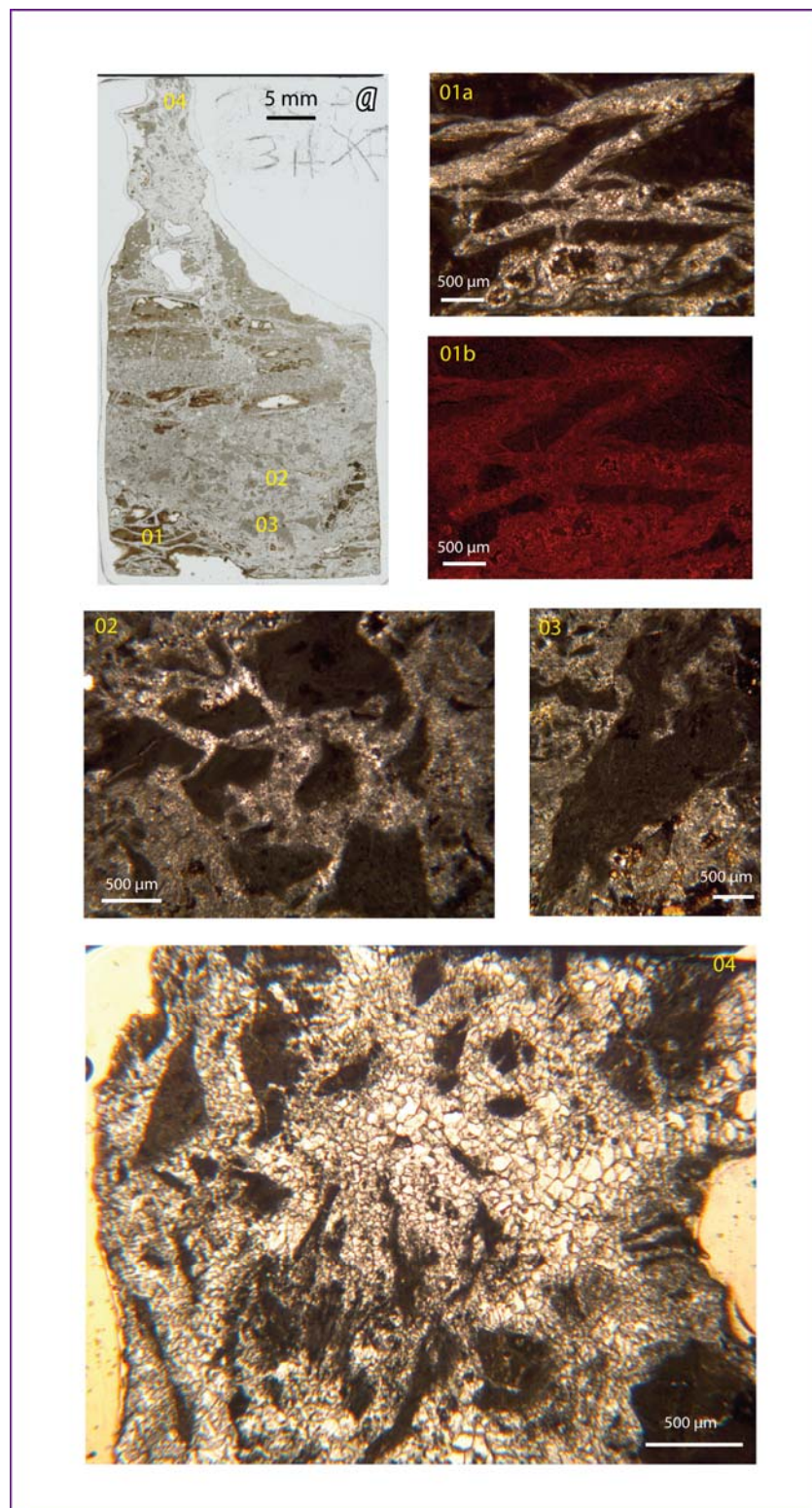
Fig. 4.2.18 - Rossano Basin - Sample CROP 3A (Appendix 3), microfacies (**a**).
Microbrecciation and fluidification features were detected (**01**-**04**): dull/NL pelitic fragments associated to zoned microsparry (**01 a-b**, coupled transmitted light - CL view); microbial fragments (**02**), also occurring in the main vein (**04**); fluidized microbialite (**03**).
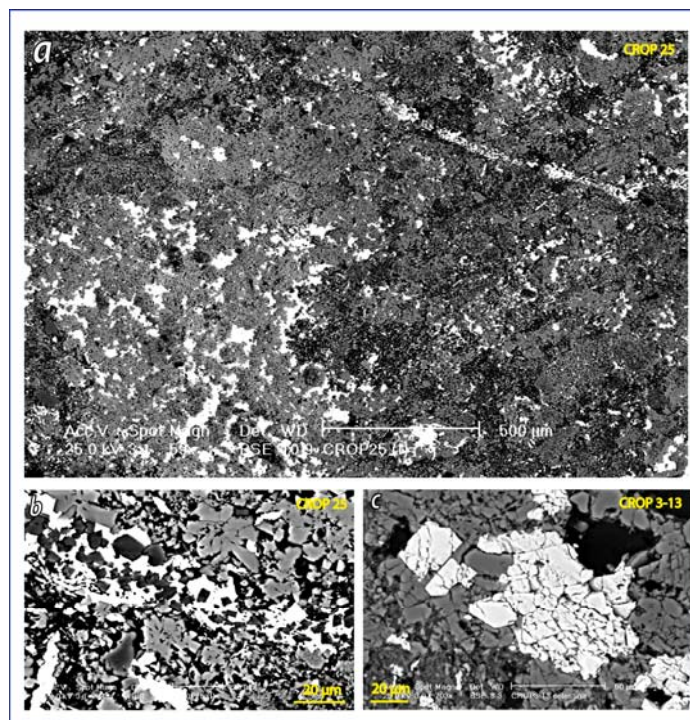
Fig. 4.2.19 - Rossano Basin - Different microfabric patterns in the celestite, occurring as: diffused interparticle cement (**a**); microveins containing dolomitic rhombs (**b**); crystals (**c**).
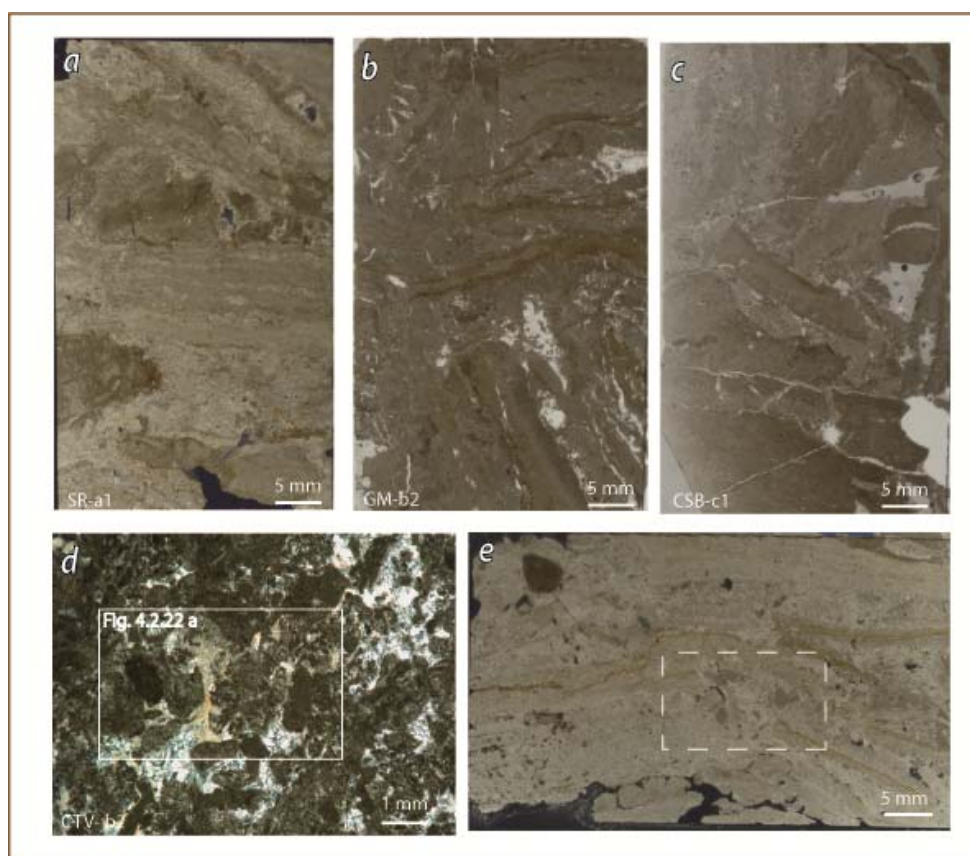
Fig. 4.2.20 - Crotone Basin - Main microfacies association. Microbial laminae, chaoticized and disrupted, locally microbrecciated (**e**, dashed box), with a microbial texture accompanied by a gypsum-anhydritic cement (**d**).
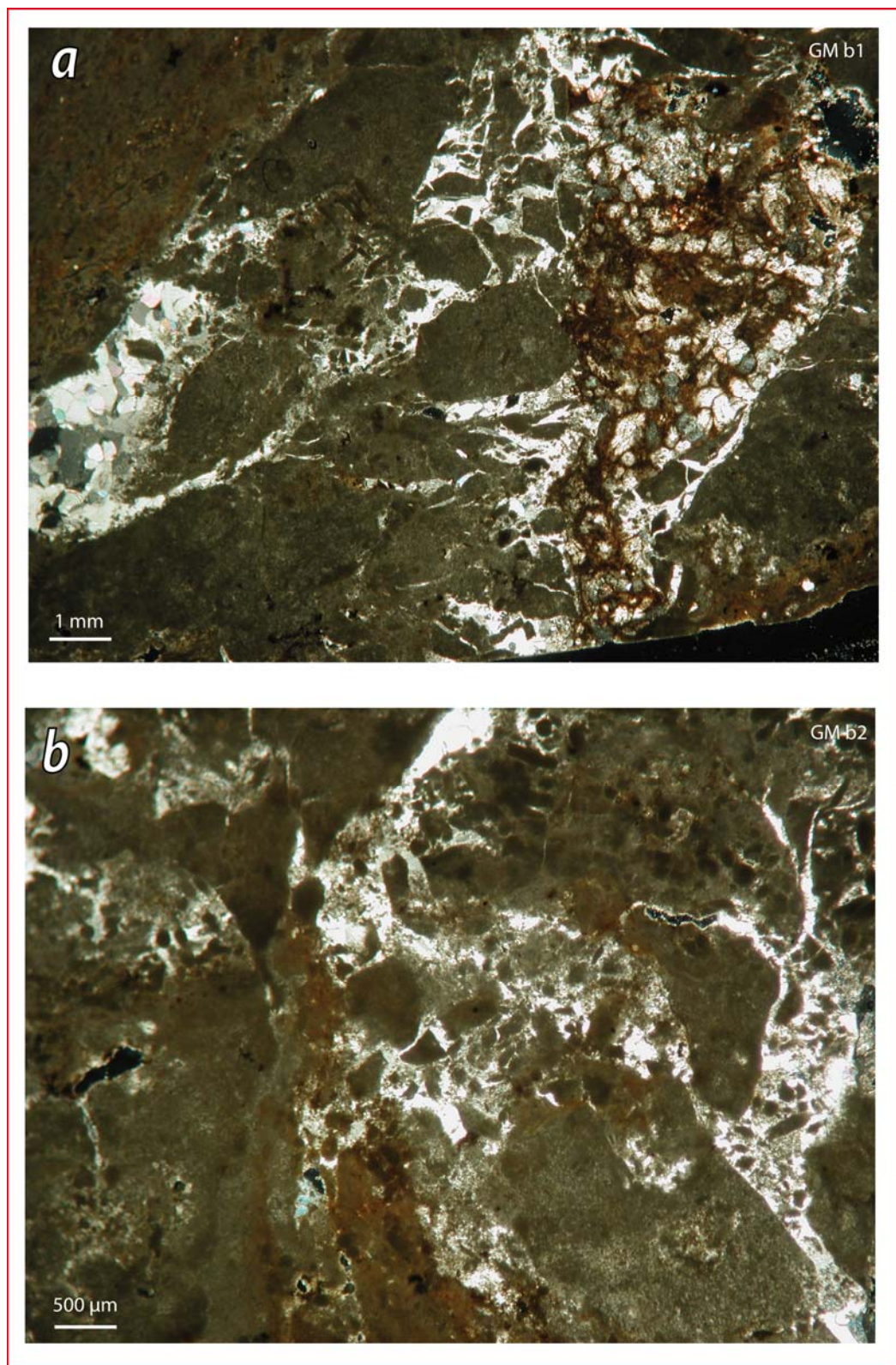
Fig. 4.2.21 - Crotone Basin - localized microbrecciation in the microbial primary texture.
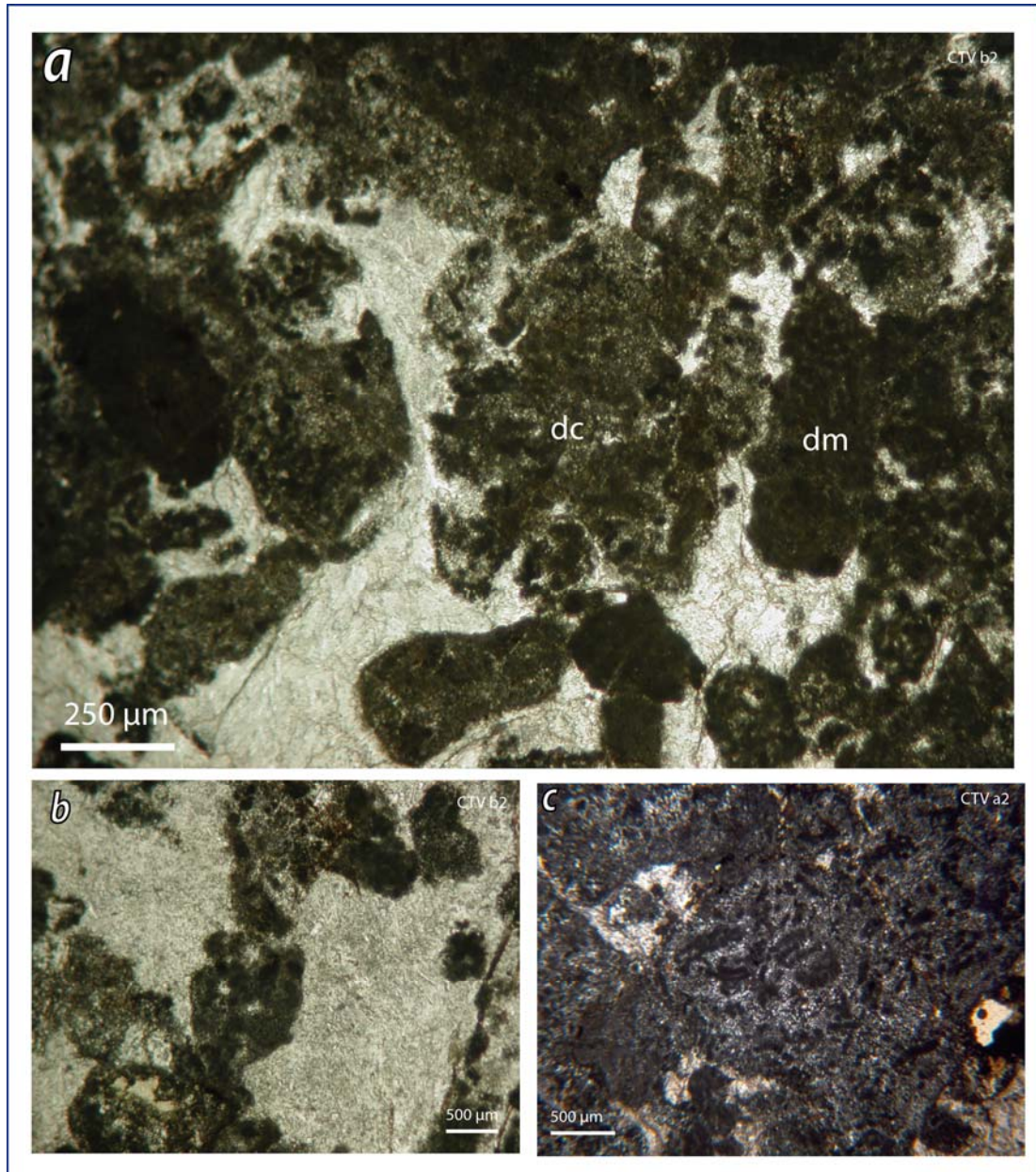
Fig. 4.2.22 - Crotone Basin - Primary facies: microbial and clotted peloidal textures associated to secondary gypsum, occurring with dendritic clumps (dc) and dense clotted microbialite (dm) (**a-b**); detail of the filamentous rod-shaped fecal pellets (**c**).
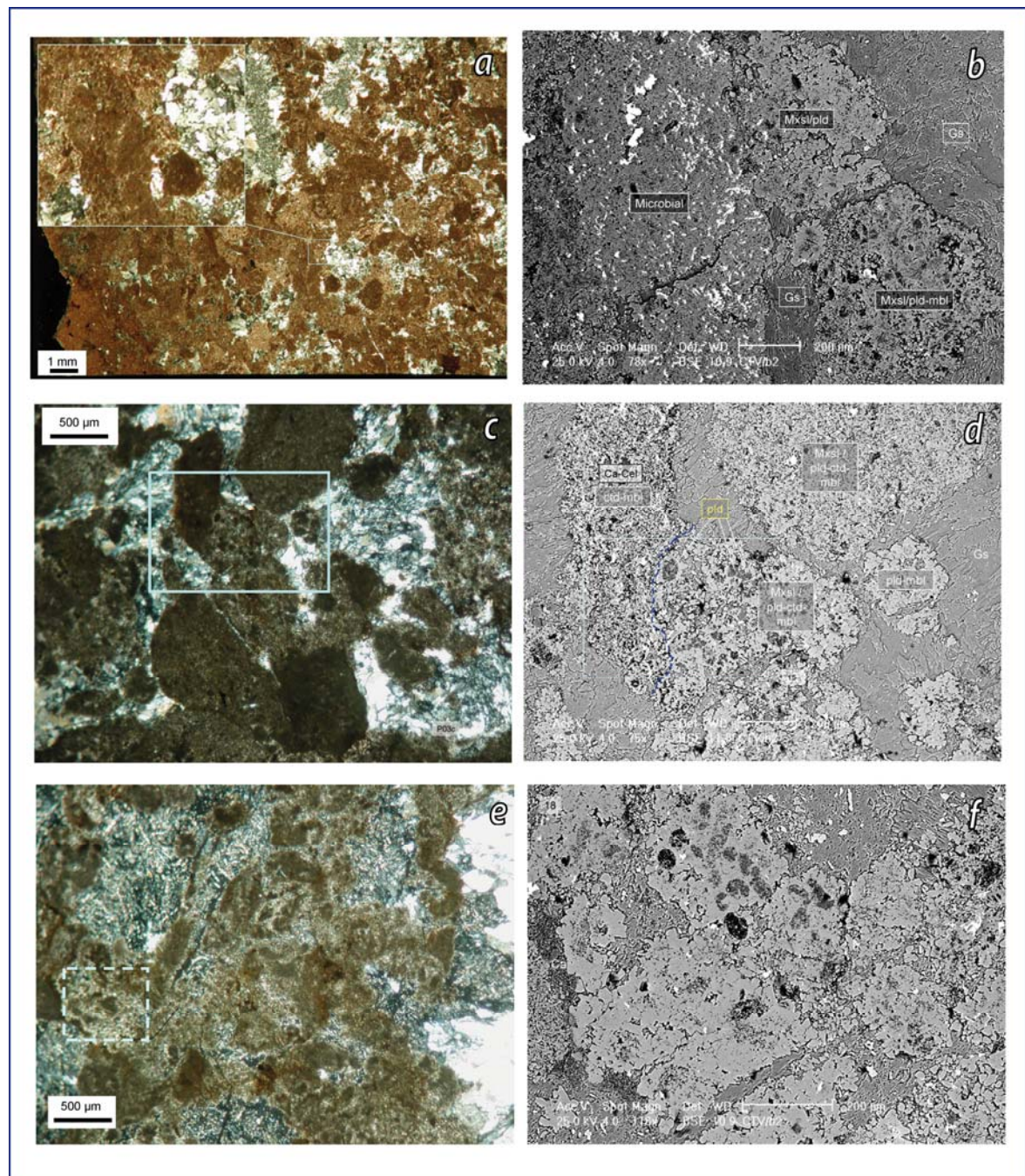
Fig. 4.2.23 - Crotone Basin - Sample CTV b2 (Appendix 3), microfacies. Coupled crossed polars and SEM views (**a**-**b**, **c**-**d**, **e**-**f**, respectively). The microfacies is microbial (mbl), clotted (ctd), peloidal (pld), microcrystalline at places (mxsl) and is accompanied by secondary gypsum (Gs) and celestite (Cel) to different extents. The texture of the cloudy nodules and the peloids contained therein is exalted in SEM view (**d**, **f**).
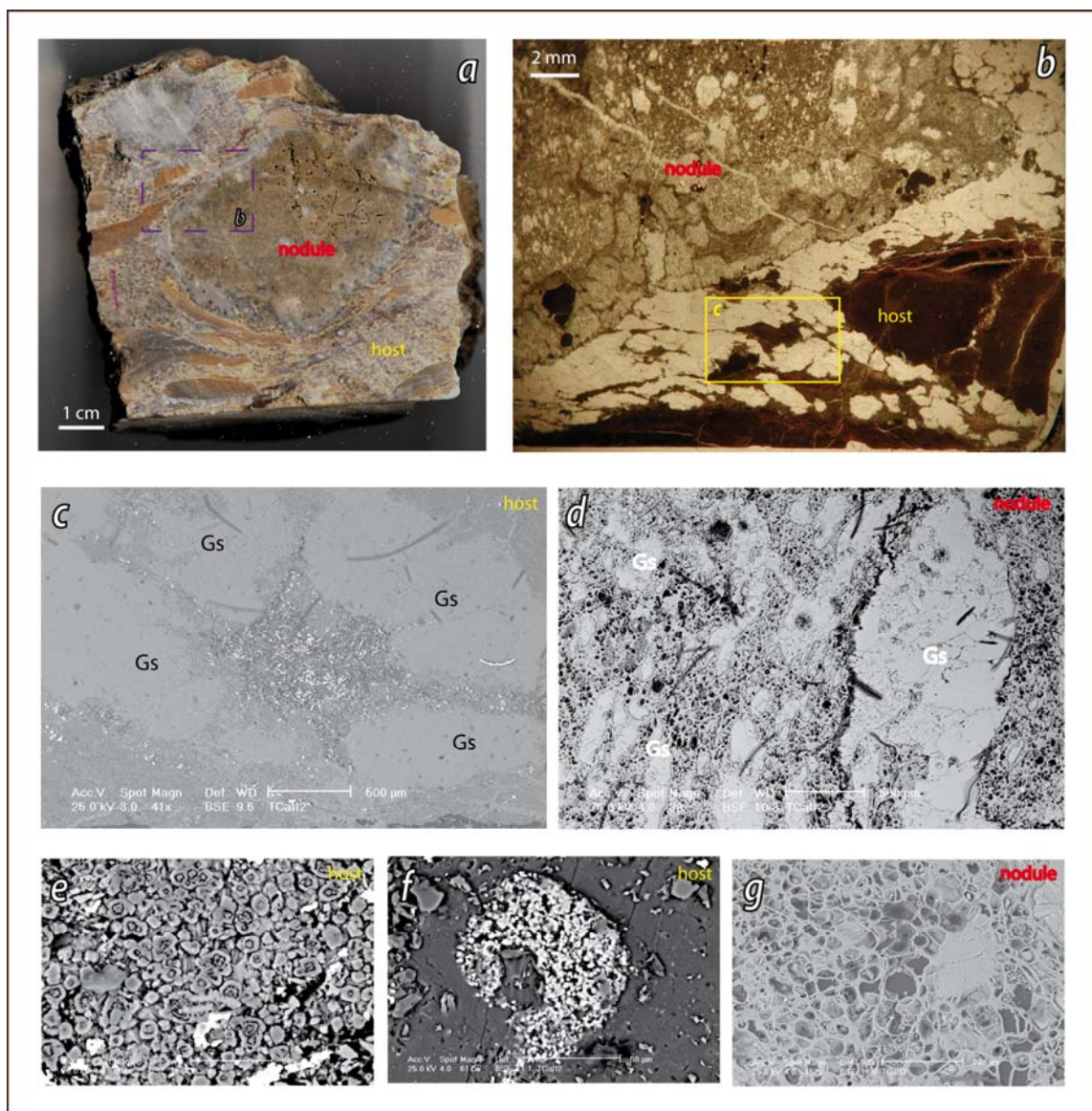
Fig. 4.2.24 - Crotone Basin - Sample TC a (Appendix 3), microfacies: sample slab (**a**), transmitted light (**b**) and SEM views (**c-g**). Vacuolar K-feldspar nodule (**d**, **g**) hosted by a mixed pelitic-carbonatic fluidized matrix (**a**, **b**). Both the subfacies are accompanied by secondary gypsum (Gs; **c-d**). The host rock is constituted by both calcite and dolomitic microtextures (**e**) and yields celestite (**c**, **e**; white in SEM view) and framboidal pyrite (**f**).

4.2.4 - Geochemical dataset: Oxygen and Carbon stable isotopes

The δ^{13}C signature in the Calabrian Calcare di Base is typified by slightly negative values, mainly comprised between 0 and -4 ‰ PDB, where the most depleted samples reach values down to ~-6 ‰ PDB (Fig. 4.2.25, Appendix 3). Generally, the more cemented facies are slightly more depleted, but no significant variation in the signal has been observed. The common occurrence of celestite revealed by facies analysis may testify the transformation of aragonite into calcite, that constitutes alone the main diagenetic process consistent with this kind of depletion in ^{13}C. Notwithstanding, the occurrence of framboidal pyrite suggests also a possible minor contribution of bacterial processes.
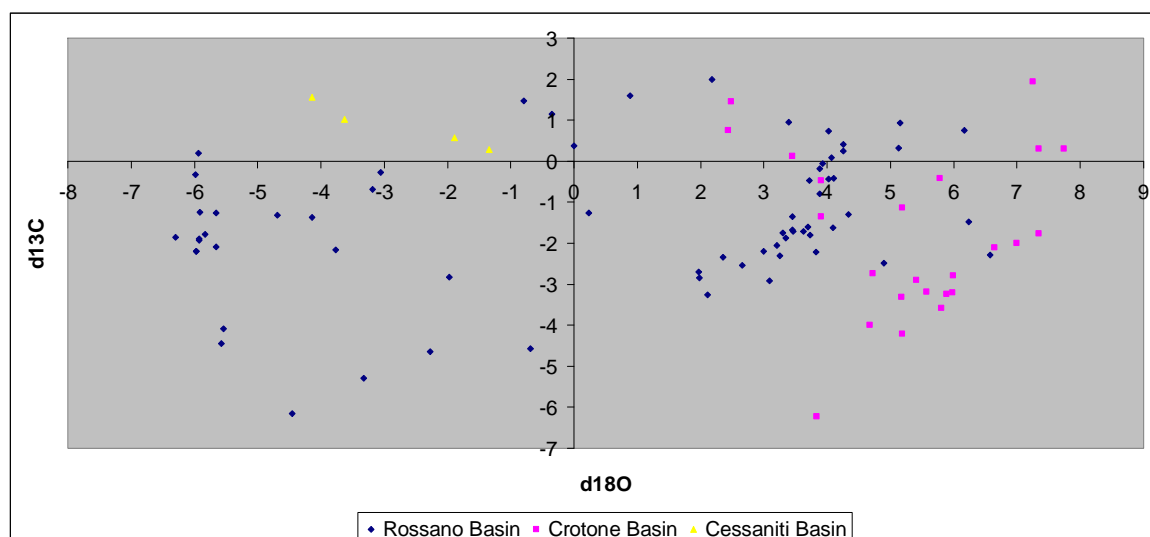
Fig. 4.2.25 - Cross plot of stable isotopes data of the Calcare di Base Fm. in the Calabrian Arc.

In terms of $\delta^{18}O$, the CdB from Crotone and Rossano must be differentiated (Fig. 4.25, Appendix 3), though to a minor extent:

- in the Crotone Basin $\delta^{18}O$ is always positive (~ +2 up to +8 ‰ PDB);

- in the Rossano Basin two distinct subsets of data can be enucleated: (a) a positive subset, with values mainly spanning between about +2 and +6 ‰ PDB, comparable to the samples from Crotone; (b) a negative subset, ranging from 0 down to about -6 ‰ PDB.

Subsampling didn't put in evidence a great variation within the signal. An exception is represented by the sample CROP 3-1 (Appendix 3). The variation within the sample can be easily explained with an increase in the $\delta^{18}O$ signal coupled to the increasing pelitic content.

Three samples of stromatolites yield an isotopic signature (Appendix 3) comprised in the common range evidenced by the authors for this kind of facies (Bellanca et al., 2001; Blanc-Valleron et al., 2002).

The $\delta^{18}O$-depleted samples in the Rossano basin were collected along the section CROP 3. The main difference between the sections CROP and CROP 3 lays in the significantly higher brecciation in the second section. According to the proposed fluid-induced brecciation model, different brecciation degrees are related to different flux rates, definitely leading to differential fluid-rock interaction: the different isotopic signature could be ascribed to such local responses in presence of ascending saline fluids (see Ch. 4.2.5.c for discussion).

The common occurrence of a positive oxygen signature in the Messinian Calcare di Base is interpreted to represent a direct marker of hypersaline conditions during precipitation (Caruso et al., 2009 and ref. therein; Manzi et al., 2010). Nonetheless, the detailed molecular study conduced by Guido et al. (2007) in the CdB of Rossano Basin clearly rules out the occurrence of such conditions, at the least in this basin. In addition, the facies analysis revealed that the Calcare

di Base in the Calabrian Arc experienced important diagenetic processes. Tentatively, the coupled positive $\delta^{18}O$ - negative $\delta^{13}C$ widely typifying the Calcare di Base both in Sicily and Calabria, can be related to gas hydrate destabilization processes, as already suggested by Pierre & Rouchy (2004). This delicate topic will be matter of discussion in the Chapter 5.

4.2.5 - Discussion

4.2.5.a - The Calcare di Base in the Calabrian Arc: stratigraphic implications

In the Calabrian Arc the Calcare di Base Fm (CdB) conformably rests above the Tripoli Fm (Tr). Laminitic dolostones, referable to stromatolitic facies, mark the gradual transition from the Tr to the CdB in the Rossano Basin. In the model recently envisaged by Manzi et al. (2010), this laminitic facies represents the sole proper basal limestone marking the onset of the Messinian Salinity Crisis; they name this subfacies of the Calcare di Base "CdB Type 2". The other two types enucleated by the authors are: the brecciated limestones ("CdB Type 3") and the sulphur bearing limestones ("CdB Type 1"). CdB Type 1, cropping out only in Sicily, is therein considered a late diagenetic counterpart of CdB Type 3, since these two types substitute laterally. The authors stress the systematic unconformable contact between CdB type 2 (basal limestone) and CdB type 1-3, through the polyphased Messinian Erosional Surface (MES). By contrast, in the Rossano Basin a gradual transition between the CdB type 2, actually marking the basal portion of the CdB, and the brecciated facies (CdB Type 3 sensu Manzi et al., 2010) has been observed. In addition, the brecciated limestones are cut on top by the MES, and don't lay above it. Therefore, the CdB of the Calabrian Arc belongs to the first step (evaporitic l.s.) of the crisis and marks its onset (cf. CIESM, 2008).

4.2.5.b - Primary facies and secondary processes

Within an integrated microfacies-biogeochemical study, Guido et al. (2007), clearly constrained the genesis of the CdB of the Rossano Basin: a microbialitic limestone precipitated in unstable marine (non-evaporitic) environment, with aperiodic freshwater inputs and with random and short-lived dysoxic/suboxic episodes.

In this work post-depositional processes affecting this primary facies were enucleated: 1) secondary nodules growth, further experiencing brecciation; 2) brecciation accompanied by diffused fluidification of an early diagenized sediment and focused fluid flow in correspondence to small- and macro-scale trajectories.

The common occurrence of celestite is related to these post-depositional events and generally considered a by-product of the early diagenetic transformation of aragonite into calcite. This is consistent with the weak depletion exhibited by the $\delta^{13}C$ signal. Considering the scattered occurrences of framboidal pyrite, a minor contribute of bacterial processes can also be invoked in correspondence to the more depleted samples.

4.2.5.c - The trigger for brecciation and fluid-rock interaction

Brecciation affects the CdB of the Calabrian Arc to different extents. The bedding planes of the brecciated bodies are always concordant to relict laminae, at places overprinted by brecciation, and even to relict pelitic interbeds within the major carbonatic strata. As a result, they constitute bedding-retentive breccias to a major extent. This, together with the occurrence of mosaic-type breccias, point to in situ brecciation phenomena. In addition, no collapse features have been observed. The CdB succession displays high variation in the brecciation degree, both vertically and laterally, thus pointing to a trigger that provokes variability in the intensity of fragmentation and is able to localize brecciation.

The main textural characters of the brecciated limestones can be summarized in the following points:

- breccias show no gravity segregation proxies;

- brecciated limestones are referable to a wide spectra of variously mud-supported to clast-supported breccias (in the Rossano Basin the first type predominates in the lower portion, whilst the second one characterizes the upper portion);

- clasts are generally subangular;

- laterally, brecciation is either pervasive or localized in microbrecciated portions;

- the rheological behaviour exhibited by some samples, show the coexistence of brittle behaviour (rock fragments) and plastic behaviour (muddy stretched elements), pointing to a phenomenon taking place in early diagenized sediments;

- brecciation affects not only the limestones beds, but is revealed at the microscale, even by the basal stromatolitic beds and by the major pelitic horizons (lithology-independent brecciation);

- breccias yield scale independent patterns, typically associated to fluid-induced brecciation (Turcotte, 1997).

These elements, together with the occurrence of fluidification textures exhibited by the microbial component, converge to depict a fluid migration scenario, where the release of overpressured fluids could have likely triggered brecciation, diffused but localized.

Two end-members were found within the array of breccia types in the Rossano Basin: 1) mud-supported breccias, with clasts of different nature floating in a very fine grained matrix; 2) clast-supported breccias, in which the nature of the clasts is the same as the host rock, small exotic microbial elements were found only within the cement precipitated in the fine network among the clasts (Fig. 4.2.14).

Interestingly, these variations could be explained in terms of mud volcano deposits. The latter actually generally comprise a variety of clasts and rock fragments in a clay rich matrix: the ratio of clasts to matrix
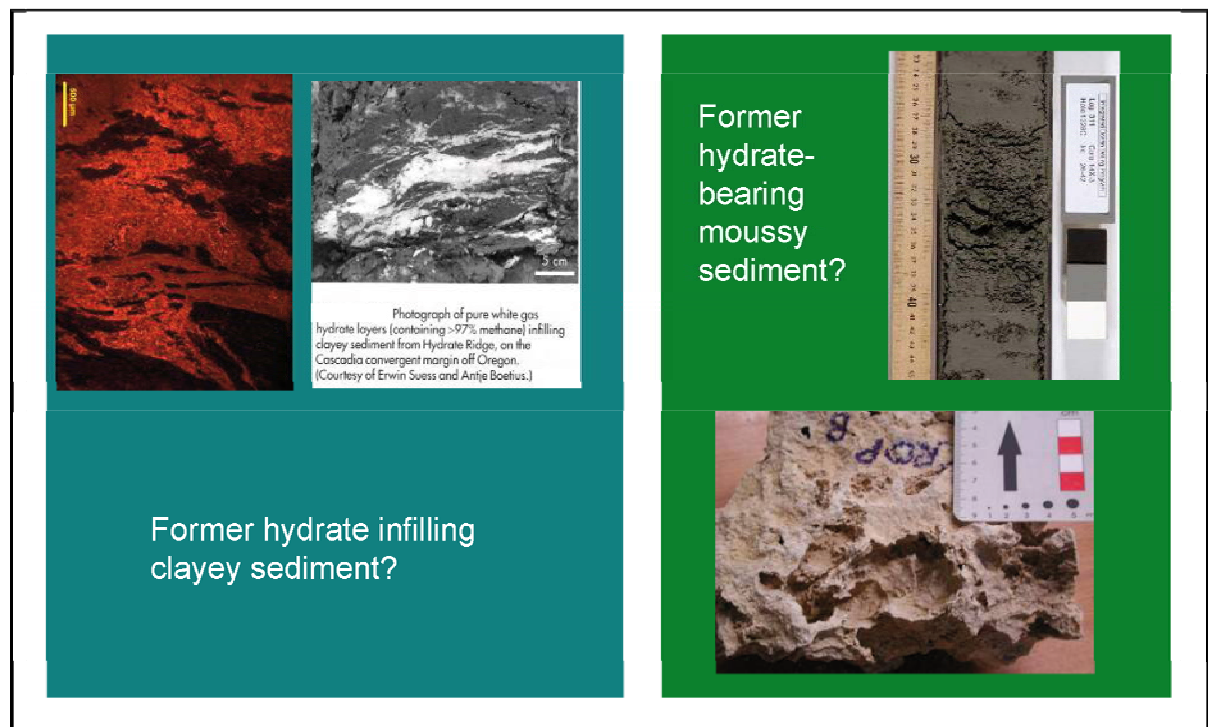
Fig. 4.2.26 - Gas-hydrate resembling textures in the Calcare di Base of the Calabrian Arc.
Pelite (sample CROP 3-13) infilled by carbonatic cement in cathodoluminescence view, strictly resembling the texture resulting from gas hydrates infilling fine sediments in the Hydrate Ridge (left side).
Common texture of the concretions of the CdB in the Rossano Basin, possibly inherited from a former hydrate-bearing moussy sediment (right side).

covers the entire spectrum from clast-supported deposits to virtually clast-free homogeneous mud (Kopf, 2002). In this view, the aforementioned clast-supported breccias from Rossano basin can be referred as to parent bed-related breccias, where a parent bed is defined as "a stratigraphic horizon that provides the bulk material that ascends and extrudes; often undercompacted and rich in clay or fluids" (Kopf, 2002). In the specific case the clay content is negligible, the mud fraction is rather represented by a microbial sediment (Guido et al., 2007). The suggested mud volcano scenario must be considered only as a working hypothesis for the moment.

The sedimentological data lead to rule out the clastic origin envisaged for the Calcare di Base of the Rossano and Crotone basins:

o   no bed gradation was observed;

o   no erosional bases were detected, but irregular surfaces, isolating portions with higher brecciation degree;

o   no clay chips were found, but rather relict pelitic interbeds (fls);

o   no load structures were found, but rather fluid-related features;

o the clastic gypsum claimed by the authors within the CdB, is herein rather interpreted as secondary gypsum filling porosity, possibly related to hypersaline fluid circulation: the cemented gypsum infillings could have eventually in turn experienced fragmentation.

The negligible detrital input is confirmed by NRD proxies, that independently rule out the occurrence of resedimented processes.

Only in the Crotone basin, locally hybrid resedimented breccias were found associated to the Calcare di Base unit. In this case, local resedimentation processes could have likely accompanied the main fluid release event, possibly acting in interplay with the active tectonic of upper Messinian times, to destabilize sediments.

The depicted diagenetic environment was possibly accompanied by gas hydrate formation, as suggested by some peculiar fabrics (Fig. 4.2.26). Nonetheless, the δ^{13}C signature never reaches extremely depleted values, nor is coupled to positive δ^{18}O, therefore, even in case of effective gas hydrate occurrences, no fluid-rock interaction would have taken place during their possible release. This scenario doesn't seem reasonable, but must be notwithstanding taken into account. More likely, the nature of the fluids involved was not rich in hydrocarbons, but rather saline. The occurrence of saline fluids on one hand explains the positive oxygen signature without contrasting the genetic model of Guido et al. (2007), that rules out an evaporitic setting for the Calcare di Base Fm; on the other hand is consistent even with the negative δ^{18}O signature recorded in the group of samples from CROP 3 section (Rossano Basin): along CROP3 section a high brecciation typifies the CdB, presumably resulting from significantly higher overpressures of ascending fluids. Higher overpressures of fluids from below are generally coupled to higher flux rates and consequent low fluid-rock interaction: in this view, the contribute of the supposed saline fluids was not recorded in isotopic signal of the breccias collected form CROP3 section. The scenario could envisage the upward migration of saline fluids interacting with a sedimentary column to different extents, according to highly variable flux rates. The hypothesized saline nature of the fluids involved is based on a possible interpretation of the isotopic data and needs further investigations.

4.2.6 - Major remarks

• In the Calabrian Arc the Calcare di Base Fm. crops out as an alternation of thick-bedded massive carbonate and pelites, conformably overlaying the pre-evaporitic unit (Tripoli Fm.).

• The transitional contact between the Tripoli Fm. and the Calcare di Base Fm. is marked by the occurrence of laminitic dolostones, representing stromatolites, defining both the topmost interval fo the Tripoli Fm and the base of the Calcare di Base.

• The Calcare di Base is represented by mud- to clast-supported breccias accompanied by concretions: their occurrence isolates relict laminae, witnessing the primary deposits.

- Bedding planes are always concordant to relict lamination and to relict pelitic interbeds as well, thus defining primary bedding-retentive breccias and pointing to in situ-brecciation phenomena.

- The sedimentological features yield by the breccias, together with their scale independent and lithology-independent pattern, their localization at the small scale, the occurrence of fluidification textures affecting the primary microbial facies and the occurrence of small scale channels, point to fluid-induced brecciation phenomena.

- In the Rossano Basin, brecciation remarkably increases upward and shows an irregular lateral variability, accounting for variable flux rates through space and time, and consequent variations in the fluid-rock interaction.

- Brecciation was experienced by an early diagenized sedimentary column - as shown by the complex rheology exhibited by the facies - where earlier cementation, resulting in growth of nodules, was taking place.

- The inventory of facies found in the Rossano Basin, in view of the depicted environment, could possibly be related to a mud volcano structure.

- The nature of the fluids involved remains obscure, but a saline nature is tentatively suggested; the occurrence of gas hydrates, as a speculative hypothesis, is not even ruled out.

- Contextually to the development of the Messinian Erosional Surface, cutting the CdB on top in the Calabrian Arc, high depressurization due to sea level drop took place: this likely enhanced a catastrophic migration of previously overpressured fluids from below.
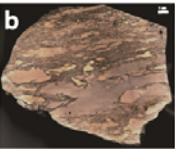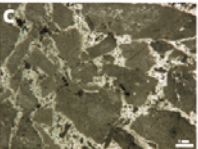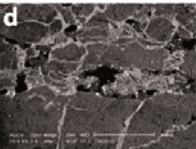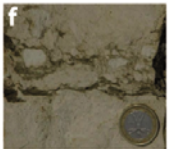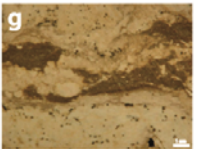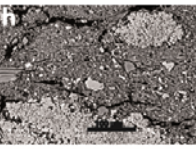
Fig. 4.2.27 - Scale-independent processes in the Calcare di Base of the Calabrian Arc: brecciation (**a-d**) and secondary growth of nodules (**e-h**).

4.3 - The *Calcare di Base* in Sicily

4.3.1 - Geological setting and the Messinian record in the area

The Messinian basin of Caltanissetta, in central Sicily (Fig. 4.3.1), displays the most complete sedimentary successions present in the Mediterranean uplifted basins. The anatomy of the basin was typified by a series of thrust-related synclines, resulting into tectonically separated several sub-basins (Butler et al., 1995). They represent the outer part of the Maghrebian Chain in a zone between the Northern Sicilian Mountains (European plate) and the Hyblean Plateau (African foreland). The Caltanissetta or Central Sicilian Basin corresponds to a broad belt, trending NE-SW across the island, that experienced deformation since the middle-late Miocene, due to continued migration of the orogenic front towards the external (African foreland) areas. This basin was then tectonically uplifted towards the end of the Pliocene, due to major thrusting on the outer margin of the Maghrebian orogen (Kastens and Mascle, 1990).

Late Miocene deposition was consequently controlled by the development of localized but deep basinal depressions and corridors favouring the accumulation of vast thicknesses of evaporites. In the central part of the Caltanissetta Basin the evaporitic succession, which can be compared to the one known in the deep Mediterranean troughs, is intercalated between deep-water deposits of Tortonian-early Messinian and Zanclean age (Schreiber et al., 1976; Rouchy, 1982; Schreiber, 1988). In this area, the classic stratigraphic model recognizes two main evaporitic units separated by an intra-Messinian tectonic unconformity (Fig. 4.3.2; Decima & Wezel, 1971; Butler et al., 1995; Rouchy & Caruso, 2006). From bottom to top, the lower unit consists of the Tripoli Formation, Calcare di Base Formation, Lower Gypsum and Salt. According to the classic view, the Calcare di Base was deposited in the shallow portion of the Caltanissetta Basin and represents the stratigraphic equivalent of the Lower Gypsum that occurs in the deepest portion of the basin. The upper unit is formed by the Upper Gypsum overlain by the Arenazzolo Formation, siliciclastic lacustrine and fluvial/alluvial facies (Decima & Wezel, 1973; Cita & Colombo, 1979), in turn capped by the pelagic Early Pliocene Trubi Formation, which marks the re-establishment of normal marine conditions as a consequence of flooding from the Atlantic (Cita, 1975; Di Stefano et al., 1999; Rouchy et al., 2001). According to Roveri et al. (2001) and Manzi et al. (2007), in Sicily, as well as in the Northern Apennines, the Lower Gypsum includes both primary gypsum (shallow water facies) and resedimented gypsum (deep water facies). In Sicily, the Primary Lower Gypsum was deposited only in the innermost wedge-top basins and in the Hyblean foreland ramp basins, and is not associated with the Salt and/or the Calcare di Base (Roveri et al., 2008). For many authors, the Calcare di Base is laterally equivalent

to the Lower Gypsum and marks the onset of the MSC, preceding the deposition of the sulphate and salt evaporites of the Gessoso-Solfifera Formation (McKenzie, 1985; Bellanca & Neri, 1986;
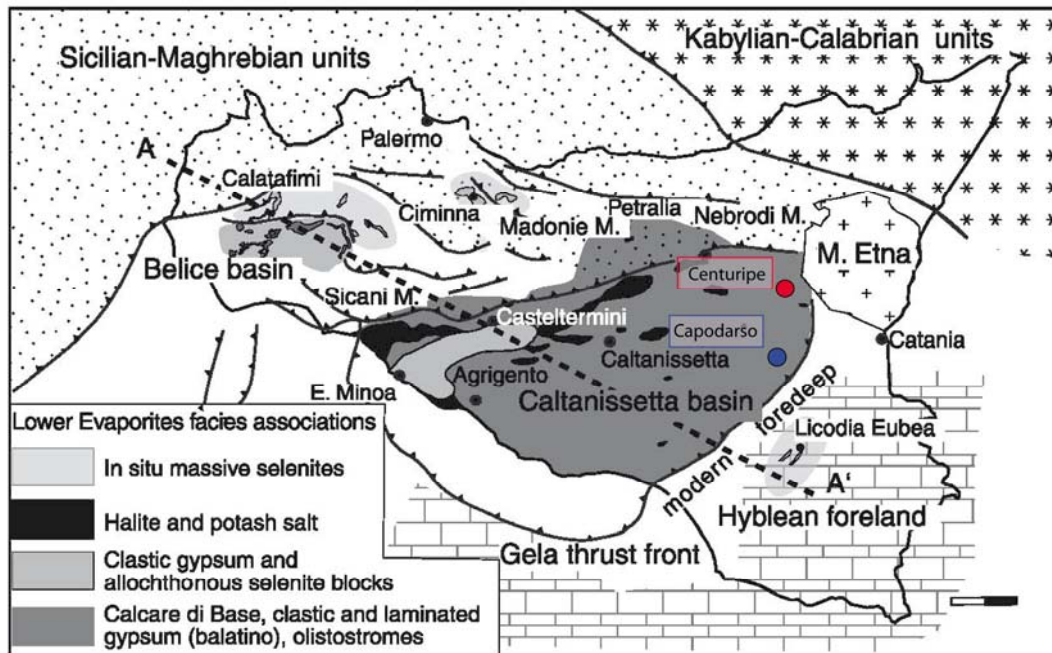
Fig. 4.3.1 - Schematic geological map of Sicily (after Roveri et al., 2006) and location of the study areas in the Caltanissetta Basin.
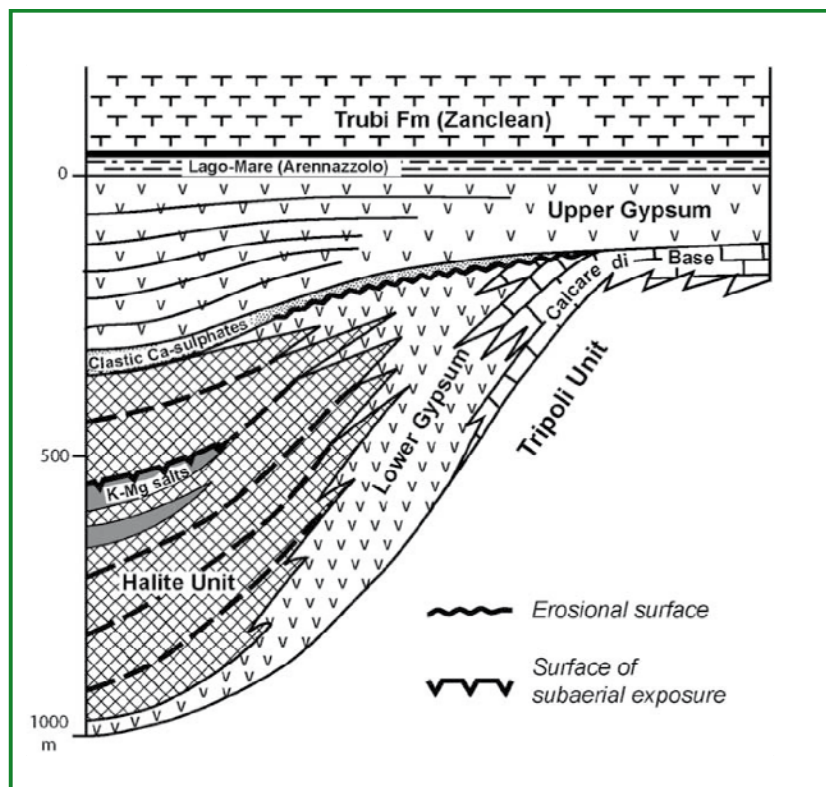
Fig. 4.3.2 - Simplified three-step model of the MSC record in the Central Sicilian Basin (after Rouchy & Caruso, 2006). The stratigraphic position of both the Calcare di Base and the Salt unit is still highly debated and recently ascribed to the second phase (CIESM, 2008; Roveri et al., 2008).

Decima et al., 1988; Caruso et al., 1997; Bellanca et al., 2001; Rouchy & Caruso, 2006). In contrast, taking the view that the Calcare di Base is mostly a non in situ brecciated limestone, Roveri et al. (2008) argue that its base represents a regional-scale unconformity and that it does not mark the onset of the MSC. Roveri et al. (2008) support Hilgen & Krijgsman (1999) in recognizing the dolostones above the Tripoli Formation as the only part of the Calcare di Base representing a lateral equivalent of the primary Lower Gypsum. The diachronous vs. synchronous character of the onset of MSC evaporite deposition in Sicily is also still controversed (Gautier et al., 1994; Krijgsman et al., 1999; Cavazza & Wezel, 2003; Butler et al., 1995, 1999; Riding et al., 1998).

4.3.2. - Field data: stratigraphy and main lithofacies

<u>Capodarso</u>

The Messinian Capodarso succession, located in central Sicily, was laid down in the northern marginal belt of the Late Neogene Enna-Caltanissetta piggyback basin, which developed above a Tertiary roof-thrust complex. At Monte Capodarso (Fig. 4.3.1), in correspondence to a former sulphur mine, crops out the well known extremely δ^{13}C-depleted sulphur-bearing limestone Auctt. It has been deeply studied and generally considered a late diagenetic by-product of bacterial sulphate reduction (Manzi et al., 2010 and ref. therein). Recently, Ziegenbalg et al. (2010), through an accurate geochemical investigation accompanied by microfacies analysis, rather pointed out the syngenetic character of their mineral authigenesis, likely fuelled by methane.

The contribute of the present work lies in the detection of peculiar structures in the facies and their comparison to the more refined results obtained in the correlatable units of the Maiella Basin and the Calabrian Arc.

The sulphur-bearing limestones transitionally rest above the Tripoli Fm and are overlain by a clastic gypsum unit (Ziegenbalg et al., 2010; Manzi et al., 2010). Patches of highly recrystallized brecciated limestone also lie above a gypsum-laminites unit, pointing to their strata-bound character.

The limestones are arranged in thick beds organized in multiple centimetric bedsets (Fig. 4.3.3), where the mesofacies is a clast-supported breccias, with subrounded to subangular clasts associated to mosaic-type breccias (Fig. 4.3.3 a). Sulphur-bearing veins, native sulphur inclusions and impregnations commonly occur. On the top surfaces of the beds peculiar carbonate and gypsum tubular features have been observed, presumably representing pipes structures, never noticed in the previous literature (Fig. 4.3.4).

Fig. 4.3.3 - Capodarso - Bedding retentive breccia (**a**); detail of the subrounded to subangular clasts (**b**) and mosaic breccia type (**c**)
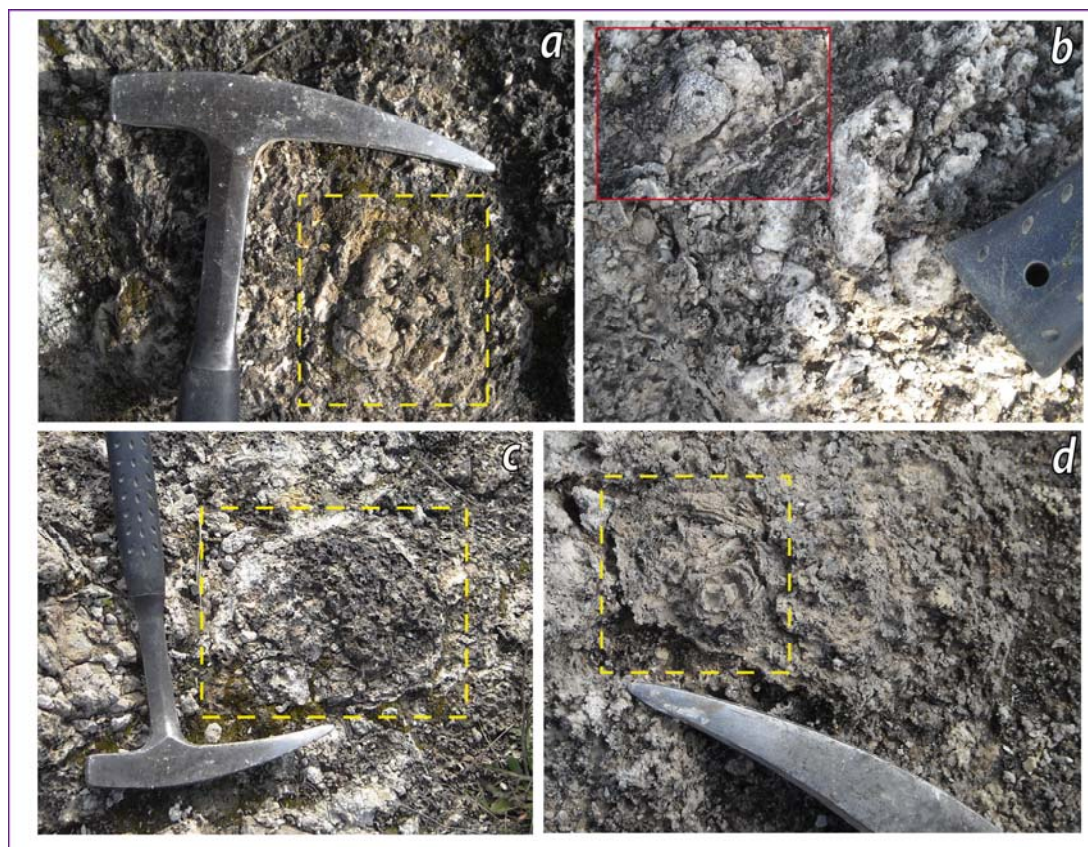
Fig. 4.3.4 - Capodarso - Fluid escape features at the mesoscale. Top views of the brecciated beds, showing carbonatic (**a**) and gypsum (**b**) cylindrical concretions, and gypsum internal conduits with concentric structures (**c-d**).

Centuripe
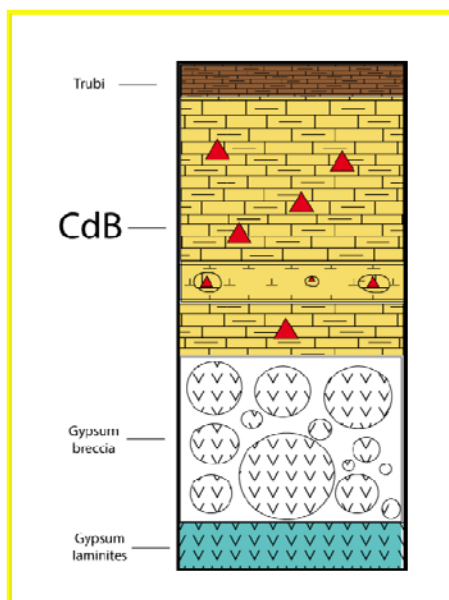
Fig. 4.3.5 - Simplified log showing part of the Messinian record in the nearby of Centuripe. Here the Calcare di Base rests above a gypsum breccia and is directly topped by the Pliocene marls (Trubi Fm).

The units cropping out in Centuripe, a village at the foot of the Etna, belong to the north-eastern sector of the Caltanissetta Basin (Fig. 4.3.1). The CdB in this area has been known since the beginning of the previous century (Di Stefano, 1902): it was described as an ocraceous to white spar-rich siliceous concretioned limestone, resting both at the base and locally intercalated to the gypsum-bearing unit. In that work the attention of the author was placed on the undoubtedly occurrence of Lucina spp. within the unit, though he pointed out their scarce preservation potential, within a few years. These occurrences were reported to be in correspondence to the

- 122 -

road connecting the village of Centuripe to Catenanuova, but today these Lucina-bearing geobodies don't crop out anymore.

Fig. 4.3.6 - Centuripe - Brecciated limestones (**a-b**) and gypsum breccia (**c**). The cemented brecciated limestones are typified by centimetric to subcentimetric clasts randomly oriented and showing no gradational patterns.

In correspondence to this site it was possible to reconstruct the following stratigraphy (Fig. 4.3.5):

1) gypsum laminites passing up-section to unconsolidated gypsum breccias (Fig. 4.3.6 c), made up of decimetric to submetric clasts (Resedimented Gypsum);

2) marly limestone breccias (Calcare di Base), associated to laminated portions and carbonate nodules;

3) marls and clays rich in foraminifera (Trubi Fm, Pliocene).
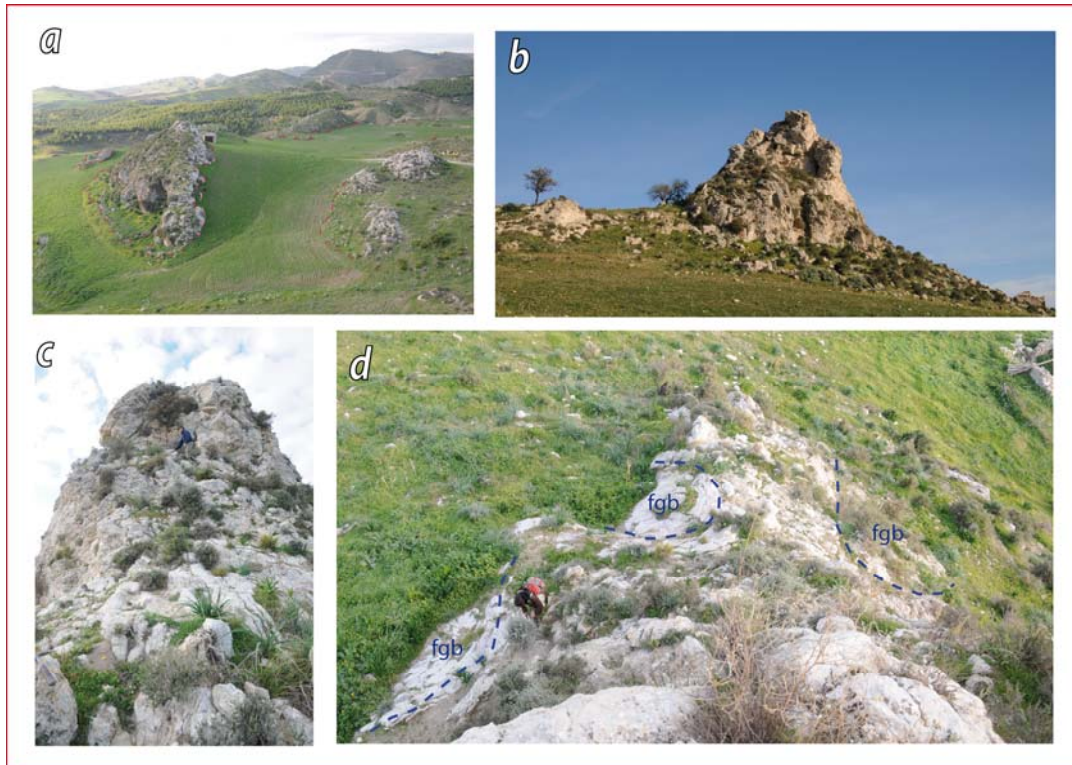
Fig. 4.3.7 - Centuripe - Isolated carbonate brecciated bodies, interpreted as outcrop-scale plugs (**a**) and chimneys (**b-d**). The plug is possibly dissected by a fault on its right side (**a**); the base of the chimney (**d**) is typified by fluidized gypsum-bearing facies association (fgp; see Fig. 4.3.9 d for details).

The Calcare di Base consists of thick bedded highly cemented breccias, yielding irregularly shaped subangular clasts, with no gradational pattern (Fig. 4.3.6 a-b).

In the vicinity of Centuripe, isolated CdB geobodies forming huge structures, with plug- and pipe- like shapes, crop out (Fig. 4.3.7). The main body is typified by variously subangular to subrounded clast-supported breccia (Fig. 4.3.8), laterally passing to verticalized laminae and brecciated horizons (Fig. 4.3.9 a, c). The facies association also contemplates: irregular carbonate encrustations (Fig. 4.3.10 a), patches of amorphous silica-bearing laminites (Fig. 4.3.10 b) and siliceous pore-filling cement (Fig. 4.3.10 c). All around the base of the supposed huge pipe, a gypsum bearing facies association yielding tear features was detected (Fig. 4.3.7 d). It encompasses: gypsum showing concentric textures (Fig. 4.3.9 b) and small fluid migration conduits arranged in complex cross-cutting patterns (Fig. 4.3.9 d). These structures contain secondary gypsum, carbonate breccias and siliceous-carbonatic laminae.
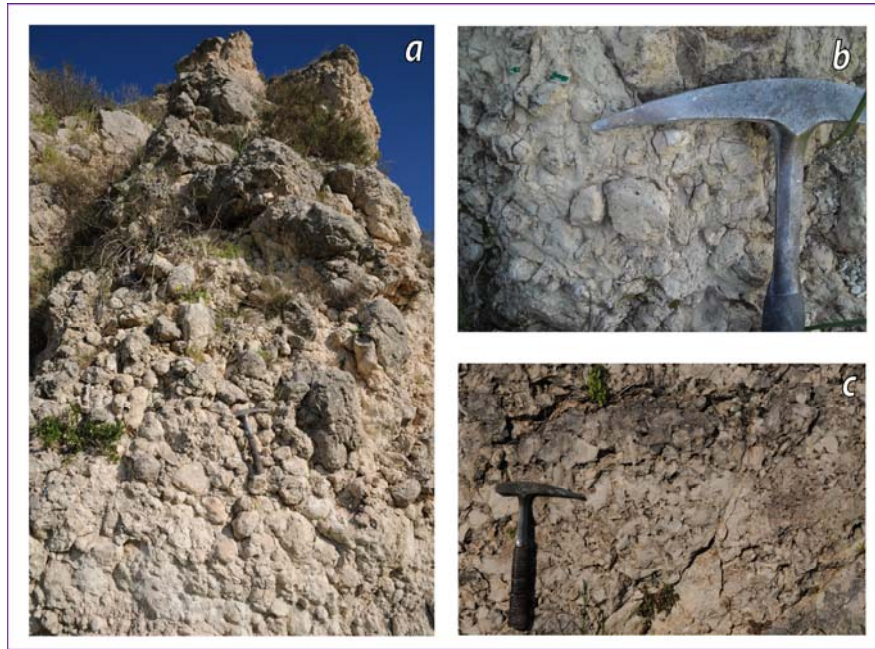
Fig. 4.3.8 - The structures interpreted as conduits are characterized by densely packed clast-supported breccias, typified by both subrounded/rounded (**a**-**b**) and subangular clasts with articulated shapes(**c**). Locally the first type is also matrix-supported, with the clasts floating in a muddy matrix (**b**).
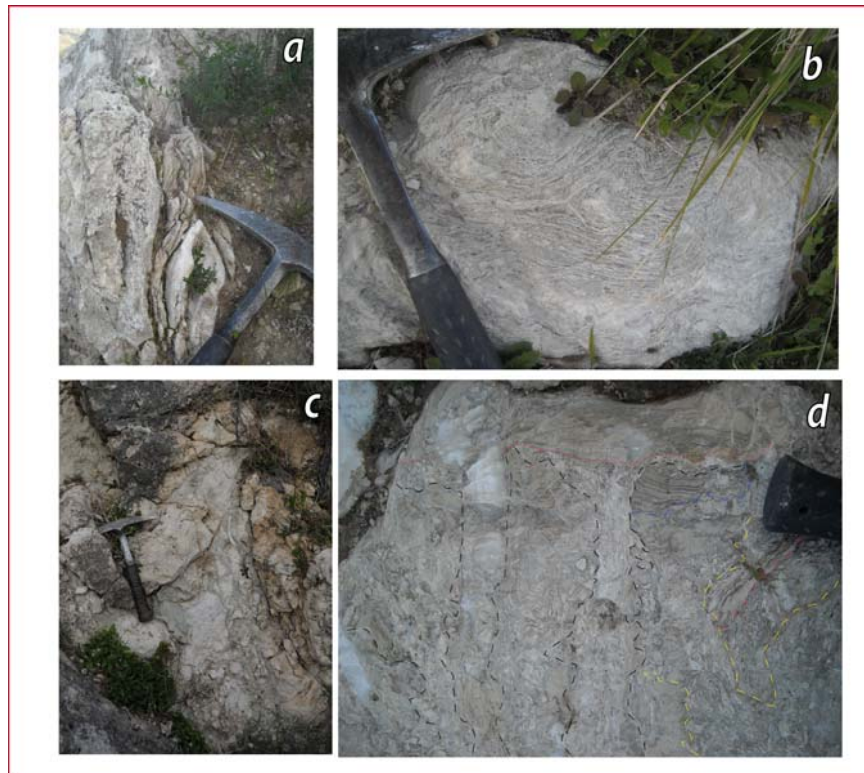
Fig. 4.3.9 - Centuripe - Fluid migration features at the mesoscale: locally verticalized limestone laminites (**a**) and breccias (**c**); possibly fluidized concentric structures in gypsum, top view (**b**); complex cross-cutting relationships in mesoscale fluid-migration feeders, typifying the basal portion of the chimney (Fig. 4.3.7 d, fgb): it is constituted by secondary gypsum, carbonatic breccias (host) and siliceous-carbonatic laminae (**d**).
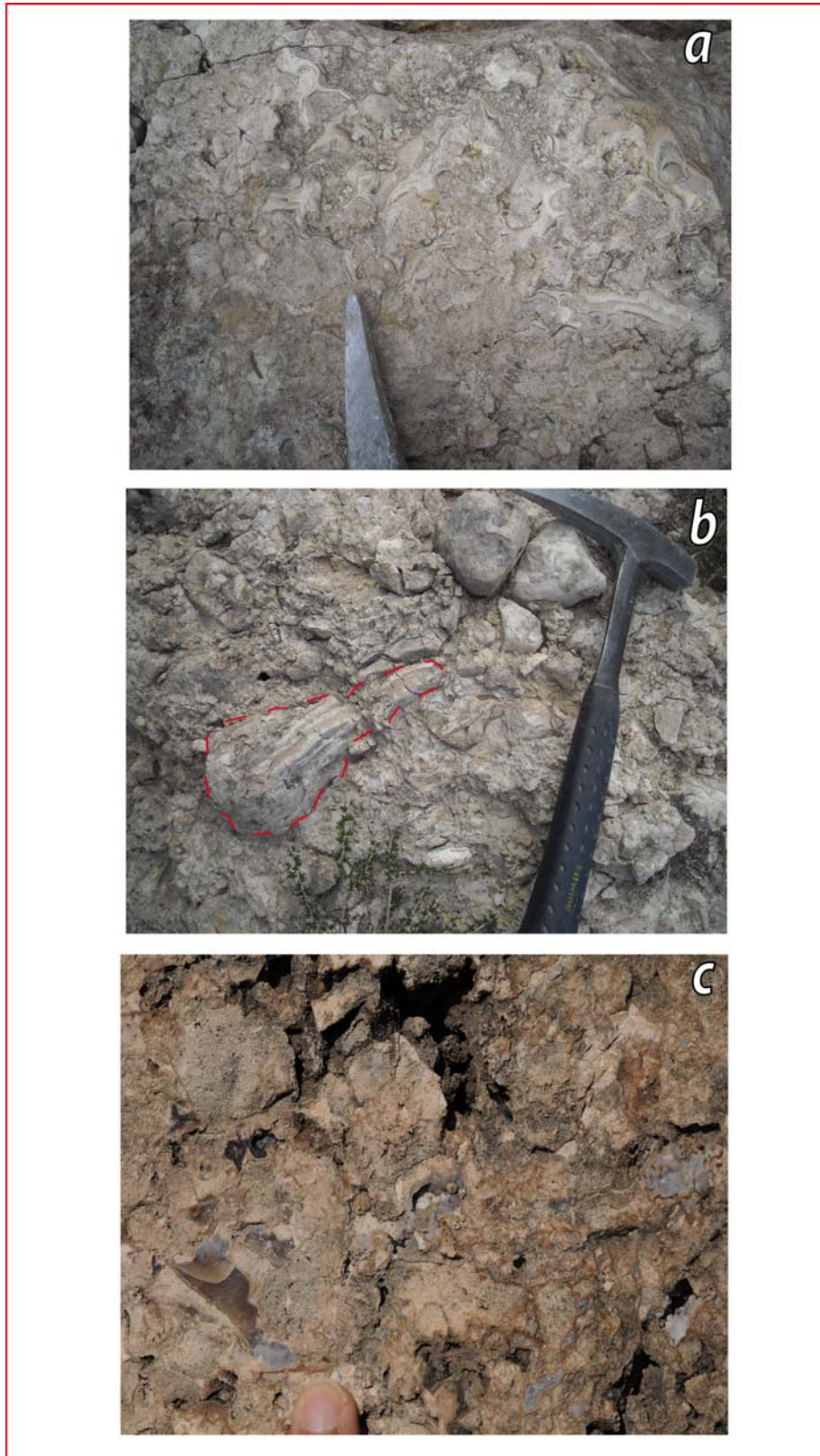
Fig. 4.3.10 - Centuripe - Breccias facies association: irregular carbonatic encrustations (**a**); amorphous silica-bearing patchy laminites (**b**) and siliceous pore-filling cements (**c**).

4.3.3 - Facies analysis

<u>Capodarso</u>

The sulphur-bearing limestones show at the fresh cut a dark cemented matrix infilled by a white cement with different patterns, variously fringing, interlayering or resulting in fragmentation (Figs. 4.3.11-12 a).

The cement is associated to relict pseudo-oolitic features (Figs. 4.3.12 b, 01) and encloses microbial portions (Figs. 4.3.12 b, 02). Abundant barite and celestite typify the cement as well. Ziegenbalg et al. (2010) also noticed the occurrence of Fe-rich dolomites as a component of the cement.

The matrix is completely defined by small microbial-microspar filled pseudomorph after lenticular gypsum (Figs. 4.3.12 b, 03). Therefore, lenticular gypsum microbial mud possibly testify the primary facies, pointing to an original OM-rich environment, where lenticular gypsum crystallization is typically favoured (Cody & Cody, 1988).
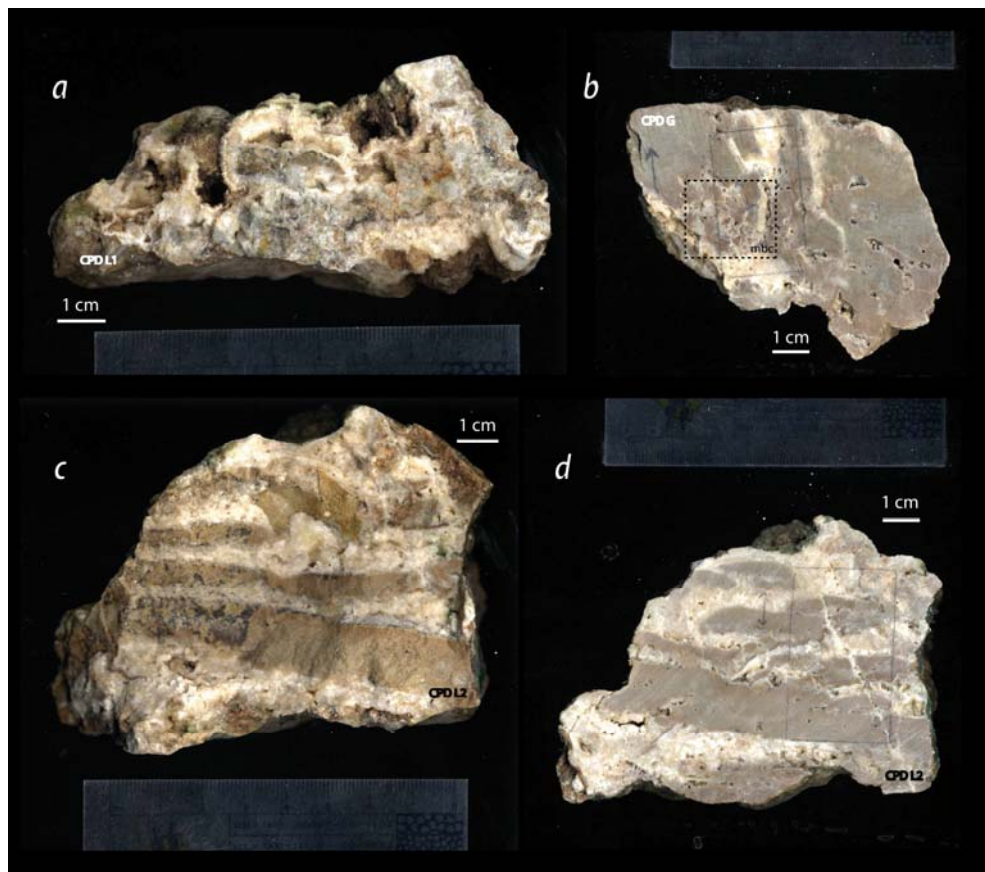
Fig. 4.3.11 - Capodarso - Sulphur-bearing limestones facies. Different patterns of cement associated to the dark cemented matrix: fringing (**a**); fragmenting (**b**, localized microbrecciation - mbc - in the dashed box); interlayered, with local microinjections (**c-d**).
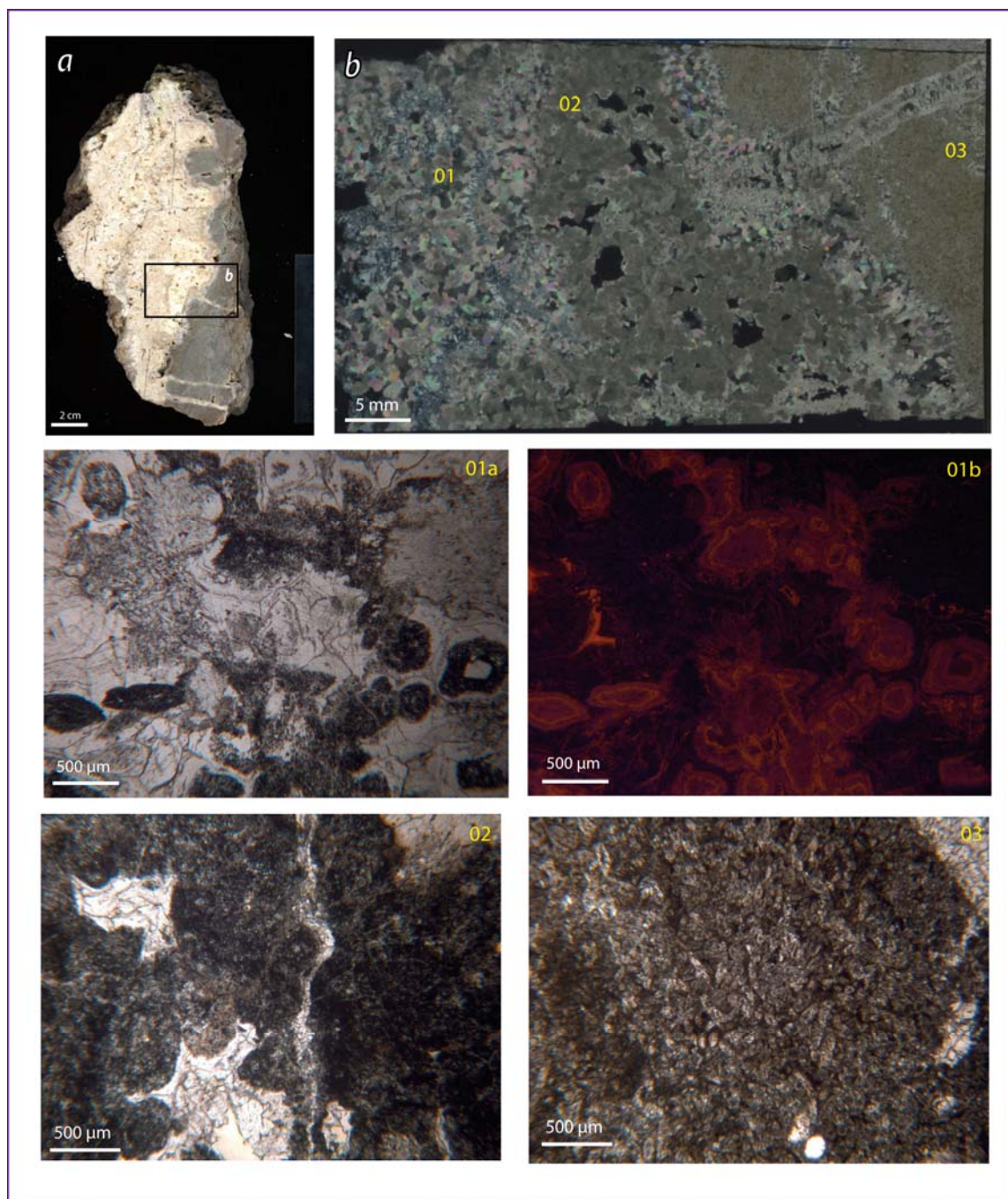
Fig. 4.3.12 - Capodarso - Sample CPD 1, microfacies.

Sulphur-bearing limestone (**a**, rock slab; **b**, crossed polars optical view).

Supposed relict pseudo-ooids (**01a-b**, coupled transmitted light-CL view) and altered microbial (**02**) are associated to the dull carbonate cement (**b 01**, **02**).

Densely packed small pseudomorphs after lenticular gypsum, filled by microcrystalline calcite (**03**) entirely typify the dark-brown cemented subfacies (**b 03**), presumably testifying the primary microfacies.
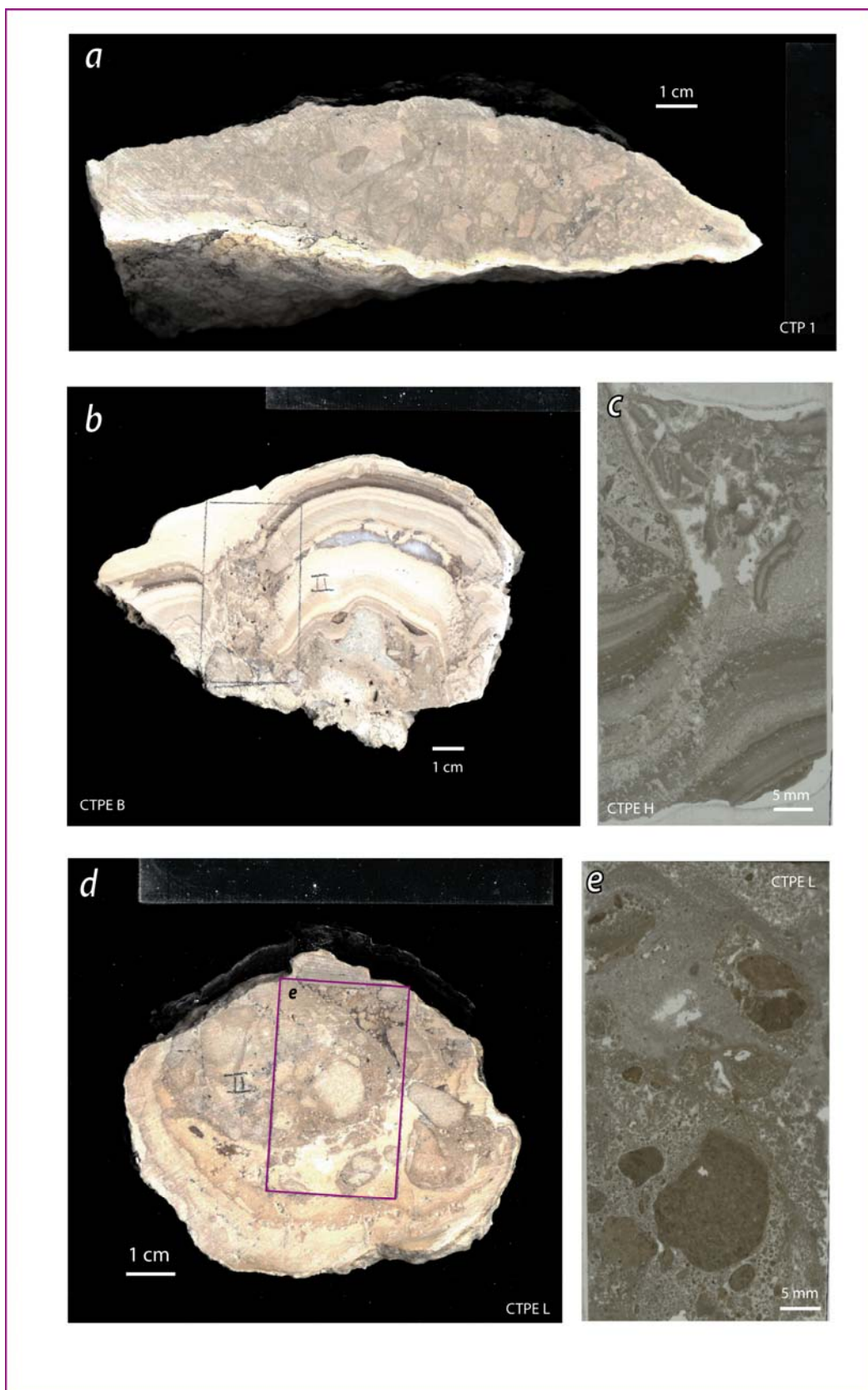
Fig. 4.3.13 - Centuripe - Facies association.
Brecciated limestone with a marly matrix (**a**); amorphous silica-bearing limestone, made up of thinly laminated encrustations, locally microbrecciated (**b**, rock slab; **c**, polished thin section).
Silica-bearing nodule, with rounded microbial elements (**d**, rock slab; **e**, polished thin section).
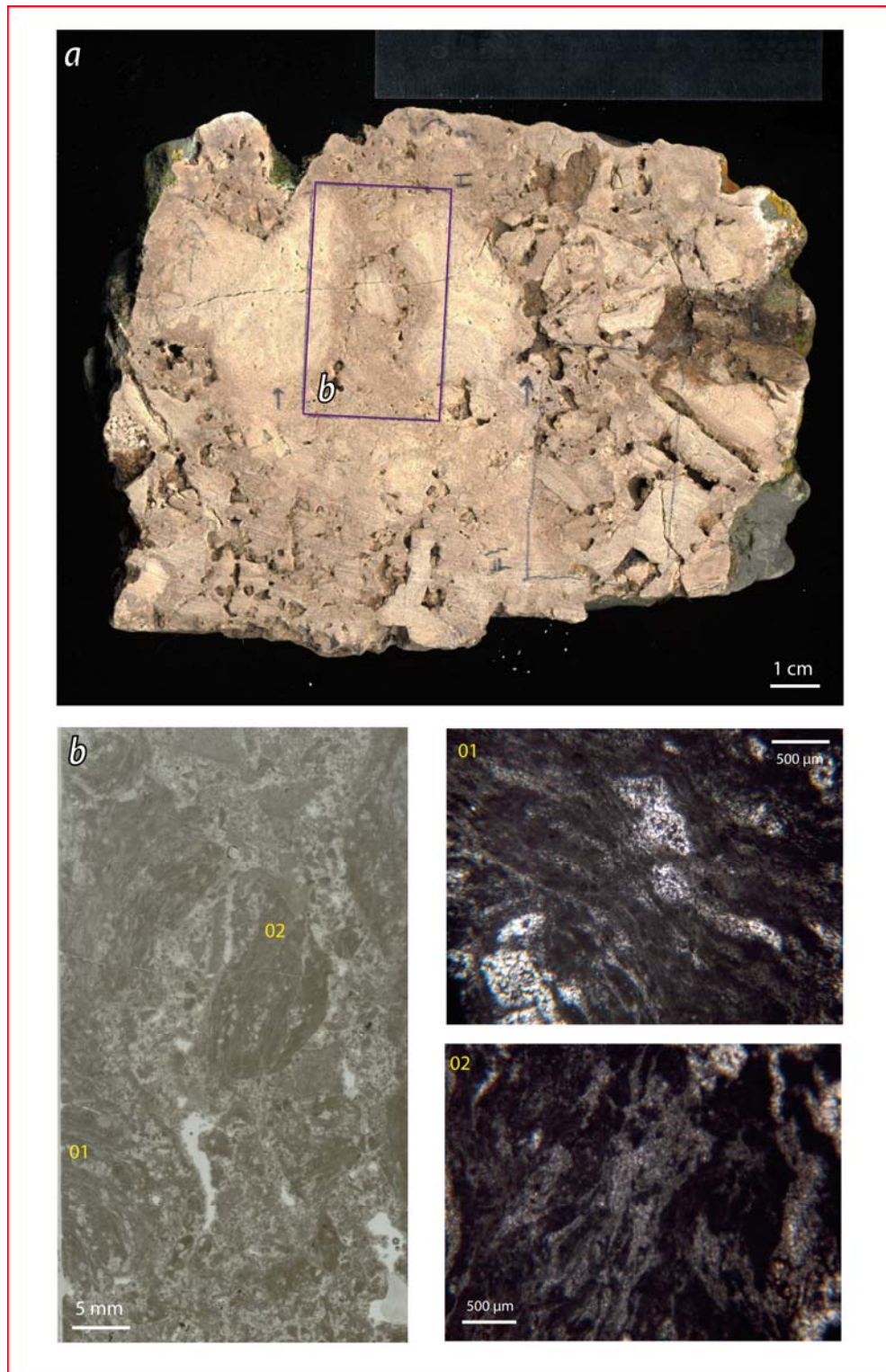
Fig. 4.3.14 - Centuripe - Sample CTPE SA (collected from the plug body), microfacies.
Limestone breccia with subangular clasts (**a**), constituted by a primary microbial microfacies both in the matrix and in the clast components (**b**); details of the fluidized patterns (**01**-**02**).
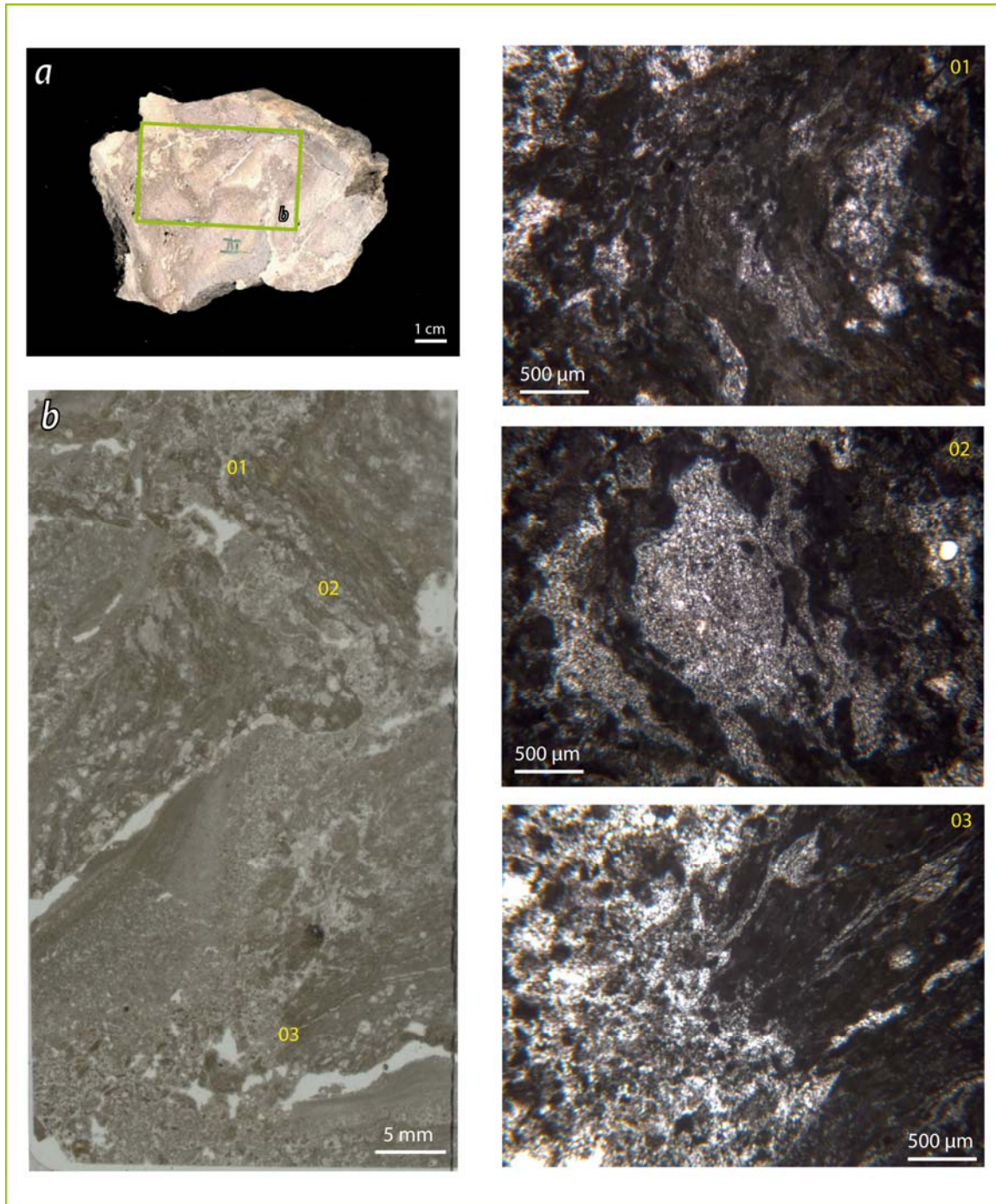
Fig. 4.3.15 - Centuripe - Sample CTPE E (collected from the supposed chimney), microfacies.
Limestone breccia (**a**) with a highly chaoticized microtexture (**b**); details of the microfacies, displaying the fluidification experienced by the clotted microbialite (**01**-**03**).
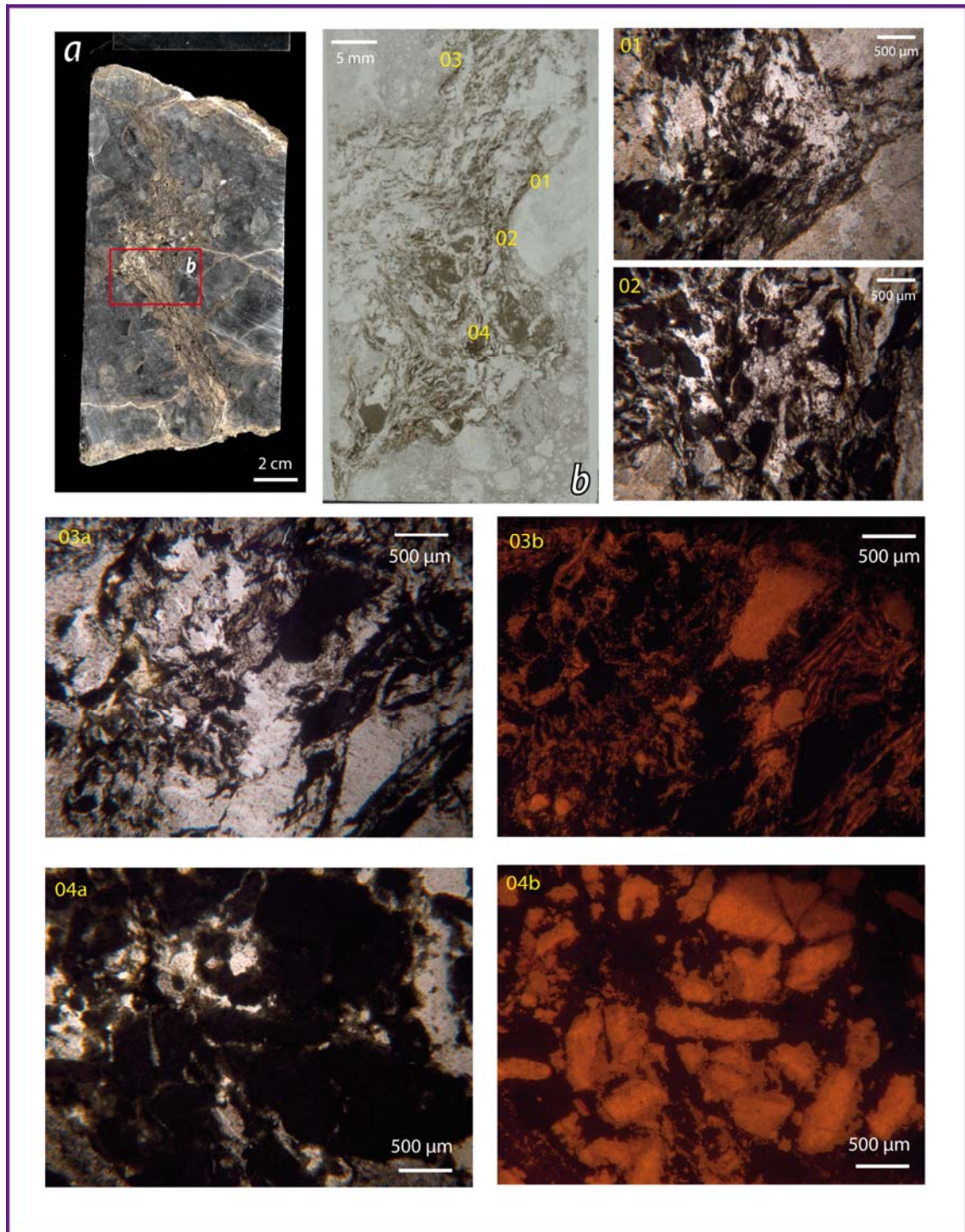
Fig. 4.3.16 - Centuripe - Sample CTP 1d, microfacies.
Gypsum breccia (sample slab, **a**; polished thin section, **b**), with supposed fluid migration pathways (**b**; detail in **01**) and microbrecciation both in the host gypsum rock and within the microchannel (**02**). In the microchannel gypsum is associated to a microbial component (**03a**, **04a**, transmitted light), whose fluidized and microbrecciated hidden texture is somewhat revealed and exalted in CL views (**03b**, **04 b**).

<u>Centuripe</u>

The microfacies of the brecciated limestones from the site of Centuripe, perfectly resemble, to a smaller scale, the textural pattern evidenced at the outcrop scale (Figs. 4.3.13 a, 4.3.14-15). It is typified by subangular randomly oriented subcentimetric (or even centimetric) clasts, with a complex fluid migration network around the clasts. Both the matrix and clasts have a microbial origin, eventually fluidized by brecciation processes (Figs. 4.3.14-15).

Silica-bearing facies yield in turn microbial features. They are represented by: 1) fine amorphous silica-bearing laminites, accompanied by localized microbrecciation (Fig. 4.3.13 b-c); 2) nodules typified by rounded clasts (Fig. 4.3.13 b-c). This shape, in a general context dominated by subangular fragments representing the breccia types, could easily be explained by the occurrence of aggressive fluids or even frictional processes (Chen, pers. comm.). In addition, rounded clasts dominate important portion of the aforementioned conduit (Fig. 4.3.8).

The single elements of the gypsum breccia underlying the brecciated limestones (Figs. 4.3.5, 4.3.6 c) are in turn brecciated when observed at the macro- and the microscale (Fig. 4.3.16). They are cut by microbial-bearing microchannels where microbrecciation commonly occurs.

4.3.4 - Geochemical dataset: Oxygen and Carbon stable isotopes

The geochemical signatures of the two study sites in Sicily are remarkably different (Fig. 4.3.17).

The samples from Capodarso are extremely depleted in ^{13}C, exhibiting values broadly comprised in the range -30 to -40 ‰ PDB; their δ^{18}O is typified by positive values (Appendix 4). Subsampling didn't yield noticeable differences in the subfacies response, but a systematic negligible less negative δ^{13}C signal in the cement if compared to the one characterizing the coupled dark cemented matrix.

The δ^{13}C signature of the CdB samples is comprised in a very narrow range (suggesting less probable mixing in the signal, at a first glance), that contains slightly negative values approximating 0. The oxygen signature resemble to a major extent the one shown by the sulphur-bearing limestones of Capodarso, and in general exhibited by almost the entire Calcare di Base geochemical dataset enlarged through times (Caruso et al., 2009; Manzi et al., 2010, and ref. therein). Negative values are also present, but in general they are related to mixed facies, i.e. the carbonatic fraction associated to pelites or to gypsum (Appendix 4).

The isotopic signature in the sulphur-bearing limestones, coupled to the observed facies and microfacies, is perfectly consistent with the hypothesis recently carried out by Ziegenebalg et al. (2010), pointing to a syngenetic character of their mineral authigenesis through sulphate reduction microbial pathways, likely fuelled by methane.
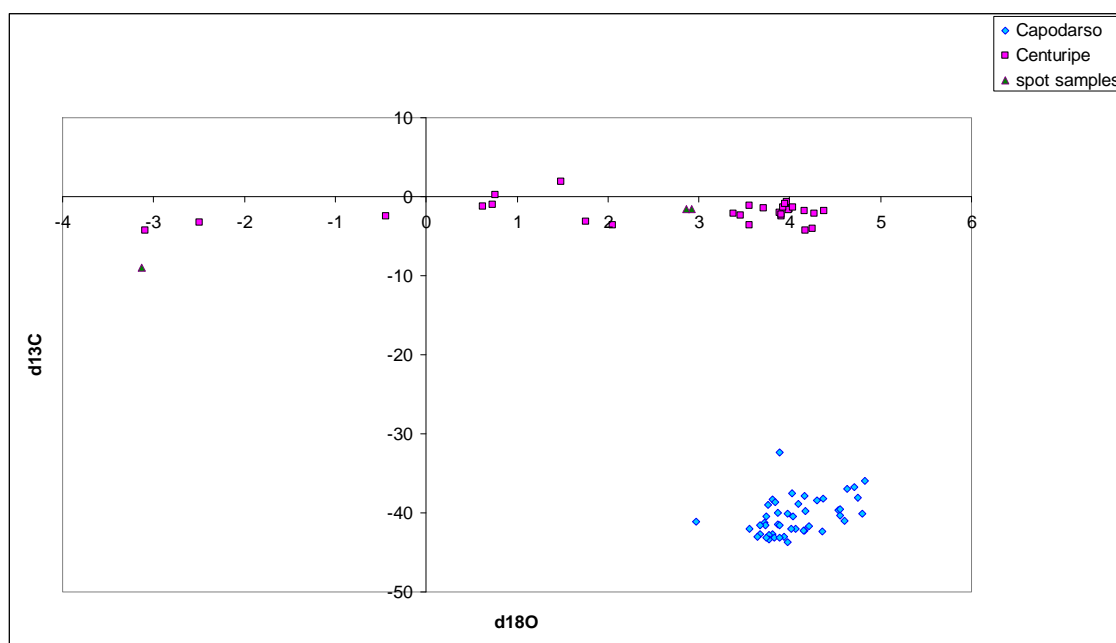
Fig. 4.3.17 - Cross plot of stable isotopes data of the Calcare di Base in the studied areas in Sicily.

The carbon isotopic signature in the Calcare di Base of Centuripe, can be explained with the absence of fluid-rock interaction during similar hydrocarbons migration, or, most likely, simply with the common diagenetic processes intervening during early carbonate diagenesis (i.e. calciticization of aragonite). In the latter hypothesis, the nature of the fluids invoked to explain the sedimentological features, remains obscure and requires further investigations.

According to many authors the positive $\delta^{18}O$ signal is indicative of evaporitic conditions during the Calcare di Base primary facies deposition (Caruso et al., 2009; Manzi et al., 2010 and ref. therein). Even in this case, like already mentioned in the Ch. 4.2.4, the geochemical signal with generally coupled positive $\delta^{18}O$ - negative $\delta^{13}C$ widely typifying the Calcare di Base both in Sicily and Calabria, can be tentatively related to gas hydrate destabilization processes, as already suggested by Pierre & Rouchy (2004). Herein, it must be stressed that, excluding the case of the sulphur-bearing limestones, this ^{13}C depletion is generally weak. This delicate topic will be matter of discussion in the Chapter 5.

4.3.5 - Discussion

4.3.5.a - Brecciation phenomena

The Calcare di Base in Sicily is extensively brecciated. Brecciation occurs in the CdB at different stratigraphic levels: both in limestones transitionally resting above the Tripoli Fm. and in limestones intercalated to clastic gypsum. In the second case, strata-bound brecciation thus takes place, thus pointing to compartmentalized brecciation. Nonetheless, this study evidenced

how sometimes even clastic gypsum levels are affected by brecciation, showing fabric relationships perfectly resembling the ones shown in the limestone facies counterpart (Fig. 4.3.16; lithology-independent brecciation).

Breccias are concordant to the primary beds and don't show erosional bases. Rock fragments are randomly oriented and show no gravity segregation; they are mostly subangular, but are also associated to subrounded clasts. In the sulphur-bearing limestones, brecciation at the microscale is extremely localized. In the CdB of Centuripe the microfacies revealed that both the clasts and the matrix are made up of microbialites, yielding in turn a fluidized microtexture.

These textural proxies, together with the occurrence of conduits at any scale of observation, converge to invoke fluid migration as a trigger for brecciation. In this view, the local co-occurrence of subrounded and subangular clasts can be explained with aggressive fluids and/or frictional processes accompanying fluid migration.

With respect to the models for brecciation in the CdB already proposed in the geological literature, the following considerations can be stated herein:

- None of the sedimentological features envisaged in the model proposed by Manzi et al. (2010) were found: the authors suggest early erosion and sedimentation processes responsible for the emplacement of the breccias, thus believed to represent mass-flow deposits.

- The classical model for brecciation invokes in situ brecciation phenomena, resulting from doline collapse of lime mudstones during exposure to meteoric waters by dissolution of evaporitic minerals (Pedley & Grasso, 1993; Rouchy & Caruso, 2006 and ref. therein). Though the model proposed herein agree with the in situ brecciation character, no collapse features and related textures were found, but rather fluid-migration proxies, detected at any scale of observation (Par. 4.3.5.b).

4.3.5.b - Fluid migration proxies

Small pipes and internal conduits with gypsum concentric structures were observed in the sulphur- bearing limestone of Capodarso. These sedimentological data, and the comparable geochemical signature obtained, perfectly fit the hypothesis recently claimed by Ziegenbalg et al. (2010): syngenetic authigenesis processes fuelled by methane drove precipitation of sulphur-bearing limestones. Therein, the proposed methane source is either the OM-rich Tripoli Fm (already suggested by Decima et al., 1988) or contemporaneous biogenic methanogenesis taking place in the underlying sediment. The fluid migration pathways clearly point to migrated fluids interacting with the early diagenized sediments (syngenetic character), and are hardly compatible with the late bacterial sulphate reduction of original clastic gypsum invoked by Manzi

et al., 2010. The coupled ^{18}O-enriched-^{13}C-depleted isotopic signature could tentatively point to gas hydrates destabilization processes. Furthermore, the patterns of cementation resemble gas-

Fig. 4.3.18 - Gas-hydrate resembling textures in the Calcare di Base of Sicily. The layered cement infillings in the sulphur-bearing limestone of Capodarso (left side), resemble the gas-hydrate infillings in fine-grained sediments (right side; sample from the Gulf of Mexico), resulting in rise to comparable fabrics.

hydrate-bearing sediments fabric (Fig. 4.3.18). Yet, this hypothesis remains speculative, but cannot be directly ruled out, sustained by both isotopic and facies results.

In the second study area (Centuripe) even huge outcrop-scale chimneys occur; they are typified by breccias eventually verticalized and cut by a complex network of fluid migration channels. The main brecciation event was thus followed by successive fluid-migrations. Fluidification-related microstructures were revealed by the microfacies analysis: both the brecciated clasts and the matrix are constituted by fluidized microbialite; the latter represents the primary facies, accompanied by a consistent siliceous fraction, possibly pointing to deeper environments. A paper published at the beginning of last century (Di Stefano, 1902), reported Lucina spp. occurrences near the village of Centuripe, within a unit that can be easily ascribed, for its stratigraphic position and its facies, to the CdB Fm. Lucina Limestones represent a common methane-derived lithofacies in many ancient cold seeps (Campbell, 2006 and ref. therein). This, together with the fluid migration pathways occurring at different scales of observation, could depict a past cold seep environment in the area. The extremely weak δ^{13}C depletion isotopic signal obtained, seems nonetheless to contrast this hypothesis. With respect to the positive δ^{18}O signal, in the CdB it is commonly envisaged as a primary signal (Caruso et al., 2009 and ref. therein), related to precipitation lead by evaporation from variously poor-ventilated, hypersaline or brackish marine seawater; occasional continental influxes are held responsible for lower values. In the revealed fluid migration context, as already suggested for the Calabrian CdB, the

positive δ^{18}O isotopic signature could rather account for ascending saline fluids. In this view, the variations within the isotopic dataset are explained with different degrees of interaction of the fluids with the sedimentary column, according to flux rates variable through space and time. The suggested nature of the fluids must be confirmed by more detailed investigations, as already highlighted for the case of the Calabrian Arc.

Even in the case of Centuripe, many fluidification features are actually constituted by gypsum, that was therefore actively involved in the fluid-migration event. This stresses once more in this study, how the role of evaporites in fluid migration is not merely the role of a seal, as often claimed on the basis of the seismic-scale scenarios.

The herein claimed interpretation of the vertical structures of Centuripe as chimneys has been suggested first by their morphology, and secondarily by their association with brecciated patches and fluid migration proxies. Yet, this interpretation needs to be corroborated, in future investigations, by more detailed facies and microfacies data.

4.3.6 - Major remarks

- In Sicily the brecciated facies referred to the Calcare di Base Fm. (including its sulphur-bearing subfacies) occurs at different stratigraphic levels: it conformably overlays the Tripoli Fm. and is truncated on top by the MES or is intercalated to clastic gypsum, above the MES. These two patterns point to compartmentalized brecciation phenomena, affecting only certain stratigraphic levels.

    With respect to the first case, the transitional contact between the Tripoli Fm and the Calcare di Base Fm, marked by the occurrence of laminitic dolostones, has been pointed out by Oliveri et al. (2010). This stratigraphic relationship has been accepted in the model of Manzi et al. (2010) as strictly concerning the laminitic subfacies (CdB Type 2), but not with respect to the brecciated type (CdB Type 3), nor to the sulphur-bearing subfacies (CdB Type 1): the latter are both ascribed to the post-evaporitic portion, lying above the MES.

- The Calcare di Base is represented by cemented clast-supported breccias, conformable to the primary bedding.

- Huge chimneys, macro-scale pipes to small scale fluid migration pathways, together with micro-fluidification features, co-occur with the breccias and affect also gypsum at locations.

- The brecciation is diffused at the mesoscale, but localized at the small scale.

- The sedimentological features of the breccias point to in situ brecciation and rule out the occurrence of resedimentation as trigger for brecciation.

- In Sicily, at least one major fluid migration event accompanied in situ brecciation phenomena, affecting compartmentalized horizons of Messinian early diagenized deposits.

- At Capodarso methane-rich ascending fluids, flowing through small gypsum and carbonatic pipes, triggered a syngenetic authigenesis of methane-derived carbonates, that was possibly accompanied by gas hydrate occurrences. The nature of the fluids ascending through huge chimneys at Centuripe, remains obscure, but a saline character is suggested here as a working hypothesis.

- The huge sea level drop occurred in the Mediterranean Basin was likely the original trigger for fluid migration: as already suggested in the case of the brecciated limestone of the Calabrian Arc, the consequent high depressurization experienced by the sedimentary column after the removal of at least 1 km of water column, could have likely favoured a catastrophic migration of previously overpressured fluids from below.

5 – DISCUSSION

5.1 - The trigger for brecciation in the Messinian Limestones: in situ brecciation, fluid-assisted processes and primary fabric overprinting

The upper Messinian brecciated limestones show many similarities in the three main study areas, so that a similar trigger for brecciation can be easily invoked. As a whole, the main differences can be only ascribed to the different stratigraphic portions affected by brecciation in any single area and to their isotopic signature.

Their analogies are enucleated in the following points:

- The Messinian brecciated bodies are bedding-retentive, since their bedding planes are concordant to the bedding shown by the primary deposits: though often partially obliterated by the high degree of brecciation, there is a general partial preservation of the primary fabric, enough to allow its recognition.

- The bases of the breccias don't show an erosional character, but they are not even sharply planar: this kind of irregularities can be easily ascribed to their mechanism of formation.

- Breccias are predominantly monomictic and devoid of gravity segregation; no preferential distribution is exhibited by their clasts.

- They are generally clast-supported, with mostly subangular and minor subrounded clasts.

- Brecciation is diffused at the outcrop scale, but localized at the small scale; a sometimes high lateral variability in the brecciation degree was observed.

- Complex rheological behaviour is shown by textural patterns: brittle and plastic responses in the same microenvironments co-occurred during brecciation events.

- Scale invariant patterns typify breccias and lithology-invariant brecciation occurs. Interestingly, the many scale invariant geological phenomena include fluid assisted brecciation and oil fields.

- The upper Messinian brecciated limestones are accompanied by fluid migration pathways, detected at any scale of observation.

These textural features point to in situ brecciation phenomena and rule out the occurrence of processes of resedimentation: they rather point to fluid-assisted brecciation, as sustained by the independent scale patterns and the evidence of channels at any scale. Even the extreme localization of microbrecciation occurring in many lithofacies is difficult to explain with processes other than localized overpressure of the fluids. In fact, the pressure of ascending fluids is extremely variable laterally, due to the primary inhomogenities within the sedimentary pile passed throughout (primary facies variation and/or disharmonic diagenesis, or even tectonic

discontinuities) and due to the lateral different energy input carried out by the fluids themselves. This results in different brecciation degrees; occurrence of focused vs. pervasive fluid flow; different flux rates and consequently different fluid-rock interactions.

In future studies, a quantitative approach to validate the brecciation model is required. This can be achieved through a research addressed to the characterization of the mechanism triggering brecciation, including particle size distribution and fractal analyses. Breccia clast size distribution and morphology can be quantified using fractal analysis. The morphology of the fragments allows chemical and mechanical breccias to be distinguished; the particle size distribution is considered a function of the energy input during breccia formation.

5.2 - Expulsion-related structures and the multifaceted record of flow trajectories

The fluid expulsion-related structures recognized in this work at any scale of observations encompasses a large inventory of typologies.

At the mesoscale mushroom-shaped conduits typified by fluidized, possibly allochthonous pelites and minor carbonatic content were found in the Maiella area, they cut the succession below the Messinian Erosional Surface throughout (Primary Lower Gypsum and underlying ramp carbonates).

Huge structures were also observed at Centuripe (Sicily), where metric carbonatic chimneys, constituted by brecciated facies are cut by variously gypsum-bearing and silica-bearing submetric fluid migration features. Similar outcrop scale features also occur in the Crotone Basin. These structures are localized, pointing to focused fluid flow in correspondence to them.

Carbonatic and gypsum centimetric pipes, accompanied by gypsum internal conduits with concentric structures were observed in the Calcare di Base of Centuripe and Capodarso.

Fluidized textures in the common microbial primary sediment are widely occurring in the microfacies of any single study area; the microbial sediment nonetheless showed also a brittle behaviour (localized microbrecciation), and the pelitic fraction as well. This possibly accounts for differential pressures in the fluids and/or variation in the early cementation of the sediment. Microscale channels were also often observed.

These different typologies and their different frequency point to a phenomenon that pervasively interested the sedimentary column, but with localized major energy input (diffused but localized). The different energy input results: 1) at the mesoscale, in more focused fluid flow in correspondence to the huge conduits, where possibly higher flux rates took place; 2) at the microscale, in localized microbrecciated portions.

Gypsum was actively involved in the fluid migration processes and didn't act as a simple seal: in the Maiella area Primary Lower Gypsum, in correspondence to localized fluid flow, behaved in brittle way; on the other hand, in Sicily, they acted as centimetric scale conduits, yielding peculiar fluidification concentric features.

5.3 - Fluid seep scenarios during the Messinian Salinity Crisis, brecciated Limestones and MSC phases. A timing for the breccia deposits or for the "brecciation" event?

Brecciation occurred at different stratigraphic levels, but always in early diagenized, partially lithified sediments. Brecciated limestones are always intimately related to the Messinian Erosional Surface, given the occurrence of brecciated bodies immediately above or/and immediately below the MES, sometimes giving rise to compartmentalized brecciation (Calcare di Base in Sicily). More specifically, brecciated bodies occurs in correspondence to evaporitic onset carbonates (CdB in the Calabrian Arc and in Sicily) and of post-evaporitic carbonates (Maiella Mts; Sicily).

These bodies experienced similar fluid-driven processes, but the nature of the fluids involved is different at the various locations.

The age of these breccias is controversial: in situ collapse breccias experienced by basal (MSC onset) limestones (Pedley & Grasso, 1993; Rouchy & Caruso, 2006 and ref. therein) vs. resedimented breccias emplaced above the MES during the post-evaporitic phase (Manzi et al., 2010). In the latter model the supposed diachronous nature of the base of the CdB is rejected, given the intrinsically erosional character of this surface at a regional scale.

Herein is not suggested an age for the breccias as deposits, but more properly an age for the brecciation event, driven and accompanied by a widespread fluid migration event, occurring in upper Messinian times after the major drawdown of the Mediterranean Sea. These processes affected the sedimentary succession to different extents, locally leading to compartmentalized brecciation according to different rheological responses of the lithofacies (typically clastic gypsum vs. microbial limestones).

The primary trigger for fluid migration, leading in turn to the diffused brecciation, is presumably related to the major drawdown of the Mediterranean Sea recorded by the MES: it took to a huge drop of the confining pressure after the removal, in a relative short time span (the gap envisaged by Krijsgmann et al., 1999), of 1000-1500 m of water column. The consequently high depressurization most likely favoured a catastrophic migration of overpressured fluids from below.

It has been already clearly stated that fluids are able to flow across and out of the MES and that water within the MES may results from gypsum-anhydrite conversion, thus pointing to saline fluids; nonetheless these processes are thought to have taken place in post-Messinian times (CIESM, 2008 and ref. therein).

More specifically, the hypothesis proposed in the present work was already speculated by Ryan (2009). A well-known case of upper Messinian methane-derived limestones is from the Tertiary Piedmont Basin (Clari et al., 2009 and ref. therein; Dela Pierre et al., 2010 and ref. therein): they are thought to have been precipitated both within an emipelagic succession and on the seafloor, according to the different lithofacies (Lucina-bearing Lucina-free concretions and Lucina-bearing mud breccias of Marmorito Quarry). Their formation has been linked to gas hydrate destabilization on the basis of coupled microfacies and geochemical data.

Considering the basin-scale, Pierre & Rouchy (2004), suggested a major event of dissociation of gas hydrates during the Messinian times in the western Mediterranean margins, invoking the main sea level drop as a trigger as well. Gas hydrates, already contained in the sediments of the margins, would have been destabilized when the water depth reached a critical low level. Their previous formation was likely favoured by the occurrence of methane-rich sediments, formed during the long period of suboxic/anoxic conditions accompanying the progressive isolation of the Mediterranean Sea (restricted marine environments).

In this view, the facies observed herein supposed to resemble gas-hydrate bearing sediments, must be taken into account for more detailed investigations, though the coupled isotopic signal remains controversial. The cited study cases, thus fit and endorse the hypothesis suggested in the present work.

5.4 - The sedimentological tool for the detection of ancient seep environments and the textural proxies for fluid-induced brecciation processes in limestones. How can we recognize in situ brecciation in the geological record and investigate the role of fluid overpressure as a trigger?

In the geological literature of the last decades the term "seep limestone" has been used to define methane-derived or hydrocarbon-derived carbonates. Their nature is generally primarily inferred by the typical ^{13}C- depleted isotopic signature. The use of the sole geochemical dataset to define seep limestones is often controversial, due to the different carbon sources involved in the carbonatogenesis process: the sources are difficult to be separated in terms of relative

contribution and this represents an even more complicated issue in ancient limestone (see Ch. 2.1.1.c). The contribution of different carbon sources, together with the possible occurrence of dominantly thermogenic parent methane for example (significantly less depleted respect to the biogenic type), can lead sometimes to complicated interpretation of the geochemical signal, that can be explained in multiple ways, not necessarily implying the contribution of hydrocarbon-rich fluids.

The present study showed that peculiar brecciated facies, associated to fluid-escape structures, typify seep limestones, whatever the nature of the fluid involved. They show the same textural patterns, both in case they are actually methane/hydrocarbon-derived carbonates (Maiella Mts; Capodarso), and in case they are generally fluid-related. In this view, herein is suggested the general use of the term "seep limestones", not necessarily implying a critical role played by methane or hydrocarbons, but independent from the nature of the fluids. In order to have an insight on the latter, the geochemical signature represents in any case only the first step (Ch. 5.5.).

The following remarkable textural proxies pointing to fluid assisted processes in a sedimentary succession were enucleated:

(a) geobodies with high lateral variability in terms of facies and brecciation degree;

(b) bedding-retentive character, accompanied by primary fabric overprinting;

(c) peculiar textural characters of the breccias (absence of gravity segregation; generally subangular clast-supported and with minor allochthonous clasts; localized microbrecciation);

(d) scale-invariant textures;

(e) lithology-independent patterns

(f) complex rheology in the breccias and the associated concretions, thus pointing to the coexistence of brittle and plastic behavior (differential rheological responses).

In addition to them, fabric resembling gas-hydrate infilling sediments have also been observed, but the nature of such hypothesis is so far speculative.

5.5 - Open questions: nature of the possible fluids involved, flux rates and fluid-rock interactions

Many textural and mesoscopic proxies clearly testify the role of ascending fluids as trigger for the widespread brecciation experienced by limestones bodies in correspondence to the major drawdown of the Mediterranean sea level in upper Messinian times. The nature of the fluids involved in the process suggested herein remains an open question. The role played by hydrocarbons is local (Maiella Mts; Capodarso in Sicily). In other cases the nature of the fluids is

tentatively inferred on the basis of the geochemical dataset (Fig. 5.1). Nonetheless it represents only a first approach to investigate the fluid composition. Additionally, the sole nature of the fluids and of the different carbon sources involved in carbonatogenesis are not the only factors to be considered when interpreting the isotopic signal in fluid-release environments: flux rates and fluid-rock interaction must be accurately evaluated as well. In case of focused fluid flow for example, presumably higher flux rates were locally taking place, and presumably lower fluid-rock interaction was occurring. In such example, the further analyzed rock sample must not be interpreted as to inherit the parent-fluid signature.

Some insights in fluid composition can be interestingly offered by REE elements investigations: REE in the early microcrystalline phases of seep limestones inherit the REE concentration of seep fluids, and yield information about changes in fluid flow regime and variability in redox conditions.
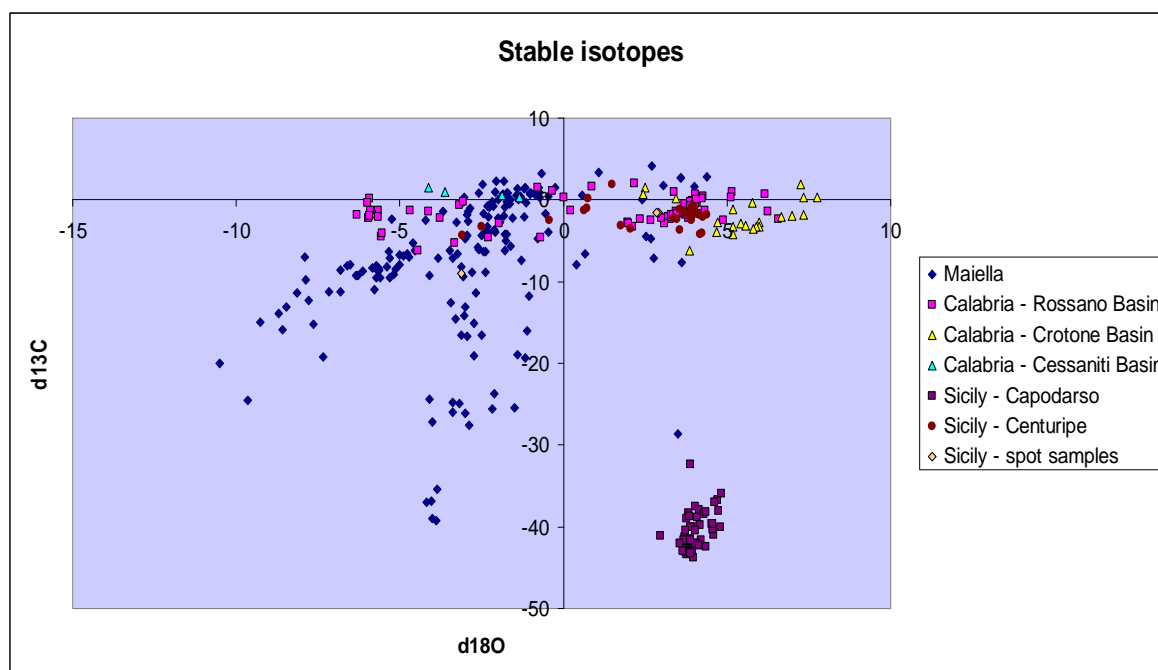
Fig. 5.1 - Cross plot of stable isotopes data of the Brecciated Limestones/Calcare di Base in the main studied areas.

6 - MAJOR REMARKS AND CONCLUSIONS

- The Messinian breccias are made up of limestones exhibiting high variability in facies and thickness: their geometry varies from a patchy distribution within a host sediment to massive or stratified thick bodies interbedded with pelitic horizons. The carbonatic beds consist of locally brecciated marly lime mudstones, cemented and concretioned to different degrees: generally brecciation overprints the primary sediment, but even in the more intensively brecciated beds, relict primary proxies allow the recognition of the original fabric. This results in fabric-retentive breccias.

- Breccias are generally highly cemented and always devoid of gravity segregation; they are mostly monomictic and clast-supported. Their clasts are mostly sub-angular and exhibit no preferential distribution.

- Brecciation yields scale-invariant and lithology-independent patterns.

- Brecciation, accompanied by fluid migration pathways occurring at any scale of observation, is a diffused phenomenon at the mesoscale, but localized at the microscale. This possibly accounts for variation in the energy input of the fluids, supposed to have triggered brecciation.

- Plastic and brittle behaviours co-existing even at the small scale, point to fluidification and associated brecciation phenomena taking place in a partly unlithified sedimentary column, typified by differential diagenesis.

- Brecciation occurred in situ: resedimentation phenomena leading to brecciation cannot be ruled out everywhere, but they must be considered as a local response accompanying the general upward fluid release.

- Textures resembling gas-hydrate bearing sediments were observed, but the contextual widespread dissociation of gas hydrates in the Western Mediterranean Sea remains a challenging issue, to be investigated more accurately.

- Important sedimentological proxies for the detection of seep limestones have been enucleated; a revisiting of the term "seep limestone" is proposed.

- The upper Messinian brecciated limestones occur in correspondence to different phases of the Messinian Salinity Crisis, but are strictly related to the regional unconformity: the MES played a critical role in the brecciation processes. There is no evidence to consider the upper Messinian breccias as a stratigraphic unit: the process of brecciation and the widespread fluid migration took place, involving different stratigraphic levels, according to their rheology and to the structural local setting. The age of these processes is constrained to the early upper Messinian phase, before the development of the Lago-Mare event.

- The major drawdown of the Mediterranean Sea recorded by the MES corresponds to a huge sea level drop: this most likely represents the primary trigger for fluid migration. In fact, the high depressurization experienced by the sedimentary column after the removal of at least 1 km of water column, could have likely favoured a catastrophic migration of overpressured fluids from below.

- Only indirect evidences (geochemical data; facies analysis) of the nature of the fluids has been provided: in the Maiella Basin and at Capodarso (in the Caltanissetta basin), they were enriched in hydrocarbons, so that we can state that they gave rise respectively to hydrocarbon-derived and methane-derived limestones; in the Calcare di Base of the Calabrian Arc and of Centuripe (in the Caltanissetta basin) the nature of the fluids, possible saline, remains object of future investigation.

7 – REFERENCES

Agosta F., Alessandroni M., Tondi E. & Aydin A., 2009. Oblique-slip normal faulting along the northern edge of the Majella anticline: inferences on hydrocarbon migration and accumulation. *Journal of Structural Geology*, **31**, 774-690.

Agosta F., Alessandroni M., Antonellini M., Tondi E. & Giorgioni M., 2010. From fractures to flow: A field-based quantitative analysis of an outcropping carbonate reservoir. *Tectonophysics*, **490***, 197–213.

Aloisi G., Pierre C., Rouchy J.-M., Foucher J.-P., Woodside J. and the M EDINAUT Scientific Party, 2000. Methane-related authigenic carbonates of eastern Mediterranean Sea mud volcanoes and their possible relation to gas hydrate destabilisation. *Earth and Planetary Science Letters*, **184**, 321-338.

APAT, 2005. Carta Geologica d'Italia, Scala 1:50.000, Foglio 360 - Torre dei Passeri, S.EL.CA., Firenze.

Baco A.R. & Smith C.R., 2003. High species richness in deep-sea chemoautotrophic whale skeleton communities. *Marine Ecology, Progress Series*, **260**, 109–114.

Bassetti M.A., Ricci Lucchi F. & Roveri M., 1994. Physical stratigraphy of the Messinian post-evaporitic deposits in central-southern Marche area (Apennines, central Italy). *Mem. Soc. Geol. Ital.*, **48**, 275–288.

Bassetti M.A., Ricci Lucchi F., Roveri M. & Taviani M., 1998. Messinian facies in a critical section of northern Apennines (Montepetra-Perticara, Pesaro). *Giorn. Geol.*, **60**, 261–263.

Bassetti M. A., Manzi V., Lugli S., Roveri M., Longinelli A., Ricci Lucchi F. & Barbieri M., 2004. Paleoenvironmental significance of Messinian post-evaporitic lacustrine carbonates in the northern Apennines, Italy. Sedimentary *Geology*, **172**, 1 –18.

Beauchamp B., 2004. Natural gas hydrates: myths, facts and issues. *Comptes Rendus Geoscience*, **336** (9), 751-765.

Belenkaia I., 2000. Gas-derived carbonates: reviews in morphology, mineralogy, chemistry and isotopes (data collected during the TTR programme cruises during 1995-1999). In: *Abstracts of the Sixth International Conference on Gas in Marine Sediments.* St. Petersburg, VNIIOkeanologia, 9-10.

Bellanca A. & Neri R., 1986. Evaporite carbonate cycles of the Messinian, Sicily: stable isotopes, mineralogy, textural features, and environmental implications. J. Sed. Petrol., **56**, 614–621.

Bellanca A., Calderone S. & Neri R., 1983. Evidenze geochimiche e mineralogiche di episodi evaporitici nella sequenza diatomitica (Messiniano pre-evaporitico) di Sutera (Sicilia centrale). *Rend. Soc. Ital. Miner. Petro.l*, **38**, 1271–1280.

Bellanca A., Calderone S. & Neri R., 1986. Isotope geochemistry, petrology and depositional environments of the diatomite-dominated Tripoli Formation (Lower Messinian), Sicily. *Sedimentology*, **33**, 729–743.

Bellanca A., Caruso A., Ferruzza G., Neri R., Rouchy J.M., Sprovieri M. & Blanc-Valleron M.M., 2001. Transition from marine to hypersaline conditions in the Messinian Tripoli Formation from the marginal areas of the central Sicilian Basin. Sed. Geol., **140**, 87–105.

Benson R.H. & Rakic-el Bied K., 1991. Biodynamics, saline giants and Late Miocene catastrophism. *Carbonates and Evaporites*, **6**, 127–168.

Berner R.A., 1980. Early diagenesis: A theoretical approach. Princton Univ. Press, Princton, NY, 241 pp.

Bertini A., 2006. The Northern Apennines palynological record as a contribute for the reconstruction of the Messinian palaeoenvironments. *Sed. Geol.*, **188–189**, 235–258.

Bishop J.K.B., 1988. The barite-opal-organic carbon association in oceanic particulate matter. *Nature*, **331**, 341–343.

Bigi G., Castellarin A., Catalano R., Coli M., Cosentino D., Dal Piaz G.V., Lentini F., Parotto M., Patacca E., Praturlon A., Salvini F., Sartori, R., Scandone P. & Vai G.B., 1989. Synthetic structural–kinematic map of Italy. Scale 1:2,000,000. CNR Finalizzato Geodinamica, Sottoprogetto: Modello Strutturale Tridimensionale. Stabilimento L. Salomone, Roma.

Blanc-Valleron M.-M., Pierre C., Caulet J.P., Caruso A., Rouchy J.M., Cespuglio G., Sprovieri R., Pestrea S. & Di Stefano E., 2002, Sedimentary, stable isotope and micropaleontological records of palaeoceanographic change in the Messinian Tripoli Formation (Sicily, Italy). *Palaeogeography*, **185**, 255–286.

Boetius A., Ravenschlag K., Schubert C. J., Rickert D., Widdel F., Gieseke A., Amann R., Jørgensen B. B., Witte U. & Pfannkuche O., 2000. A marine microbial consortium apparently mediating anaerobic oxidation of methane. *Nature*, **407**, 623–626.

Bohrmann G., Suess E., Greinert J., Teichert B. & Naehr T., 2002. Gas hydrate carbonates from Hydrate ridge, Cascadia convergent margin: indicators of near-seafloor clathrate deposits. In: Proceedings of 4th International Conference of Gas Hydrates, Yokohama, Japan, pp 102–107.

Bond D., Wignall P.B. & Racki G., 2004. Extent and duration of marine anoxia during the Frasnian-Famennian (Late Devonian) mass extinction in Poland, Germany, Austria and France. *Geol. Mag.*, **141**, 173–193.

Bohrmann G., Greinert J., Suess E. & Torres M., 1998. Authigenic carbonates from Cascadia Subduction Zone and their relation to gas hydrate stability. *Geology,* **26/7**, 647-650.

Borsetti A. M., Curzi P. V., Landuzzi V., Mutti M., Ricci Lucchi F., Sartori R., Tomadin L. & Zuffa G.G., 1990. Messinian and pre-Messinian sediments from ODP Leg 107 sites 652 and 654 in the Tyrrhenian Sea: Sedimentologic and petrographic study and possible comparisons with Italian sequences. In: *Proc. Ocean Drill. Prog. Sci. Results* (K.A. Kastens, J. Mascle, C. Auroux, E. Bonatti, C. Broglia, J. Channell, P. Curzi, K.C. Emeis, G. Glacon, S. Hasegawa, W. Hieke, F. McCoy, J. McKenzie, J. Mendelson, C. Muller, J.P. Rehault, A. Robertson, R. Sartori, R. Sprovieri & M. Torii, eds.), **107**, 169–184.

Botz R., Wehner H., Schmitt M., Worthington T.J., Schmidt M. & Stoffers P., 2002. Thermogenic hydrocarbons from the offshore Calypso hydrothermal field, Bay of Plenty, New Zealand. *Chem. Geol.*, **186**, 235–248.

Burhan R.Y.P., Trendel J.M., Adam P., Wehrung P., Albrecht P. & Nissenbaum A., 2002. Fossil bacterial ecosystem
at methane seeps: origin of organic matter from Be'eri sulfur deposit, Israel. *Geochim. Cosmochim. Acta*, **66**, 4085-4101.

Butler R.W.H., Lickorish W.H., Grasso M., Pedley H.M. & Ramberti, L., 1995. Tectonics and sequence stratigraphy in Messinian basins, Sicily: constraints on the initiation and termination of the Mediterranean salinity crisis. *Geological Society of America Bulletin*, **107**, 425–439.

Butler R.W.H., McClelland E. & Jones R.E., 1999. Calibrating the duration and timing of the Messinian salinity crisis in the Mediterranean: linked tectonoclimate signals in thrust-top basins of Sicily. J. Geol. Soc.London, **156**, 827–835.

Campbell K. A., 2006. Hydrocarbon seep and hydrothermal vent paleoenvironments and paleontology: Past developments and future research directions. *Palaeog., Palaeoclim., Palaeoec.*, **232**, 362– 407.

Campbell K.A. & Bottjer D.J., 1993. Fossil cold seeps. *Natl. Geog. Res. Explor.*, **9**, 326– 343.

Campbell K. A., Farmer J. D. & Des Marais D., 2002. Ancient hydrocarbon seeps from the Mesozoic convergent margin of California: carbonate geochemistry, fluids and palaeoenvironments. *Geofluids*, **2** (2), 63-94.

Campbell K.A., Francis D. A., Collins M., Gregory M. R., Campbell S. N., Greinert J., Aharon P., 2008. Hydrocarbon seep-carbonates of a Miocene forearc (East Coast Basin), North Island, New Zealand. *Sedimentary Geology*, **204**, 83–105.

Canet C., Prol-Ledesma R. M., Escobar-Briones E., Mortera-Gutiérrez C., Lozano-Santa Cruz R., C. Linares, Cienfuegos E. & Morales-Puente P., 2006. Mineralogical and geochemical characterization of hydrocarbon seep sediments from the Gulf of Mexico. *Marine and Petroleum Geology*, **23**, 605–619.

Carbonnel G., 1978. Le zone a Loxoconcha djaffarovi Schneider (Ostracoda, Miocène supérieur) ou le Messinien de la Vallée du Rhòne. *Rev. Micropaleontol.*, **21** (3), 106-118.

Caruso A., Di Stefano E., Rouchy J.M. & Sprovieri R., 1997. Biostratigraphy, cyclostratigraphy and sedimentology controls of the transition Tripoli-Calcare di Base (Lower Messinian) from Caltanissetta Basin (Sicily). Eighth Workshop of the ILP Task Force, Origin of Sedimentary Basins, Palermo, Abstr.

Caruso A., Pierre C., Rouchy J.-M. & Blanc-Valleron M. M., 2009. Depositional and diagenetic environments of the Messinian Calcare di Base and sulfur-bearing carbonates from Sicily and Calabria. Abstract Book ACTA NATURALIA de "L'Ateneo Parmense", **45** (1/4), 330-331.

Catalano R., Di Stefano E., Nigro F., Vitale F.P., 1993. Sicily mainland and its offshore: a structural comparison. In: Max M.D., Colantoni P. (eds) Geological development of the Sicilian-Tunisian Platform.UNESCO Report in Marine Science 58, pp 19–24.

Catenacci V., 1974. Note illustrative della carta geologica d' Italia - Foglio 147 Lanciano. Servizio Geologico d'Italia, Roma, 87 pp .

Cavagna S., Clari P. & Martire L., 1999. The role of bacteria in the formation of cold seep carbonates: geological evidence from Monferrato (Tertiary, NW Italy). *Sed. Geol.*, **126**, 253–270.

Cavazza W. & Wezel F.C., 2003. The Mediterranean region a geological primer. *Episodes*, **26**, 160–168.

Centamore E. & Nisio S., 2003. Significative events in the Periadriatic Foredeeps Evolution (Abruzzo - Italy). *Studi Geologici Camerti*, num. Spec. 2003, 39-48.

Chand S., Rise L., Ottesen D., Dolan M.F.J., Bellec V. & Bøe R., 2009. Pockmark-like depressions near the Goliat hydrocarbon field, Barents Sea: Morphology and genesis. *Marine and Petroleum Geology*, **26**, 1035–1042.

Chen J., CHOUGH S. K., CHUN S. S. & HAN Z., 2009. Limestone pseudoconglomerates in the Late Cambrian Gushan and Chaomidian Formations (Shandong Province, China): soft-sediment deformation induced by storm-wave loading. *Sedimentology*, **56**, 1174–1195.

CIESM, 2008. The Messinian Salinity Crisis from mega-deposits to microbiology – A consensus report, N° 33. In: *CIESM Workshop Monographs* (F. Briand, ed.), 168 pp. CIESM, Monaco.

Cipollari P., Cosentino D. & Parotto M., 1995. Modello cinematico-strutturale dell'Italia centrale. *Studi Geologici Camerti*, vol. spec. 1995/2, 135-143.

Cipollari P., Cosentino D. & Gliozzi, E., 1999. Extension- and compression-related basins in central Italy during the Messinian Lago-Mare event. *Tectonophysics*, **315**, 163– 185.

Cipollari P., Cosentino D., Di Bella L., Gliozzi E. & Pipponzi G., 2003. Inizio della sedimentazione d'avanfossa nella Maiella meridionale: la sezione di Fonte dei Pulcini (Taranta Peligna). *Studi Geologici Camerti*, num. Spec. 2003, 63-71.

Cita M.B., 1975. The Miocene-Pliocene boundary: history and definition. In: Late Neogene Epoch Boundaries (Eds T. Saito and L.H. Burkle), *Micropaleontology Press*, Spec. Publ. **1**, 1–30.

Cita M.B. & Colombo L., 1979. Sedimentation in the latest Messinian at Capo Rossello (Sicily). *Sedimentology*, **26**, 497–522.

Cita M.B. & Corselli C., 1990. Messinian paleogeography and erosional surfaces in Italy: an overview. *Palaeogeogr. Palaeoclimatol. Palaeoecol.*, **77**, 67–82.

Cita M.B., Santambrogio S., Melillo B. & Rogate F. 1990. Messinian paleoenvironments: new evidence from the Tyrrhenian Sea (ODP Leg 107). In: *Proc. Ocean Drill. Prog. Sci. Results* (K.A. Kastens, J. Mascle, C. Auroux, E. Bonatti, C. Broglia, J. Channell, P. Curzi, K.C. Emeis, G. Glacon, S. Hasegawa, W. Hieke, F. McCoy, J. McKenzie, J. Mendelson, C. Muller, J.P. Rehault, A. Robertson, R. Sartori, R. Sprovieri & M. Torii, eds.), **107**, 211–227.

Clari P., Cavagna S., Martire L. & Hunziker J., 2004. A Miocene mud volcano and its plumbing system: a Chaotix Complex revisited (Monferrato, NW Italy). *Journ. of Sed. Res.*, **74** (5), 662-676.

Clari P., Dela Pierre F., Martire L. & Cavagna S., 2009. The Cenozoic CH4-derived carbonates of Monferrato (NW Italy): A solid evidence of fluid circulation in the sedimentary column. *Marine Geology,* **265**, 167–184.

Clauzon G., Suc J.P., Gautier F., Berger A. & Loutre M., 1996. Alternate interpretation of the Messinian Salinity Crisis: controversy resolved? *Geology*, **24**, 363–366.

Cody R.D. & Cody A.M., 1988. Gypsum nucleation and crystal morphology in analog saline terrestrial environments. *Journal of Sedimentary Petrology*, **58**, 247-255.

Colella A. & Vitale F.P., 1998. Eustacy, tectonics and their controls on the depositional patterns of clinostratified shoreface carbonates (late Pliocene, Sicily). In: Colella A. (ed) Strata and sequences on

shelves and slopes, SEPM, Research Conference, Catania-Sicily, September 1998, Excursion Guidebook, pp. 29–69.

Cornée J.J., Ferrandini M., Saint Martin J.P., Münch Ph., Moullade M., Ribaud-Laurenti A., Roger S., Saint Martin S. & Ferrandini J., 2006. The late Messinian erosional surface and the subsequent reflooding in the Mediterranean: New insights from the Melilla-Nador basin (Morocco). *Palaeogeogr. Palaeoclimatol. Palaeoecol.*, **230**, 129– 154.

Cosentino D., Cipollari P., Lo Mastro S. & Giampaolo C., 2005. High-frequency cyclicity in the latest Messinian Adriatic foreland basin: insight into palaeoclimate and palaeoenvironments of the Mediterranean Lago-Mare episode. *Sed. Geol.*, **178**, 31-53.

Cosentino D., Federici I., Cipollari P. & Gliozzi E., 2006. Environments and tectonic instability in central Italy (Garigliano Basin) during the late Messinian Lago-Mare episode: New data from the onshore Mondragone 1 well. *Sed. Geol.*, 188–189, 297–317.

Cosentino D., Darbaş G. & Gürbüz K., 2010. The Messinian Salinity Crisis in the marginal basins of the Peri-Mediterranean orogenic systems: examples from the Central Apennines (Italy) and the Adana Basin (Turkey). *European Geoscience Union, General Assembly 2010, Vienna.*

Costa G.P., Colalongo M.L., De Giuli C., Marabini S., Masini F., Torre D. & Vai, G.B., 1986. Latest Messinian vertebrate fauna preserved in a Paleokarst-neptunian dike setting. *Grotte Ital.*, **12**, 221–235.

Crescenti U., 1975. Sul substrato pre-pliocenico dell'avanfossa appenninica dalle Marche allo Jonio. *Boll. Soc. Geol. It.*, **94** (3), 583-634.

Crescenti V., Crostella A., Donzelli G. & Raffi G., 1969. Stratigrafia della serie calcarea dal Lias alMiocene nella regione marchi giano-abruzzese (Parte 11: litostratigrafia, biostratigrafia , paleogeografia). *Mem. Soc. Geol. It.*, **8**, 343-420.

Crescenti U., Biondi R., Raffi I., Rusciadelli G., 2002. The S. Nicolao section (Montagna della Maiella): a reference section for the Miocene–Pliocene boundary in the Abruzzi area. *Boll. Soc. Geol. Ital.*, Vol. Spec. **1**, 509– 516.

Critelli S., 1999. The interplay of lithospheric flexure and thrust accommodation in forming stratigraphic sequences in the Southern Apennines foreland basin system, Italy. Accademia Natuale dei Lincei, *Rendiconti Lincei Scienze Fisiche e Naturali*, serie IX, **10**, 257-326.

Dahlmann A. & de Lange G. J., 2003, Fluid-sediment interactions at Eastern Mediterranean mud volcanoes: a stable isotope study from ODP Leg 160. *Earth and Planetary Science Letters*, **212** (3-4), 377-391.

Davidson D. W., 1983. Oxygen-18 enrichment in the water of a clathrate hydrate. *Geochim. Cosmochim. Acta*, 47, 2293–2295.

De Beer D., Sauter E., Niemann H., Kaul N., Foucher J., Witte U., Schlüter M. & Boetius A., 2006. In situ fluxes and zonation of microbial activity in surface sediments of the HåkonMosby Mud Volcano, *Limnol. Oceanogr.*, **51**, 1315–1331.

DeCelles P.G. &Giles K.A., 1996. Foreland basin system. *Basin Reasearch*, **8**, 105-123.

Decima A. & Wezel F.C., 1973. Late Miocene evaporites of the central Sicilian basin, Italy. In: Initial Reports of the Deep Sea Drilling Projects (Eds W.B.F. Ryan, K.J. Hsü, M.B. Cita, P. Dumitrica, J.M. Lort, W. Mayne,

W.D. Nesteroff, G. Pautot, H. Stradner and F.C. Wezel), **13**, pp. 1234–1240. US Government Printing Office, Washington.

Decima A., McKenzie J.A., Schreiber B.C., 1988. The origin of "evaporitive" limestones: an example from the Messinian of Sicily (Italy). *J. Sediment. Petrol.*, **58**, 256–272.

Dela Pierre F., Martire L., Natalicchio M., Clari P. & C. Petrea, 2010. Authigenic carbonates in Upper Miocene sediments of the Tertiary Piedmont Basin (NW Italy): Vestiges of an ancient gas hydrate stability zone? *GSA Bulletin*, **122** (7/8), 994–1010.

Dessau G., Jensen M.L. & Nakai N., 1962. Geology and isotopic studies of Sicilian sulphur deposits. *Economic Geology*, 57, 410–438.

Dickens G.R., 2001. The potential volume of oceanic methane hydrates with variable external conditions, *Org. Geochem.*, **32**, 1179–1193.

Di Napoli Alliata E., 1964. Il Miocene superiore della Valle dell'Orte presso Bolognano (Pescara). *Geol. Rom.* **3**, 3-32, 3 Tavv.

Di Stefano G., 1902. Il calcare con grandi Lucine dei dintorni di Centuripe in provincia di Catania. *Atti Acc*. Serie 4° Vol. **XVI** - Mem. XII., 1-71, 4 Tavv.

Di Stefano E., Cita M.B., Spezzaferri S. & Sprovieri R., 1999. The Messinian-Zanclean Pissouri section (Cyprus, Eastern Mediterranean). *Mem. Soc. Geol. Ital.*, **54**, 133–144.

Distel D.L., Baco A.R., Chuang E., Morrill W., Cavanaugh C. & Smith C.R., 2002. Marine ecology: do mussels take wooden steps to deep-sea vents? *Nature*, **403**, 725.

Eberli G.P., Bernoulli D., Sanders D. & Vecsei A., 1993. From aggradation to progradation, the Maiella platform, Abruzzi, Italy, gradual eustatic rise, and eutrophication of shallow water environments. In *Amer. Assoc. Petroleum. Geol. Memoir*, **56**, 213-231.

Emerson S. & Hedges J.I., 1988. Processes controlling the organic carbon content of open ocean sediments. *Paleoceanography*, **3**, 621–634.

Escutia C. & Maldonado A., 1992. Palaeogeographic implications of the Messinian surface in the Valencia trough, north-western Mediterranean Sea. *Tectonophysics*, **203**, 263–284.

Feng D., Chen D. & Roberts H. H., 2009. Petrographic and geochemical characterization of seep carbonate from Bush Hill (GC 185) gas vent and hydrate site of the Gulf of Mexico. *Marine and Petroleum Geology*, **26**, 1190–1198.

Flügel E., 2004. Microfacies of carbonate rocks. Analysis, Interpretation and Application. Springer-Verlag, Berlin. 976 pp.

Formolo M. J., Lyons T. W., Zhang C., Kelley C., Sassen R., Horita J. & Cole D. R., 2004. Quantifying carbon sources in the formation of authigenic carbonates at gas hydrate sites in the Gulf of Mexico. *Chemical Geology*, **205**, 253- 264.

Fortuin A.R., Kelling J.M.D. & Roep Th.B., 1995. The enigmatic Messinian-Pliocene section of Cuevas del Almanz- ora (Vera Basin, SE Spain) revisited: erosional features and strontium isotope ages. *Sed. Geol.,* **97**, 177–201.

Gaillard C., Rio M., Rolin Y. & Roux M., 1992. Fossil chemosynthetic communities related to vents or seeps in sedimentary basins: the pseudobioherms of southeastern France compared to other world examples: *Palaios*, **7**, 451–465.

Gamberi F. & Rovere M., 2010. Mud diapirs,mud volcanoes and fluid flowing in the rear of the Calabrian Arc Orogenic Wedge (southeastern Tyrrhenian sea). *Basin Research*, **22**, 452–464.

Gennari R. & Iaccarino S., 2004. An overview of the Messinian 'Lago-Mare' paleontological record. *The Messinian Salinity Crisis Revisited, 4th International congress 'Environment and Identity in the Mediterranean 2004', Corte, 19-25 July, 2004. Abstract volume*, 43.

Giampaolo C. & Lo Mastro S., 2000. Analisi (semi)quantitativa delle argille mediante diffrazione a raggi X. In: Fiore, S. (Ed.), Incontri. Scientifici., vol. II. Istituto di Ricerca Sulle Argille, pp.109– 146.

Gliozzi E., Cipollari P. & Cosentino D., 2002. The Messinian Lago-Mare event in central Italy: palaeogeographical reconstruction using geological data and ostracod assemblages. *Bull Acad Serbe Sci Arts, Cl Sci Nat*, **41**, 121– 152.

Goldberg D.S., Collett T.S., Hyndman R.D., 2000. Ground truth: in situ properties of hydrate, in: M.D. Max (Ed.), Natural Gas Hydrate in Oceanic and Permafrost Environments, Kluwer Academic, Dordrecht, 2000, pp. 295–310.

Gontharet S., Pierre C., Blanc-Valleron M.-M., Rouchy J.M., Fouquet Y., Bayon G, Foucher J.P., Woodside J. & Mascle J., The Nautinil Scientific Party, 2007. Nature and origin of diagenetic carbonate crusts and concretions from mud volcanoes and pockmarks of the Nile deep-sea fan (eastern Mediterranean Sea). *Deep-Sea Research II*, **54**, 1292–1311.

Gonzales F. J., Somoza L., Lunar R., Martínez-Frías J., Martín Rubí J. A. & Díaz del Río V., 2007. Fe-Mn nodules associated with hydrocarbon seeps: the new discovery of the Gulf of Cadiz (eastern Central Atlantic). *Episodes*, **30** (3), 187-196.

Guennoc P., Gorini C. & Mauffret A., 2000. Histoire ge´ologique du Golfe du Lion et cartographie du rift oligo-Aquitanien et de la surface messinienne*. Géol. Fr.*, **3**, 67–97.

Guido A., Jacob J., Gautret P., Laggoun-Défarge F., Mastandrea A. & Russo F., 2007. Molecular fossils and other organic markers as palaeoenvironmental indicators of the Messinian Calcare di Base Formation: normal versus stressed marine deposition (Rossano Basin, northern Calabria, Italy). *Palaeogeogr., Palaeoclim., Palaeoecol.*, **255**, 265–283.

Guillemin M. & Honzay J.P., 1982. Le Néogène post-nappe et le Quaternaire du Rif nord-oriental (Maroc). Stratigraphie et tectonique des bassins de Melilla, du Kert, de Boudinar et du piedmont des Kebdana. *Notes Mém. Serv. Géol. Maroc*, **314**, 7–238.

Hinrichs K.U. & Boetius A.B., 2002. The anaerobic oxidation of methane: new insights in microbial ecology and biogeochemistry. In: Wefer G., Billett D., Hebbeln D., Jørgensen B.B., Schlüter, M., van Weering, T. (Eds.), Ocean Margin Systems. Springer-Verlag, Heidelberg, pp. 457–477.

Hovland M., 1982. Pockmarks and the recent geology of the central section of the Norwegian Trench. *Mar. Geol.*, **47**, 283-301.

Hovland M., 1984. Gas-induced erosion features in the North Sea. *Earth Surf. Proc. Landforms*, **9**, 209-228.

Hovland M. & Judd A.G., 1988. Seabed Pockmarks and Seepages: Impact on Geology, Biology and the Marine Environment. Graham and Trotman, London, 144 pp.

Hovland M., Talbout M., Qvale H., Olausson S. & Aasberg L., 1987. Methane-related carbonate cements in pockmarks of the North Sea. J. *Sediment. Petrol*,. **57**, 881 - 892.

Hsü K.J., Cita M., Ryan B., 1973a. The origin of the Mediterranean evaporites. In: Ryan,W.F.B., Hsü, K.J., et al. (Eds.), *Initial Reports of the Deep Sea Drilling Project*, **13**. U.S. Government Printing Office, Washington, pp. 1203–1231.

Hsü K.J., Ryan W.B.F. & Cita MB., 1973b. Late Miocene desiccation of the Mediterranean. *Nature*, **242**, 240–244.

Huuse M., Jackson C. A.-L., Van Rensbergen P., Davies R. J., Flemings P. B. & Dixon R. J., 2010. Subsurface sediment remobilization and fluid flow in sedimentary basins: an overview. *Basin Research*, **22**, 342–360.

Jolivet L., Augier R., Robin C., Suc J.-P. & J. M. Rouchy, 2006. Lithospheric-scale geodynamic context of the Messinian salinity crisis. *Sedimentary Geology*, **188–189**, 9–33.

Jones B. & Manning D.A.C., 1994. Comparison of geochemical indices used for the interpretation of paleoredox conditions in ancient mudstones. *Chem. Geol.*, **111**, 111–129.

Judd A.G. & Hovland M., 1992. The evidence of shallow gas in marine sediments. *Cont. Shelf Res.*, **12**, 1081-1095.

Judd A.G. & Hovland M., 2007. Seabed Fluid Flow: The Impact on Geology, Biology, and the Marine Environment. Cambridge University Press, Cambridge. 475 pp.

Kastens K. & Mascle J., 1990. The geological evolution of the Tyrrhenian Sea: an introduction to the scientific results of ODP Leg 107. *Proc. ODP Sci. Results*, **107**. ODP, College Station, TX, 3-26.

Kelly S.R.A., Ditchfield P.W., Doubleday P.A. & Marshall J.D., 1995. An Upper Jurassic methane - seep limestone from the fossil Bluff Group forearc basin of Alexander Island, *Antarctica. J. Sediment. Res.*, **A65**, 274-282.

King L.H. & MacLean B., 1970. Pockmarks of the Scotian Shelf. *Geol. Soc. Am. Bull.*, **81**, 3141-3148.

Kopf A., 2002. Significance of mud volcanism. *Rev. Geophys.*, **40**, 1-51.

Kopf A., Sample J. C., Bauer P., Behrmann J. H. & Erlenkeuser H., 1995. Diagenetic carbonates from Cascadia margin: textures, chemical compositions, and oxygen and carbon stable isotope signatures. In: Carson, B., Westbrook, G. K., Musgrave, R. J., and Suess, E., (Eds.), *Proc. ODP, Sci. Results,* **146** *(Pt. 1)*, College Station, TX (Ocean Drilling Program), 117–136.

Krijgsman W., Hilgen F.J., Marabini S. & Vai G.B., 1999a. New palaeomagnetic and cyclostratigraphic age constraints on the Messinian of the Northern Apennines (Vena del Gesso Basin, Italy). *Mem. Soc. Geol. Ital.*, **54**, 25–33.

Krijgsman W., Hilgen F.J., Raffi I., Sierro F.J. & Wilson D.S., 1999b. Chronology, causes and progression of the Messinian salinity crisis. *Nature*, **400**, 652– 655.

Kvenvolden K.A., 1988. Methane hydrate—a major reservoir of carbon in the shallow geosphere?. *Chem. Geol.*, **71**, 41–51.

Kvenvolden K.A., 1993. Gas hydrates - geological perspective and global change. *Rev. Geophys.*, **31**, 173-187.

Kvenvolden K. A., 1998. A primer on the geological occurrence of gas hydrates. In: Henriet J.-P. and Mienert, J., (eds.), *Gas Hydrates - Relevance to World Margin Stability and Climate Change: London, The Geological Society*, 9-30.

Gautier F., Clauzon G., Suc J.P., Cravatte J. & Violanti D., 1994. Age et durée de la crise de salinité messinienne. CR

Acad. Sci. Paris, **318**, 1103–1109.

Ghisetti F. & Vezzani L., 2002. Normal faulting, extension and uplift in the outer thrust belt of the central Apennine (Italy): role of the Caramanico Fault. Basin Res. 14, 225– 236.

Grossi F., Gliozzi E. & Cosentino D., 2008. Late Messinian Lago-Mare ostracods and palaeoenvironments of the

central and eastern Mediterranean Basin. *Bollettino della Società Paleontologica Italiana, 47* (2), 131-146.

Hilgen F.J. & Krijgsman W., 1999. Cyclostratigraphy and astrochronology of the Tripoli diatomite formation (preevaporite Messinian, Sicily, Italy). *Terra Nova*, **11**, 16–22.

Iaccarino S. & Bossio A., 1999. Paleoenvironment of uppermost Messinian sequences in the Western Mediterranean (sites 974, 975 and 978). In: *Proc. Ocean Drill. Prog. Sci. Results* (R. Zahn, M.C. Comas and A. Klaus, eds), **161**, 529–541.

Iaccarino S., Castradori D., Cita M.B., Di Stefano E., Gaboardi S., McKenzie J.A., Spezzaferri S. & Sprovieri R., 1999. The Miocene -Pliocene boundary and the significance of the earliest Pliocene flooding in the Mediterranean. *Mem. Soc. Geol. lt.*, **54**, 109-131.

Lampert S.A., Lowrie W., Hirt A.M., Bernoulli D. & Mutti M., 1997. Magnetic and sequence stratigraphy of redeposited Upper Cretaceous limestones in the Montagna della Maiella, Abruzzi, Italy. *Earth and Planetary Science Letters*, **150**, 79-93.

Lofi J., Gorini C., Berne S., Clauzon G., DosReis A.T., Ryan W.B.F. & Steckler M.S., 2005. Erosional processes and paleo-environmental changes in the western Gulf of Lions (SW France) during the Messinian Salinity Crisis. *Mar. Geol.*, **217**, 1–30.

MacDonald I.R., Sager W.W. & Peccini M.B., 2003. Gas hydrate and chemosynthetic biota in mounded bathymetry at mid-slope hydrocarbon seeps: Northern Gulf of Mexico. *Mar. Geol.*, **198**, 133– 158.

Maillard A., Gorini C., Mauffret A., Sage F., Lofi J. & Gaullier V., 2006. Offshore evidence of polyphase erosion in the Valencia Basin (Northwestern Mediterranean): scenario for the Messinian Salinity Crisis. *Sed. Geol.*, **188–189**, 69–91.

Manzi V., Lugli S. & Roveri M., 2007. New insights on the Messinian Upper Evaporites of Sicily (Italy). *Geoitalia, Epitome*, **2**, 393. Rimini, 12–14 September 2007.

Manzi V., Lugli S., Roveri M., Schreiber B.C., 2009. A new facies model for the Upper Gypsum of Sicily (Italy): chronological and palaeoenvironmental constraints for the Messinian salinity crisis in the Mediterranean. *Sedimentology*, **56**, 1937–1960.

Manzi V., Lugli S., Roveri M., Schreiber B.C. & Gennari R., 2010. The Messinian "Calcare di Base" (Sicily, Italy) revisited. Geological Society of America Bulletin, doi: 10.1130/B30262.1.

Marchegiani L., Van Dijk J. P., Gillespie P. A, Tondi E. & Cello G., 2006. Scaling properties of the dimensional and spatial characteristics of fault and fracture systems in the Majella Mountain, central Italy. *Geological Society, London, Special Publications*, **261**, 113-131.

Martire L., Natalicchio M., Petrea C., Cavagna S., Clari P. & Dela Pierre F., 2010. Direct petrographic evidence of the past occurrence of gas hydrates in the sediment column. examples from the Oligocene-Miocene of the Tertiary Piedmont Basin (NW Italy). *Geo-Marine Letters*, **30**, 461–476.

Mattei M., Cipollari P., Cosentino D., Argentieri A., Rossetti F., Speranza F & Di Bella L., 2002. The Miocene tectono-sedimentary evolution of the southern Tyrrhenian Sea: stratigraphy, structural and palaeomagnetic data from the on-shore Amantea basin (Calabrian Arc, Italy). *Basin Research*, **14**, 147-168.

Mazzini A., Jonk R., Duranti D., Parnell J., Cronin B. & Hurst A., 2003. Fluid escape from reservoirs: implications from cold seeps, fractures and injected sands. Part I. The fluid flow system. *Journal of Geochemical Exploration*, **78-79**, 293-296.

McKenzie J.A., 1985. Stable isotope mapping in Messinian evaporative carbonates of central Sicily. *Geology*, **13**, 851-854.

McKenzie J.A., Jenkyns H.C. & Bennet G.G., 1979–1980. Stable isotope study of the cyclic diatomite-claystones from the Tripoli formation, Sicily: a prelude to the Messinian salinity crisis. *Palaeogeogr. Palaeoclimatol. Palaeoecol.*, **29**, 125–142.

Milkov A. V., 2004. Global estimates of hydrate-bound gas in marine sediments: how much is really out there? *Earth-Sci. Rev.*, **66** (3 - 4), 183 -197.

Mozley P.S. & Burns S.J., 1993. Oxygen and carbon isotopic composition of marine carbonate concretions: an overview. *J. Sed. Petrol.*, **63**, 73–83.

Naehr T.H., Rodriguez N.M., Bohrmann G., Paull C.K. & Botz R., 2000. Methane-derived authigenic carbonates associated with gas hydrate decomposition and fluid venting above the Blake Ridge Diapir. *Proceedings of the Ocean Drilling Program, Scientific Results*, **164**, 285-300.

Natalicchio M., 2010. Methane-derived carbonates in the Messinian sediments of the Tertiary Piedmont Basin: relation to gas hydrates formation and dissociation and to the emplacement of chaotic deposits. *PhD Thesis*, 158 pp. Dipartimento di Scienze della Terra, Università degli Studi di Torino.

Niemann H., Lösekann T., De Beer D., Elvert M., Nadalig T., Knittel K., Amann R., Sauter E. J., Schlüter M., Klages M., Foucher J. P. & Boetius A., 2006. Novel microbial communities of the Haakon Mosby mud volcano and their role as a methane sink. *Nature*, **443** (7113), 854–858.

Nyman S.L., Nelson C.S. & Campbell K.A., 2010. Miocene tubular concretions in East Coast Basin, New Zealand: Analogue for the subsurface plumbing of cold seeps. *Marine Geology*, **272**, 319-336.

Odin G.S., Ricci Lucchi F., Tateo F., Cosca M., Hunziker J.C., 1997. Integrated stratigraphy of the Maccarone section late Messinian (Marche region, Italy). In: Montanari, A., Odin, G.S., Coccioni, R. (Eds.), Miocene Stratigraphy: An Integrated Approach. Elsevier, Amsterdam, pp. 531–545.

Ogniben L., 1955. Le argille scagliose del crotonese. *Mem e note Ist. Geol. Appl. Napoli*, **6**, 1– 72.

Ogniben L., 1957. Petrografia della Serie Solfifera Siciliana e considerazioni geologiche relative. *Mem. Descr. Carta Geol. Ital.*, **33**, 275 pp.

Ogniben L., 1962. Le Argille Scagliose e i sedimenti messiniani a sinistra del Trionto (Rossano, Cosenza). *Geol. Rom.*, 1, 255 –82.

Ogniben L., 1963a. Sedimenti halitico-calcitici a struttura grumosa nel Calcare di Base Messiniano in Sicilia. *Giorn. Geol.*, **31**, 509–542.

Ogniben L., 1963b. Relazione sulle ricerche di salgemma nel Rossanese.

Ogniben L., 1973. Schema geologico della Calabria in base ai dati odierni. *Geol. Rom.*, **12**, 243– 585.

Oliveri E., Neri R.,. Bellanca A. & Riding R., 2010. Carbonate stromatolites from a Messinian hypersaline setting in the Caltanissetta Basin, Sicily: petrographic evidence of microbial activity and related stable isotope and rare earth element signatures. *Sedimentology*, **57**, 142–161.

Orphan V. J., House C. H., Hinrichs K.-U., McKeegan K. D. & DeLong E. F., 2001. Methane-consuming archaea revealed by directly coupled isotopic and phylogenetic analysis. *Science*, **293** (5529), 484–487.

Patacca E., Scandone P, Bellatalla M.,Perilli N. & Santini U., 1992. La zona di giunzione tra l'arco appenninico settentrionale e l'arco appenninico meridionale nell 'Abruzzo e nel Molise. *Studi Geologici Camerti*, vol. spec. 1991/2, 417-441.

Paull C.K., Chanton J. P., Neumann A. C., Coston J. A., Martens C. S. & Shower W., 1992. Indicators of methane-derived carbonates and chemosynthetic organic carbon deposits: examples from the Florida Escarpment. *Palaios*, **7**, 361-375.

Paull C.K., Brewer P. G., Ussler W. III, et al., 2003. An experiment demonstrating that methane slumping is a mechanism to transfer methane from seafloor gas-hydrate deposits into the upper ocean and atmosphere. *Geo-Marine Letters*, **22**, 189-203.

Pearson M. J., Grosjean E., Nelson C. S., Nyman S. L. & Logan G. A., 2010. Tubular concretions in New Zealand petroliferous basins: lipid biomarkers evidence for mineralisation around proposed Miocene hydrocarbon seep conduits. *Journal of Petroleum Geology*, **33**(3), 205-220.

Peckmann J. & Thiel V., 2004. Carbon cycling at ancient methane-seeps. *Chemical Geology, 205*, 443– 46.

Peckmann J., Thiel V., Michaelis W., Clari P., Gaillard C., Martire L. & Reitner J., 1999a. Cold seep deposits of Beauvoisin (Oxfordian; southeastern France) and Marmorito (Miocene; northern Italy): microbially induced authigenic carbonates. *International Journal of Earth Sciences*, **88** (1), 60-75.

Peckmann J., Walliser O.H., Riegel W. & Reitner J., 1999b. Signatures of hydrocarbon venting in a Middle Devonian carbonate mound (Hollard Mound) at the Hamar Laghdad (Antiatlas, Morocco). *Facies*, **40**, 281–296.

Peckmann J., Goedert J.L., Thiel V., Michaelis W. & Reitner J., 2002. A comprehensive approach to the study of methane–seep deposits from the Lincoln Creek Formation, western Washington State USA. *Sedimentology*, **49**, 855- 873.

Peckmann J., Reitner A., Luth U., Luth C., Hansen B.T., Heinicke C., Hoefs C. & Reitner J., 2001. Methane-derived carbonates and authigenic pyrite from the northwestern Black Sea. *Mar. Geol.*, **177**, 129-150.

Peckmann J., Gischler E., Oschmann W. & Reitner J., 2001a. An Early Carboniferous seep community and hydrocarbon-derived carbonates from the Harz Mountains, Germany. *Geology*, **29**, 271–274.

Peckmann J., Goedert J.L., Heinrichs T., Hoefs J. & Reitner J., 2003. The Late Eocene Whiskey Creek methane-seep deposit (western Washington State) - Part II: petrology, stable isotopes, and biogeochemistry. *Facies*, **48**, 241–254.

Pedley H.M. & Grasso M., 1993. Controls on faunal and sediment ciclicity within the Tripoli and Calcare di Base basins (Late Miocene) of central Sicily. *Palaeogeogr., Palaeoclim., Palaeoecol.*, **105**, 337-360.

Pierre C. & Rouchy J.M., 2004. Isotopic compositions of diagenetic dolomites in the Tortonian marls of the Western Mediterranean margins: Evidence of past gas hydrate formation and dissociation. *Chemical Geology*, **205**, 469-484.

Pierre C., Rouchy J.M. & Blanc-Valleron, M.M., 1998, Sedimentological and stable isotope changes at the Messinian-Pliocene boundary in the eastern Mediterranean (Holes 968A, 969A, 969B): Proc. O.D.P., Scient. Res., v. 160, p. 3-7.

Pierre C., Rouchy J. M. & Blanc-Valleron M. M., 2002. Gas hydrate dissociation in the Lorca Basin (SE Spain) during the Mediterranean Messinian salinity crisis. *Sed. Geol.*, **147** (3-4), 247-252.

Pilcher R. & Argent J., 2007. Mega-pockmarks and linear pockmark trains on the West African continental margin. *Mar. Geol.*, **244**, 15-32.

Raiswell R., 1987. Non-steady state microbiological diagenesis and the origin of concretions and nodular limestones. In: Marshall, J.D. (Ed.), Diagenesis of sedimentary sequences: Geological Society Special Publication, 36, pp. 41–54.

Reeburgh W. S., 1996. "Soft spots" in the global methane budget. In: Microbial Growth on C1 Compounds, edited by: Lidstrom M. E. and Tabita F. R.; Kluwer, Dordrecht, 334–342, 1996.

Reeburgh W. S., 2007. Oceanic methane biogeochemistry. *Chem. Rev.*, **107**(2), 486–513.

Riding R., Braga J.C., Martín J.M. & Sanchez-Almazo I.M., 1998. Mediterranean Messinian Salinity Crisis: constraints from a coeval marginal basin, Sorbas, southeastern Spain. *Mar. Geol.*, **146**, 1–20.

Riding R., Braga J.C. & Martín J.M., 1999. Late Miocene Mediterranean desiccation: topography and significance of the ''Salinity Crisis'' erosion surface on-land in southeast Spain. *Sed. Geol.*, **123**, 1–7.

Ritger S., Carson B. & Suess E., 1987. Methane-derived authigenic carbonates formed by subduction-induced pore-water expulsion along the Oregon/Washington margin. *Geological Society of American Bulletin*, **98**, 147-156.

Roberts H. H., 2001. Fluid and gas expulsion on the northern Gulf of Mexico continental slope: mud-prone to mineral-prone responses. In: C.K. Paull and W.P. Dillon, Editors, Natural Gas Hydrates: Occurrence, distribution and dynamics, American Geophysical Union, p. 131–143.

Roberts H.H. & Aharon P., 1994. Hydrocarbon-derived carbonate buildups of the northern Gulf of Mexico continental slope: a review of submersible investigations. *Geo Mar. Lett.* **14**, 135– 148.

Roda C., 1964. Distribuzione e facies dei sedimenti neogenici del Bacino di Crotonese. *Geol. Rom.*, **3**, 319–366.

Roda C., 1970. I depositi pliocenici della regione costiera Ionica dell'Italia Meridionale. *Boll. Accad. Gioenia Sci. Nat. Catania*, **10** (5), 364– 78.

Roda C., 1971. I depositi miocenici della Calabria. Boll. Accad. Gioena Sci. Nat. Catania, **10** (6), 237– 45.

Rodriguez N.M., Paull C.K. & Borowski W.S., 2000. Zonation of authigenic carbonates within gas hydrate-bearing sedimentary sections on the Blake Ridge: offshore Southeastern North America. In: Paull C.K., Matsumoto R., Wallace P.J. and Dillon W.P. (Eds.), 2000. Proceedings of the Ocean Drilling Program, Scientific Results, **164**, 301-312.

Rouchy J.M., 1982. La genèse des evaporites messiniennes de Mediterranee, *Mem. Mus. Nat. Hist. Nat.*, Paris.

Rouchy J.M. & Caruso A., 2006. The Messinian salinity crisis in the Mediterranean basin: a reassessment of the data and an integrated scenario. *Sed. Geol.*, **188-189**, 35-67.

Rouchy J.M., Orszag-Sperber F., Blanc-Valleron M.M., Pierre C., Rivière, M., Combourieu-Nebout N. & Panaydes I., 2001. Paleoenvironmental changes at the Messinian-Pliocene boundary in the eastern Mediterranean: southern Cyprus basins. *Sed. Geol.*, **145**, 93–117.

Rouchy J.-M., Pierre C., Et-Touhami M., Kerzazi K., Caruso A. & Blanc Valleron M.M., 2003. Late Messinian to Early Pliocene paleoenvironmental changes in the Melilla Basin (NE Morocco) and their relation to Mediterranean evolution. *Sed. Geol.*, **163**, 1–27.

Roveri M., Bassetti M.A. & Ricci Lucchi F., 2001. The Mediterranean Messinian salinity crisis: an Apennine foredeep perspective. *Sed. Geol.*, **140**, 201–214.

Roveri M., Lugli S., Manzi V., Gennari R., Iaccarino S. M., Grossi F. & Taviani M., 2006 (a). The Record of the Messinian Events in the Northern Apennines Foredeep Basins. *ACTA NATURALIA de "L'Ateneo Parmense"*, **42** (1).

Roveri M., Manzi V., Lugli S., Schreiber B.C., Caruso A., Rouchy J.-M., Iaccarino S.M., Gennari R. & Vitale F.P., 2006 (b). Clastic vs. primary precipitated evaporites in the Messinian Sicilian basins. RCMNS IC Parma 2006 "The Messinian salinity crisis revisited II", post-congress field-trip guidebook. Acta Naturalia de "L'Ateneo Parmense" 42-1, pp. 65.

Roveri M., Lugli S., Manzi V. & Schreiber B.C., 2008. The Messinian Sicilian stratigraphy revisited: new insights for the Messinian salinity crisis. *Terra Nova*, **20** (6), 483–488.

Ryan W.B.F., 1969. The floor of the Mediterranean Sea. PhD thesis, Columbia Univ., NY.

Ryan W.B.F., 1973. Geodynamic implications of the Messinian crisis of salinity. In: C.W. Drooger (Editor), Messinian Events in the Mediterranean. North Holland, Amsterdam, pp. 26-38.

Ryan W.B.F., 2009. Decoding the Mediterranean salinity crisis. *Sedimentology*, **56**, 95–136.

Sackett W.M., 1978. Carbon and hydrogen isotope effects during the thermocatalytic production of hydrocarbons in laboratory simulation experiments. *Geochim. Cosmochim. Acta*, **42**, 571- 580.

Sampalmieri G., 2006. Profili γ–ray di superficie come strumento per l'analisi di bacino: metodologia e applicazioni alle successioni mioceniche dell'Italia Centrale. *PhD Thesis*, 186 pp. Dipartimento di Scienze Geologiche, Università Roma Tre.

Sampalmieri G., Cipollari P., Cosentino D., Iadanza A., Lugli S. & Soligo M., 2008. Evaporites of the Messinian salinity crisis: natural radioactivity of the Gessoso-Solfifera Fm in the Maiella Mts (Abruzzi, central Italy). *Boll. Soc. Geol. It.*, **127** (1), 25-36.

Sampalmieri G., Iadanza A., Cipollari P. & Cosentino D., 2009. Natural radioactivity of pre-evaporitic/evaporitic succession outcropping in the Adriatic Foreland domain (Maiella Mts, Central Italy). 13th Congress RCMNS 2nd-6th September 2009 Naples (Italy), ACTA Naturalia de "L'Ateneo Parmense" Vol. 45 n. 1/4 2009.

Sampalmieri G., Iadanza A., Cipollari P., Cosentino D. & Lo Mastro S., 2010. Palaeoenvironments of the Mediterranean Basin at the Messinian hypersaline/hyposaline transition: evidence from natural radioactivity and microfacies of post-evaporitic successions of the Adriatic sub-basin. *Terra Nova*, **22**(4), 239–250.

Sample J.C. & Kopf A., 1995. Occurrences and geochemistry of syntectonic carbonate cements and veins from ODP Leg 146: implications for hydrogeologic evolution of the Cascadia margin. In: Carson, B., Westbrook, G. K., Musgrave, R. J., et al.: *Proc. ODP, Sci. Results*, **146**, College Station, TX (Ocean Drilling Program), 137-150.

Sauter E., Muyakshin S., Charlou J., Schlüter M., Boetius A., Jerosch K., et al., 2006. Methane discharge from a deep-sea submarine mud volcano into the upper water column by gas hydrate-coated methane bubbles. *Earth Planet. Sc. Lett.*, **243**, 354–365.

Savard M. M., Beauchamp B. & Veizer J., 1996. Significance of aragonite cements around Cretaceous marine methane seeps. *Journal of Sedimentary Research*, **66** (3), 430-438.

Schreiber B.C., 1988. Subaqueous evaporite deposition. In: Schreiber, B.C. (Ed.), *Evaporites and Hydrocarbons*. Columbia University Press, New York, pp. 182-255.

Schreiber B.C., Friedman G.M., Decima A. & Schreiber E., 1976. Depositional environments of Upper Miocene (Messinian) evaporite deposits of the Sicilian Basin. *Sedimentology*, **23**, 729-760.

Scisciani V., Calamita F., Bigi S., De Girolamo C. & Paltrinieri W., 2000. The influence of synorogenic normal fault on Pliocene thrust system development: the Maiella structure (central Apennines, Italy). *Mem. Soc. Geol. It.*, **55**, 193–204.

Scotti P., Chiaramonte M.A. & Paccaloni G., 1998. The Source Rock: a keypoint for Hydrocarbon Exploration. ENI-Agip, E&P Division, Corporate Technical Services - Quaderno Tecnico n. 8, pp. 1-20.

Selli R., 1973. An outline of the Messinian. In: Drooger C.W. (Ed), Messinian Events in the Mediterranean. 150-171, Amsterdam.

Sibuet M.& Olu K., 1998. Biogeography, biodiversity and fluid dependence of deep-sea cold seep communities at active and passive margins. *Deep- Sea Research*, **45** (1-3), 517-567.

Soria J.M., Caracuel J.E., Yébenes A., Fernández J. & Viseras C., 2005. The stratigraphic record of the Messinian Salinity crisis in the northern margin of the Bajo Segura Basin (SE Spain). *Sed. Geol.*, **179**, 225–247.

Suess E., Torres M.E., Bohrmann G., Collier R.W., Rickert D., Goldfinger C., Linke P., Heuser A., Sahling H., Heeschen K., Jung C., Nakamura K., Greinert J., Pfannkuche O., Trehu A., Klinkhammer G., Whiticar M.J.,

Eisenhauer A., Teichert B. & Elvert M., 2001. Sea floor methane hydrates at Hydrate Ridge, Cascadia margin. In: Paull C.K. & Dillon W.P. (Eds.), Natural Gas Hydrates: Occurrence, Distribution, and Detection. *Am. Geophysical Union, Geophys. Monogr. Ser.,* **124**, 87–98.

Tamajo E., 1961. Probabili tracce di vita in livelli ritenuti azoici della formazione zolfifera siciliana. *Riv. Min. Siciliana*, **67**, 6–14.

Tansi C., Muto F., Critelli S. & Iovine G., 2007. Neogene-Quaternary strike-slip tectonics in the central Calabrian Arc (southern Italy). *Journal of Geodynamics*, **43**, 393–414.

Thiel V., Peckmann J., Seifert R., Wehrung P., Reitner J. & Michaelis W., 1999. Highly isotopically depleted isoprenoids: molecular markers for ancient methane venting. *Geochim. Cosmochim. Acta*, **63**, 3959–3966.

Tréhu A.M., Bangs N.L. & Guerin G., 2006. Near-offset vertical seismic experiments during Leg 204. In: Tréhu A.M., Bohrmann G., Torres M.E. & Colwell, F.S. (Eds.), *Proc. ODP, Sci. Results*, **204**: College Station, TX (Ocean Drilling Program), 1–23.

Turcotte D.L., 1997. Fractals and Chaos in Geology and Geophysics. Cambridge University Press 2nd edition, 385 pp.

Tryon M. D., Brown K. M. & Torres M. E., 2002. Fluid and chemical flux in and out of sediments hosting methane hydrate deposits on Hydrate Ridge, OR, II: Hydrological processes. *Earth Planet. Sc. Lett.*, **201**, 541–557.

Ussler W. III & Paull C.K., 1995. Effects of ion exclusion and isotopic fractionation on pore water chemistry during gas hydrate formation and decomposition. *Geo-Marine Letters*, **15**, 37–44.

Ussler III W. & Paull C. K., 2001. Ion exclusion associated with marine gas hydrate deposits. In: Paull, C. K., and Dillon, W.P. eds., Natural Gas Hydrates: Occurrence, Distribution, and Detection: American Geophysical Union Geophysical Monograph, 124, p. 41–51.

Van Dijk J.P., Bello M., Brancaleoni G.P., Cantarella G., Costa V., Frixa A., Golfetto F., Merlini S., Riva M.,Torricelli S., Toscano C. & Zerilli A., 2000. A regional structural model for the northern sector of the Calabrian Arc (southern Italy).*Tectonophysics*, **324**, 267-320.

Van Dover C.L., 2000. The Ecology of Deep-sea Hydrothermal Vents. Princeton University Press, Princeton, New Jersey, pp. 1–424.

Vezzani L. & Ghisetti F., 1998. Carta Geologica dell'Abruzzo, Scala 1:100.000. S.EL.CA., Firenze.

Vismara-Schilling A., Stradner H., Cita M.B. & Gaetani M., 1976. Stratigraphic investigations on the late Neogene of Corfou (Greece) with special reference to the Miocene ∕ Pliocene boundary and to its geodynamic significance. *Mem. Soc. Geol. Ital.*, **16**, 279–317.

Wang C.Y. & Manga M., 2009. Mud Volcanoes. *Lecturer Notes in Earth Sciences*, **114**, 33-43.

Wegener G. & Boetius A., 2009. An experimental study on short-term changes in the anaerobic oxidation of methane in response to varying methane and sulfate fluxes. *Biogeosciences*, **6**, 867–876.

Whiticar M.J., 1999. Carbon and hydrogen isotope systematics of bacterial formation and oxidation of methane. *Chem. Geol.*, **161**, 291-314.

Whiticar M.J., Faber E. & Schoell M., 1986. Biogenic methane formation in marine and freshwater environments: CO_2 reduction vs. acetate fermentation - Isotope evidence. *Geochim. Cosmochim. Acta*, **50**, 693–709.

Wignall P.B., 1994. Black Shales. Claredon Press, Oxford, 127 pp.

Wignall P.B., Newton R. & Brookfield M.E., 2005. Pyrite framboid evidence for oxygen-poor deposition during the Permian–Triassic crisis in Kashmir. *Palaeogeogr. Palaeoclimatol. Palaeoecol.*, **216**, 183–188.

Wilkin R.T. & Barnes H.L., 1997. Formation processes of framboidal pyrite. *Geochim. Cosmochim. Acta*, **61**, 323–339.

Wilkin R.T., Barnes H.L. & Brantley S.L., 1996. The size distribution of framboidal pyrite in modern sediments: an indicator of redox conditions. *Geochim. Cosmochim. Acta*, **60**, 3897–3912.

Wilkin R.T., Arthur M.A. & Dean W.E., 1997. History of water-column anoxia in the Black Sea indicated by pyrite framboid size distributions. *Earth Planet. Sci. Lett.*, **148**, 517–525.

Zecchin M., Massari F., Mellere D., Prosser G., 2004. Anatomy and evolution of a Mediterranean-type fault bounded basin: the lower Pliocene of the northern Crotone basin (southern Italy). *Basin Res.*, **16**, 117–143.

Zhang C.L. & Lanoil B., 2004. Geomicrobiology and biogeochemistry of gas hydrates and cold seeps. *Chemical Geology*, **205**, 187–194.

Ziegenbalg S.B., Brunner B., Rouchy J.M., Birgel D., Pierre C., Böttcher M.E., Caruso A., Immenhauser A. & Peckmann J., 2010. Formation of secondary carbonates and native sulphur in sulphate-rich Messinian strata, Sicily. *Sedimentary Geology*, **227**, 37–50.

Appendix 1 - Summary of: concentrations of U_{ppm}, Th_{ppm} and % K2O; U/Th and Th/K ratios; U_{aut} and U_{det} contents (after Sampalmieri et al., 2010) in the brecciated limestones of the northwestern Maiella area

Lithology	Sample	U (ppm)	K₂O (%)	Th (p.p.m.)	U/Th	Th/K	Uaut (ppm)	Udet (ppm)	Uaut (%)
Brown laminated shale	RM 39	1.38	7.71	0.71	1.962	0.091	1.15	0.24	83.01
Brecciated carbonate	RM 40 a	1.30	3.58	0.30					
Grey marl	RM 41	1.36	6.79	0.62	2.175	0.092	1.15	0.21	84.68
Brecciated carbonate	RM 43	5.29	0.89	0.21					
Red laminated shale	RM 45	2.94	8.74	1.02	2.875	0.117	2.60	0.34	88.41
Yellow mud carbonate	RM 47	5.31	4.10	0.41					
Brecciated carbonate	RM 48	5.49	1.68	0.14					
Brecciated carbonate	RM 49	4.27	0.76	0.09					
Yellow laminated marl	CV 1	3.46	7.29	0.79	4.391	0.108	3.20	0.26	92.41
Vacuolar carbonate	CV 2	3.59	1.65	0.22					
Volcaniclastic layer	CV 6	3.67	17.75	5.02					
Volcaniclastic layer	CV 7	1.95	12.94	2.58					
Volcaniclastic layer	CV 8	2.09	10.93	2.44					
Grey marl	CV 9	4.18	6.84	0.95	4.420	0.138	3.86	0.32	92.46
Grey marl	CV 11a	7.36	7.88	0.91	8.130	0.115	7.06	0.30	95.90
Grey laminated marl	CV 12	8.30	6.76	0.67	12.304	0.100	8.07	0.22	97.29

Appendix 2 - List of the δ^{18}O and δ^{13}C results in the Brecciated Limestones unit of the Maiella area

lithofacies		sample	facies	δ^{18}O	δ^{13}C
Patchy limestones	guest carbonates	RM 50L	cemented brecciated concretion	-2,51	-16,6
		RM 34	vuggy limestone with pore-filling tar	-1,4	-19
		RM 34a	vuggy limestone with pore-filling tar	-4,18	-37,01
		RCM/A6	brecciated limestone	-3,91	-20,78
		RCM/A7	cemented marl	-1,72	-0,2
		RCM/A8	brecciated limestone	-2,70	-22,94
		RM 38	microbrecciated limestone	-3,87	-35,4
		RM 40a	cemented brecciated marl	-3,9	-39,27
		RM 41	laminated marl	-4,03	-36,85
		RM 43	cemented microbrecciated concretion	-3,46	-12,5
	host sediment	RM 44	brown marl	2,67	-4,69
		RM 44 (mbc)	microbrecciated grain (subsampled brown marl)	-6,83	-11,27
		RM 44 (tb)	microtubular structures (subsampled brown marl)	-5,31	-9,53
		RM 44 (V)	vein (subsampled brown marl)	-5,73	-9,56
		RM 45	laminated red pelites	-6,34	-9,25
		RM 45 (tb)	microtubular structures (subsampled laminated red pelites)	-5,78	-11,03
		RM 46	laminated grey pelites	-1,61	-5,71
		RM 46 (mbc)	microbrecciated grain (subsampled laminated grey pelites)	-7,16	-11,29
		RM 46 (tb)	microtubular structures (subsampled laminated grey pelites)	3,50	-28,69
		RM 47	yellow marl	-5,33	-6,32
		RM 47 (tb)	microtubular structures (subsampled yellow marl)	-4,00	-39,05
	guest carbonates	RM 48	weakly cemented concretion	2,75	-7,16
		RM 49	cemented concretion	-3,03	-14,1
		RM 54	concretioned brecciated limestone	-0,46	-3,92
		RM 55	concretioned brecciated limestone	-3,03	0,29
		RM 56 (a)	mostly dark brown cemented portion (subsampled microbrecciated concretion)	0,41	-7,96
		RM 56 (b)	impregnated laminite (subsampled microbrecciated concretion)	2,7	4,14
		RM 56 (c)	mixed impregnated and cemented portion, with white microconcretions (subsampled microbrecciated concretion)	0,67	-6,6
		RM 56 (d)	muddy concretion (subsampled microbrecciated concretion)	-1,05	-11,81
		RM 56 (e)	cemented matrix (subsampled microbrecciated concretion)	-1,1	-16,04
		RM 57 (a)	laminated portion (subsampled brecciated limestone)	-1,8	-6,18
		RM 57 (b)	brecciated portion (subsampled brecciated limestone)	-3,4	-7,1
		RM 58 (a)	dark brown pelitic portion (subsampled microbrecciated limestone)	3,05	1,72
		RM 58 (b)	yellow marly portion (subsampled microbrecciated limestone)	-2,13	-3,62
		RM 58 (c)	cemented pink portion (subsampled microbrecciated limestone)	-2,43	-6,37
		RM 59 (a)	highly cemented portion (cemented microbrecciated limestone)	-3,3	-14,55
		RM 59 (b)	chaotic cemented yellow portion (cemented microbrecciated limestone)	-4,09	-9,28
		RM 59 (c)	cloudy microconcretion (cemented microbrecciated limestone)	-3,13	-8,2
		RM 60	weakly cemented dark brown homogeneous concretion	3,59	2,68
		RM 61 (a)	impregnated portion (subsampled cemented dark brown microbrecciated concretion)	2,42	0,1
		RM 61 (b)	impregnated portion and interparticle cement (subsampled cemented dark brown microbrecciated concretion)	-0,54	-1,69

lithofacies		sample	facies	δ¹⁸O	δ¹³C
Patchy limestones	*guest carbonates*	RM 61 (c)	microbrecciatted impregnated portion with major interparticle cement (subsampled cemented dark brown microbrecciated concretion)	-2,08	-3,94
		RM 62	cemented carbonatic laminae	-2,38	-8,83
		RM 63a	carbonatic fraction (subsampled chaoticized brecciated limestone)	-2,39	-6,28
		RM 63b	dark brown pelitic flames (subsampled chaoticized brecciated limestone)	-2,69	-11,39
		RM 63c	mixed chaoticized microfacies (subsampled chaoticized brecciated limestone)	-2,41	-4,1
		RM 64	laminated limestone	-1,33	0,43
		RM 65 (a)	clasts matrix (subsampled cemented dark brown brecciated concretion)	-2,6	0,82
		RM 65 (b)	clast matrix and interparticle cement (subsampled cemented dark brown brecciated concretion)	-2,47	1,96
		RM 66	brown marly lens	2,52	-4,52
	guest carbonates (altered)	RM 1-1 (a)	ocraceous cemented portion (subsampled brecciated limestone)	-1	0,89
		RM 1-1 (b)	bulk portion: mixed microfacies (subsampled brecciated limestone)	-2,07	2,31
		RM 1-1 (c)	laminated calcarenitic microfacies (subsampled brecciated limestone)	-1,82	2,31
		RM 1-2 (a)	ocraceus matrix microfacies (subsampled brecciated limestone)	-1,54	-2,16
		RM 1-2 (b)	laminated calcarenitic microfacies (subsampled brecciated limestone)	-1,19	1,38
		RM 1-3	cemented carbonatic laminae	-2,6	-6,09
		RM 1-4 (a)	rim porton, yellow matrix-dominated (subsampled clast within a concretion)	-2,8	-8,89
		RM 1-4 (b)	bulk portion: mixed microfacies (subsampled clast within a concretion)	-2,75	-19,04
		RM 1-4 (c)	core portion: sparry cement-dominated (subsampled clast within a concretion)	-2,73	-15,1
		RM 1-5	brecciated concretions occurring as single elements	-3,06	-9,41
		RM 1-6	weakly cemented brecciated limestone	-3	-13,11
		RM 1-7	calcarenite	-3,09	-0,31
		RM 50	finely laminated marl	-2,29	-2,09
		RM 51	homogeneous marl	-2	-2,19
	uppermost portion of the Bcl Unit (alternation of laminated and bioturbated marls and pelites)	CV 1	laminated ocraceous marl	-3,48	-6,23
		CV 1a	cemented limestone	-2,92	-2,65
		CV 2	weakly cemented laminated marl	-0,8	-4,72
		CV 3	ocraceous laminated marl	-2,61	-5,79
		CV 4	ocraceous laminated marl	-3,82	-7,11
		CV 5	reddish laminated marly limestone	-3,28	-2,78
		CV 7	carbonatic matrix associated to volcaniclastics	-2,94	-16,71
		CV 7a	carbonatic matrix associated to volcaniclastics	-3,38	-24,76
		CV 8	carbonatic matrix associated to volcaniclastics	-3,12	-16,53
		CV 9 (a)	reddish laminae associated to concretion (subsampled pale cream homogeneous marl)	-3,67	-1,46
		CV 9 (b)	concretioned portion (subsampled pale cream homogeneous marl)	-0,77	1,57
		CV 10	ocraceous laminites	-2,94	-4,34
		CV 11	homogeneous marl	-1,82	-1,96
		CV 12	grey laminated marl	-2,32	-3,25
	guest carb.	CGS/A	vuggy microbrecciated limestone	-4,89	-6,81
		CGS/B	concretioned limestone	-6,51	-7,98

lithofacies	sample	facies	$\delta^{18}O$	$\delta^{13}C$
Brecciated limestones	ABB 1	brecciated limestone: pale cream microbial limestone partially impregnated	-1,86	0,74
	ABB 2A (a)	grey microconcretion (subsampled brecciated limestone: pale cream microbial limestone partially impregnated)	-3,11	-0,41
	ABB 2A (b)	bulk portion: mixed microfacies (subsampled brecciated limestone: pale cream microbial limestone partially impregnated)	-0,68	3,19
	ABB 2A (c)	impregnated brown microfacies (subsampled brecciated limestone: pale cream microbial limestone partially impregnated)	1,07	3,34
	ABB 2A (d)	pale cream microbial microfacies (subsampled brecciated limestone: pale cream microbial limestone partially impregnated)	-1,43	0,55
	ABB 3	brecciated limestone: pale cream microbial limestone partially impregnated	-1,38	-0,02
	ABB 4a	impregnated brown microfacies (subsampled brecciated limestone: pale cream microbial limestone partially impregnated)	-0,26	1,47
	ABB 4b	pale cream microbial microfacies (subsampled brecciated limestone: pale cream microbial limestone partially impregnated)	-1,41	1,35
	ABB 5a	matrix-dominated microfacies (subsampled cemented brecciated dark-brown concretion)	-1,71	0,37
	ABB 5b	bulk portion: mixed microfacies (subsampled cemented brecciated dark-brown concretion)	-2,01	0,08
	ABB 6	impregnated limestone	-1,64	-0,46
	ABB 7	cloudy concretions pale cream microbial limestone associated to brecciated impregnated portion with interparticle cement	-1,61	0,01
	ABB 8A (a)	prevailing impregnated portion (subsampled cemented breccia with localized impregnations)	-2,27	-0,83
	ABB 8A (b)	bulk portion: mixed microfacies (subsampled cemented breccia with localized impregnations)	-0,46	0,44
	ABB 8B	dark brown silt	4,01	1,66
	ABB 8C	highly cemented impregnated dark brown limestone	0,57	0,52
	ABB 8D (a)	cemented dark brown portion (subsampled impregnated cemented breccia)	-1,29	0,12
	ABB 8D (b)	cement (subsampled impregnated cemented breccia)	-1,8	0,43
	ABB 9a (a)	prevailing grey microconcretions (subsampled brecciated concretion)	-0,85	0,64
	ABB 9a (b)	mixed microfacies (subsampled brecciated limestone with red matrix)	-1,03	0,75
	ABB 9a (c)	white clasts and reddish matrix (subsampled brecciated limestone with red matrix)	-0,73	0,36
	ABB 9b (a)	white concretion (subsampled brecciated limestone with red matrix)	-1,01	0,82
	ABB 9b (b)	mixed microfacies (subsampled brecciated limestone with red matrix)	-0,75	1
	ABB 10 (a)	cement (subsampled impregnated cemented breccia)	-1,17	1,57
	ABB 10 (b)	cemented dark brown laminated portion (subsampled impregnated cemented breccia)	-1,7	0,9
	ABB 11	dark concretioned patch	3,6	2,68
	ABB 12	very dark brown pelites associated to the brecciated limestones	-1,78	-0,89
	ABB 13	trapped green-reddish pelites	-1,15	-0,39
	ABB 14	dark concretioned laminated patch	4,4	2,81
	ABB 15	dark brown cemented brecciated limestone	-1,73	0,87
	CC/A	chaoticized concretion	-1,21	-2,06
	CC/B (a)	prevailing cement (subsampled brecciated limestone)	-1,72	-4,2
	CC/B (b)	mixed microfacies (subsampled brecciated limestone)	-1,75	-4,95
	CCT	brecciated limestone	-5,13	-8,47
	MP/A (a)	cemented microncretion (subsampled brecciated limestone)	-2,33	-0,78
	MP/A (b)	cement (subsampled brecciated limestone)	-2,16	-0,81
	MP/B	vuggy limestone	-2,17	-0,19

lithofacies	sample	facies	δ¹⁸O	δ¹³C
	LET 1	tar-bearing recrystallized sulphur-bearing limestones	-3,99	-27,18
	LET 2	tar-bearing recrystallized sulphur-bearing limestones	-2,18	-25,61
	LET 3a	tar-bearing recrystallized sulphur-bearing limestones	-3,40	-26,02
	LET 3b	tar-bearing recrystallized sulphur-bearing limestones	-4,09	-24,34
	LET 4	tar-bearing recrystallized sulphur-bearing limestones	-2,11	-23,67
	LET 5	tar-bearing recrystallized sulphur-bearing limestones	-3,19	-24,94
	LET 6	tar-bearing recrystallized sulphur-bearing limestones	-2,90	-27,52
	LET 7	tar-bearing recrystallized sulphur-bearing limestones	-3,00	-26,07
	LET 8	tar-bearing recrystallized sulphur-bearing limestones	-1,5	-25,48
Oil-bearing brecciated limestones	MM/a1	tar-bearing vuggy limestone	-5,02	-7,92
	MM/b1 (a)	microcrystalline cement (subsampled tar-bearing vuggy limestone)	-7,8	-12,27
	MM/b1 (b)	bulk portion: mixed microfacies (subsampled tar-bearing vuggy limestone)	-6,8	-8,62
	MM/b1 (c)	tar-bearing spar (subsampled tar-bearing vuggy limestone)	-8,14	-11,43
	MM/c1	tar-bearing vuggy limestone	-7,91	-6,93
	MM/e1 (a)	tar dominated portion (subsampled tar-bearing vuggy limestone)	-8,72	-13,95
	MM/e1 (b)	brown cemented microfacies (subsampled tar-bearing vuggy limestone)	-8,47	-13,1
	MM/e1 (c)	prevailing cement (subsampled tar-bearing vuggy limestone)	-8,58	-15,83
	MM/f (a)	tar-bearing vuggy limestone	-7,87	-9,84
	MM/f (b)	vein (subsampled tar-bearing vuggy limestone)	-7,64	-15,23
	GP/A (a)	botryoidal aragonite (subsampled cemented bituminous limestone)	-1,18	-19,4
	GP/A (b)	microspar (subsampled cemented bituminous limestone)	-1,28	-7,35
	DEC 1-2	mudstone	-5,24	-2,41
	DEC 1-3 (a)	white concretion (subsampled bituminous pelites and marls)	-5,83	-8,38
	DEC 1-3 (b)	pelite and concretion (subsampled bituminous pelites and marls)	3,62	-7,63
	DEC 1-3 (c)	pelite and concretion (subsampled bituminous pelites and marls)	-5,19	-9,1
	DEC 1-5	chaoticized and concretioned pelite	-5,64	-8,6
	DEC 1-7	laminated brown pelite with white microconcretions	-6,28	-9,31
	DEC 1-8	concretions associated to pelites	-6,61	-8,06
	DEC 14	mixed facies: brown pelite with concretions	-2,43	-1,74
Fluidized sediments	DEC 15	cemented brecciated concretion	-4,2	-2,47
	DEC 16	dark brown concretioned pelitie	-1,78	-4,15
	DEC 16 a	concretions associated to brown pelites	-4,79	-6,59
	DEC 16 b	reddish concretion	-2,5	-4,27
	DEC 16 c	concretioned microconglomerate	-1,95	-2,79
	DEC 1-6	homogeneous mud	-6,14	-8,73
	CT 1	vuggy reddish clast	-2,08	0,98
	CT 2 (a)	opalescent micronodules - bulk	-3,04	-4,41
	CT 2 (b)	white concretion (associated to pale blue micronodules)	-5,6	-9,53
	CT 3	opalescent micronodules	-2,31	-4
	CT 4	vuggy laminated limestone	-2,91	-1,42
	CT 6	laminated marl with variously white, brown and black flames	-7,36	-19,2
	CT 7	botryoidal aragonite	-9,64	-24,5

Appendix 2 (continued)

lithofacies	sample	facies	δ¹⁸O	δ¹³C
Fluidized sediments	CT 8 (a)	fibrous cement (subsampled vuggy scoria-like limestone with botryoidal aragonite)	-9,28	-14,9
	CT 8 (b)	cemented carbonate (subsampled vuggy scoria-like limestone with botryoidal aragonite)	-10,5	-20
	BUN 3	homogeneous white concretion	-5,67	-8,37
	BUN 4	white concretion	-5,75	-8,32
	BUN 5	vuggy scoria-like limestone	-2,86	-1,04
	CBU 3c - 1 (a)	brown-greenish pelites	-5,65	-8,7
	CBU 3c - 1 (b)	white concretions	-5,41	-8,2
	CBU 3c - 1 (c)	calcarenitic clasts with a white matrix	-5,73	-8,07
	CBU 3c - 1 (d)	vuggy scoria-like limestone	-5,32	-7,1
	CBU 3c - 2 (a)	chaoticized brown pelite	-5	-6,76
	CBU 3c - 2 (b)	carbonate clast	-5,67	-8,5
	CBU 3c - 3 (a)	green-reddish pelite	-4,55	-6,24
	CBU 3c - 3 (b)	white concretions	-4,72	-6,95
	CBU 3c - 3 (c)	white concretions with minor pelite	-3,23	-6,55
	CBU 3c - 3 (d)	vuggy scoria-like limestone with minor veins	-2,99	-4,78
	CBU 3c - 4 (a)	homogeneous white concretions (subsampled fluidized pelite)	-5,65	-8,27
	CBU 3c - 4 (b)	brown pelite (subsampled fluidized pelite)	-4,61	-5,29
	CBU 3c - 5	vuggy scoria-like limestone	-2,93	-1,82

Appendix 3 - List of the δ^{18}O and δ^{13}C results in the *Calcare di Base* of the Calabrian Arc

area	SAMPLE	facies/microfacies	d18O	d13C
	CROP 04	diatomite	6,57	-2,29
	CROP 18a	mudstone	5,15	0,94
	CROP 18b	mudstone	5,13	0,32
	CROP 20	stromatolithe	4,26	0,41
	CROP 21	concretion	6,24	-1,47
	CROP 23	cemented diatomite	4,9	-2,48
	CROP E	*cnd-fls*	4,1	-0,41
	CROP D	stromatolite	6,17	0,76
	CROP 25	*fls*-bearing mudstone	4,02	0,74
	CROP 26	pelitic mudstone with *cnd-fls*	4,25	0,24
	CROP 28	mudstone	4,02	-0,43
	CROP 29 (a)	*cnd* in a muddy matrix (subsampled *cnd-fls*)	3,72	-0,48
	CROP 29 (b)	mudstone (subsampled *cnd-fls*)	3,93	-0,05
	CROP 30	pelitic-rich mudstone	3,88	-0,19
	CROP 31 (a)	microsparry (subsampled *cnd-fls*)	-4,46	-6,15
	CROP 31 (b)	*fls* in a muddy matrix (subsampled *cnd-fls*)	2,11	-3,26
	CROP 33	concretion	2,35	-2,34
	CROP 34	concretion	2,66	-2,54
	CROP B	concretion	-3,32	-5,29
	CROP A	stomatolite	3,39	0,95
Rossano Basin	CROP SP4	mudstone	3,88	-0,8
	CROP 35	concretion	4,07	0,09
	CROP 37	cemented concretion	3,25	-2,31
	CROP 38	*cnd-fls*	3,2	-2,06
	CROP 39	concretion in a pelitic matrix	3,45	-1,36
	CROP 40	*cnd-fls*	4,34	-1,3
	CROP 43	concretion	3,82	-2,22
	CROP 45	microbrecciated carbonatic grains in a fine green matrix	3,45	-1,67
	CROP 46	mudstone with abundant marly matrix and *fls*	3,3	-1,75
	CROP 47	concretion with minor pelitic fraction	3,09	-2,92
	CROP 49 (a)	muddy fraction and *cld* (fluidized breccia)	3,63	-1,71
	CROP 49 (b)	*cnd* (single) (fluidized breccia)	1,97	-2,71
	CROP 49 (c)	muddy fraction (fluidized breccia)	4,09	-1,62
	CROP 52	concretion	2,99	-2,2
	CROP 53	concretion	3,34	-1,87
	CROP 54	cemented mudstone with *cld-fls*	3,73	-1,8
	CROP 55	concretion with small *cnd*	3,46	-1,71
	CROP 56	mudstone with *cld-fls*	1,98	-2,84
	CROP SP7	carbonatic grains in a fine matrix	3,69	-1,6
	CROP C	mudstone with cnd and veins	-4,14	-1,37
	CROP3-1	yellow mudstone with interparticle cement	-0,69	-4,57
	CROP3-4	marl associated to microsparry and pore-filling cement	-2,28	-4,64
	CROP3-5	cemented concretion	-5,93	-1,92
	CROP3-6	cemented concretion	-6,3	-1,85
	CROP3-7	concretion with pelitic fraction	-1,97	-2,83
	CROP3-10	mudstone	-3,77	-2,16
	CROP3-10 v (a)	vein (concretion cut by a vein)	-5,66	-1,27

Appendix 3 (continued) - (*cnd*: cloudy nodules; *fls*: flames-like pelitic structures)

area	SAMPLE	facies/microfacies	d18O	d13C
Rossano Basin	CROP3-10 v (b)	mudstone (concretion cut by a vein)	-5,97	-2,2
	CROP3-12	concretion with *cnd*	0,23	-1,27
	CROP3-13v	vein	-5,97	-2,2
	CROP3-14	mudstone	-5,94	0,2
	CROP3-15	concretion	-4,69	-1,31
	CROP3-15a	concretion	-0,79	1,47
	CROP3-15b	concretion with cement	-5,83	-1,78
	CROP3-15c	pelitic mudstone	-3,18	-0,68
	CROP3-15d	mudstone with veins and *fls*	-5,58	-4,45
	CROP3-16 (a)	pelitic fraction prevailing (microbrecciated laminated pelite)	2,18	2
	CROP3-16 (b)	carbonatic grains prevailing (microbrecciated laminated pelite)	-0,35	1,14
	CROP3-16 (c)	pelitic mudstone (microbrecciated laminated pelite)	0,88	1,6
	CROP 3-17	mudstone	-5,54	-4,09
	CROP3-18b	mudstone	5,13	0,37
	CROP3-18c	concretion with pelite	-3,06	-0,28
	CROP3-19	mudstone	-5,91	-1,24
	CROP 3-A	pelitic mudstone with interparticle cement and veins	-5,66	-2,09
	CROP 3-B (a)	vein (concretion cut by a vein)	-5,98	-0,33
	CROP 3-B (b)	concretion (concretion cut by a vein)	-5,93	-1,9
Cessaniti Basin	BRI	mosaic breccia with a microbial peloidal microfacies	-3,63	1,02
	BRI/A	mosaic breccia with a microbial peloidal microfacies	-4,14	1,56
	BRI 1	mosaic breccia with a microbial peloidal microfacies	-1,34	0,29
	BRI/B	mosaic breccia with a microbial peloidal microfacies	-1,89	0,57
Crotone Basin	CTV a1	microbreccia	2,48	1,46
	CTV a2	microbreccia with gypsum cement	2,43	0,75
	CTV b1	finely laminated calcarenite	3,91	-0,47
	CTV b2	microbreccia with gypsum cement	3,45	0,12
	CTV b3	microbreccia with gypsum cement	3,91	-1,35
	SR/a1	laminite	5,78	-0,42
	SR/a2	concretioned bituminous limestone	5,19	-1,13
	GM/b1	chaoticized laminae	5,41	-2,9
	GM/b2	chaoticized laminae	5,18	-3,32
	GM/b3	chaoticized laminae	4,72	-2,74
	GM/c	contorted chaoticized laminae	7,25	1,93
	GM/d	nodule	7,35	0,31
	CSB/c1(a)	laminae (subsampled chaoticized laminae with dark concretions)	5,57	-3,19
	CSB/c1(b)	concretion (subsampled chaoticized laminae with dark concretions)	7,74	0,3
	CSB/c2	chaoticized laminae	5,99	-2,8
	CSB/c3(a)	cemented concretion (subsampled brecciated limestone)	5,98	-3,21
	CSB/c3(b)	mixed microfacies (subsampled brecciated limestone)	4,67	-3,99
	CSB/c4	laminites and microbreccias	5,19	-4,22
	CSB/c5	chaoticized laminae	5,89	-3,24
	CSB/c6	chaoticized laminae	5,8	-3,58
	CSB/c7	chaoticized laminae	3,84	-6,23
	CSB/c8	chaoticized laminae	6,65	-2,11
	CSB/d1	marly limestone with secondary gyspum (mesobreccia)	6,99	-2
	CSB/d2	brecciated limestones with clay partings	7,35	-1,77

Appendix 4 - List of the δ^{18}O and δ^{13}C results in the *Calcare di Base* of Sicily

area	SAMPLE	facies/microfacies	d18O	d13C
	CPD/B	brecciated carbonatic concretions associated to gypsum	4,6	-41
	CPD/C	brecciated carbonatic concretions associated to gypsum	4,36	-42,4
	CPD/D	brecciated carbonatic concretions associated to gypsum	4,09	-38,9
	CPD/F (a)	cement (subsampled sulphur-bearing brecciated limestone)	3,98	-40,1
	CPD/F (b)	dark cemented matrix (subsampled sulphur-bearing brecciated limestone)	3,87	-40
	CPD/G (a)	dark cemented matrix (subsampled dark sulphur-bearing brecciated limestone rich in sparry calcite)	3,72	-41,2
	CPD/G (b)	cement (subsampled dark sulphur-bearing brecciated limestone rich in sparry calcite)	2,97	-41,1
	CPD/H (a)	cement (subsampled dark sulphur-bearing brecciated limestone rich in sparry calcite)	3,81	-38,3
	CPD/H (b)	dark cemented matrix (subsampled dark sulphur-bearing brecciated limestone rich in sparry calcite)	3,73	-41,6
	CPD/I (a)	cement (subsampled dark sulphur-bearing brecciated limestone rich in sparry calcite)	4,03	-37,5
	CPD/I (b)	dark cemented matrix (subsampled dark sulphur-bearing brecciated limestone rich in sparry calcite)	3,76	-39
	CPD/L1 (a)	fibrous cement (subsampled dark sulphur-bearing brecciated limestone rich in sparry calcite)	3,84	-38,7
	CPD/L1 (b)	dark cemented matrix (subsampled dark sulphur-bearing brecciated limestone rich in sparry calcite)	3,67	-41,6
	CPD/L2 (a)	dark layer (subsampled dark sulphur-bearing brecciated limestone rich in sparry calcite)	4,8	-40,1
	CPD/L2 (b)	dark layer (subsampled dark sulphur-bearing brecciated limestone rich in sparry calcite)	3,74	-40,5
Capodarso	CPD/M	carbonatic concretion	4,71	-36,7
	CPD1/B	brecciated limestone	4,16	-37,9
	CPD1/C	brecciated limestone	4,53	-39,7
	CPD1/D	sulphur-bearing vein	4,3	-38,4
	CPD1/E1 (a)	brecciated limestone	4,83	-35,9
	CPD1/E1 (b)	vein (subsampled brecciated limestone)	4,75	-38,1
	CPD1/E2	brecciated limestone	4,63	-37
	CPD1/F	brecciated limestone with primary lamination preserved	4,16	-42,2
	CPD1/G (a)	dark cemented matrix (subsampled brecciated limestone)	4,55	-40,3
	CPD1/G (b)	cement (subsampled brecciated limestone)	4,55	-39,6
	CPD1/H	brecciated limestone	4,37	-38,2
	CPD2/1	carbonate concretion associated to gypsum	3,89	-32,4
	CPD2/2	brecciated carbonate concretion associated to gypsum	4,17	-39,8
	CPD2/3 (a)	cement (subsampled dark sulphur-bearing brecciated limestone rich in sparry calcite)	3,81	-42,7
	CPD2/3 (b)	mixed microfacies (subsampled dark sulphur-bearing brecciated limestone rich in sparry calcite)	3,77	-42,8
	CPD2/4	brecciated sulphur-bearing limestone with high porosity	3,87	-41,5
	CPD2/5	highly cemented brecciated sulphur-bearing limestone	3,77	-43,4
	CPD2/6 (a)	cement (subsampled sulphur-bearing brecciated limestone)	4,21	-41,7
	CPD2/6 (b)	dark cemented matrix (subsampled sulphur-bearing brecciated limestone)	3,98	-43,7
	CPD2/7	highly cemented brecciated sulphur-bearing limestone	4,06	-42
	CPD2/8 (a)	dark cemented matrix (subsampled sulphur-bearing brecciated limestone)	3,94	-43
	CPD2/8 (b)	cement (subsampled sulphur-bearing brecciated limestone)	3,83	-43,1
	CPD2/9 (a)	rim cement (subsampled sulphur-bearing brecciated limestone)	4,04	-40,4
	CPD2/9 (b)	core dark cemented matrix (subsampled sulphur-bearing brecciated limestone)	3,74	-43,1

area	SAMPLE	facies/microfacies	d18O	d13C
Capodarso	CPD2/A	brecciated sulphur-bearing limestone	3,67	-42,7
	CPD2/B	brecciated sulphur-bearing limestone	3,89	-43,2
	CPD2/C	brecciated sulphur-bearing limestone	4,02	-42
	CPD2/D	brecciated sulphur-bearing limestone	3,89	-41,6
	CPD2/E	brecciated sulphur-bearing limestone	4,15	-42,3
	CPD2/F	brecciated sulphur-bearing limestone	3,64	-43
	CPD2/G	brecciated sulphur-bearing limestone	3,56	-42
Centuripe	CTPE/A	moderately brecciated limestone	4,38	-1,79
	CTPE/B (a)	cemented laminated portion (subsampled amorphous silica-bearing limestone)	4	-1,59
	CTPE/B (b)	amorphous silica-bearing limestone	3,56	-1,17
	CTPE/C	marly calcareous patch	4,17	-4,25
	CTPE/D	weakly cemented brecciated limestone	4,27	-2,13
	CTPE/E1	brecciated limestone	3,99	-1,71
	CTPE/E2	brecciated limestone	4,16	-1,83
	CTPE/F	clay horizon	-2,49	-3,24
	CTPE/G	brecciated limestone with a fine matrix	3,38	-2,18
	CTPE/H (a)	cemented nodule (subsampled amorphous silica-bearing limestone)	3,71	-1,49
	CTPE/H (b)	laminae (subsampled amorphous silica-bearing limestone)	3,46	-2,35
	CTPE/I	gypsum-carbonate contact	-0,44	-2,46
	CTPE/L	nodules	4,25	-4,05
	CTPE/M	altered breccia	2,05	-3,59
	CTPE/N	laminated limestone	3,56	-3,62
	CTPE/O	brecciated concretion	4,04	-1,39
	CTPE/SA (a)	concretioned clasts (subsampled limestone breccia)	3,91	-2,44
	CTPE/SA (b)	matrix (subsampled limestone breccia)	3,89	-1,99
	CTPE/SB (a)	clasts (subsampled limestone breccia)	3,97	-0,69
	CTPE/SB (b)	matrix (subsampled limestone breccia)	3,91	-2,23
	CTPE/SC (a)	matrix (subsampled limestone breccia)	3,93	-1,36
	CTPE/SC (b)	clast (subsampled limestone breccia)	3,95	-0,93
	CTP 1	brecciated marly limestone	1,48	1,89
	CTP/1c	carbonatic porous vein associated to gypsum	-3,09	-4,27
	CTP/2	carbonatic vein associated to gypsum	0,76	0,23
	CTP/3	marly laminites	1,76	-3,09
	CTP/4	carbonatic nodules	0,62	-1,27
	CTP/5	marly limestone breccia	0,73	-0,96
spot samples	MGB-P	brecciated and laminated limestone	-3,13	-8,96
	CG4-F (a)	clast-dominated microfacies (subsampled brecciated concretion)	2,92	-1,56
	CG4-F (b)	matrix-dominated microfacies (subsampled brecciated concretion)	2,86	-1,61

Appendix 5 - Rock characterization parameters (TOC, S1, S2, HI, T_{max} and PI) and bitumen characterization (PM, i.e. biodegradation index; $\delta^{13}C$ of bitumen) on selected samples from the Maiella study area.

PI indicates the production index, given by the ratio (S1/S1+S2); see text (Ch. 3.4.3) for explanations on the other parameters.

Facies	sample nr	Sample type	TOC Wt%	S1 mg/g	S2 mg/g	HI	Tmax °C	PI	PM	δ13C
bituminous concretition weakly cemented	ABB 11	superficie	5,76	3,38	28,17	489	420	0,11	10	-27,80
	ABB 11	superficie-ws	0,70	0,04	1,40	200	425	0,03		
bituminous cemented concretion-breccia	ABB 14	superficie	8,64	9,62	47,54	550	420	0,17	10	-27,72
	ABB 14	superficie-ws	1,63	0,03	1,78	109	424	0,02		
brecciated bituminous limestone - dark brown mf	ABB 2A (c)	superficie	2,01	2,82	12,02	598	421	0,19	7/8	-26,87
	ABB 2A (c)	superficie-ws	0,26	0,03	0,98	377	427	0,03		
brown pelite with carbonate clasts	CBU 3C-4	superficie	0,10							
clayey-marly laminae with dark and whte flames	CT 06	superficie	1,74	0,15	1,35	78	390	0,10		
bituminous pelite and marls	DEC 1-3	superficie	0,66	1,35	1,35	205	390	0,50		-26,3
	DEC 1-3	superficie-ws	0,53	0,14	1,01	191	367	0,12		
tar infilling	PIL	superficie	4,55	3,45	27,51	605	428	0,11	9	-28,21
	PIL	superficie-ws	0,54	0,03	3,56	659	427	0,01		
dark pelite	RM 58 (a)	superficie	0,75	0,67	3,94	525	423	0,15	7	-27,56
	RM 58 (a)	superficie-ws	0,49	0,02	1,19	243	429	0,02		
weakly cemented bituminous concretion	RM 60	superficie	2,24	0,84	12,37	552	425	0,06	10	-28,39
	RM 60	superficie-ws	1,07	0,03	1,85	173	430	0,02		
cemented bituminous concretion	RM 61	superficie	1,00	0,59	5,05	505	422	0,10	7	-27,59
	RM 61	superficie-ws	0,67	0,01	1,07	160	426	0,01		
xsl vacuolar bitumen-bearing limestone	MM / a1	superficie	0,66	0,09	3,56	539	431	0,02		
	MM / a1	superficie-ws	0,43	0,09	1,48	344	433	0,06		
xsl vacuolar bitumen-bearing limestone	MM / b1	superficie	5,55	0,47	9,64	174	426	0,05	9	-27,51
	MM / b1	superficie-ws	0,46	0,02	1,27	276	434	0,02		
xsl vacuolar bitumen-bearing limestone	MM / e1	superficie	1,32	0,16	7,73	586	425	0,02	10	-28,66
	MM / e1	superficie-ws	0,40	0,02	1,18	295	433	0,02		
xsl vacuolar bitumen-bearing limestone	MM / f	superficie	0,84	0,27	4,51	537	429	0,06		
	MM / f	superficie-ws	0,31	0,04	0,96	310	432	0,04		
cemented bituminous limestone	LET	superficie	11,07	13,22	75,49	682	433	0,15	9/10	-28,6
	LET	superficie-ws	0,25	0,04	1,13	452	433	0,03		